

Drug-repurposing approaches to target bacterial respiratory complexes

Thesis for the degree of PhD in Microbiology

School of Biosciences

Division of Natural Sciences

University of Kent

Number of Pages: 201

Samantha Amoy Henry

2024

Declaration

I declare that no part of this thesis has been previously submitted in support of an application for any degree or qualification at either the University of Kent, or any other university or higher education learning institution.

Samantha Henry

April 29, 2024

Abstract

Antimicrobial resistance is a global health problem that resulted in an estimated 1.2 million deaths in 2019. It is predicted that antimicrobial resistance will result in an estimated 10 million deaths annually by 2050 if urgent action is not taken (Pulingam *et al.* 2022). This has fuelled various research aimed at discovering new antimicrobials to combat this issue. Within the past few decades, a myriad of drug targets has surfaced such as cytochrome *bd*. Cytochrome *bd* is an oxidoreductase that is found only in prokaryotes and archaea and is a promising drug candidate for numerous reasons. Cytochrome *bd* has been proven to increase virulence in some of the most pathogenic strains of bacteria such as *Mycobacterium* species, as deletion of the enzyme causes severe attenuation. The oxidase is also highly expressed and induced by the innate immune response during infection. High resolution structures of cytochrome *bd* from various organisms have been published which means that the oxidase can be studied computationally. These characteristics make cytochrome *bd* an attractive drug candidate and therefore forms the basis of this study.

Lambda-red mutagenesis was previously employed by the host lab to create *E. coli* mutant strains that express only a single respiratory oxidase (i.e., cytochrome *bd-I* or *bo'*) and numerous attempts were made to engineer an *E. coli* 'cytochrome *bd-II* only' strain but these were unsuccessful. The current work aimed to characterise *E. coli* WT and respiratory mutant strains and develop an assay to measure oxygen consumption activity in membranes of these strains. Plasmid-based approaches were used to express *E. coli* cytochrome *bd-I* and cytochrome *bd-II* in an *E. coli* 'EcoM4' strain that lacked all respiratory oxidases. The strains were successfully engineered with a CO difference spectral analysis showing peaks at 640 nm. Further genetic work introduced amino acid mutations to the quinol site of *E. coli* cytochrome *bd-I* to perform future studies on antibiotic resistance. Of five amino acids that were mutated,

only strains harbouring mutations in residues F269A and L253A were able to grow. Interestingly, spectral analysis revealed a distinctive peak at 640 nm for strain harbouring F269A mutation which is representative of the assembly of cytochrome *bd-I*. However, strain harbouring L253A mutant did not have any peaks that suggested the assembly of cytochrome *bd-I*.

In this project both *in silico* and *in vitro* microbiological approaches were used to search for novel inhibitors of cytochrome *bd*. Initially, reductive approaches were undertaken to test the natural compounds madecassic acid 1 and 2-hydroxy-1,4-naphthoquinone for inhibition of *E. coli* cytochrome *bd-I* and *bo'*. Both compounds were inhibitory to *E. coli* cytochrome *bd-I* and *bo'* but madecassic acid 1 exhibited significantly lower IC₅₀ of $23.62 \pm 7.9 \mu\text{g/mL}$ ($46.80 \pm 15.7 \mu\text{M}$) and $1019 \pm 260 \mu\text{g/mL}$ ($6443 \pm 1644 \mu\text{M}$), respectively. Three derivatives of madecassic acid 1 were further tested to assess whether derivatisation could improve binding of the compound to cytochrome *bd-I*. The addition of an acetoxy group to madecassic acid 2 and 3 have shown to improve binding to cytochrome *bd-I* with significantly lower IC₅₀ of $8.8 \pm 3.5 \mu\text{M}$ ($5.6 \pm 2.2 \mu\text{g/mL}$) and $10.2 \pm 1.1 \mu\text{M}$ ($8 \pm 0.9 \mu\text{g/mL}$), respectively.

A drug repurposing pipeline was set-up to screen a library of FDA-approved drugs for their ability to bind to *E. coli* cytochrome *bd-I*. Steroid compounds (ethinylestradiol, quinestrol and mestranol) were identified within the top hits, and these steroid compounds were docked to the quinol site of *S. aureus* CydA subunit of cytochrome *bd*. Preliminary oxygen consumption experiments with isolated *E. coli* membranes identified ethinylestradiol and quinestrol as inhibitors of *E. coli* cytochrome *bd-I*. Quinestrol was the more potent compound causing inhibition of '*bd-I* only' membranes with an IC₅₀ of $0.2 \pm 0.04 \mu\text{g/mL}$ ($0.5 \pm 0.1 \mu\text{M}$), so this drug was selected for further analyses. Similar oxygen consumption experiments also confirmed quinestrol as an inhibitor of MRSA USA300 cytochrome *bd*. Growth assays showed that quinestrol completely abolished growth of MRSA USA300 WT and single oxidase mutant

strains, while the growth of *E. coli* strains was inhibited with low IC₅₀ values, but complete growth inhibition could not be achieved at higher concentrations of quonestrol. Survival assays demonstrated that quonestrol was lethal to MRSA *bd*-only cells with a median lethal concentration (LC₅₀) of 5.6 ± 0.3 µg/mL (13.7 ± 0.7 µM). However, viability assays showed that *E. coli* was completely resistant to the quonestrol. This study identified novel inhibitors of cytochrome *bd* which will pave the way for future studies on steroid drugs as antimicrobials.

Acknowledgements

I would like to extend my deepest gratitude to all the individuals who assisted me to see this project to completion. Firstly, I want to express my appreciation to my PhD supervisor, Dr Mark Shepherd, for providing me endless support and guidance. Dr Shepherd went above and beyond to ensure that my PhD journey was a success by not only giving me first-class supervision but also aiding me with career development by creating publication and conference opportunities. I also thank my co-supervisor, Prof Neil Kad, for his unwavering support and for delivering useful ideas that were essential for the progression of my research.

An immense thank you to Calum Webster, a past PhD student of the Shepherd lab, for providing me training on how to perform experimental procedures as well as data analysis. Thanks to Dr Gary Robinson for always having an open office to provide me academic and non-academic support. I would like to acknowledge the University of Kent for providing me hardship grants throughout my studies to assist with maintenance and support to attend conferences.

A huge thanks to my family members and friends that supported my PhD journey in numerous ways that I cannot account for. The main person is my father, Samuel Henry, who immensely assisted with my maintenance which allowed me to live comfortably whilst completing my studies. I also want to thank my sister in America, Tracy-Ann Young; my fiancé, Samson Akhigbe; my friend, Georgia Bennett; and my grandmother, Pancheta Golding, for always being present when I needed emotional support.

Finally, I would like to share my favourite quote that kept me going throughout the hardest times on this four-year journey, “It doesn't matter who you are, where you come from. The ability to triumph begins with you - always.” – Oprah Winfrey.

Presentations and Publications

Publications:

Henry, S. A., Webster, C. M., Shaw, L. N., Torres, N. J., Jobson, M-E., Totzke, B. C., Jackson, J. J., McGreig, J. E., Wass, M. N., Robinson, G.K. and Shepherd, M. (2024) Steroid drugs inhibit bacterial respiratory oxidases and are lethal towards methicillin-resistant *Staphylococcus aureus*. *Journal of Infectious Diseases*. Oxford University Press.

<https://doi.org/10.1093/infdis/jiad540>

Hilton, K. L. F., Karamalegkos, A. A., Allen, N., Gwynne, L., Streater, B., White, L. J., Baker, K. B., Henry, S. A., Williams, G. T., Shepherd, H. J., Shepherd, M., Hind, C. K., Sutton, M. J., Jenkins, T. A., Mulvihill, D. P., Tullet, J. M. A., Ezcurra, M., & Hiscock, J. R. (2023). Controlling the structure of supramolecular fibre formation for benzothiazole based hydrogels with antimicrobial activity against methicillin resistant *Staphylococcus aureus*. *Journal of Materials Chemistry. B*, <https://doi.org/10.1039/d3tb00461a>

Rutkauskaite, A., White, L. J., Boles, J. E., Hilton, K. L., Clifford, M., Patenall, B., Streater, B. R., Mulvihill, D. P., Henry, S. A., Shepherd, M., Sutton, J. M., Hind, C. K., & Hiscock, J. R. (2023). Adamantane appended antimicrobial supramolecular self-associating amphiphiles. *Supramolecular Chemistry*, 1–10. <https://doi.org/10.1080/10610278.2022.2161902>

Presentations and Awards:

Postgraduate Research Festival (Awarded Best Presentation Talk)

Presentation title: Drug repurposing approaches to target a bacterial respiratory complex: *Cytochrome bd*

20th July 2023, University of Kent

The Tetrapyrrole Discussion Group Meeting (Awarded Best Presentation Talk)

26th – 27th April 2023, Kent, England

Presentation title: Drug repurposing approaches to target a bacterial respiratory complex: *Cytochrome bd*

International Conference on Oxygen Binding and Sensing Proteins (Poster Presentation)

Sept 6th – 9th 2022, Rome, Italy

Presentation title: Drug repurposing approaches to target a bacterial respiratory complex:
Cytochrome bd

The Microbiology Society Annual Conference (Poster Presentation)

4th – 7th April 2022, Belfast, Northern Ireland

Presentation title: Drug repurposing approaches to target a bacterial respiratory complex:
Cytochrome bd

Abbreviations

AMR	Antimicrobial Resistance
CIO	Cyanide Insensitive Oxidases
ETC	Electron Transport Chain
FAD	Flavin Adenine Dinucleotide
FDA	Food and Drug Administrative
FMN	Flavin Mononucleotide
GBS	Group B Streptococcus
MRSA	Methicillin-resistant <i>S. aureus</i>
NO	Nitric Oxide
OD ₆₀₀	Optical density at 600nm
PCR	Polymerase Chain Reaction
PDB	Protein Data Bank
PMF	Proton Motive Force
REDOX	Oxidation-Reduction
ROS	Reactive Oxygen Species
RPM	Revolutions Per Minute
RNS	Reactive Nitrogen Species
SOB	Sugar Optimal Broth
SOC	Super Optimal Broth with Catabolite Repression
TSB	Tryptone Soy Broth
TTFA	2-thenoyltrifluoroacetone
UPEC	Uropathogenic <i>E. coli</i>
UQ	Ubiquinone
UTI	Urinary Tract Infection

Table of Contents

Declaration.....	2
Abstract.....	3
Acknowledgements.....	6
Presentations and Publications.....	7
Abbreviations.....	9
Table of Contents.....	10
List of Figures.....	15
List of Tables.....	18
Supplementary Data.....	19
Chapter 1.....	20
Introduction.....	21
1.1. Antibiotics: Past, Present and Future.....	21
1.1.1. History of Antibiotics.....	21
1.1.2. Antibiotic Resistance: A Global Health Threat.....	22
1.1.2.1. AMR Occurrence.....	22
1.1.2.2. Examples of Mechanisms.....	24
1.1.2.3. The Future of Antibiotics.....	25
1.2. Respiratory Chains.....	26
1.2.1. Overview of Respiratory Chains.....	26
1.2.2. <i>E. coli</i> Electron Transport Chain compared to other Bacteria.....	28
1.2.3. Cytochrome Oxidase Families.....	29
1.3. <i>E. coli</i> Terminal Oxidases.....	30
1.3.1. <i>E. coli</i> Cytochrome <i>bo'</i>	30
1.3.2. <i>E. coli</i> <i>bd</i> -type oxidases.....	30
1.3.2.1. <i>E. coli</i> cytochrome <i>bd</i> -I.....	31
1.3.2.2. <i>E. coli</i> cytochrome <i>bd</i> -II.....	36
1.4. Physiological Functions of <i>E. coli</i> Cytochrome <i>bd</i>	37
1.4.1. Oxygen-reactive Oxidase in Anaerobes.....	37
1.4.2. Oxygen-scavenging role for Cytochrome <i>bd</i>	37
1.5. <i>S. aureus</i> Aerobic Respiratory Chain.....	38
1.6. Cytochrome <i>bd</i> and effects on environmental stressors.....	39
1.7. Cytochrome <i>bd</i> oxidase as a drug target.....	42
1.7.1. Cytochrome <i>bd</i> is a good drug target.....	42
1.7.2. <i>Bd</i> -type Oxidases as a Drug Target in various Bacteria.....	43
1.7.2.1. Uropathogenic <i>E. coli</i> (UPEC).....	44
1.7.2.2. Group B Streptococcus.....	44

1.7.2.3. <i>Mycobacterium tuberculosis</i>	45
1.8. Known Inhibitors of Cytochrome <i>bd</i>	45
1.9. Aims of Study.....	48
Chapter 2.....	50
Materials and Methods.....	51
2.1. Bacterial Strains and Growth Conditions.....	51
2.1.1. Bacterial Strains.....	52
2.1.2. Bacterial Plasmids.....	52
2.1.3. Oligonucleotides.....	53
2.1.4. Chemicals and Water.....	56
2.1.5. Media and Buffer Solutions.....	56
2.1.5.1. Luria-Bertani (LB) Medium.....	56
2.1.5.2. M9 Minimal Medium.....	56
2.1.5.3. Tryptic Soy Broth (TSB) Medium.....	56
2.1.5.4. Super Optimal Broth (SOB) Medium.....	57
2.1.5.5. Super Optimal Broth with Catabolite Repression (SOC).....	57
2.1.5.6. Tris/HCl buffer.....	57
2.1.5.7. Sonication Buffer.....	57
2.1.5.8. Tris-acetate-EDTA (TAE) Buffer.....	57
2.1.5.9. Phosphate-buffered Saline (PBS).....	58
2.1.5.10. Succinate.....	58
2.1.5.11. HEPES (4-(2-hydroxyethyl)-1-piperazineethanesulfonic acid) Buffer.....	58
2.1.5.12. Glycerol Stocks.....	58
2.1.6. Antibiotics.....	58
2.1.7. Drugs Tested.....	59
2.2. Bacterial Assays.....	59
2.2.1. Growth Conditions.....	59
2.2.2. Optical Density Readings.....	60
2.2.3. CO Difference and Reduced <i>minus</i> Oxidised Spectra.....	60
2.2.4. Membrane Preparation.....	61
2.2.5. Oxygen Consumption Assays and Drug Screen.....	62
2.2.6. Succinate-dehydrogenase Assays.....	62
2.2.7. Growth Curves.....	63
2.2.8. Plate Reader Assays.....	63
2.2.9. Viability Assays.....	64
2.2.10. Data Analysis.....	65
2.3. Genetic Methods.....	65
2.3.1. Isolation of DNA plasmid.....	65
2.3.2. Polymerase Chain Reaction (PCR).....	65
2.3.3. DNA Purification.....	65
2.3.4. Agarose Gel Electrophoresis.....	65
2.3.5. Cloning of <i>E. coli</i> cytochrome <i>bd</i> -II oxidase using Gibson Assembly....	66
2.3.5.1. PCR Reactions to Amplify Cytochrome <i>bd</i> -II Oxidase and Vector Backbone.....	66

2.3.5.2. Gibson Assembly.....	66
2.3.5.3. Screening PCR to identify pSU2718G_ <i>appCBX</i>	67
2.3.5.4. Isolation of pSU2718G_ <i>appCBX</i> plasmid	67
2.3.6. Expression of recombinant cytochrome <i>bd</i> complexes in oxidase null mutant.....	67
2.3.6.1. Preparation of <i>E. coli</i> chemically competent cells.....	67
2.3.6.2. Transformation of cytochrome <i>bd</i> complexes into <i>E. coli</i> chemically competent cells.....	68
2.3.6.3. Restriction Enzyme Digest.....	68
2.3.7. Site-directed Mutagenesis of <i>E. coli</i> Cytochrome <i>bd</i> -I Operon	69
2.3.7.1. DNA Plasmid Isolation.....	69
2.3.7.2. Restriction enzyme digest to quantify plasmid.....	69
2.3.7.3. Q5 Site-directed Mutagenesis.....	69
2.3.7.4. Transformation of <i>E. coli</i> cytochrome <i>bd</i> -I plasmid into competent cells.....	69
2.3.7.5. Restriction digest to identify mutation of interest.....	70
2.4. <i>In silico</i> Methods.....	70
2.4.1. Structural Modelling.....	70
2.4.2. Analysis of Ligands.....	71
2.4.3. Molecular Docking.....	71
2.4.4. Analysis of Molecular Docking.....	72
Chapter 3.....	73
Engineering and characterisation of <i>E. coli</i> strains that express single respiratory oxidases.....	74
3.1. Summary.....	74
3.2. Introduction.....	75
3.2.1. Antimicrobial Resistance of UPEC.....	75
3.3. Results.....	77
3.3.1. Determining the growth and spectral properties for <i>E. coli</i> EC958 WT strains and terminal oxidase mutants.....	77
3.3.2. Spectral analysis of <i>E. coli</i> EC958 cytochrome <i>bd</i> -I only membranes	81
3.3.3. Optimisation of an oxygen consumption assay to assess the inhibition of cytochrome <i>bd</i> activity in purified membranes.....	82
3.3.4. Recombinant expression of terminal oxidases in <i>E. coli</i> strain lacking all terminal respiratory oxidases.....	83
3.3.4.1. CO difference spectra of <i>E. coli</i> MG1655 'EcoM4' strain lacking all terminal respiratory oxidases.....	83
3.3.4.2. Cloning and transformation of cytochrome <i>bd</i> -II plasmid to construct <i>bd</i> -II only recombinant strain in <i>E. coli</i> MG1655 'EcoM4'..	87
3.3.4.3. Restriction digest to confirm cytochrome <i>bd</i> -II plasmid in newly expressed <i>E. coli</i> recombinant strain.....	88
3.3.4.4. Growth and spectral properties of newly expressed recombinant strains expressing <i>E. coli</i> cytochrome <i>bd</i> -I and <i>bd</i> -II oxidases.....	90
3.3.4.5. Oxygen consumption assay of recombinant strain expressing <i>E.</i>	

<i>coli</i> EC958 cytochrome <i>bd</i> -II only recombinant strain with TTFA....	93
3.3.5. Development of quinol site mutants to investigate drug resistance...	94
3.3.5.1. Identifying important residues for mutation.....	94
3.3.5.2. Residues F269A and L253A were successfully mutated.....	96
3.3.5.3. F269A mutant led to oxygen consumption in purified membranes.....	99
3.4. Discussion.....	102
3.4.1. Characterisation of <i>E. coli</i> EC958 cytochrome <i>bd</i> -I WT and mutant Strains.....	102
3.4.2. Designing experimental tools to repurpose drugs that target cytochrome <i>bd</i> oxidases.....	103
3.4.3. Development of quinol site mutants to investigate drug resistance....	104
3.4.4. Future Studies.....	105
Chapter 4.....	107
Assessing known antimicrobials as inhibitors of cytochrome <i>bd</i>	102
4.1. Summary.....	108
4.2. Introduction.....	109
4.2.1. Madecassic Acid, Atovaquone and 1,4-Naphthoquinone as potential quinol site targets of <i>E. coli</i> Cytochrome <i>bd</i> -I.....	109
4.3. Results.....	111
4.3.1. Docking of known antimicrobials to the AlphaFold 2 models of <i>E. coli</i> cytochrome <i>bd</i> -I and cytochrome <i>bo'</i>	111
4.3.2. Investigation of Drug Efficacy/Specificity.....	114
4.3.2.1. Preliminary investigation of Atovaquone's efficacy/specificity..	114
4.3.2.2. Oxygen consumption assays of madecassic acid 1 and 2- hydroxy-1,4-naphthoquinone against <i>E. coli</i> EC958 cytochrome <i>bd</i> -I and <i>bo'</i> -only membranes.....	115
4.3.2.3. Growth and Survival Assays of Madecassic Acid 1 and 2- hydroxy-1,4-naphthoquinone against <i>E. coli</i> WT, cytochrome <i>bd</i> -I only and cytochrome <i>bo'</i> -only cells.....	117
4.3.3. Assessing derivatives of madecassic acid 1 as <i>E. coli</i> cytochrome <i>bd</i> -I Inhibitors.....	124
4.3.3.1. <i>In silico</i> analysis of madecassic acid 1 derivatives.....	124
4.3.3.2. Oxygen Consumption, Growth and Lethality of Madecassic Acid derivatives against <i>E. coli</i> EC958 cytochrome <i>bd</i> -I only cells...	126
4.4. Discussion.....	132
4.4.1. Development of <i>in silico</i> and experimental tools to identify new potential inhibitors of cytochrome <i>bd</i> -I.....	132
4.4.2. Known antimicrobials as inhibitors of cytochrome <i>bd</i>	133
4.4.3. Derivatisation enhances inhibitory activity of madecassic acid against <i>E. coli</i> EC958 cytochrome <i>bd</i> -I.....	135
Chapter 5	137
Drug screening approaches to identify novel inhibitors of cytochrome <i>bd</i>	137
5.1. Summary.....	138
5.2. Introduction.....	139

5.2.1. Drug Repurposing Progresses and Challenges.....	139
5.2.2. Approaches for Drug Repurposing	141
5.3. Results.....	143
5.3.1. <i>In silico</i> drug screen identified FDA-approved steroid drugs as potential inhibitors of cytochrome <i>bd</i>	143
5.3.2. <i>In vitro</i> approaches to confirm FDA-approved steroid drugs as inhibitors of cytochrome <i>bd</i>	148
5.3.2.1. FDA-approved steroid drugs inhibit oxygen consumption activity in <i>E. coli</i> EC958 <i>bd</i> -I only membranes and MRSA ‘ <i>bd</i> -only’ membranes..	148
5.3.2.2. Kinetic assays confirm that quinestrol does not inhibit succinate dehydrogenase activity in <i>E. coli</i> EC958 <i>bd</i> - I only membranes.....	152
5.3.2.3. Growth assays demonstrate that quinestrol inhibits the growth of bacterial cells expressing only cytochrome <i>bd</i> as their terminal respiratory	
5.3.2.4. Development of a PEG quinestrol derivative.....	158
5.4. Discussion.....	161
5.4.1. Pharmacology of FDA-approved steroid drugs.....	161
5.4.2. Novel inhibitors of cytochrome <i>bd</i>	152
5.4.3. Derivatisation improves mode of binding of quinestrol	164
5.4.4. Quinestrol as a novel inhibitor of cytochrome <i>bd</i>	164
5.4.6. Future Work.....	165
Chapter 6.....	166
Final Discussion.....	166
6.1. Background.....	167
6.2. Conclusions.....	169
6.2.1. Engineering and characterisation of <i>E. coli</i> strains that express single respiratory oxidases.....	162
6.2.2. Cytochrome <i>bd</i> as a modern drug target.....	170
6.2.3. Drug screening approaches to identify novel inhibitors of cytochrome <i>bd</i>	
.....	171
6.3. Future Work.....	173
References.....	175
Appendix.....	192

List of Figures

Figure 1.1. Antibiotic discovery and resistance timeline.....	22
Figure 1.2. The layout and function of <i>CydABXH</i> in the electron transport chain of <i>E. coli</i>	32
Figure 1.3. Cryo-EM structure of cytochrome <i>bd-I</i> oxidase from <i>E. coli</i>	35
Figure 1.4. Proposed MRSA aerobic respiratory chain.....	39
Figure 1.5. The functions of cytochrome <i>bd</i> oxidases.....	42
Figure 2.1. SDB4 Spectrophotometer.....	61
Figure 2.2. Oxygen Electrode Apparatus.....	62
Figure 2.3. Molecular Docking Pipeline.....	72
Figure 3.1 Aerobic growth curves for <i>E. coli</i> WT, <i>bd-I</i> and <i>bo'</i> -only cells.....	77
Figure 3.2 CO difference whole cell spectra of WT, <i>bd-I</i> only and <i>bo'</i> -only.....	79
Figure 3.3. Reduced <i>minus</i> oxidised whole cell spectra of WT, <i>bd-I</i> only and <i>bo'</i> -only.....	80
Figure 3.4. Difference spectra of <i>E. coli</i> EC958 cytochrome <i>bd-I</i> only membranes.....	81
Figure 3.5. Oxygen consumption assay of <i>E. coli</i> EC958 cytochrome <i>bd-I</i> membranes with TTFA.....	83
Figure 3.6. CO difference spectra of <i>E. coli</i> MG1655 'EcoM4' strain lacking all oxidases	84
Figure 3.7. Plasmid map of <i>E. coli</i> cytochrome <i>bd-I</i> plasmid with 6*His tag.....	86
Figure 3.8. Transformation of <i>E. coli</i> cytochrome <i>bd-I</i> plasmid with <i>E. coli</i> MG1655 'EcoM4' strain lacking all terminal respiratory oxidases.....	86
Figure 3.9. Screening PCR for confirming the cloning of <i>E. coli</i> cytochrome <i>bd-II</i> plasmid	88
Figure 3.10. Plasmid map of <i>E. coli</i> cytochrome <i>bd-II</i> plasmid.....	89
Figure 3.11. Restriction digest to confirm <i>E. coli</i> cytochrome <i>bd</i> plasmids in strains.....	90
Figure 3.12. Aerobic growth curves for recombinant strains.....	92
Figure 3.13. CO Difference spectral analysis of membranes isolated from recombinant strains expressing either <i>E. coli</i> EC958 <i>bd-I</i> only or <i>bd-II</i> only oxidases.....	93

Figure 3.14. Oxygen consumption assay on membranes of recombinant strain expressing only <i>E. coli</i> cytochrome <i>bd-II</i> with TTFA.....	94
Figure 3.15. Residues of significance in the functioning of the quinol binding site of the <i>cydA</i> subunit of cytochrome <i>bd-I</i>	95
Figure 3.16. Plasmid map and restriction digest for F269A mutagenesis.....	97
Figure 3.17. Plasmid map and restriction digest for L253A mutagenesis.....	97
Figure 3.18. Aerobic growth curves of quinol site mutants F269A and L253A.....	98
Figure 3.19. Whole cell spectra of quinol <i>E. coli</i> cytochrome <i>bd-I</i> quinol site-directed mutants	99
Figure 3.20. Oxygen consumption membrane assay on <i>E. coli</i> cytochrome <i>bd-I</i> quinol site- directed mutants.....	100
Figure 3.21. Oxygen consumption assay for <i>E. coli</i> cytochrome <i>bd-I</i> quinol site mutant (F269A) with TTFA.....	101
Figure 4.1. Pharmacological properties of 1,4-Naphthoquinone, Atovaquone and Madecassic Acid.....	110
Figure 4.2. Docking images of known antimicrobial compounds and ubiquinol-8 bound to <i>cydA</i> of <i>E. coli</i> cytochrome <i>bd-I</i>	113
Figure 4.3. Docking images of known antimicrobial compounds and ubiquinol-8 bound to subunit 1 of <i>E. coli</i> cytochrome <i>bo'</i>	114
Figure 4.4. Oxygen consumption assay of <i>E. coli</i> EC958 cytochrome <i>bd-I</i> and cytochrome <i>bo'</i> only membranes against atovaquone.....	115
Figure 4.5. Dose inhibition curves of madecassic acid 1 and 2-hydroxy-1,4-naphthoquinone activities against <i>E. coli</i> EC958 cytochrome <i>bd-I</i> only membranes.....	116
Figure 4.6. Dose inhibition curves of madecassic acid 1 and 2-hydroxy-1,4-naphthoquinone activities against <i>E. coli</i> EC958 cytochrome <i>bo'</i> -only membranes.....	117
Figure 4.7. Growth Assays of 2-hydroxy-1,4-naphthoquinone against <i>E. coli</i> EC958 WT, cytochrome <i>bd-I</i> only and cytochrome <i>bo'</i> -only cells.....	119
Figure 4.8. Growth Assays of madecassic acid 1 against <i>E. coli</i> WT, cytochrome <i>bd-I</i> only and cytochrome <i>bo'</i> -only cells.....	120
Figure 4.9. Viability assays of 2-hydroxy-1,4-naphthoquinone against <i>E. coli</i> EC958 WT, cytochrome <i>bd-I</i> only and cytochrome <i>bo'</i> -only cells.....	122
Figure 4.10. Viability assays of madecassic acid 1 against <i>E. coli</i> EC958 WT, cytochrome <i>bd-I</i> only and cytochrome <i>bo'</i> -only cells.....	123

Figure 4.11. Madecassic acid derivatives docked to <i>E. coli</i> AlphaFold 2 cytochrome <i>bd-I</i> model.....	126
Figure 4.12. Madecassic acid derivatives inhibit <i>E. coli</i> EC958 cytochrome <i>bd-I</i> only membranes.....	128
Figure 4.13. Madecassic acid derivatives inhibit the growth of <i>E. coli</i> EC958 cytochrome <i>bd-I</i> only cells.....	130
Figure 4.14. Madecassic acid derivatives survival assay on <i>E. coli</i> EC958 cytochrome <i>bd-I</i> only cells.....	131
Figure 5.1. Docking of FDA-approved steroid drugs to the quinol binding site of <i>E. coli</i> cytochrome <i>bd-I</i> AlphaFold2 model.....	147
Figure 5.2. Docking of FDA-approved steroid drugs to the quinol site of <i>S. aureus</i> CydA subunit.....	148
Figure 5.3. FDA-approved steroid drugs inhibit oxygen consumption activity in <i>E. coli</i> EC958 <i>bd-I</i> only membranes.....	150
Figure 5.4. Quinestrol inhibits <i>E. coli</i> cytochrome <i>bd-II</i>	151
Figure 5.5. Quinestrol inhibits oxygen consumption activity of MRSA USA300 ‘ <i>bd-only</i> ’ membranes.....	152
Figure 5.6. Succinate dehydrogenase (SDH) <i>E. coli</i> <i>bd-I</i> only membrane assay with quinestrol and ethinylestradiol.....	153
Figure 5.7. Quinestrol inhibits the growth of <i>E. coli</i> EC958 cells.....	155
Figure 5.8. Quinestrol inhibits the growth of MRSA USA300.....	156
Figure 5.9. Quinestrol kills MRSA cells but not <i>E. coli</i>	158
Figure 5.10. PEG quinestrol derivative.....	159
Figure 5.11. ¹ H NMR of the quinestrol PEG derivative and the original quinestrol compound	160
Figure 5.12. Quinestrol derivative inhibits oxygen consumption activity in <i>E. coli</i> <i>bd-I</i> only membranes.....	160
Figure 6.1. Summary of <i>in silico</i> and <i>in vitro</i> drug screening pipeline.....	168

List of Tables

Table. 1.1. Compounds with inhibitory effects on the respiratory activity of cytochrome <i>bd</i>	48
Table. 2.1. List of Bacterial Strains.....	51
Table 2.2. Bacterial Plasmids.....	52
Table 2.3. List of Oligonucleotides.....	53
Table 2.4. List of Antibiotics.....	58
Table 2.5. List of Drugs Tested.....	59
Table 3.1. Prevalence of antibiotic resistance in developed and developing countries.....	76
Table 4.1. Docking of known antimicrobials to the ubiquinol sites in CydA of <i>E. coli</i> cytochrome <i>bd</i> -I and subunit 1 of <i>E. coli</i> cytochrome <i>bo'</i>	112
Table 4.2. Madecassic acid derivatives structures and predicted binding affinities.....	125
Table 5.1. Modern drug repurposing approaches compared to de novo drug discovery.....	140
Table 5.2. Top 70 potential <i>E. coli</i> cytochrome <i>bd</i> -I inhibitors ranked by predicted affinity to the quinol binding site of the AlphaFold 2 modelled structure.....	146
Table 5.3. FDA-approved steroid compounds and their binding affinities to the quinol binding site of <i>E. coli</i> cytochrome <i>bd</i> -I.....	146
Table 5.4. FDA-approved steroid compounds and their binding affinities to the quinol binding site of <i>S. aureus</i>	147

Supplementary Data

Appendix A.1. Raw traces of oxygen consumption TTFA assay with <i>E. coli</i> cytochrome <i>bd</i> -I only membranes.....	193
Appendix A.2. Sequence alignment to identify conservation of amino acid residues in mutagenesis study.....	194
Appendix A.3. Raw traces of <i>E. coli</i> ‘ <i>bd</i> -only’ growth curves in the presence of quineestrol	200
Appendix A.4. Solubility assay for quineestrol against <i>E. coli</i> cells.....	201

Chapter 1

Introduction

1. Introduction

1.1. Antibiotics: Past, Present and Future

1.1.1. History of Antibiotics

Antibiotics are one of the greatest medical discoveries that caused a major difference in clinical science. Prior to the discovery of antibiotics during the 20th century, now treatable conditions such as pneumonia and diarrhoea were the leading cause of deaths globally. In addition, antibiotics allowed other medical procedures to be performed successfully such as organ transplants and cancer treatment (Hutchings, Truman and Wilkinson 2019). Microbes capable of producing antibiotics dates back to 1550 BC where bread containing mould as well as soil were used by the Eber's papyrus to treat open wounds (Haas, 1999). It was the accidental discovery of penicillin in 1928 by Sir Alexander Fleming that marked the beginning of the antibiotic revolution and the first development of an antibacterial drug (Adedeji, 2016).

The golden age of antibiotic discovery resulted in the development of many antibiotics between the 1950s and 1970s (Adedeji 2016; Hutchings, Truman and Wilkinson 2019). This era introduced many antibiotic classes including glycopeptides, quinolones, and macrolides (Figure 1.1). Classes of antibiotics were produced from actinomycetes (e.g., macrolides), fungi (e.g., penicillin's), other bacteria (e.g., polypeptides) and some were synthetically made (e.g., phenazines) (Hutchings, Truman and Wilkinson 2019). Following the golden era, a huge decrease in antibiotic discovery was seen and by the 1980s, the last class of antibiotic known as daptomycin was discovered (Durand, Raoult and Dubourg 2019). The achievements of the antibiotic era have been threatened by antibiotic resistance which have led to bacteria becoming resistant to many antibiotics that were once potent (Figure 1.1). Between 2000 to 2010, it was reported that antibiotic use was increased by over 65% globally (Walsh *et al.* 2023). By 2015,

antimicrobial resistance (AMR) was declared a global health threat, and an action plan was put in place by the World Health Organization to combat this (Walsh *et al.* 2023).

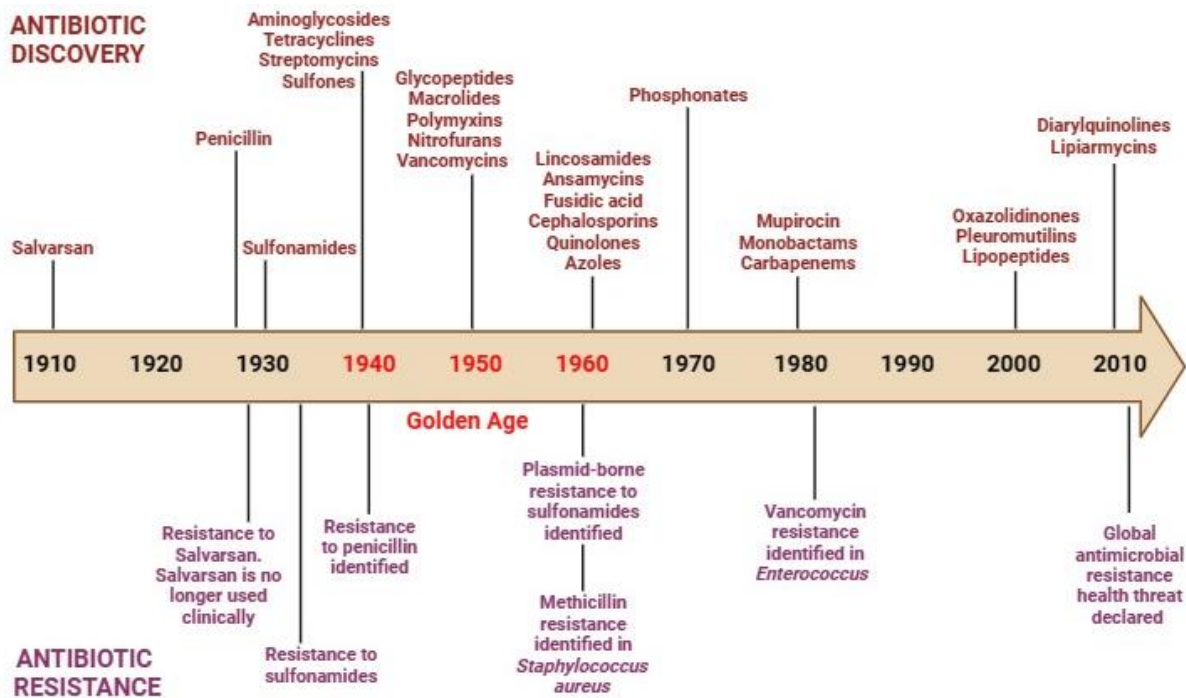


Figure 1.1. Antibiotic discovery and resistance timeline. Timeline showing the rich history of antibiotic discovery and resistance of chosen antibiotics (Hutchings, Truman and Wilkinson 2019).

1.1.2. Antibiotic Resistance: A Global Health Threat

1.1.2.1. AMR Occurrence

AMR is a global health emergency that was declared as one of the top ten global health threats that affects humans (World Health Organization, 2021). It was estimated that 1.2 million deaths in 2019 were caused by bacterial antimicrobial resistance (Murray *et al.* 2022) and will result in an estimated 10 million deaths yearly by 2050 if not resolved (Pulingam *et al.* 2022). Despite AMR being a natural phenomenon, its occurrence is accelerated heavily by the misuse of antibiotics. Hospitals are one of the primary sites for antimicrobial-resistant bacteria which emphasises the need for practicing good hygiene and the appropriate

administration of antimicrobial prescriptions. The UK government had introduced a monetary incentive in a scheme called the Quality Premium scheme aimed at rewarding general practitioners for reducing the administration of antimicrobials to patients inappropriately (EClinicalMedicine, 2021).

AMR is the umbrella term that describes resistance to drugs by microbes such as bacteria, virus, fungi and other pathogens. Alternatively, antibiotic resistance refers specifically to the ability of bacteria to evade the antibacterial actions of antibiotics that they were once sensitive to (Pulingam *et al.* 2022). The first notable sign of antibiotic resistance was in 1940 when Abraham and Chain reported that an *E. coli* strain had produced penicillinase which inactivated penicillin (Lobanovska and Pilla, 2017). By 1942, penicillin resistance was officially documented when four *S. aureus* strains demonstrated resistance to penicillin after being administered to patients in a hospital (Rammelkamp and Maxon, 1942; Lobanovska and Pilla, 2017).

The mechanisms of AMR and antibiotic resistance are similar and allow the microbe to evade the antimicrobial properties of a drug. All mechanisms of antibiotic resistance fall under intrinsic resistance where the resistance was always expressed in the species or acquired resistance where resistance is developed after exposure to antibiotics (Reygaert, 2018). Acquired resistance are transferred via horizontal gene transfer and occur via routes of either transduction, transformation or conjugation (Hasegawa *et al.* 2018). Transduction and conjugation involve the transfer of DNA from a donor to recipient. Conjugation features the use of conjugative pili while transduction utilises phage virions (Hasegawa *et al.* 2018). Transformation occurs when the recipient cell takes up DNA extracellularly from the environment (Hasegawa *et al.* 2018). Intrinsic and acquired mechanisms of antibiotic resistance mainly fall under these categories: (i) modification of the antibiotic compound; (ii) the production of enzymes capable of chemically altering the antibiotic; (iii) through direct

destruction of the antibiotic and (iv) through decreased antibiotic penetration and efflux (Munita and Arias, 2016).

1.1.2.2. Examples of Mechanisms

Over the past decades, bacteria have developed a high level of resistance to some of the most clinically used antibiotics. β -lactams antibiotic group was the first to be discovered and include highly effective antibiotics such as penicillin and cephalosporin (Mora-Ochomogo and Lohans, 2021). In fact, β -lactams are ranked as the most used antibiotics globally (Mora-Ochomogo and Lohans, 2021). β -lactams mode of action is via the inhibition of bacterial transpeptidases that are involved in the synthesis of peptidoglycan (Oelschlaeger, 2021). This leads to the inhibition of bacterial growth, consequently resulting in the lysis of bacteria (Oelschlaeger, 2021). However, bacteria have developed ways of resisting β -lactam antibiotics via the production of serine β -lactamase enzymes (Mora-Ochomogo and Lohans, 2021). The production of β -lactamase enzymes by bacteria hydrolyses the β -lactam ring which leads to the inactivation the drug (Bush and Bradford, 2016).

Aminoglycosides is a broad-spectrum group of antibiotics which are used in the treatment of several Gram-negative and some Gram-positive infections (Garneau-Tsodikova and Labby, 2016). Most importantly, aminoglycosides are used in the treatment of multidrug-resistant tuberculosis infections (Garneau-Tsodikova and Labby, 2016). Antibiotics found within this group include streptomycin and gentamicin (Garneau-Tsodikova and Labby, 2016). Aminoglycosides exert their mode of action via the inhibition of bacterial ribosomes which inhibits protein translation (Garneau-Tsodikova and Labby, 2016). The mechanisms of bacterial resistance to aminoglycosides are varied and occur via: (i) inactivation of aminoglycosides by aminoglycoside-modifying enzymes; (ii) removal by drug efflux pumps; (iii) decreased uptake or (iv) alterations to the target site that prevents binding (Bonomo, 2014).

Fluoroquinolones are synthetically derived antibiotics that have been used in the treatment of several antibiotic-resistant infections since the 1980s (Redgrave *et al.* 2014). This broad-spectrum group of antibiotics includes antibiotics such as ciprofloxacin and levofloxacin. Fluoroquinolones inhibit bacterial activity by inhibiting DNA gyrase and topoisomerase enzymes which are vital for bacterial DNA replication (Redgrave *et al.* 2014). The main mechanism of fluoroquinolone resistance is target-site mutation to DNA gyrase and topoisomerase enzymes (Redgrave *et al.* 2014). Mutations occur at the quinolone resistance-determining region also known as the short DNA sequence, resulting in amino acid substitutions and alteration of the target protein structure (Redgrave *et al.* 2014).

1.1.2.3. The Future of Antibiotics

Since the 1980s, no new classes of clinically-used antibiotics have been discovered while many bacteria are growing resistant to already-discovered antibiotics (Hutchings, Truman and Wilkinson 2019). However, many terrestrial environments have not been sampled or studied which highlights opportunities to discover new soil bacteria that produce antibiotics (Hutchings, Truman and Wilkinson 2019). Also, improved accessibility to marine environments has led to the discovery of natural products capable of producing new clinical antimicrobials. Sequencing approaches have been successful in locating multiple natural products biosynthetic gene clusters across bacteria phyla such as Actinobacteria (Donia *et al.* 2014). Lugdunin, an antibacterial compound extracted from nasal *Staphylococcus lugdunensis*, 2016, is under investigation and is active in animal models (Zipperer *et al.* 2016).

Up to December 2020, it had been reported that there were 43 antibiotics in phases 1, 2 and 3 of clinical trials or pending approval (Cook and Wright 2022). The future of antibiotics is heavily dependent on the discovery of new approaches which might be different to conventional methods. *In silico* drug development pipelines are at the forefront of drug

discovery due to their ability to accelerate the process and reduce costs, time, and effort (Shaker *et al.* 2021). This is also applicable to drug repurposing approaches as *in silico* pipelines which allow researchers to screen for multiple drug candidates at once. Indeed, this thesis describes *in silico* approaches to find new inhibitors of cytochrome *bd* from a library of FDA-approved drugs.

1.2. Respiratory Chains

1.2.1. Overview of Respiratory Chains

Respiration involves a sequence of coupled oxidation and reduction reactions that facilitate the transfer of electrons from an electron donor to an electron acceptor (Kelly, Hughes and Poole, 2014). There are two types of respiration: aerobic and anaerobic respiration. Aerobic respiration involves a final electron transfer to oxygen which reduces water and generates a proton electrochemical gradient (Kelly, Hughes and Poole, 2014). Anaerobic respiration involves a final electron transfer to a molecule other than oxygen (Kelly, Hughes and Poole, 2014). Both aerobic and anaerobic respiration provide energy for an organism in the form of adenosine triphosphate (ATP) through conversion of the proton electrochemical gradient by ATP synthase (Kelly, Hughes and Poole, 2014).

Respiratory chain is also referred to as an electron transport chain (ETC). There are a series of proteins located in the ETC that facilitate the transfer of electrons. The ETCs of eukaryotes are located in the inner mitochondrial membrane. However, the ETC of photosynthetic eukaryotes are found on the thylakoid membrane. In eukaryotic organisms, the proteins in an ETC are generally ordered as such: complex I (ubiquinone oxidoreductase), complex II (succinate dehydrogenase), coenzyme Q (ubiquinone [CoQ]), complex III (cytochrome c reductase), cytochrome C, and complex IV (cytochrome c oxidase) (Ahmad, Wolberg and Kahwaji, 2023). Complex I comprises of NADH dehydrogenase, flavin

mononucleotide and iron sulphur clusters (Ahmad, Wolberg and Kahwaji, 2023). NADH donated from glycolysis and citric acid cycle succumbs to oxidation, subsequently passing two electrons to flavin mononucleotide (FMN) (Ahmad, Wolberg and Kahwaji, 2023). These electrons are then shuttled to the iron sulphur clusters and finally to coenzyme Q. In complex II, succinate is oxidised into fumarate and flavin adenine dinucleotide (FAD) accepts two electrons. FAD shuttles these electrons to iron sulphur clusters and then to coenzyme Q (Ahmad, Wolberg and Kahwaji, 2023). Coenzyme Q's main function is to shuttle electrons to complex III (Ahmad, Wolberg and Kahwaji, 2023). In the Q cycle (quinol cycle), coenzyme Q is reduced to semiquinone and ubiquinol (Ahmad, Wolberg and Kahwaji, 2023). Complex III comprises of cytochrome *b*, cytochrome *c* proteins and Rieske subunits (Ahmad, Wolberg and Kahwaji, 2023). Cytochromes contain haem groups which alternate between ferrous and ferric forms during electron transfer (Ahmad, Wolberg and Kahwaji, 2023). Cytochrome *c* can only accept one electron at a time, so this process occurs twice which forms the Q cycle (Ahmad, Wolberg and Kahwaji, 2023). At the end of the Q cycle, complex III releases four protons which largely contributes to the formation of a proton electrochemical gradient (Ahmad, Wolberg and Kahwaji, 2023). Cytochrome *c* shuttles the electrons to complex IV which oxidises cytochrome *c* and transfers the electrons to oxygen, the final electron acceptor in aerobic respiration (Ahmad, Wolberg and Kahwaji, 2023).

Embedded in the plasma membrane, the ETC of prokaryotes vary among different species but generally involves a series of redox reactions between membrane embedded proteins that lead to the generation of an electrochemical gradient and oxidative phosphorylation (Kracke, Vassilev and Krömer, 2015). Prokaryotic ETCs consist of numerous electron donors and acceptors (Kaila and Wikström, 2021). There are three levels at which electrons can enter a prokaryotic ETC: dehydrogenase level, quinone pool, or at the cytochrome electron carrier level (Kaila and Wikström, 2021). In bacteria, numerous dehydrogenases,

oxidases, reductases and electron donors can be used to start a reaction. In bacteria, for example, NADH or succinate can be used as an electron source which would start the reaction at NADH dehydrogenase or succinate dehydrogenase, respectively (Kaila and Wikström, 2021). Though NADH is comparable to mitochondrial complex I and succinate dehydrogenase is comparable to mitochondrial complex II, the terminologies of ‘complexes’ are not generally used to describe the proteins found in prokaryotic ETCs.

1.2.2. *E. coli* Electron Transport Chain compared to other Bacteria

A major difference between the structure and function of bacterial respiratory chains is how they are branched. *E. coli* falls into a group of bacteria that oxidises reduced electron carriers and transfer these electrons directly to the quinone pool (Shepherd and Poole, 2013). These reduced quinones are then oxidised by terminal oxidoreductases (Soballe and Poole, 1999). Other bacteria, such as the genus *Paracoccus*, express cytochrome *bc*₁ complexes, which cause further branching of the respiratory chain and can involve transfer of electrons to terminal oxidoreductases by periplasmic *c*-type cytochromes (Shepherd and Poole, 2013). All bacteria that have a cytochrome *bc*₁ complex usually contain at least one other ubiquinol oxidase pathway that can bypass the cytochrome *bc*₁ complex (Shepherd and Poole, 2013). It has also been found that having a second respiratory chain in these bacteria may provide some protection against competing microbes that produce toxins that inhibit cytochrome *bc*₁. However, some bacteria such as *E. coli* lack a cytochrome *bc*₁ complex (Shepherd and Poole, 2013).

Though there are distinctive differences between the ETC of *E. coli* and other bacteria, there are some commonalities between both groups. The ETCs of *E. coli* and other bacteria transfer electrons from NADH to various electron acceptors and all bacteria generate a proton gradient across the plasma membrane during an ETC reaction which is comparable to that of

the eukaryotic ETC. However, the ETC branch of *E. coli* is generally shorter than other bacteria and consists of two types of terminal oxidases: cytochrome *bd* (*bd*-I and *bd*-II) and cytochrome *bo'* oxidases (Kaila and Wikström, 2021). On the other hand, some bacteria have longer ETC branches. *Pseudomonas aeruginosa*, for example, has five aerobic terminal oxidases: *bo'*-type oxidase (Cyo), cyanide-insensitive oxidase (CIO), *aa*₃-type cytochrome *c* oxidase (*aa*₃), and two *cbb*₃-type cytochrome *c* oxidases (Arai *et al.*, 2014).

1.2.3. Cytochrome Oxidase Families

The two main classes of bacterial terminal oxidases are haem copper oxidases, or HCOs, (such as cytochrome *bo'*) and quinol oxidoreductases (such as cytochrome *bd*) (Borisov and Siletsky, 2019). HCOs are a superfamily that include cytochrome oxidases of mitochondria from eukaryotes and most aerobic prokaryotes (Hemp and Gennis, 2008). HCOs catalyse electron transfer from quinols to oxygen with the generation of a proton motive force (Siletsky, 2013). HCOs differ to cytochrome *bd* oxidases because HCOs generate proton motive force via the transfer of electrons and protons to the catalytic centre from various sides of the membrane (Borisov and Siletsky, 2019). The classification of HCOs is mainly based on the organisation of their intraprotein transfer channels that connect the catalytic centre with the cytoplasmic side of the membrane (Borisov and Siletsky, 2019). This classification system further divides HCOs into three subcategories known as the A, B and C families (Borisov and Siletsky, 2019). In contrast to HCOs, *bd*-type oxidases are found in the terminal region of bacterial and archaeal electron transport chains and have not been detected in eukaryotes (Forte *et al.* 2017). In addition, amino acid sequence alignment has been conducted and no homology was observed between HCOs and *bd*-type oxidases (Borisov *et al.* 2011). The most explored cytochrome *bd* oxidase is from *E. coli* (Borisov and Siletsky, 2019). *E. coli* cytochrome *bd* consists of two large subunits which are CydA and CydB (Borisov and Siletsky, 2019). The other two subunits are CydX and the most recently discovered, CydH (Safarian *et al.* 2019).

1.3. *E. coli* Terminal Oxidases

1.3.1. *E. coli* Cytochrome *bo'* oxidase

Cytochrome *bo'* (otherwise called cytochrome *bo*₃) is a member of the heme-copper oxidase family and is encoded by the *cyoABCDE* operon (Chepuri *et al.* 1990; Calhoun, Newton and Gennis 1991; Forte *et al.* 2019). Cytochrome *bo'* is structurally comparable to mammalian cytochrome *c* oxidase (Weiss *et al.* 2009). Cytochrome *bo'* comprises of four subunits and catalyses the oxidation of ubiquinol-8 and the reduction of oxygen to water. Subunits I, II and III are homologues of cytochrome *c* oxidase while the function of subunit IV remains unclear. Subunit I is the largest subunit and contains low-spin heme *b*, high-spin heme *o* and a copper ion (Cu_B) (Sousa *et al.* 2012). Ubiquinol-8 is the natural substrate for *E. coli* cytochrome *bo'* (Li *et al.* 2021). There are two ubiquinol sites present in cytochrome *bo'*: a low affinity site which is the site for binding ubiquinone and a high affinity site involved in stabilisation of semiquinone intermediates during catalysis (Laemmli *et al.* 1991; Weiss *et al.* 2009). The binding of ubiquinone at the low affinity site occurs within subunit II at the periplasmic domain (Sato-Watanabe *et al.* 1994) while subunit I contains the high affinity site (Abramson *et al.* 2000). The expression of cytochrome *bo'* is enhanced when cells are grown under high oxygen conditions (Forte *et al.* 2019), and this complex has a low affinity for oxygen (D'Mello *et al.* 1995; Forte, Siletsky and Borisov 2020). Deoxygenation kinetics revealed the K_m values of cytochrome *bo'* to be 0.43 μ M for oxymyoglobin and 0.026 μ M for oxyleghemoglobin (D'Mello *et al.* 1995).

1.3.2. *E. coli* *bd*-type oxidases

Cytochrome *bd* complexes are respiratory oxidoreductases found exclusively in the inner membrane of prokaryotes, namely bacteria and archaea (Borisov, Gennis, *et al.* 2011). The main function of these '*bd*-type' is to facilitate the reduction of molecular oxygen into

water subsequently conserving energy as a proton motive force used in the production of ATP (Borisov *et al.* 2020). In *E. coli*, there are two types of cytochrome *bd* complexes recognised thus far; cytochrome *bd-I* and cytochrome *bd-II* (Giuffrè *et al.* 2014). *E. coli* cytochrome *bd-I* has a high affinity for oxygen with a K_m of 0.54 μM (D'Mello *et al.* 1996) and is maximally expressed under microaerobic conditions under the control of ArcA and FNR (Fu *et al.* 1991). Cytochrome *bd-II* expression has been shown to be enhanced during phosphate starvation and during the approach to stationary phase (Brøndsted and Atlung 1996).

1.3.2.1. *E. coli* cytochrome *bd-I*

Bd-type oxidases have *d*-type haem groups that are redox-reactive, have no copper atoms present, and protons are translocated across the membrane (Borisov, Gennis, *et al.* 2011). *Bd* oxidases have two other haem groups, haem *b*₅₉₅ and haem *b*₅₅₈ (Figure 1.2) (Borisov *et al.* 2015). All three haem groups are located towards the periplasmic side of the membrane (Safarian *et al.* 2016). Haem *d* binds directly to O₂ and is involved in its four-electron reduction to H₂O while haem *b*₅₅₈ is involved in quinol oxidation. It has been reported that haem *b*₅₉₅ forms a haem-haem binuclear centre with haem *d* subsequently resulting in the reduction of both haems (Mogi *et al.* 2009). Cytochrome *bd-I* of *E. coli* has two major subunits, CydA and CydB, which both consist of 9 transmembrane (TM) helices (Giuffrè *et al.* 2014). They are homologous proteins and the *cydA* and *cydB* genes have emerged due to gene duplication events. *CydA*, *cydB* and *cydX* are all located on the same operon. There is a 4kDa single helix protein known as CydX that is essential for the functioning of *bd-I* oxidase (Vanorsdel *et al.* 2013). In addition, there is a recently identified 3 kDa subunit in *E. coli* *bd-I* oxidase located between TM domains 1 and 9 of CydA known as CydH (Safarian *et al.* 2019). CydH is encoded by a different gene called *ynhF* that is not a part of *cyd* (*bd-I*) nor the *app* (*bd-II*) operon. This

subunit binds the hydrophobic region of CydA and blocks oxygen accessibility to haem *b*₅₉₅ from the hydrophobic lipid bilayer (Safarian *et al.* 2019).

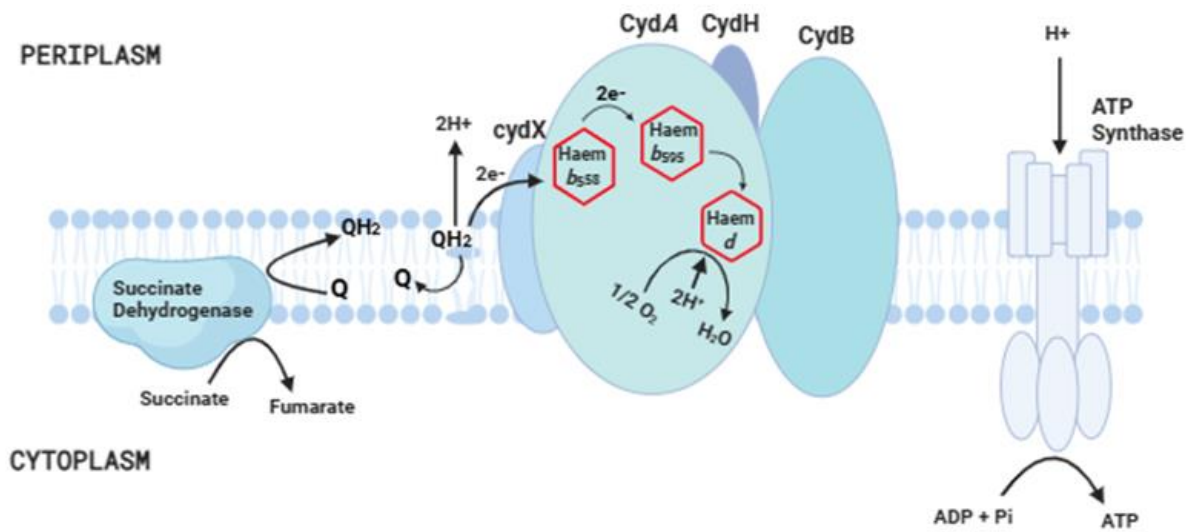


Figure 1.2. The layout and function of CydABXH in the electron transport chain of *E. coli*. CydA, CydB, CydX and CydH are the four subunits that form cytochrome *bd* which sits in the electron transport chain of a prokaryotic cell membrane. Succinate dehydrogenase oxidises succinate into fumarate with the reduction of ubiquinone (Q) to ubiquinol (QH₂). Two electrons are released and shuttled across the haems present in CydA. Haem *d* has the highest affinity for oxygen and is the site of oxygen binding. A proton motive force is generated which is used by ATP synthase to produce ATP.

The single membrane subunit, CydX, has roles in promoting the assembly and stability of the *bd-I* oxidase complex (Hoeser *et al.* 2014). *E. coli bd-I* CydABX has an architecture similar to that of S-subfamily *bd* oxidase from *Geobacillus thermodenitrificans* where *E. coli* CydX has a similar location to that of CydS on *G. thermodenitrificans* (Safarian *et al.* 2016). This suggests that *E. coli* CydX may be an analogue of *G. thermodenitrificans* CydS. There are several homologues of *CydH*, all have been exclusively found in proteobacteria and correlate with the L-subfamily *bd* oxidases. The precise role of *CydH* is still unclear but some authors proposed its role in blocking the entry route of O₂ to haem *b*₅₉₅ in *E. coli bd-I*. Respiratory studies in *G. thermodenitrificans* where *CydH* is absent demonstrated that channels remained open allowing O₂ to be transported to haem *d*, which is in the place of *E. coli* haem *b*₅₉₅ (Safarian *et al.* 2016).

All known members of the cytochrome *bd* family are quinols, where ubiquinol and menaquinol serve as electron donor substrates (Borisov *et al.* 2011). Cytochrome *bd* has three major subtypes that display differences in the ‘Q-loop’, a hydrophilic region that forms a part of the quinol binding site (Matsumoto *et al.* 2006): sub-type A, sub-type B and cyanide insensitive oxygen reductases (CIO). Members of sub-type A have an insert in the C terminal domain of the Q-loop giving them a characteristic “long Q-loop”. Well-characterised examples are found in *Azotobacter vinelandii* and *Escherichia coli* (Osborne and Gennis 1998). CIO have ‘short Q-loops’ (sub-type B) which severely reduces the amount of haem *d* present (Borisov *et al.* 2011). Previous studies that have characterised CIO demonstrated that respiration occurs in these enzymes even in the presence of 1 mM KCN (Cunningham and Williams, 1995). However, diagnostic spectroscopic analysis of membranes does not show the signature peak for haem *d* at 630 nm in these instances (Cunningham and Williams, 1995; Quesada *et al.* 2007). Microorganisms that contain CIO include *P. aeruginosa* (Cunningham and Williams, 1995), *P. putida* (Morales *et al.* 2006), *C. jejuni* (Jackson *et al.* 2007) and *S. carnosus* (Voggu *et al.* 2006).

The Q-loop was examined in its normal isolated state without substrate to determine its role. A synthetic quinone substrate (UQ-1) was used in the presence of AD3-11, an aurachin-D-type competitive inhibitor. The Q-loop begins near the periplasmic section of TM helix 6 and there is a helix break at Asp^{239.A} close to haem *b*₅₅₈ (Figure 1.3D). The hydrogen/deuterium exchange mass spectrometry (HDX-MS) results data showed that binding of AD3-11 specifically affects flexibility and disorders the N-terminal domain of the Q-loop (Q_N) (Figure 1.3E). This had no effect on the C-terminal domain of the Q-loop (Q_C) which insinuates that this insertion has no roles in substrate binding in the L-subfamily of *E. coli*. Except for interactions with the Q_N-loop, the inhibitor AD3-11 nor the substrate

UQ-1 had no effect on the overall structure of *bd-I* which strengthens the argument that other substrate binding sites do not exist on the enzyme.

Safarian *et al.* (2019) used cryo-electron microscopy (cryo-EM) to determine the structure of L-subfamily *E. coli bd-I* oxidase in lipid nanodiscs with a bound Fab fragment to 2.7 Å resolution (Figure 1.3). It confirmed that *bd-I* oxidase is a hetero-oligomer consisting of a CydAB core dimer and two smaller single TM subunits, CydX and CydH (Figure 1.3A). CydA and CydB share a common architecture where they both have two four-helix bundles and an additional peripheral helix (Figure 1.3C). The oxygen reduction reaction is localised to CydA where haem *d* facilitates the reduction of O₂ into H₂O (Safarian *et al.* 2016). The CydB subunit has a structural ubiquinone-8 (UQ-8) molecule bound in a hydrophobic pocket similar, which occupies an internal cleft that is similar to the pocket that is occupied by *b*-type haems in CydA (Figure 1.3C). This UQ-8 is positioned 3.5 nm away from haem *d* and so its role in electron transfer or oxygen reduction is unlikely. However, there have been suggestions of its participation in the assembly of the CydAB dimer (Safarian *et al.* 2019).

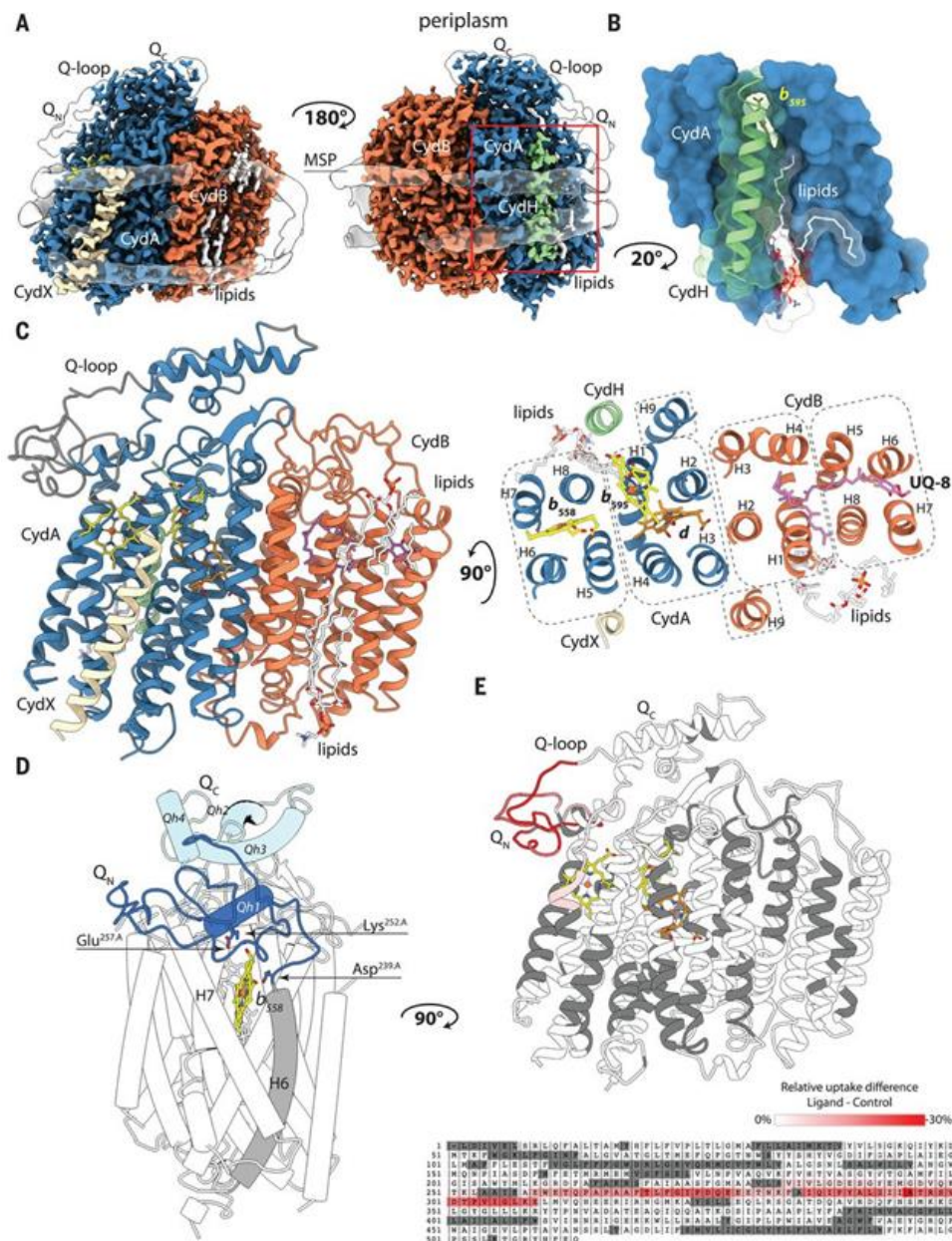


Figure 1.3. Cryo-EM structure of cytochrome *bd-I* oxidase from *E. coli*. (A) Surface representation of *bd-I* oxidase cryo-EM density map at 2.68 Å resolution. (B) The CydH subunit binds to the hydrophobic cleft in CydA. (C) There are 20 membrane-spanning helices in *E. coli bd-I*. (D) The Q-loop is divided into Q_N segments that are rigid and Q_c that are well ordered. (E) AD3-11 is an aurachin-D-type competitive inhibitor of *bd-I* quinone substrate that reduces deuterium exchange rate in the Q_N region. The relative differences of deuterium uptake are mapped on the structure and the CydA amino acid sequence (Safarian *et al.* 2019).

1.3.2.2. *E. coli* cytochrome *bd-II*

E. coli *bd-I* oxidase is well-studied, but less is known about *E. coli* cytochrome *bd-II*. The first high-resolution structure of cytochrome *bd-II* was published recently, and more studies are ongoing to further characterise this enzyme complex (Grund *et al.* 2021). Early work reported a new locus *appCB* that encoded a novel cytochrome *bd* complex in *E. coli* (Dassa *et al.* 1991; Sturr, Krulwich and Hicks 1996), and later analyses confirmed the presence of a third gene to make *appCBX* (Serra *et al.* 2013). The AppCB proteins exhibited 60% identity to the CydA and CydB proteins of *E. coli* (Borisov, Murali, *et al.* 2011; Grauel *et al.* 2021), and spectroscopic techniques confirmed the presence of haem *d*, haem *b*₅₉₅ and haem *b*₅₅₈ in the *bd-II* complex (Sturr, Krulwich and Hicks 1996; Grauel *et al.* 2021). The *appCB* and *appB* genes are part of the same operon and expression is elevated under O₂-limited conditions and carbon/phosphate starvation, and when entering stationary phase (Atlung *et al.* 1997). However, there is a notable structural difference between cytochromes *bd-I* and *bd-II*, one being that the CydH subunit is missing in the latter, meaning that the haem *b*₅₉₅ of *bd-II* the haem *b*₅₉₅ cofactor is accessible from the membrane (Grauel *et al.* 2021).

Initially, flux analysis that involved glucose catabolism and respiration had implied that *E. coli* *bd-II* could operate via a mechanism that is fully uncoupled from proton translocation (Bekker *et al.* 2009). However later studies opposed this and suggested that PMF is generated in membranes expressing cytochrome *bd-II* with a H⁺/e⁻ stoichiometry estimation ratio of 0.94 +/-0.18 (Borisov, Gennis, *et al.* 2011). It was concluded that the *bd-II* complex releases protons into the periplasm via quinol oxidation, performing a vectorial translocation mechanism identical to that of cytochrome *bd-I* (Borisov, Gennis, *et al.* 2011).

1.4. Physiological Functions of *E. coli* Cytochrome *bd*

The predominant roles of terminal oxidases are oxygen reduction (mainly to water), moving protons across the membrane and energy consumption (i.e., ubiquinol). However, cytochrome *bd* oxidases possess physiological functions beyond these that are of huge interest to scientists (Figure 1.5).

1.4.1. Oxygen-reactive Oxidase in Anaerobes

An anaerobe may be defined as a microbe that cannot grow in the presence of dissolved oxygen that exceeds 5 μM (Baughn and Malamy 2004). Interestingly, several anaerobes can survive below this level and their survival is linked to the presence of cytochrome *bd* oxidases. *Bacteroides fragilis*, an obligate anaerobe, encodes cytochrome *bd*-oxidase that allows it to consume oxygen at appreciable rates. However, studies show that *cydAB* mutants were defective in performing oxygen uptake. This is also the case for other obligate anaerobes where *cyd* genes are widely distributed including *Geobacter*, *methanosarcina* and *Moorella* (Baughn and Malamy 2004).

Alternatively, facultative anaerobes such as *E. coli* require the presence of cytochrome *bd* to survive at low oxygen concentrations. A study that assessed the importance of *E. coli* cytochrome *bd* in mice intestinal colonisation demonstrated that mutants lacking cytochrome *bd* oxidase had failed to colonise the intestines (Jones *et al.* 2007). This study provides evidence that aerobic respiration caused by cytochrome *bd* oxidase is essential for the survival of commensal and pathogenic *E. coli* (Jones *et al.* 2007).

1.4.2. Oxygen-scavenging role for cytochrome *bd*

Cytochrome *bd* complexes in nitrogen-fixing bacteria have previously been shown to have an oxygen scavenging role that protects the nitrogenase enzyme from oxygen-mediated

inactivation. Indeed, a double knockout strain of *Azorhizobium caulinodans* lacking cytochromes *bd* and *cbb₃* was shown to be unable to fix nitrogen (Kaminski *et al.* 1996). Additionally, nitrogen fixation was completely impaired in a *cyd* mutant of *Klebsiella pneumoniae* even at low concentration of oxygen. Studies with *Azotobacter vinelandii* demonstrated that cytochrome *bd* is essential for aerotolerant nitrogen fixation (Edwards *et al.* 2000) and fixing nitrogen when environmental oxygen concentrations were reduced to 1.5% (v/v).

1.5. *S. aureus* Aerobic Respiratory Chain

The characterisation of *S. aureus* is more recent when compared to *E. coli*, and as such, most of the data presented on its respiratory chain are speculative. However, some details are certain such as Staphylococcal species use menaquinones (vitamin K₂) as their sole quinones (Götz and Mayer 2013). A series of bioinformatics and biochemical analysis have proposed that *S. aureus* encodes two or three terminal oxidases (Taber and Morrison 1964; Tynecka *et al.* 1999; Clements *et al.* 1999; Voggu *et al.* 2006; Hammer *et al.* 2013). Figure 1.4 proposes that there is a main cytochrome *aa₃* oxidase that is encoded by the *qoxABCD* locus that is proton-pumping. A second oxidase, cytochrome *bd*, is encoded by *cydAB* and is microaerophilic and non-proton pumping (Götz and Mayer 2013). It is uncertain whether cytochrome *bo'* is a third oxidase found in *S. aureus* but if it is, it is proposed to be proton-pumping and aerophilic (Götz and Mayer 2013). However, it was initially thought that *S. aureus* expressed a cytochrome *bo'* complex that did not pump protons (Tynecka *et al.* 1999). Cytochrome *bd* in *S. aureus* is expressed under microaerophilic conditions (Hammer *et al.* 2013). A *cydB qoxB* double knockout mutant was constructed to evaluate the importance of the oxidases in survival during infection (Hammer *et al.* 2013). Results confirmed that both cytochrome *aa₃* and cytochrome *bd* in *S. aureus* are required for aerobic respiration and pathogenesis in *S. aureus* (Hammer *et al.* 2013). It was also proposed that cytochrome *aa₃* and

cytochrome *bd* are more likely to be the only oxidases present during aerobic respiration in *S. aureus* (Hammer *et al.* 2013).

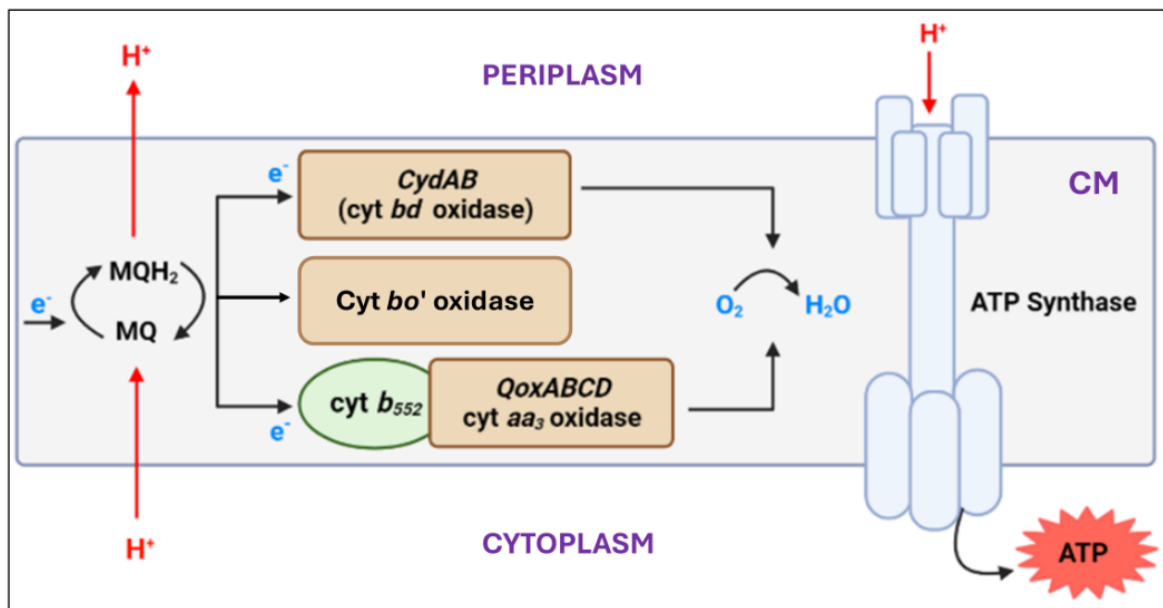


Figure 1.4. Proposed MRSA aerobic respiratory chain. The respiratory chain of MRSA is situated in the cytoplasmic membrane (CM). It is proposed that menaquinone (MQ) is reduced to menaquinol (MQH₂), which then transfers electrons (e⁻) to different terminal oxidases. The proposed main oxidase is cytochrome aa₃ (QoxABCD) which is composed of cytochromes a₆₀₂ and b₅₆₁. Cytochrome *bd* oxidase (CydAB), is proposed to function under microaerobic conditions while a third terminal oxidase, cytochrome *bo'*, consists of cytochrome b₅₅₅ and a possible cytochrome b₅₅₇. Cytochrome *bd* is proposed to not be proton-pumping while cytochrome aa₃ and cytochrome *bo'* are proton-pumping and work under aerophilic conditions. ATP synthase uses the electrochemical gradient generated to produce ATP. This diagram is an adaptation of Götze and Mayer 2013 and is speculative.

1.6. Cytochrome *bd* and environmental stressors

Cytochrome *bd* has been linked to having effects on certain environmental stressors such as nitric oxide, peroxide, chromate, and sulphide (Figure 1.5). This can result in increasing the tolerance of bacterial pathogens to stresses encountered during infection, which makes cytochrome *bd* a good candidate for drug targeting.

A. **Peroxide.** Cytochrome *bd* complexes may play a role in providing protection against hydrogen peroxide (H₂O₂)-induced stress. Both cytochrome *bd*-I and *bd*-II have shown

contribution towards the elimination of ROS such as H₂O₂ in *E. coli* (Borisov, Nastasi and Forte, 2023). These oxidases are believed to act as antioxidants that result in the decomposition of H₂O₂ and subsequently creates a redox balance which protects the bacteria from oxidative stress (Borisov, Nastasi and Forte, 2023). Further research demonstrated that knockout mutants of *E. coli* K12 strains with defect in cytochrome *bd* had shown high sensitivity to H₂O₂ (Lindqvist *et al.* 2000). This testifies to the importance of cytochrome *bd* in providing bacterial resistance to ROS such as H₂O₂. Another study demonstrated that the expression of cytochrome *bd* was increased upon addition of exogenous H₂O₂ or via elevation endogenous ROS production (Charbon *et al.* 2017). This was also observed in *Staphylococcus aureus* where exposure to H₂O₂ resulted in elevated expression of cytochrome *bd* (Chang *et al.* 2006). These studies have highlighted the importance of cytochrome *bd* oxidases in providing redox balance in bacterial species and creating bacterial resistance to H₂O₂.

B. Nitric Oxide. Nitric oxide is produced by the host during an immune response to eliminate the invading pathogen. Cells of the innate immune system (i.e., neutrophils, macrophages and natural killer cells), identify invading pathogens via the use of their pattern recognition receptors (Tripathi *et al.* 2007). Macrophages release nitric oxide when activated to inhibit the replication of invading pathogens (Tripathi *et al.* 2007). Comparative studies showed that nitric oxide caused greater growth inhibition in cytochrome *bd*-deficient mutant *E. coli* cells than in cytochrome *bo'*-deleted mutants (Mason *et al.* 2009). In *Salmonella enterica*, cytochrome *bd* also played a role in NO tolerance and has been shown to increase virulence (Jones-Carson *et al.* 2016). In a mouse model, cytochrome *bd*-I contributed to the survival of uropathogenic *E. coli* after two days of infection which testifies to the importance of the oxidase in host colonisation (Shepherd *et al.* 2016). Further studies demonstrated that upon exposure to nitric oxide in *E. coli*, genes encoding cytochrome *bd*-I were upregulated at the

transcriptional level (Hyduke *et al.* 2007). These studies have highlighted the importance of cytochrome *bd* in being a valuable defence tool for the survival of bacteria under NO-induced stressed.

C. **Sulphide.** Cytochrome *bd* has been proven to elicit resistance against sulphide in several bacterial species. A study conducted on isolated enzymes demonstrated that cytochrome *bd* was insensitive to sulphide even at high concentrations of 58 μ M while cytochrome *bo'* was severely inhibited (Forte *et al.* 2016). It was hypothesised that cytochrome *bd* oxidase was functioning as a sulphide-insensitive oxidase after sulphide was shown to inhibit cytochrome *c* oxidase in bacteria (Nicholls *et al.* 2013). In these bacteria, an exposure to sulphide led to energy depletion and cell death (Nicholls *et al.* 2013). In cytochrome *bd*-deficient mutants, sulphide potently inhibits oxygen growth and respiration when administered both exogenously and endogenously (Korshunov, Imlay and Imlay 2016). The direct reason for the sulphide insensitivity exhibited by cytochrome *bd* oxidase remains a question but has been proposed to be caused by the lack of copper site in the oxidase (Borisov *et al.* 2015). This conclusion was drawn based on a transient binding of hydrogen sulphide (H_2S) to copper (Cu_b) during sulphide's inhibition of cytochrome *c* (Nicholls *et al.* 2013).

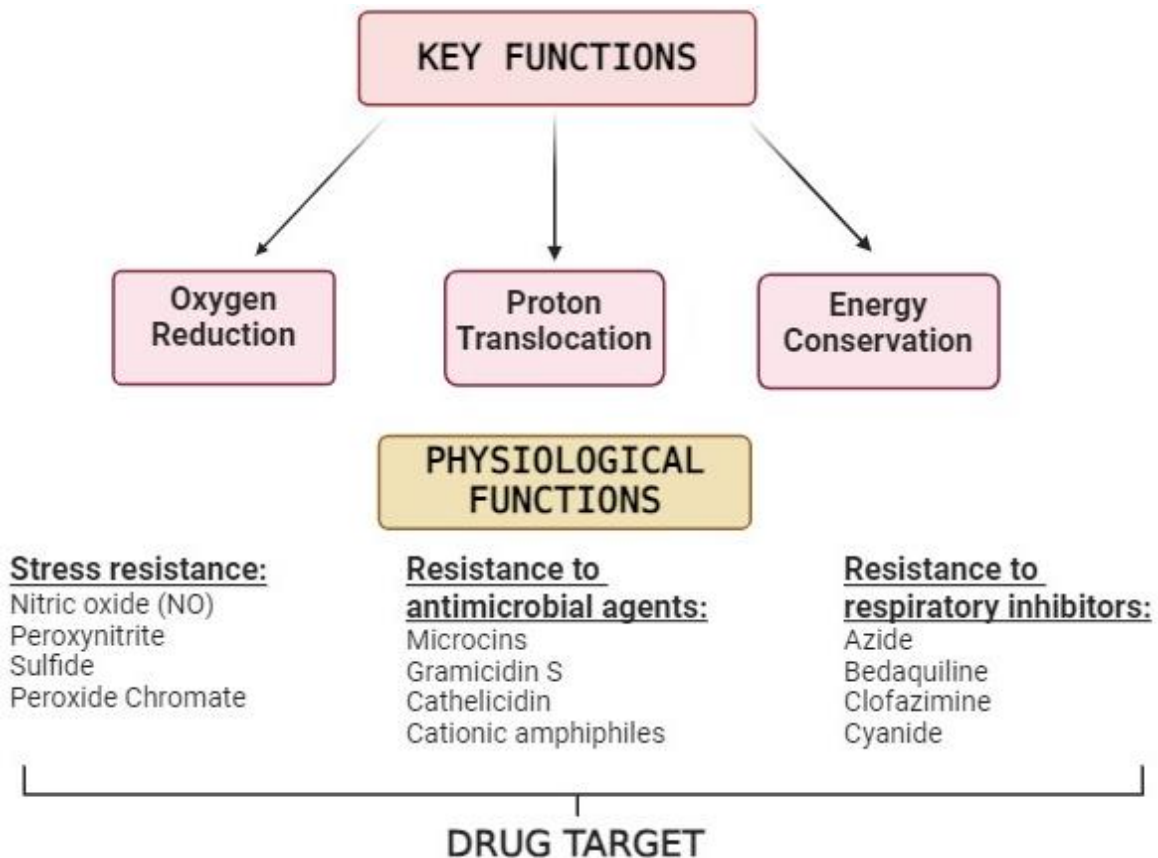


Figure 1.5. The functions of cytochrome *bd* oxidases. The key functions of *bd*-type oxidases are to perform oxygen reduction proton translocation (independent of a proton pump) and energy conservation. The physiological functions identified so far include resistance to stress, resistance to antimicrobial agents and resistance to respiratory inhibitors.

1.7. Cytochrome *bd* as a drug target

1.7.1. Cytochrome *bd* is a good drug target

Cytochrome *bd* is a good drug target for numerous reasons. High resolution structures exist for various cytochrome *bd* complexes from multiple organisms which makes it easy to study the enzyme (Safarian *et al.* 2019; Grauel *et al.* 2021; Safarian *et al.* 2021; Friedrich, Wohlwend and Borisov 2022). *Bd*-type have been linked to virulence and stress tolerance in some of the most pathogenic strains of bacteria including *Salmonella* (Turner *et al.* 2003) group B *Streptococcus* (Yamamoto *et al.* 2005), Staphylococcal species and *Pseudomonas aeruginosa* (Voggu *et al.* 2006), *Burkholderia pseudomallei* (Price *et al.* 2018), *Brucella*

abortus (Loisel-Meyer *et al.* 2005; Endley, McMurray and Ficht 2001), *Shigella flexneri* (Way *et al.* 1999), and *M. tuberculosis* (Shi *et al.* 2005) (for a detailed review see Borisov *et al.* 2021).

Cytochrome *bd* oxidases are highly expressed under anaerobic and growth-limiting conditions such as iron deficiency (Borisov and Verkhovsky 2009) and acts as an oxygen scavenger by protecting oxygen-sensitive enzymes such as nitrogenase from being inactivated (Dincturk, Demir and Aykanat 2011). In *Mycobacterium tuberculosis*, murine studies demonstrated an upregulation of *bd* oxidases in the lung of mice when the infection transitioned from acute to chronic state (Shi *et al.* 2005). In the fight to produce novel anti-tuberculosis drugs, a new compound imidazopyridine Q203 was found to target cytochrome *bcc* complex (Lu *et al.* 2018). Biochemical assays using the cytochrome *bcc* inhibitor Q203 were studied as the compound suppressed the growth of *Mycobacterium tuberculosis* at nanomolar concentrations but was unable to kill the pathogen (Lu *et al.* 2018). Inhibition of cytochrome *bd*, another respiratory oxidase found in *Mycobacterium tuberculosis*, largely improved the bactericidal activity of compound Q203 (Lu *et al.* 2018).

CIO is one of the five terminal oxidases that are found to be expressed in the opportunistic pathogen, *Pseudomonas aeruginosa*. However, the CIO possessed by this organism have shown great resistance to cyanide toxin which is also produced by the bacteria (Zlosnik *et al.* 2006). The virulent characteristics of cytochrome *bd* oxidases, the presence of high-resolution structures and their existence in solely prokaryotes make them excellent antibacterial drug targets.

1.7.2. *Bd*-type oxidases as drug target in various bacteria

Pathogenic bacteria are exposed to extreme hostile environments upon invasion of a host. They are introduced to an O₂-deprived environment as well as other harsh conditions such

as the presence of RNS and ROS produced during immune defence. In addition, the respiratory inhibitor H₂S is produced by bacteria that coexists in the host (Borisov *et al.* 2020). These unfavourable conditions are detrimental to the survival of the bacteria in the host and explains the need for an increased expression of cytochrome *bd* oxidases. Cytochrome *bd* complexes can function in O₂-limited conditions due to their high affinity for oxygen. Studies demonstrate that cytochrome *bd* has also conferred resistance to hydrogen sulphide that is produced in the gut (Korshunov *et al.* 2016). As shown in Figure 1.5, cytochrome *bd* oxidases are resistant to ROS and RNS mediated stress which increases the virulence of the *bd* oxidase-containing bacterium.

1.7.2.1. Uropathogenic *E. coli* (UPEC)

UPEC is the primary cause of urinary tract infections (UTIs) (Whelan *et al.* 2023). UTI is a global health issue and the most common nosocomial infection (Gastmeier, 2001; Asadi Karam, Habibi and Bouzari 2019). Cytochrome *bd* is believed to have vital roles in the virulence of this organism by conferring NO resistance during infection (Shepherd *et al.* 2016). This study investigated the relative contributions of various mechanisms to the tolerance of NO, including the iron cluster repair protein YtfE, NO detoxification systems (Hmp, NorVW, NrfA) and expression of the NO-tolerant cytochrome *bd-I* oxidase. As predicted, the major contributors to NO tolerance were cytochrome *bd-I* and Hmp. Cytochrome *bd-I* also induced resistance to neutrophil-mediated killing and conferred greater survival in macrophages.

1.7.2.2. Group B Streptococcus

Group B Streptococcus (GBS) is a commensal bacterium that usually resides in the genital and gastrointestinal tracts of individuals. The existence of GBS in the vagina flora is usually harmless to women but could be life-threatening for new-borns during childbirth that could develop sepsis. GBS was assumed to partake only in fermentative respiration, but a study

discovered its ability to respire aerobically if the environment provides quinone and haem requiring cytochrome *bd* (Yamamoto *et al.* 2005). ‘Environmental’ quinone and haem are believed to be supplied by residential flora that synthesise haem and menaquinone in the lower gastrointestinal or genital tracts (Yamamoto *et al.* 2005). The study also showed that an inactivation of *cydA* in GBS leads to a decrease in growth in human blood (Yamamoto *et al.* 2005).

1.7.2.3. *Mycobacterium tuberculosis*

There has been a lot of ongoing research on the characterisation of cytochrome *bd* in *M. tuberculosis*, the causative agent of tuberculosis. Considering that tuberculosis is a global health concern with an estimated 10 million new cases and 1.6 million deaths in 2021 (Villar-Hernández *et al.* 2023), a lot needs to be done to create new therapeutics. *M. tuberculosis* can persist under severely deprived oxygen conditions inside its host but cannot proliferate (Cook *et al.* 2014). The ETC of *M. tuberculosis* consists of two terminal oxidases: a *bd*-type oxidase and an *aa₃*-type cytochrome *c* oxidase that forms a super complex with *bc₁* (Borisov *et al.* 2020). The role that cytochrome *bd* plays in mycobacterial virulence is believed to occur during the transition from the acute to chronic stage of an infection. A transcriptomic study using a murine infection model demonstrated that cytochrome *bd* and a nitrate transporter were upregulated between the acute and chronic stages of the disease (Shi *et al.* 2005).

1.8. Known Inhibitors of Cytochrome *bd*

Bd oxidases have been associated with bacterial virulence and thus far have been only identified in prokaryotes making them excellent drug targets. Consequently, there have been a surge in research aimed towards discovering inhibitors of *bd*-type oxidases. There have been many compounds shown to inhibit respiratory activity of *bd* oxidases (Table 1.1). Thus far, there are two recognised forms of quinol oxidase inhibitors against cytochrome *bd*: (1) Q-like

compounds that binds at the *Q* binding site and (2) haem ligands that act at the *Q*₂ binding/reducing site (Borisov, Gennis, *et al.* 2011). Q-like inhibitors include aurachin C and haem ligands include nitric oxide (NO), cyanide and azide. Advancements are being made as it relates to cytochrome *bd* oxidase inhibition and drug repurposing of Food and Drug Administrative (FDA) approved drugs. NO is a potent and reversible inhibitor of cytochrome *bd*, similarly to that observed in cytochrome *c* oxidase (Sarti *et al.* 2012). This inhibition was demonstrated with *E. coli* cells (Mason *et al.* 2009) and with cytochrome *bd* that was isolated from *E. coli* and *A. vinelandii* (Borisov *et al.* 2004).

An ATP synthase inhibitor, bedaquiline, was recently approved for treating multi-drug-resistant strains of *Mycobacterium tuberculosis* which highlighted that oxidative phosphorylation plays a major role in *Mycobacterium tuberculosis* survival (Bajeli *et al.* 2020). Early studies demonstrated that *Mycobacterium tuberculosis* was sensitive to bedaquiline in mutants where cytochrome *bd* had been knocked out (Berney, Hartman and Jacobs 2014), highlighting the importance of cytochrome *bd* in virulence of pathogens. Bedaquiline was proven to be an ineffective inhibitor of cytochrome *bd* on its own but when combined with Talacebec (Q203), a phase two drug, respiration, and ATP homeostasis were inhibited (Lee *et al.* 2020). A recent study identified a series of 2-aryl-quinolone as novel inhibitors of *Mycobacterium tuberculosis* cytochrome *bd* (Jeffreys *et al.* 2023). However, combination therapies that involve inhibitors of both branches of Mycobacteria terminal oxidases were shown to improve the overall antimycobacterial activity of the compounds (Jeffreys *et al.* 2023).

Inhibitor	Organism	Substrate	Inhibitory Activity	Unit of Measurement
Antimycin A	<i>E. coli</i>	Duroquinol Oxidase	50 μ M, 80%	Conc. and % Inhibition
Aurachin A	<i>E. coli</i>	Duroquinol Oxidase	700 μ M, 27%	Conc. and % Inhibition
Aurachin C	<i>E. coli</i>	Duroquinol Oxidase	214 nM, 90%	Conc. and % Inhibition
Aurachin D	<i>E. coli</i>	Duroquinol Oxidase	400 nM, 93%	Conc. and % Inhibition
Carbon monoxide	<i>A. vinelandii</i>	Ascorbate-2, 6-dichlorophenolindophenol Oxidase	0.5–1 mM, 80%	Conc. and % Inhibition
decyl-aurachin D	<i>A. vinelandii</i>	Ubiquinol-1 Oxidase	13 nM	Inhibition Constant (K_i)
(1,5-Dimethylhexyl)quinazolinamide	<i>E. coli</i>	Duroquinol Oxidase	100 μ M, 88%	Conc. and % Inhibition
2,6-Dimethyl-<i>p</i>-benzoquinone	<i>B. stearothermo philus</i>	Duroquinol Oxidase	65 μ M	IC ₅₀
Dibromothymoquinone	<i>E. coli</i>	Duroquinol Oxidase	100 μ M, 38%	Conc. and % Inhibition
Gramicidin S	<i>E. coli</i>	Ubiquinol-1 Oxidase	5.3 μ M	IC ₅₀
Hydrogen Peroxide	<i>E. coli</i>	Duroquinol Oxidase	120 mM	IC ₅₀
2-<i>n</i>-heptyl-4-hydroxyquinoline N-oxide	<i>E. coli</i>	Duroquinol Oxidase	7 mM	IC ₅₀
(1-Methyldecyl)quinazolinamide	<i>E. coli</i>	Duroquinol Oxidase	100 μ M, 85%	Conc. and % Inhibition
Nigericin	<i>E. coli</i>	Duroquinol Oxidase	100 μ M, 44%	Conc. and % Inhibition

Nitric oxide (NO)	<i>E. coli</i>	Ubiquinol-1 Oxidase	100 nM	Inhibition Constant (K_i)
Potassium cyanide or Sodium cyanide	<i>E. coli</i>	Ubiquinol-1 Oxidase	2 mM	IC ₅₀
Piericidin A	<i>E. coli</i>	Ubiquinol-1 Oxidase	15 μ M	IC ₅₀
Pentachlorophenol (PCP)	<i>E. coli</i>	Ubiquinol-1 Oxidase	200 μ M	Inhibition Constant (K_i)
<i>p</i>-benzoquinone	<i>B. stearothermo philus</i>	Duroquinol Oxidase	120 μ M	IC ₅₀
Sodium azide (NaN₃)	<i>E. coli</i>	Ubiquinol-1 Oxidase	400 mM	IC ₅₀
Stigmatellin	<i>E. coli</i>	Duroquinol Oxidase	200 μ M, 14%	Conc. and % Inhibition
2-Thenoyl trifluoroacetone (TTFA)	<i>E. coli</i>	Ubiquinol-1 Oxidase	1 mM, 35%	Conc. and % Inhibition
Undecylhydroxy dioxo-benzothiazole	<i>E. coli</i>	Duroquinol Oxidase	20 μ M, 18%	Conc. and % Inhibition
Zinc sulphate or Zinc Chloride	<i>E. coli</i>	Ubiquinol-1 Oxidase	60 μ M	IC ₅₀
2-aryl-quinolones	<i>Mycobacterium tuberculosis</i>	Glucose	20–200 μ M	Conc. and % Inhibition

Table. 1.1. Compounds with inhibitory effects on the respiratory activity of cytochrome *bd*. *All *E. coli* data refers specifically to cytochrome *bd-I* (Borisov *et al*, 2011).

1.9. Aims of Study

The first aim of this study was to create and characterise EC958 *E. coli* strains that express single respiratory oxidases. This allowed for the enzyme to be easily studied in a highly pathogenic *E. coli* strain that was isolated from a patient with urinary tract infection. The

second main aim was to assess known antimicrobials as inhibitors of cytochrome *bd*. There are multiple published compounds with antibacterial activity and/or are known for binding to quinol sites. It was important to establish the effect of these compounds on cytochrome *bd* and determine whether they are potent inhibitors of the enzyme. The final main aim of the study was to employ computational (molecular docking), *in vitro*, and *in vivo* approaches to develop drug repurposing pipeline to identify novel inhibitors of cytochrome *bd*. This strategy involved the screening of an FDA library via a molecular docking pipeline followed by the screening of the top hits in the lab to determine their effects. Experimental assays included but were not limited to oxygen consumption assays, growth assays and viability assays.

Chapter 2

Materials and Methods

2. Materials and Methods

2.1. Bacterial Strains and Growth Conditions

2.1.1. Bacterial Strains

All bacterial strains used throughout this project are listed in Table 2.1. All *E. coli* strains are derived from a clinical strain isolated from a patient with UTI (Lau *et al.* 2008). The MRSA strain used is the well-characterised USA300 LAC isolate (Kennedy *et al.* 2008), a community-associated MRSA strain isolated from the Los Angeles County Jail. All MRSA mutant strains were generated by phage transduction of the relevant transposon mutant from the Nebraska Transposon Mutant Library (Bae *et al.* 2007) into strain USA300 LAC using methods described previously (Fey *et al.* 2013), generating clean insertions in the loci of interest and conferring erythromycin resistance. For the purposes of this thesis, the MRSA *qoxA::Tn* strain will be referred to as 'bd-only' while the *cydA::Tn* strain will be referred to as 'aa₃-only'.

Table. 2.1. List of Bacterial Strains

Strain	Characteristics	Reference
MS402	<i>E. coli</i> TOP10 harbouring pSU2718-G- <i>cydABX</i>	(Shepherd <i>et al.</i> 2016)
MS628	<i>E. coli</i> ST131 EC958 Δ <i>cyoA</i> <i>appCB::Cm</i>	Webster, C.M. (2023) PhD thesis, University of Kent)
MS629	<i>E. coli</i> ST131 EC958 Δ <i>cydAB</i> <i>appCB::Cm</i>	Webster, C.M. (2023) PhD thesis, University of Kent)
MS631	DH5 α containing pSU2718- G- <i>cydABX</i> -6*HIS	Webster, C.M. (2023) PhD thesis, University of Kent)
MS662	<i>E. coli</i> EC958 wild type strain from clonal group ST131	(Lau <i>et al.</i> 2008)

MS667	<i>E. coli</i> MG1655 'EcoM4' Δ (<i>cydAB appBC cyoABCD ygiN</i>):FRT-kan-FRT	Shepherd Laboratory
MS681	<i>E. coli</i> 'EcoM4' Δ (<i>cydAB appBC cyoABCD ygiN</i>)	This Work
MS682	Methicillin-resistant <i>Staphylococcus aureus</i> LAC (USA300) WT	(Kennedy <i>et al.</i> 2008)
MS685	MRSA LAC Δ <i>cydA</i> :+n	NARSA
MS688	MRSA LAC Δ <i>qoxA</i> :+n	NARSA
MS694	<i>E. coli</i> MG1655 'EcoM4' Δ (<i>cydAB appBC cyoABCD ygiN</i>):FRT-kan-FRT harbouring pSU2718G_ <i>cydABX</i> F269A	This Work
MS695	<i>E. coli</i> MG1655 'EcoM4' Δ (<i>cydAB appBC cyoABCD ygiN</i>):FRT-kan-FRT harbouring pSU2718G_ <i>cydABX</i> L253A	This Work
MS696	<i>E. coli</i> MG1655 'EcoM4' Δ (<i>cydAB appBC cyoABCD ygiN</i>):FRT-kan-FRT	This Work
MS697	<i>E. coli</i> MG1655 'EcoM4' Δ (<i>cydAB appBC cyoABCD ygiN</i>):FRT-kan-FRT harbouring pSU2718G_ <i>cyoABCD</i>	This Work

2.1.2. Bacterial Plasmids

The plasmids used throughout this project are shown in Table 2.2.

Table 2.2. Bacterial Plasmids

Plasmid	Characteristics	Antibiotic Resistance	Reference
pSU2718-G-<i>cydABX</i>	Δ <i>cydAB</i> complementation plasmid	Gent ^R	(Shepherd <i>et al.</i> 2016)
pSU2718G-appCBX-6HIS	Δ <i>appCB</i> complementation plasmid	Gent ^R	Unpublished (Shepherd Lab)
pSU2718-G-<i>cydABX</i>-6HIS	<i>E. coli</i> EC958 <i>cydABX</i> -6HIS expression plasmid	Gent ^R	(Webster, C.M. (2023) PhD thesis, University of Kent)

pSU2718-G-cyoABCD-7HIS	Expression plasmid for <i>E. coli</i> EC958 <i>cyoABCD-7HIS</i>	Gent ^R	(Webster, C.M. (2023) PhD thesis, University of Kent)
-------------------------------	---	-------------------	---

2.1.3. Oligonucleotides

SnapGene (SnapGene®, n.d.) was used to design the oligonucleotides used throughout this project which are listed in Table 2.3. GC content was between 40-60%. Oligonucleotides were purchased from Integrated DNA Technologies and the purification type was standard desalting.

Table 2.3. List of Oligonucleotides

Primer	Sequence (5'-3')	Use	Shepherd Lab primer number	Direction
1RNew_pSU2718	ATGCCTGCAGGT CGACTCTAGAA ATTCAATGGTGA TGGTGATGGTG ATGTCTTCTTGA CCGGCTTTGCCT GATTC	Amplification of <i>CydABX</i> from pSU2718 or EC958 with 6*His-tag, XbaI and GA to pSU2718	406	Forward
<i>CydABX_F_EC958</i>	CGGGGATCCTTA AAGAGGAGAAA GGTACATGATGT TAGATATAGTCG AAC TGTCGCG	Reverse primer for 406. Used with vector primers 431 and 432.	407	Reverse
2F_New_pSU2718	ATTTCTAGAGTC GACCTGCAGGC ATGCAAG	Amplification of pSU2718-G backbone.	431	Forward
2R_New_pSU2718	GTACCTTTCTCC TCTTTAAGGATC CCCGGG	Amplification of pSU2718-G backbone.	432	Reverse

<i>appCBX_F_v2</i>	CGGGGATCCTTA AAGAGGAGAAA GGTACATGTGGG ATGTCATTGATT TATCGCGCTGG	Cloning of <i>appCBX</i> operon from EC958 into pSU2718. Used with vector primers 404 and 453.	476	Forward
<i>appCBX_R_v2</i>	TAGAAATTCAAT GGTGATGGTGAT GGTGACTTTTCA GACGCGGGTCC AGCCATACCAA	Reverse primer for 476	477	Reverse
pSU_his_F	CACCATCACCAT CACCATTTGAATT TCTAGA	Amplification of vector backbone PSU2718G HIS6.	453	Forward
2R_pSU2718	GTACCTTTCTCC TCTTTAAGGATC	Reverse vector primer for 453	404	Reverse
pSU2718seq_200_F	GTCGGGTGATG CTGCCAACT	Screening of pSU2718G_ <i>appCBX</i>	275	Forward
pSU2718seq_200_R	GCAGCTGGCAC GACAGGTTT	Reverse primer for 275	276	Reverse
<i>cydA_L253A_F</i>	GAAAACCAAAG CAGCTGCTATTG AAGCCGA	Mutagenesis of L253A in <i>CydA</i> of pSU2718G- <i>appCBX</i> -6HIS.	466	Forward
<i>cydA_L253A_R</i>	CAATAGCAGCTG CTTTGGTTTTCT GCACGT	Reverse for primer 466.	467	Reverse
<i>cydA_F269A_F</i>	TGCTGCCGCCA CTCTGTTCGGTA TTCCTGA	Mutagenesis of F269A in <i>CydA</i> of pSU2718G- <i>appCBX</i> -6HIS.	474	Forward
<i>cydA_F269A_R</i>	CGAACAGAGTG GCGGCAGCAGG TGCAGGTT	Reverse primer for 474.	475	Reverse

cydA_Y387A_F	AGCGCCGCTGG CATTCGCGTTCC GTATCAT	Mutagenesis of Y387A in CydA of pSU2718G- appCBX-6HIS.	468	Forward
cydA_Y387A_R	GGAACGCGAAT GCCAGCGGCGC TACACGCG	Reverse primer for 468.	469	Reverse
cydA_F390A_F	GTACTTCGCGG CGCGCATCATG GTGGCGTG	Mutagenesis of F390A in CydA of pSU2718G- appCBX-6HIS.	470	Forward
cydA_F390A_R	CCATGATGCGC GCCGCGAAGTA CAGCGGCG	Reverse primer for 470.	471	Reverse
cydA_I295A_F	GCTGGGCATCG CCGCAACGCGT TCCGTGGA	Mutagenesis of I295A in CydA of pSU2718G- appCBX-6HIS.	472	Forward
cydA_I295A_R	AACGCGTTGCG GCGATGCCAG CGCGTAAG	Reverse primer for 472.	473	Reverse
cydA_S241A_F	GGGTGATGAAG CCGGCTACGAA ATGGGCGA	Mutagenesis of S241A in CydA of pSU2718G- appCBX-6HIS.	462	Forward
cydA_S241A_R	TTTCGTAGCCGG CTTCATCACCCA GAACAA	Reverse primer for 462.	463	Reverse
cydA_Y243A_F	TGAATCCGGCG CCGAAATGGGC GACGTGCA	Mutagenesis of Y243A in CydA of pSU2718G- appCBX-6HIS.	464	Forward
cydA_Y243A_R	CGCCATTTCCGG CGCCGGATTCA TCACCCA	Reverse primer for 464.	465	Reverse

2.1.4. Chemicals and Water

Molecular biology experiments involving DNA manipulation were performed using milli-Q water. All other experiments were performed using deionized (distilled) water. Solutions were sterilised by autoclaving at 121°C for 15 min at 15 psi or via filter sterilisation using 0.22 µm Millipore filters.

All chemicals were acquired from ThermoFisher or Sigma-Aldrich unless stated otherwise. Media components such as tryptone soy broth (TSB), tryptone and yeast extract were purchased from Oxoid.

2.1.5. Media and Buffer Solutions

2.1.5.1. Luria-Bertani (LB) Medium

One litre of LB broth contained 10 g tryptone, 10 g NaCl and 5 g yeast. For LB agar medium, 15 g of agar was added to the ingredients in the LB broth.

2.1.5.2. M9 Minimal Medium

A 200 mL solution of 5x M9 salts was prepared by adding 16.05g Na₂HPO₄·2H₂O, 3 g KH₂PO₄ and 0.5 g NaCl. This mixture was autoclaved and left to cool. A 500 mL of 1 x M9 was made by mixing 100 mL of 5 x M9, 20 mL of a 50% glycerol (filter-sterilised), 1 mL of 1 M MgSO₄ solution (autoclaved), 50 µL of 1 M CaCl₂ solution (autoclaved), 25 mL of a 2% casein hydrolysate solution (autoclaved) and 353.96 mL of autoclaved water.

2.1.5.3. Tryptic Soy Broth (TSB) Medium

A 1 L solution of TSB was made by adding 30 g of TSB medium into 1 L water. To prepare 1 L of tryptic soy agar (TSA), 15 g of agar was added to a 1L TSA solution. Solution was autoclaved and cooled before being stored at room temperature.

2.1.5.4. Super Optimal Broth (SOB) Medium

To make a 1 L solution of SOB medium, 20 g of bacto-tryptone, 5 g of yeast, 0.5 g NaCl, 0.186 g KCl was added to 1 L of water. SOB⁺⁺ was made by having a final concentration of 10 mM MgCl₂ and 10 in SOB medium.

2.1.5.5. Super Optimal Broth with Catabolite Repression (SOC) Medium

SOC medium is SOB medium with catabolite repression. SOC media was made by adding 20 mM of filter sterilised glucose (final concentration) to previously autoclaved and cooled SOB⁺⁺ medium.

2.1.5.6. Tris/HCl buffer

A 20 mM Tris/HCl was made by adding 2.42 g of Tris base to 1 L of water. Hydrochloric acid (HCl) was added to alter the pH to 7.4 before autoclaving the mixture.

2.1.5.7. Sonication Buffer

Sonication buffer was made by creating a solution with a final concentration of 20 mM Tris, 2 mM MgCl₂ and 1 mM EGTA. Hydrochloric acid (HCl) was added to the mixture to obtain a pH of 7.4 before autoclaving.

2.1.5.8. Tris-acetate-EDTA (TAE) Buffer

A 1 L solution of 50x TAE was made by adding 242 g of Tris, 57.1 mL of acetic acid and 50 mL of 1 M EDTA to 900 mL of distilled water. A 100 mL working solution of 1x TAE as made by adding 2 mL of 50x TAE to 98 mL of water.

2.1.5.9. Phosphate-buffered Saline (PBS)

To produce 1L of a 1x PBS solution (pH 7.4), 100 mL of a 10x concentrated PBS solution (1.37 M NaCl, 27 mM KCl, 100 mM Na₂HPO₄, and 18 mM KH₂PO₄) was added to 900 mL of distilled water. The solution was autoclaved and cooled.

2.1.5.10. Succinate

For oxygen consumption assays, 160 mM succinic acid was made up by using succinic acid. The pH of the solution was adjusted to 7.5 by using 1 M HCl, and filter sterilised.

2.1.5.11. HEPES (4-(2-hydroxyethyl)-1-piperazineethanesulfonic acid) Buffer

To make up 1 L of 50 mM HEPES buffer (Fluka, BioChemika), 11.9 g of HEPES was added to 1 L of distilled water. The pH was adjusted to 7.2 using NaOH before being autoclaved.

2.1.5.12. Glycerol Stocks

For freezing bacterial cultures, glycerol stocks were prepared by mixing 750 µL of 50% sterile glycerol with 750 µL of bacterial culture grown to stationary phase. Contents were stored in a sterile cryotube at -80°C.

2.1.6. Antibiotics

All antibiotics used throughout this study are listed in Table 2.4.

Table 2.4. List of Antibiotics

Antibiotic	Solvent	Stock Concentration (mg/mL)	Working Concentration (µg/mL)
Ampicillin	Milli-Q water	125	125
Gentamicin	Milli-Q water	30	30 and variable

Chloramphenicol	Ethanol	34	25
Lincomycin	Milli-Q water	25	25
Erythromycin	Ethanol	5	5

2.1.7. Drugs Tested

The drugs tested throughout this research are listed in Table 2.5.

Table 2.5. List of Drugs Tested

Drug	Solvent	Source
Quinestrol	DMSO	TCI, UK Ltd.
Ethinylestradiol	DMSO	TCI, UK Ltd.
Mestranol	Ethanol	Sigma-aldrich
Quinestrol PEG Derivative	DMSO	David Beal (Mark Smales' Laboratory)
Madecassic Acid & Derivatives	DMSO	Geraud Sansom (Christopher Serpell's Laboratory)
TTFA (2-thenoyltrifluoroacetone)	Ethanol	Sigma-aldrich

2.2. Bacterial Assays

2.2.1. Growth Conditions

E. coli was cultured in LB or M9 minimal media while MRSA was grown in tryptic soy broth (Oxoid), supplemented with antibiotics where appropriate.

To produce overnight cultures, a single colony from a plate containing bacteria was used to inoculate 10 mL starter cultures and left to grow overnight. A 1% (v/v) inoculum of the

overnight culture was used to inoculate fresh sterile media. *E. coli* and MRSA strains were routinely cultured at 37°C, 180 rpm unless stated otherwise.

2.2.2. Optical Density Readings

Routinely, optical density readings at 600 nm (OD₆₀₀) were performed to determine the growth of cells or turbidity of a sample. This was performed by adding 1 mL of the required sample into a cuvette with a pathlength of 1 cm and placed inside a Shimadzu UV-1800 spectrophotometer that had been blanked with the appropriate growth medium.

2.2.3. CO Difference and Reduced *minus* Oxidised Spectra

A SDB4 dual beam spectrophotometer (Poole and Kalnenieks 2000) was used to record ‘reduced *minus* oxidised’ and ‘CO difference’ spectra of *E. coli* cells as previously reported (Poole *et al.* 1989). Firstly, 100 mL cells were grown overnight in 250 mL conical flasks (37°C, 180 rpm). Next, 90 mL of the overnight culture was centrifuged at 4000 rpm for 10 mins and the pellet was resuspended in approximately 6 mL of 20 mM Tris/HCl (pH 7.4) and kept on ice (OD₆₀₀ of these dense cell suspensions ranged from 40-60). For membrane spectra, membranes were prepared as outlined in section 2.2.2. Ammonium persulphate was added to 2 mL of cell/membrane suspension to obtain the reduced samples, sodium dithionite was added to a 2 mL suspension to generate the reduced sample, and these reduced suspensions were subsequently exposed to carbon-monoxide gas for 5 min to generate the ‘CO reduced’ sample. Absorbance spectra were recorded for all samples from 400-700 nm at 0.5 nm/min, and baseline subtractions were performed to generate the CO difference spectra. N.B. CO difference = ‘CO reduced’ *minus* ‘reduced’.



Figure 2.1. SDB4 Spectrophotometer. This is a special type of spectrophotometer that can analyse highly turbid samples.

2.2.4. Membrane Preparation

Cells were grown overnight in LB agar and 1 mL were inoculated into 2 L conical flasks containing 1L of fresh LB. The culture was left to cultivate at 37°C, 150 rpm overnight after which the culture was pelleted via centrifugation for 20 mins at 4°C. The pellet was resuspended in 35 mL sonication buffer (20 mM Tris/HCl at pH 7.4, 2 mM MgCl₂, and 1 mM EGTA). The solution was then transferred to 50 mL beaker and sonicated at 15 amps six times (MRSA cells at 20 amps, twelve times) for 30s with 30s rests in between each sonication, and keeping the beaker submerged in iced water to avoid overheating. After sonication, the solution was centrifuged for 15 mins at 4°C and 12,000 rpm using a Beckman Coulter high-speed centrifuge, JA-20.50 rotor. At this point, the supernatant contained the membrane and the pellet containing debris was discarded. A second centrifugation was performed for 1 hour at 4°C and 44,000 rpm using a Beckman Coulter ultracentrifuge, rotor Ti70. The pellet was removed and weighed in Eppendorf tubes before being stored at -20°C.

2.2.5. Oxygen Consumption Assays and Drug Screen

A drug screen was performed from a list of FDA-approved drugs that were deemed “high-hit” via a series of *in silico* screening. The criteria used to determine whether the drugs were “high-hit” or not was based on how well they bound the quinol binding loop of *E. coli* cytochrome *bd-I*. The oxygen consumption rate of cytochrome *bd-I* membrane in the presence of these drugs was tested using the Rank Brother LTD Dual Digital Model 2D (refer to manual for calibration). The drugs tested were atovaquone and naphthoquinone at various concentrations in 5% DMSO. To measure the oxygen rates, 200 μL of the drugs was added to an assay volume of 4mL (3580 μL of HEPES buffer, with 20 μL of the *bd-I* membranes, and 200 μL of succinate as the electron donor).



Figure 2.2. Oxygen Electrode Apparatus. The oxygen electrode (blue) consists of chambers that are connected to temperature-controlled circulating water bath.

2.2.6. Succinate-dehydrogenase Assays

A solution containing 50 mM Tris–HCl buffer (pH 8.5) and 0.02% DDM was made. A mixture containing 400 μM PMS, 8 mM succinate and 0.5% final concentration of bacteria membranes were preincubated for 30 mins at 37° C before adding to Tris/DDM mixture. Any

drug that was being added was performed after the incubation of the PMS, succinate, and membranes after which the solution was transferred to a cuvette along with the Tris/DDM solution. To start the reaction, 50 μ M of DCPIP was added which produced a starting OD about 0.8 to 1 at 600 nm. A kinetic read was immediately performed using Cary WinUV Kinetics application on a spectrophotometer with a single run lasting about 15 mins. A set point was selected between each run and the rate of DCPIP reduction was calculated at OD₆₀₀.

2.2.7. Growth Curves

Growth curves for bacterial strains were obtained by performing the traditional conical flask method. Overnights were set up for the bacteria and 50 μ L was used to inoculate 50 mL fresh media the next day. The culture was left to grow at appropriate rpm and temperature and the optical density was measured at 600 nm every hour until stationary phase.

2.2.8. Plate Reader Assays

Cells were cultured overnight in LB medium (*E. coli*) or TSB medium (MRSA) in sterile conical flasks and supplemented with the appropriate antibiotics where necessary. The next day, 2 x 50 mL cultures were made up in 250 mL conical flasks and the media choice was M9 minimal medium for *E. coli* and TSB medium for MRSA. These cultures were inoculated with 50 μ L of the overnight culture and was left to grow at 37°C and 180 rpm until an OD of 0.6 was reached at 600 nm. Cultures that grew beyond an OD of 0.6 were diluted using the appropriate growth media. Antibiotics were excluded from the 50 mL cultures as this could affect the results of the experiment. The stock solutions of the drugs being tested were prepared in the correct solvent so that the final concentration of drug is 40x lower than working concentration. The 96 well plate (Greiner F-bottom sterile 96-well) was then prepared using a multichannel pipette by adding 100 μ L of a 2x concentrated growth medium, 61.7 μ L sterile milliQ H₂O, 5 μ L of the drug and 33.3 μ L of cell culture which was added last. This resulted in

a final OD₆₀₀ of 0.1 in the 96 well plates. A negative control was performed for each experiment which contained the solvent only and no drug. Blanks were also prepared for each experiment and consisted solely of the solvent, water, and growth medium. The plate reader settings were as follow: 145 cycles, 300s apart (totalling 12 hours) and shaking of 200 rpm double orbital pattern.

2.2.9. Viability Assays

For susceptibility assays for *E. coli* bacteria, two overnight cultures were grown in sterile conical flasks for the appropriate bacterial strain. The next day, 100 µL of an overnight culture was used to inoculate 10 mL fresh M9 medium with 0.1% casamino acids and glycerol as carbon source. The cultures grew until an OD₆₀₀ of 0.3 and was diluted to 0.125 in fresh M9 medium. The diluted cultures were statically incubated at 37°C for 30 min. Following this, 20 µL of each stock concentrations of the drug being tested was added to row A (10⁰ dilution) of a 96-well microplate. For the DMSO-only control, two wells were used so an average could be calculated for the data analysis. After the static incubation, 180 µL of the bacterial culture was added to the stock concentrations in row A. The bacteria-drug mixture was thoroughly mixed using a multichannel pipette and the microplates were placed in a 37°C incubator for 3 hours. After incubation, the microplates were placed on ice to stop further growth and 180 µL of sterile 1 x PBS was added to the remaining wells. The wells were mixed thoroughly using multichannel pipette then 1:10 dilutions were performed from the first row downwards by taking 20 µL from row A and adding to 180 µL PBS in row B. Row B was mixed and 20 µL was taken from row B and added to row C. This continued until all 8 rows were completed, which generated dilutions in the range 10¹ to 10⁷. Afterwards, 5 µL of each dilution was spotted onto a gridded LB agar plate in triplicate (for each biological repeat, 3 technical repeats were performed). The spots were left to absorb by the medium for approximately 20 min and plates were incubated overnight at 37°C.

2.2.10. Data Analysis

All Data analysis for the bacterial assays were analysed via GraphPad Prism. Dose response curves for oxygen consumption assays, viability assays and plate reader assays were fitted to the sigmoid $y = min + (max - min)/(1 + 10^{(n*(logIC_{50}-X)})}$ using nonlinear regression.

2.3. Genetic Methods

2.3.1. Isolation of DNA plasmid

To isolate DNA plasmid, QIAprep Spin Miniprep Kit (QIAGEN) was used, and instructions were followed as per the manufacturer's manual.

2.3.2. Polymerase Chain Reaction (PCR)

Colony PCR was performed to isolate the plasmid of interest in a 50 μ L total reaction volume. The mixture consisted of 25 μ L 2 x Master mix, 21.5 μ L sterile milli-Q water, 1.5 μ L forward primer and 1.5 μ L reverse primer and 0.5 μ L of resuspended colonies. The PCR solution was added to PCR tubes and the reaction was carried out in a T3000 Thermocycler (Biometra®) or Veriti Thermal Cycler (Applied Biosystems) machine. The conditions for the PCR reactions were: 94 °C initial temperature; 94°C for 15 s for 35 cycles; 50 °C for 30 s, 72 °C for 3 min and the last step was 72 °C for 5 min. The final hold temperature was 4°C.

2.3.3. DNA Purification

Purification of PCR products were performed using a QIAquick PCR Purification Kit as per the manufacturer's manual, but milli-Q waster was used instead of an elution buffer.

2.3.4. Agarose Gel Electrophoresis

The amplified PCR products were analysed via gel electrophoresis using 1% agarose gels, 10 μ L SYBR safe (per 100 mL molten agarose) and 1 x TAE buffer. Amplified DNA

samples were mixed with 6 x loading dye and a 5 µL of '1kb DNA ladder' (Promega) was loaded to determine the size of bands. The loaded gel ran for 45 min at 150 V and ~300 mA. The DNA bands were visualised using a UV transilluminator.

2.3.5. Cloning of *E. coli* cytochrome *bd-II* oxidase using Gibson Assembly

2.3.5.1. PCR Reactions to Amplify Cytochrome *bd-II* Oxidase and Vector Backbone

Two separate PCR reactions were carried out: first, the vector backbone was amplified and then the *E. coli* oxidase operon for cytochrome *bd-II* was amplified. Colony PCR was used to amplify the pSU2718G vector backbone from an *E. coli* Top10 strain harbouring pSU2718-G-*cydABX* plasmid using forward primer, pSU_his_F, and reverse primer, 2R_pSU2718. For the amplification of *E. coli* cytochrome *bd-II* oxidase operon, *appCBX*, amplified from an *E. coli* ST131 EC958 WT strain using forward primer, *appCBX_F_v2*, and reverse primer, *appCBX_F_v2*. Extraction of the DNA harbouring the *appCBX* operon was performed using a GenElute™ Bacterial Genomic DNA Kit (Sigma-Aldrich) as per the manufacturer's instruction manual.

PCR reactions consisted of the following components: 25 µL 2X Q5® High-Fidelity DNA Polymerase 2X Master Mix, 21.5 µL sterile milli-Q water, 1.5 µL forward primer (300 nM final), 1.5 µL reverse primer (300 nM final) and 0.5 µL of resuspended colony for the vector amplification or 0.5 µL of genomic DNA for the amplification of the *appCBX* operon. Thermal cycling parameters for the PCR reaction were: 94 °C for 5 min followed by 25 cycles of 94 °C for 15 s, 50 °C for 30 s, and 72 °C for 3 min. Samples were then held at 72 °C for 5 min and stored at 4°C until they could be transferred to -20 °C for storage

2.3.5.2. Gibson Assembly

A Gibson Assembly kit was used for the assembling of the amplified *E. coli* cytochrome *bd-II appCBX* operon with the linearised pSU2718G vector backbone. The Gibson assembly

was performed using the Gibson Assembly® Cloning Kit (NEB) as per the manufacturer's instructions (manualE2611_E5510). The resultant plasmid, pSU2718G_ *appCBX*, was then introduced to chemically competent NEB® 5-alpha competent *E. coli* cells.

2.3.5.3. Screening PCR to identify pSU2718G_ *appCBX*

A colony PCR was carried out to identify the presence of pSU2718G_ *appCBX* with a desired band of 3378 bp. Primers used for the screening PCR were pSU2718seq_200_F (275) and pSU2718seq_200_R (276) (Table 2.3).

2.3.5.4. Isolation of pSU2718G_ *appCBX* plasmid

Following the cloning of the *appCBX* operon with pSU2718G vector backbone, the QIAprep Spin Miniprep Kit (QIAGEN) was used for the extraction of the pSU2718G_ *appCBX* from *E. coli* DH5 α competent cells as per the manufacturer's protocol. The only alteration made to the manufacturer's protocol is that sterile milli-Q water was used instead of elution buffer.

2.3.6. Expression of recombinant cytochrome *bd* complexes in oxidase null mutant

2.3.6.1. Preparation of *E. coli* chemically competent cells

A 10 mL overnight culture was prepared by inoculating fresh LB media with the appropriate bacterial strain. 20 mM (final concentration) of glucose was added to the culture where necessary (to respiratory mutant strains that grow slowly), and the culture was incubated overnight at 37°C and 180 rpm. The overnight culture was used to inoculate 10 mL of SOC medium in a 1:1000 dilution and left to incubate at 37°C and 180 rpm until OD₆₀₀ was approximately between 0.4 and 0.6. The culture was then chilled on ice for 10 min after which 5 mL of the cell suspension was centrifuged for 10 min at 3,500 rpm and 4°C. The supernatant was discarded, and the pellet was gently resuspended in 200 μ L ice-cold TB buffer. To make

100 mL TB buffer, 10 mM HEPES pH 6.7, 15 mM CaCl₂, 55 mM MnCl₂ and 250 mM KCl were added to distilled water before being filter sterilised. The cell suspension was incubated on ice for 10 min and centrifuged for 5 min at 3,500 rpm and 4°C. The pellet was gently resuspended in 186 µL ice-cold TB buffer and 14 µL DMSO was added. The newly made competent cells were shock-frozen in liquid nitrogen and stored at -80°C.

2.3.6.2. Transformation of cytochrome *bd* complexes into *E. coli* chemically competent cells

Firstly, 0.5 µL of plasmid DNA was added to 100 µL chemically competent cells and the mixture left on ice for 1 hour. The mixture was then incubated at 42 °C for 1 min in a water bath after which it was left on ice for 20 min. 1 mL of SOC media was added to the cell/DNA mixture and incubated for 2 hours at 37 °C and 180 rpm. 100 µL of the previously incubated cell mixture was plated out on LB media supplemented with the appropriate antibiotic or supplementary carbon source, if required. The remaining cells were harvested by centrifuging for 5 min at room temperature and 3000 rpm. Cell pellets were suspended in 100 µL fresh SOC media and plated out. Both plates were incubated overnight at the appropriate temperature for maintenance of the plasmid.

2.3.6.3. Restriction Enzyme Digest

Restriction enzyme digests were carried out on purified DNA plasmids. The total digest volume was 10 µL and contained: 5.5 µL sterile milli-Q water, 1 µL of Promega buffer D, 3 µL DNA plasmid and 0.5 µL NcoI (Promega). The mixture was gently mixed and incubated at 37°C for 3h. After incubation, 2 µL of 6 x DNA loading buffer was added to the mixture and the 12 µL samples were ran on 1% TAE agarose gel alongside Promega 1Kb ladder (5 µL ladder and 1µL dye). The DNA bands were visualised using a UV transilluminator.

2.3.7. Site-directed Mutagenesis of *E. coli* Cytochrome *bd-I* Operon

2.3.7.1. DNA Plasmid Isolation

QIAprep Spin Miniprep Kit (QIAGEN) was used to isolate the plasmid, pSU2718-G-*cydABX*, from *E. coli* TOP10 cell pellets as per the manufacturer's manual instructions. The only variation from the protocol is the use of sterile milli-Q water instead of elution buffer.

2.3.7.2. Restriction enzyme digest to quantify plasmid

Restriction enzyme digest was carried out as outlined in section 2.5.2 to quantify and identify the plasmid. For this experiment, BamHI was the restriction enzyme and Cutsmart buffer was used.

2.3.7.3. Q5 Site-directed Mutagenesis

Site-directed mutagenesis was established by use of a Q5® Site-Directed Mutagenesis Kit as outlined in manufacturer's protocol (E0554). The primers used in the mutagenesis study are outlined in Table 2.3 (see section 2.1.3).

2.3.7.4. Transformation of *E. coli* cytochrome *bd-I* plasmid into competent cells

The product of the Q5 site-directed mutagenesis was transformed into NEB 5-alpha competent cells. First, 50 µL of competent cells were pipetted into transformation tubes stored on ice. Afterwards, 5 µL of the mutagenesis reaction was added to the cell mixture before the tube was carefully flicked 4-5 times. The mixture was placed on ice for 30 min and was exposed to heat shock for at 42°C for 30 s before being placed on ice for 5 min. 950 µL of sterile room temperature SOC medium was pipetted into the mixture. The mixture was incubated at 37°C for 60 min and rotated at 250 rpm. The tube containing mixture was carefully flicked 4 – 5 times before performing several 10-fold serial dilutions in SOC media. Pre-incubated (37°C) selection plates containing LB agar and gentamicin were used to spread 50-100 µL of each

dilution. The remaining cells were harvested at 3500 rpm for 5 min before being resuspended in 100 μ L fresh SOC and plated onto selection plates. Plates were incubated overnight at 37°C.

2.3.7.5. Restriction digest to identify mutation of interest

Restriction enzyme digest was carried out as outlined in section 2.5.2 to identify specific mutations to the plasmid. Agarose gels were prepared as in section 2.3.3 and visualised using a UV transilluminator. The composition of each site-directed mutagenesis restriction digest reaction is outlined below:

For F269A mutagenesis, the restriction digest mixture consisted of 6.5 μ L sterile milli-Q water, 1 μ L 10X rCutSmart™ Buffer (NEB), 2 μ L DNA plasmid and 0.5 μ L BsmI restriction enzyme.

The I295A mutagenesis restriction digest mixture contained 6.5 μ L sterile milli-Q water, 1 μ L 10X NEBuffer™ r2.1 (NEB), 2 μ L DNA plasmid and 0.5 μ L BsrDI restriction enzyme.

F390A mutagenesis restriction digest mixture contained 6.5 μ L sterile milli-Q water, 1 μ L 10X rCutSmart™ Buffer (NEB), 2 μ L DNA plasmid, 0.5 μ L BssHIII and 0.5 μ L BamHI restriction enzymes.

For L253A mutagenesis, the digest was composed of 6.5 μ L sterile milli-Q water, 1 μ L 10X NEBuffer™ r3.1, 2 μ L DNA plasmid and 0.5 μ L PvuII restriction enzyme.

The Y387A mutagenesis restriction digest mixture contained 6.5 μ L sterile milli-Q water, 1 μ L 10X rCutSmart™ Buffer (NEB), 2 μ L DNA plasmid and 0.5 μ L BsmI restriction enzyme.

2.4. *In silico* Methods

2.4.1. Structural Modelling

A 3D molecular structure of *E. coli* cytochrome *bd-I* was obtained from Protein Data Bank (PDB) and constructed using Phyre2 (Figure 2.3). The construction of *E. coli* cytochrome

bd-I and MRSA was performed via Phyre2 for homology modelling (Kelley *et al.* 2015). The modelled *E. coli bd*-I structure must be homologous to the structure present on PDB which are 6RKO (Safarian *et al.* 2019) and 6RX4 (Theßeling *et al.* 2019). Structural analyses were performed using PyMOL. All pre-molecular docking work of the protein structures were performed by host lab (Webster, C.M. (2023) PhD thesis, University of Kent).

2.4.2. Analysis of Ligands

Three-dimensional structures of 1993 FDA-approved drugs were obtained from the e-Drug3D online database with drugs that had a molecular weight of ≤ 2000 g/mol (Pihan *et al.* 2012). The drug ligands were downloaded in .sdf format and converted to .pdb using PyMOL. The .pdb format was later converted into a .pdbqt format using python script from MGL Tools (Morris *et al.* 2009).

2.4.3. Molecular Docking

As shown in Figure 2.3, the molecular docking of the protein-ligand was performed using AutoDock Vina (Trott and Olson 2010). Prior to this, AutoDock Tools (Morris *et al.* 2009) was used to determine the docking parameters that would be used for the docking of ligands into various sites on the cytochrome *bd* enzyme. PyMOL molecular visualisation software was also used to assess the binding site of the protein (Seeliger and De Groot 2010). The docking box size for the Phyre2 model of *E. coli* cytochrome *bd*-I protein structure was $28 \text{ \AA} * 28 \text{ \AA} * 30 \text{ \AA} = 23520 \text{ \AA}^3$ (Webster, 2023). For automation of docking, Bash Script (Vina_auto.sh) was used. Substrates and published inhibitors of cytochrome *bd*-I was used as controls to help determine the correct size and position of the docking box.

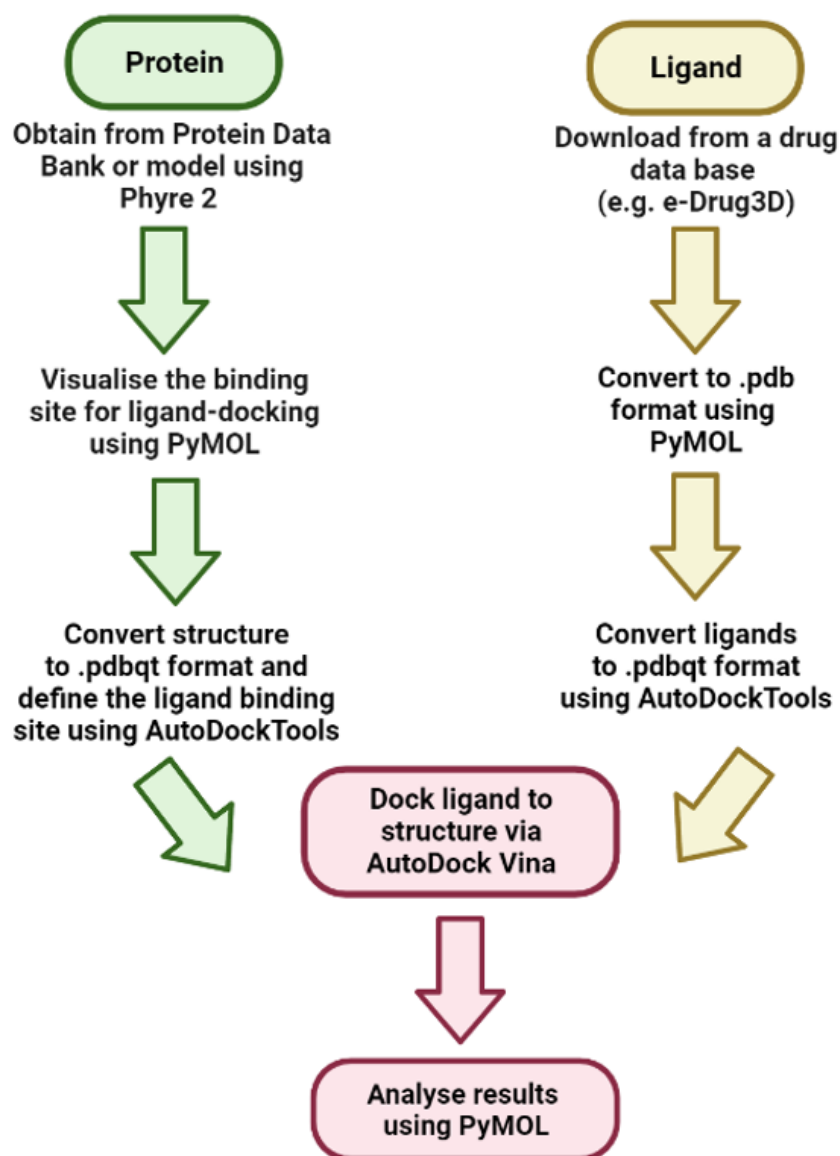


Figure 2.3. Molecular Docking Pipeline. Protein structures were obtained from PDB or modelled using Phyre2. FDA-approved drugs were downloaded from e-Drug3D database. Docking of the ligands to the structure was performed using AutoDock Vina.

2.4.4. Analysis of Molecular Docking

The results generated by AutoDock Vina docking were analysed based on predicted binding affinities (kcal/mol). The dissociation constant (K_d) was estimated using the equation $K_d = \exp(\Delta G/(R \cdot T))$ with ΔG = binding energy (kcal/mol), R = gas constant = (1.986 cal/mol*K) and T = temperature (298K). Drug ligands were manually analysed in PyMOL to identify interactions with the quinol binding site.

Chapter 3

Engineering and characterisation of *E. coli* strains that express single respiratory oxidases

3. Engineering and characterisation of *E. coli* strains that express single respiratory oxidases

3.1. Summary

Globally, urinary tract infection (UTI) is a clinical concern as it is one of the most common infections in humans. More than 80% of UTIs are caused by uropathogenic *E. coli* such as the multidrug resistant strain, EC958. The resistance of UPEC to antimicrobials are largely due to reoccurring infections which results in excessive use of antimicrobials. In developing countries, the overuse of broad-spectrum antibiotics has resulted in a massive resistance of UPEC to antimicrobials which has a huge clinical and financial impact on healthcare. The treatment choice of a UTI is dependent on the classification of the infection such as complicated versus uncomplicated UTIs. Conventional antibiotics such as amoxicillin are rarely effective against UTIs so newer forms of antibiotics such as nitrofurantoin are being used. However, UTI-causing pathogens are growing resistant to the newer antibiotics which highlights the urgency to develop new treatment methods.

The strain used in this study is an EC958 *E. coli* O25: H4-ST131 multidrug resistant strain (Lau *et al.* 2008) that was isolated from a clinical patient with UTI. Mutants were generated from this strain that expressed only cytochrome *bd-I* or cytochrome *bo'* as their sole respiratory oxidases. These strains were characterised to determine the presence of these oxidases. Recombinant oxidases were also engineered with *E. coli* EC958 cytochrome *bd-I* or cytochrome *bd-II* in an *E. coli* MG1655 'EcoM4' strain lacking all respiratory oxidases for use in future work. *In silico* analyses were performed to identify key residues for the successful binding of drugs in the ubiquinol site of CydA of *E. coli* cytochrome *bd*. Mutagenesis was performed on key residues to simulate the emergence of antimicrobial resistance.

3.2. Introduction

E. coli EC958 is a well-defined *E. coli* O25: H4-ST131 multidrug-resistant strain that is the one of the aetiological causes of UTIs worldwide (Lau *et al.* 2008; Totsika *et al.* 2011; Forde *et al.* 2014; Webster *et al.* 2022). It is reported that UTIs are the most frequently occurring infection in humans with an estimated 40% of women and 12% of men being likely to experience one UTI episode during their lifetime (Brumbaugh, Smith and Mobley 2013; Kot 2019). Overall, uropathogenic *E. coli* (UPEC) accounts for up to 80% of all UTIs (Croxall *et al.* 2011; Totsika *et al.* 2011; Bien, Sokolova and Bozko 2012). The fast-growing resistance of antimicrobials towards UPEC signals an urgent need for the study and design of new antibacterial agents.

3.2.1. Antimicrobial Resistance of UPEC

The resistance of UPEC to antimicrobials are largely due the antimicrobial treatment of recurrent UTIs (Kot 2019). This has resulted in the emergence of MDR UPEC in mainly women with recurring UTIs (Kot 2019). For a UTI to be classified as recurrent, a patient must experience three or more episodes in one year and two or less in under 6 months (Terlizzi, Gribaudo and Maffei 2017). Resistance of UPEC to antimicrobials is a clinical problem, and the resistance of UPEC to antimicrobials are increasing globally (Table 3.1). The higher prevalence of antimicrobial resistance in treating UTIs in developing countries is due to excessive use of broad-spectrum antibiotics which has serious clinical and financial implications (Bartoletti *et al.* 2016).

UTI is a complicated infection that can manifest in many ways such as asymptomatic, bacteriuria, acute, chronic, or recurrent infection (Smelov, Naber and Bjerklund Johansen 2016; Asadi Karam, Habibi and Bouzari 2019). The type of treatment that is administered to a patient is dependent on the classification of UTI or level of severity. Traditionally, antibiotics

such as amoxicillin were effectively used in the treatment of UTIs but due to drug resistance, other antibiotics are now being used. First-line treatments for uncomplicated cystitis include nitrofurantoin and Fosfomycin (Asadi Karam, Habibi and Bouzari 2019; Kot 2019). Another first-line drug used in the treatment of uncomplicated UTIs, trimethoprim-sulfamethoxazole, is now growing resistant to UPEC even in developed countries (Kot 2019) (Table 3.1).

Antibiotic	Developed Countries	Developing Countries
Amoxicillin-clavulanic acid	3.1% - 40%	48% - 83%
Trimethoprim-sulfamethoxazole	14.6% - 37.1%	54% - 82%
Ciprofloxacin	5.1% - 39.8%	55.5% 85.5%
Nitrofurantoin	<1.5% - 13.3%	
Fosfomycin	<1.5%	

Table 3.1. The resistance of uropathogenic *E. coli* to antimicrobials used in the treatment of UTIs in developed and developing countries.

In this study, *E. coli* EC958 strains that expressed either cytochrome *bd-I* or cytochrome *bo'* as their sole respiratory oxidases were characterised. Recombinant oxidases containing either *E. coli* EC958 cytochrome *bd-I* or cytochrome *bd-II* were engineered into *E. coli* MG1655 'EcoM4' strains lacking all respiratory oxidases for future work. Mutations of multiple amino acids were introduced to the quinol site of the CydA subunit of cytochrome *bd-I* to study the emergence of drug resistance to various drugs binding cytochrome *bd-I*.

3.3. Results

3.3.1. Determining the growth and spectral properties for *E. coli* EC958 WT strains and terminal oxidase mutants

Mutant strains expressing single respiratory oxidases (*bd-I* only and *bo'*-only cells) were obtained. The mutants were previously generated in the host laboratory (Webster, C.M. (2023) PhD thesis, University of Kent) from a UPEC EC958 strain which is shown as 'WT cells' in Figure 3.1. Firstly, growth curves were generated to establish the growing characteristics of the strains. All three strains grew to an OD₆₀₀ value between 1.5 and 2.0 with WT cells being the fastest grower. Cytochrome *bd-I* only cells grew the second fastest while *bo'*-only cells grew the slowest. Numerous attempts were made at engineering an *E. coli* *bd-II* only strain but there was no success.

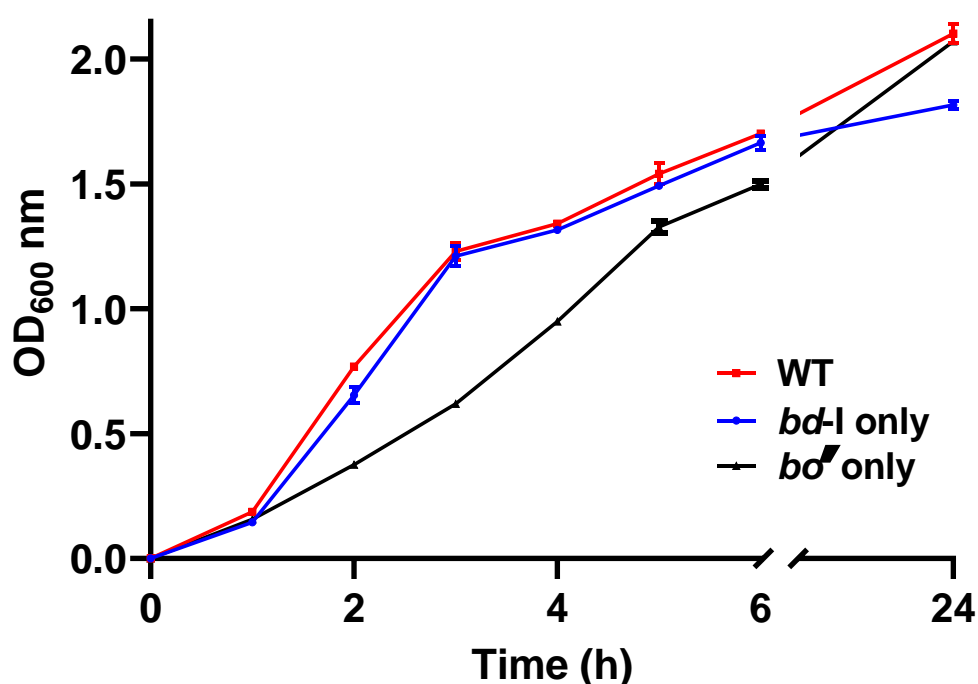


Figure 3.1. Aerobic growth curves for *E. coli* WT, *bd-I* and *bo'*-only cells. Cells were grown in LB media under aerobic conditions. Error bars represent the \pm standard deviation of 2 biological repeats. The OD₆₀₀/h for each growth curve was obtained and a one-way ANOVA performed at timepoint 2 – 5. The p-value is 0.62 which means that there is no statistical difference between the curves and the null hypothesis is accepted.

To confirm the presence of the relevant oxidase in each strain, CO difference spectra were recorded. Figure 3.2 shows whole cell CO difference spectra for *E. coli* WT, *bd-I* and *bo'*-only cells. This technique exploits the different absorption characteristics of haem cofactors in different redox and ligation states that can be used to confirm the correct assembly of a particular terminal oxidase. One of the most notable features is the presence of a peak at 640 nm which is characteristic of the CO-bound ferrous form of haem *d* (Poole *et al.* 1989). Haem *d* is not detected in mutant strains expressing only cytochrome *bo'* (Figure 3.2C). A trough at 442 nm is most likely caused by cytochromes *b₅₉₅* and *d* (Poole *et al.* 1989). The peak at around 414 nm is due to the presence of the reduced haem *o*-CO complex and can be seen in WT strain (Figure 3.3A) and strain expressing only cytochrome *bo'* (Figure 3.2C).

Figure 3.3 illustrates the reduced minus oxidised whole-cell spectra for *E. coli* EC958 WT, *bd-I* only and *bo'* only cells which showcases most of the distinctive features of each strain. *E. coli* *bd-I* only cells had a distinctive peak at 630 nm which is representative of reduced haem *d* (Figure 3.3B). As expected, the peak at 630 that is representative of haem was absent in cytochrome *bo'* only cells (Figure 3.3C). A distinctive band at 595 nm present in *bd-I* only cells is due to high-spin *b₅₉₅* (Lorence, Gennis and Koland 1986). Cytochrome *b₅₅₈* is present at the peak 558 nm which contributes to Soret band at 426 nm (Poole *et al.* 1989). The troughs at 650 and 680 nm seen in both WT (Figure 3.3A) and *bd-I* only (Figure 3.3B) are caused by the peroxy- (Poole and Williams 1988) and oxy- (Poole 1983) forms of cytochrome *bd*.

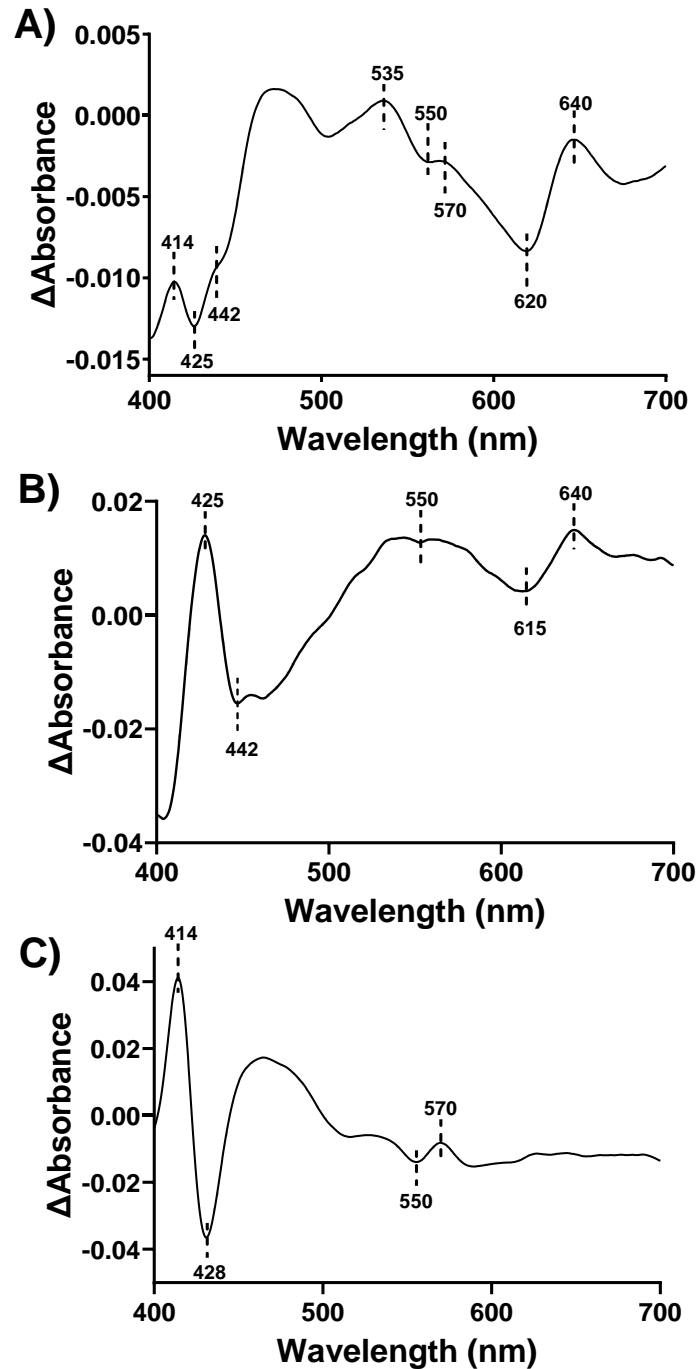


Figure 3.2. CO difference whole cell spectra of *E. coli* EC958 WT, *bd-I* only and *bo'*-only. A reduced spectrum was obtained via the addition of sodium dithionite while CO-reduced data was obtained by exposing reduced sample to carbon monoxide for 5 min. To obtain a CO difference spectrum, the CO-reduced data was subtracted from the reduced data. **A)** WT spectra with peaks representative of all three oxidases. **B)** Spectra of cells containing cytochrome *bd-I* only oxidase, represented by a peak at 640 nm. **C)** Spectra of cells containing cytochrome *bo'* only oxidase which explains the missing peak at 640 nm.

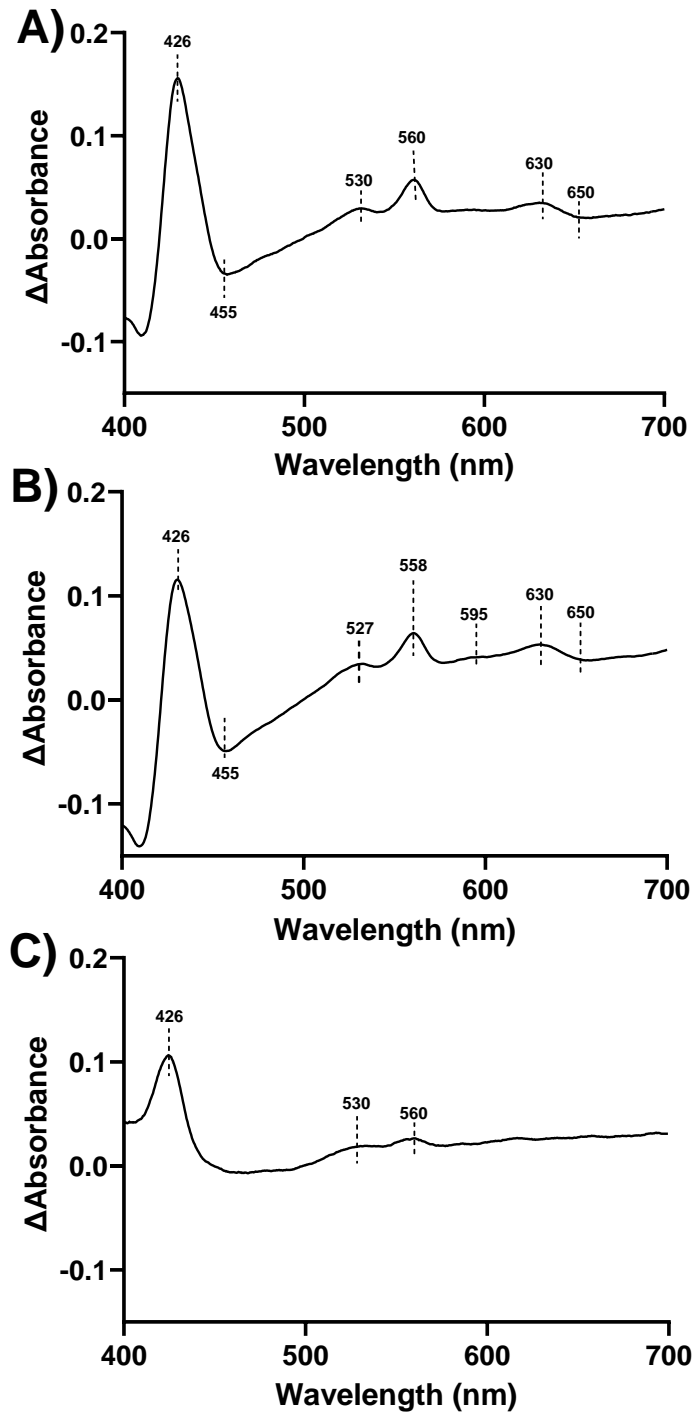


Figure 3.3. Reduced *minus* oxidised whole cell spectra of *E. coli* EC958 WT, *bd-I* only and *bo'*-only. A reduced *minus* oxidised spectra was obtained for A) WT, B) *bd-I* only and C) *bo'*-only cells. Reduced *minus* oxidised spectra were obtained by subtracting the oxidised data from the reduced data. Reduced data was obtained via the addition of sodium dithionite while oxidised data was obtained via the addition of ammonium persulphate.

3.3.2. Spectral analysis of *E. coli* EC958 cytochrome *bd-I* only membranes

To circumvent potential issues with inhibitor compounds accessing cytochrome *bd-I* in the inner membranes of whole cells, oxygen consumption assays were performed on isolated membranes of the *E. coli* EC958 *bd-I* only strain. As cytochrome *bd-I* is highly expressed under low oxygen levels, *E. coli* EC958 *bd-I* only cells were cultured under the following conditions: 1 L of medium in 2 L conical flasks grown at 130 rpm and 37 °C. As mentioned in section 3.3.1, all distinctive spectral properties relating to cytochrome *bd-I* are present in the reduced *minus* oxidised (Figure 3.4A) and CO difference (Figure 3.4B) spectra. The most distinctive feature of cytochrome *bd* are the peaks at 630 nm (reduced *minus* oxidised) and 640 nm (CO difference) (Poole *et al.* 1989). Cytochrome *b₅₅₈* contributes to the peak at 558 nm in Figure 3.3A along with the Soret band at 426 nm (Poole *et al.* 1989).

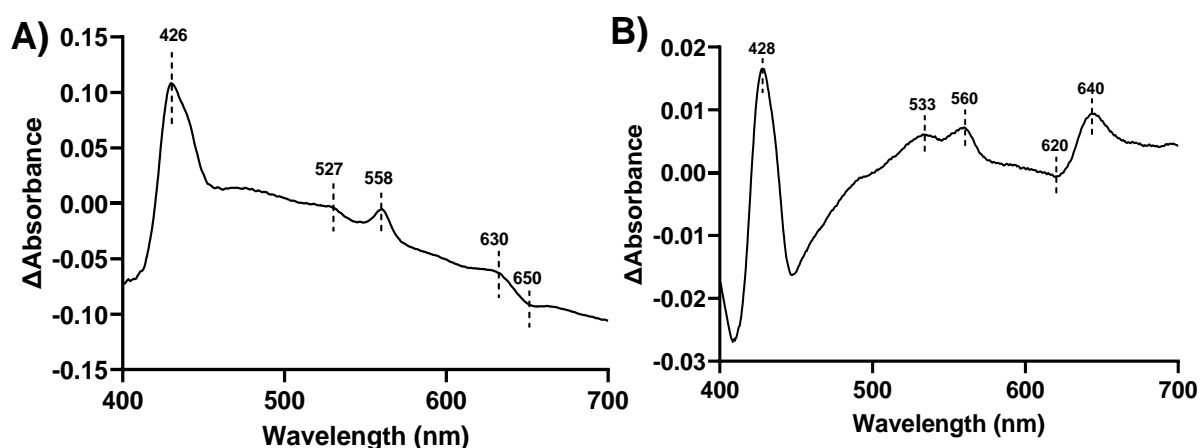


Figure 3.4. Difference spectra of *E. coli* EC958 cytochrome *bd-I* only membranes. A) Reduced *minus* oxidised spectrum with a final concentration of 50 mg/mL membranes. B) CO difference spectrum with a concentration of 50 mg/mL membranes. Oxidised spectra were recorded following the addition of ammonium persulphate. Reduced spectra were recorded following the addition of sodium dithionite, while CO-reduced spectra were recorded following exposure of reduced samples to carbon-monoxide for 5 min. Reduced *minus* oxidised spectra were obtained by subtracting the oxidised data from the reduced data. To obtain CO difference spectra, CO-reduced data was subtracted from the reduced data.

3.3.3. Optimisation of an oxygen consumption assay to assess the inhibition of cytochrome *bd* activity in purified membranes

To assess the inhibition of cytochrome *bd*-I activity, an oxygen consumption assay was developed using a known inhibitor of cytochrome *E. coli* *bd*-I oxidases, thenoyltrifluoroacetone (TTFA). TTFA is a known inhibitor of *E. coli* cytochrome *bd*-I where 1 mM of TTFA has been shown to diminish ubiquinol-1 oxidase activity of the purified enzyme by 35% (Meunier *et al.* 1995) (Borisov *et al.* 2011). A dose response curve was generated for TTFA activity against *E. coli* EC958 *bd*-I only membranes and resulted in an IC_{50} of 1.4 ± 0.1 mM (Figure 3.5). To estimate median inhibitory concentrations (IC_{50}), dose response data were fitted to the sigmoid $y=Bottom + (Top-Bottom)/(1+10^{((LogIC50-X)*HillSlope)})$ equation using nonlinear regression (GraphPad). Raw data demonstrating an example of how the fits were calculated is illustrated in Appendix A.1.

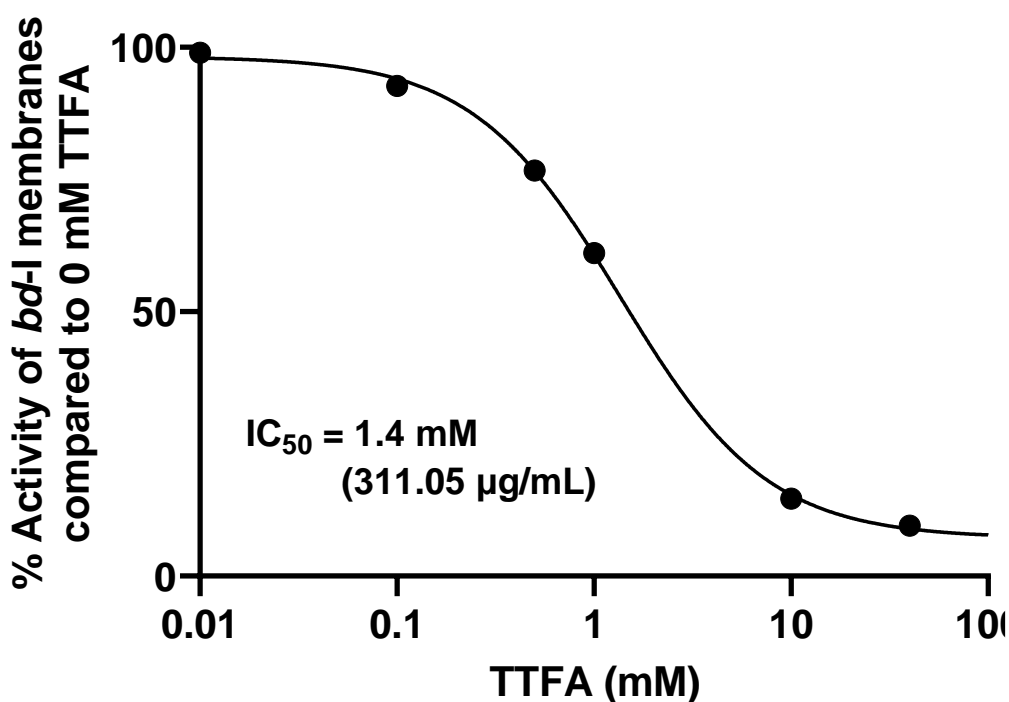


Figure 3.5. Oxygen consumption assay of *E. coli* EC958 cytochrome *bd-I* membranes with TTFA. In the reaction chamber, 500 µg/mL membranes were added to 50 mM HEPES (pH 7.5) with changing concentrations of TTFA in ethanol. The concentration of ethanol was 2.5% v/v in all samples. A final concentration of 8 mM succinate was added to start the reaction. Cytochrome *bd-I* membranes were inhibited by TTFA at an IC_{50} of 1.4 ± 0.1 mM. Data points represent single experiments. Dose response data were fitted to the sigmoid $y = Bottom + (Top - Bottom) / (1 + 10^{((LogIC_{50} - X) * HillSlope)})$ equation using nonlinear regression (GraphPad).

3.3.4. Recombinant expression of terminal oxidases in *E. coli* strain lacking all terminal respiratory oxidases

3.3.4.1. CO difference spectra of *E. coli* MG1655 'EcoM4' strain lacking all terminal respiratory oxidases

An *E. coli* MG1655 'EcoM4' Δ (*cydAB appBC cyoABCD ygiN*) strain lacking all terminal respiratory oxidases (Portnoy, Herrgård and Palsson 2008; Portnoy *et al.* 2010) was used in this experiment. This strain lacked all known terminal respiratory oxidases that are capable of consuming oxygen in *E. coli*. CO difference spectra revealed no distinctive features, which confirms the absence of terminal respiratory oxidases (Figure 3.6A).

The researcher wanted to determine whether isopropyl β -d-1-thiogalactopyranoside (IPTG), an inducer of gene expression, would have any effect on terminal oxidases being expressed in this strain. The addition of IPTG to the culture during the growth of the strain had no effect on oxidases being assembled (Figure 3.6B) which proposes that there are no terminal respiratory oxidases present in *E. coli* 'EcoM4' Δ (*cydAB appBC cyoABCD ygiN*). For transformation with terminal respiratory oxidase plasmids, chemically competent cells were produced for *E. coli* MG1655 'EcoM4' Δ (*cydAB appBC cyoABCD ygiN*) strain lacking all terminal respiratory oxidases.

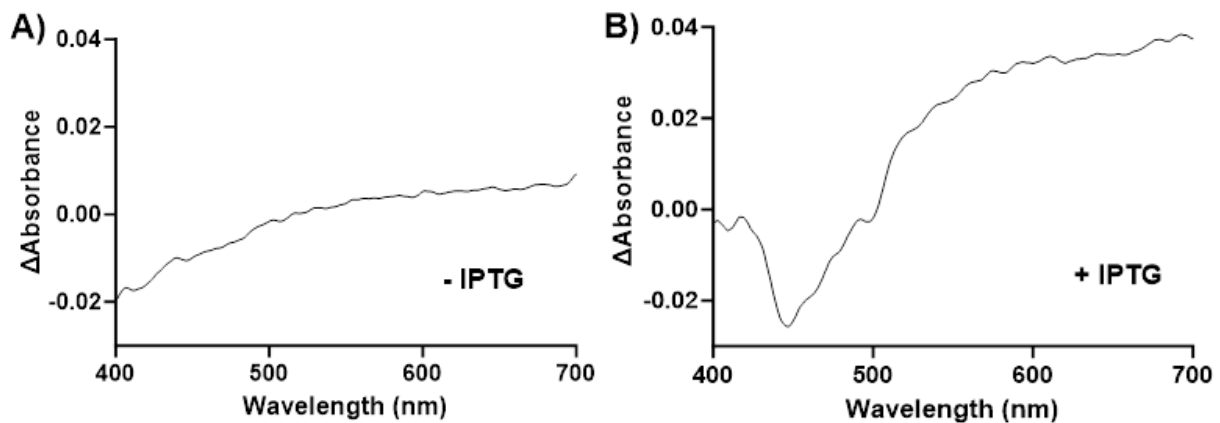


Figure 3.6. CO difference spectra of *E. coli* MG1655 'EcoM4' strain lacking all respiratory oxidases. *E. coli* MG1655 'EcoM4' Δ (*cydAB appBC cyoABCD ygiN*) was engineered by the host laboratory and lacks all terminal respiratory oxidases. Cells were grown under low aeration **A**) without IPTG and **B**) in the presence of 500 μ M IPTG to assess whether the expression of the respiratory oxidases would be induced. No distinctive spectral features were seen for both growth conditions that are indicative of the assembly of *E. coli* terminal oxidases.

E. coli *bd-I* plasmid (pSU2718G *cydABX_HIS6*) was previously cloned by the host laboratory (Webster, C.M. (2023) PhD thesis, University of Kent). The plasmid was engineered harbouring a 6His-tag to facilitate purification via affinity chromatography, if required. The vector backbone, pSU2718, was amplified from an *E. coli* TOP10 strain harbouring the pSU2718G plasmid (strain MS402, Table 2.1). The primers used to amplify the vector backbone were primers 2F_New_pSU2718 and 2R_New_pSU2718 (see Table 2.3). The

cytochrome *bd-I* operon, *cydABX*, was amplified from an *E. coli* EC958 strain via the use of primers *CydABX_F_EC958* and 1RNew_pSU2718. Gibson assembly was used for the cloning of this plasmid before being transformed into *E. coli* DH5 α (MS631, Table 2.1, Shepherd Lab). Mini prep was used to extract the plasmid for sequencing and for future experiments.

To reconfirm the size and presence of pSU2718-G-*cydABX*-6HIS, a restriction enzyme digest was performed for *E. coli* DH5 α strain (MS631, Table 2.1, Shepherd Lab) that the cloned plasmid was first transformed into. Figure 3.7 shows an operon that contains plasmid pSU2718-G-*cydABX*-6*HIS. Based on Figure 3.7, the NcoI restriction is expected to produce three bands after performing gel electrophoresis: the largest band with a size of 3727 bp; the second largest band with a size of 1505 bp; and the smallest band with a size of 698 bp (Figure 3.11).

Following this, the miniprepped *E. coli* *bd-I* (pSU2718G *cydABX*_HIS6) plasmid extracted was chemically transformed into *E. coli* MG1655 'EcoM4' Δ (*cydAB appBC cyoABCD ygiN*) cells lacking all respiratory oxidases (see section 3.3.3.1). Figure 3.8 shows the presence of colonies on the plates which contain the newly transformed *bd-I* plasmid into the *E. coli* MG1655 'EcoM4' strain lacking all oxidases. This new strain is identified as strain MS681 in the Shepherd Lab (Table 2.1).

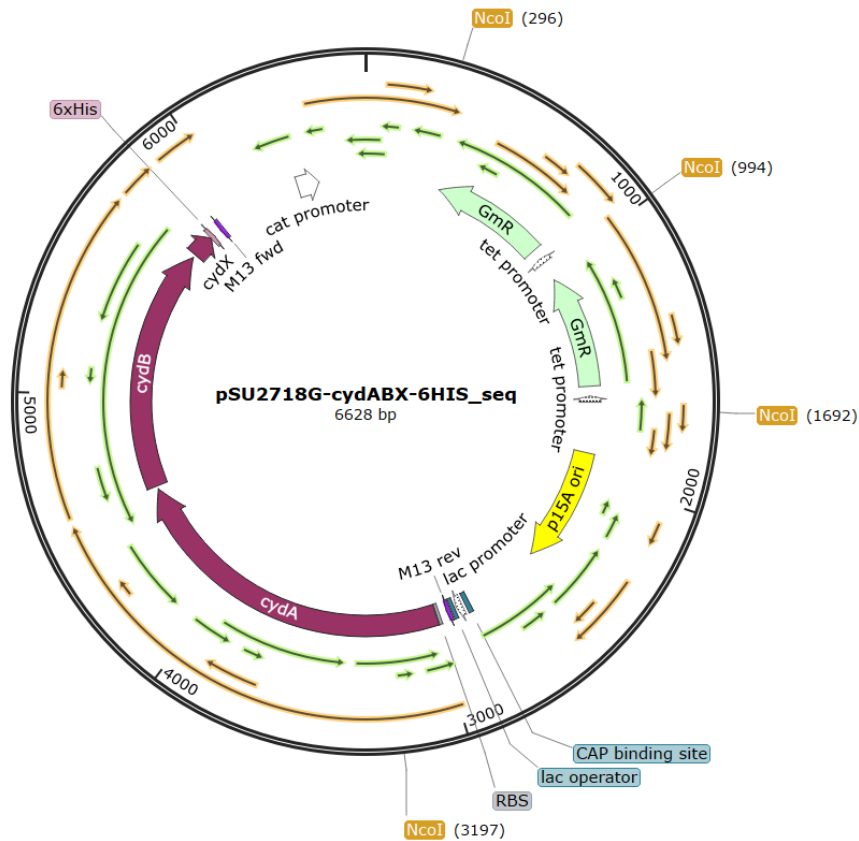


Figure 3.7. Plasmid map of *E. coli* cytochrome *bd-I* plasmid with 6*His tag. The pSU2718G *cydABX_HIS6* plasmid contains the genes *cydA*, *cydB* and *cydX* with a 6*His tag attached to *cydX*. There are two gentamicin resistance genes and four *NcoI* sites.

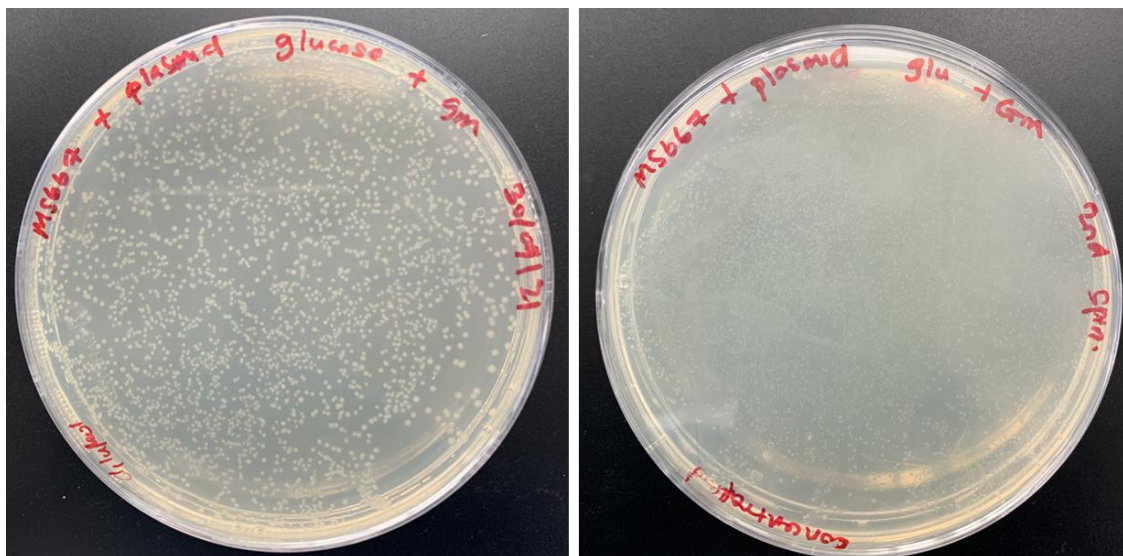


Figure 3.8. Transformation of *E. coli* cytochrome *bd-I* plasmid with *E. coli* MG1655 'EcoM4' strain lacking all terminal respiratory oxidases. *E. coli* cytochrome *bd-I* plasmid (PSU2718G *cydABX_HIS6*) was transformed into *E. coli* MG1655 'EcoM4' $\Delta(cydAB\ appBC\ cyoABCD\ ygiN)$ cells that lack all terminal respiratory oxidases. Colonies can be seen on LB agar plates that represent the new recombinant strain identified as MS681 in the Shepherd lab.

3.3.4.2. Cloning and transformation of cytochrome *bd-II* plasmid to construct *bd-II* only recombinant strain in *E. coli* MG1655 'EcoM4'

For future comparative studies between *E. coli* cytochrome *bd-I* and *bd-II*, cytochrome *bd-II* plasmid (pSU2718-G-*appCBX_6HIS*) was cloned to construct a *bd-II* only recombinant strain in *E. coli* MG1655 'EcoM4' $\Delta(\text{cydAB } \text{appBC } \text{cyoABCD } \text{ygiN})$ strain that lacks all respiratory oxidases. The plasmid was engineered harbouring a 6*His Tag to facilitate purification via affinity chromatography (introduced using the reverse cloning primer), if required. The pSU2718G vector backbone was amplified from an *E. coli* TOP10 strain (MS402, Table 2.1) using the primers pSU_his_F and 2R_pSU2718 (see Table 2.3). The *appCBX* operon was amplified from an *E. coli* EC958 strain (MS662, Table 2.1) via the use of primers *appCBX_F_v2* and *appCBX_R_v2* (see Table 2.3).

The amplified pSU2718G vector backbone and *appCBX* operon were cloned via Gibson assembly and the plasmid was chemically transformed into *E. coli* DH5 α . Following the successful cloning of cytochrome *bd-II* plasmid, colony PCR was employed to identify the colonies with the correctly cloned plasmid (Figure 3.9). The primers used for this PCR were pSU2718seq_200_F (275) and pSU2718seq_200_R (276) (Table 2.3). Lastly, the miniprep procedure (QIAGEN mini prep kit) was used to extract the plasmid for sequencing and for future experiments.

E. coli *bd-II* plasmid (pSU2718-G-*appCBX_6HIS*) was chemically transformed into *E. coli* MG1655 'EcoM4' $\Delta(\text{cydAB } \text{appBC } \text{cyoABCD } \text{ygiN})$ cells lacking all respiratory oxidases (see section 3.3.3.1). This new strain was identified as strain MS696 in the Shepherd Lab (Table 2.1).

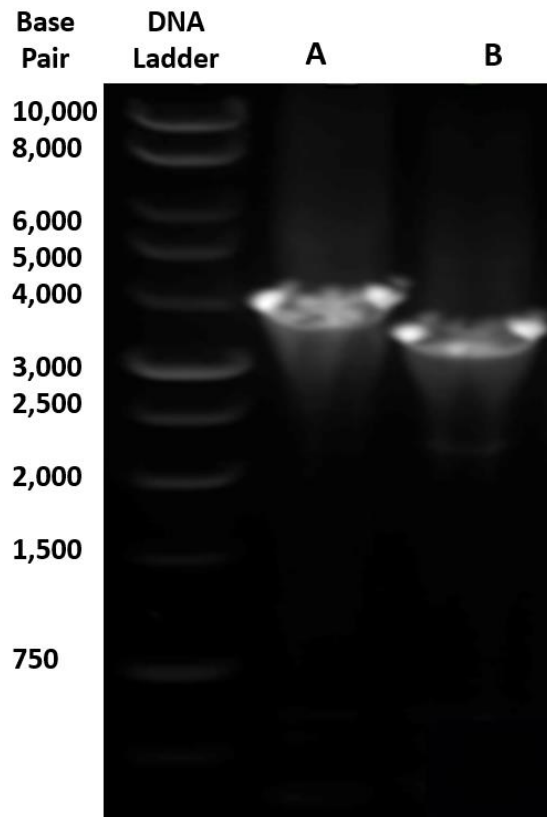


Figure 3.9. Screening PCR for confirming the cloning of *E. coli* cytochrome *bd-II* plasmid. Following the cloning of pSU2718-G-*appCBX*, a colony-PCR was performed to confirm the transformation of pSU2718-G-*appCBX* into *E. coli* DH5 α competent cells. Screening primers, pSU2718seq_200_F (forward) and pSU2718seq_200_R (reverse), were used with an expected band size of 3378 bp. This 1% Agarose gel confirms the presence of a positive hit for pSU2718-G-*appCBX* plasmid in lane B. Lane A is a failed experiment as the band is not the predicted size.

3.3.4.3. Restriction digest to confirm cytochrome *bd-II* plasmid in newly expressed *E. coli* recombinant strain

To confirm the presence of *E. coli* cytochrome *bd-II* plasmid (pSU2718-G-*appCBX_6HIS*) in strain lacking all respiratory oxidases, a restriction digest was performed (Figure 3.11). The gene map (Figure 3.10) shows the operon with the pSU2718-G-*appCBX_6HIS* plasmid and enzyme NcoI that has two sites. The restriction enzyme used for the restriction enzyme digest was NcoI with an expected band size of 5175 bp for the largest cut between two NcoI site containing the *E. coli* cytochrome *bd-II* plasmid (pSU2718-G-*appCBX_6HIS*) (see section 3.3.3.3). Two band sizes can be seen for this restriction digest with

the largest band appearing at 5175 bp and a smaller band size which represents the smaller cut for the NcoI enzymes of 695 bp (Figure 3.11).

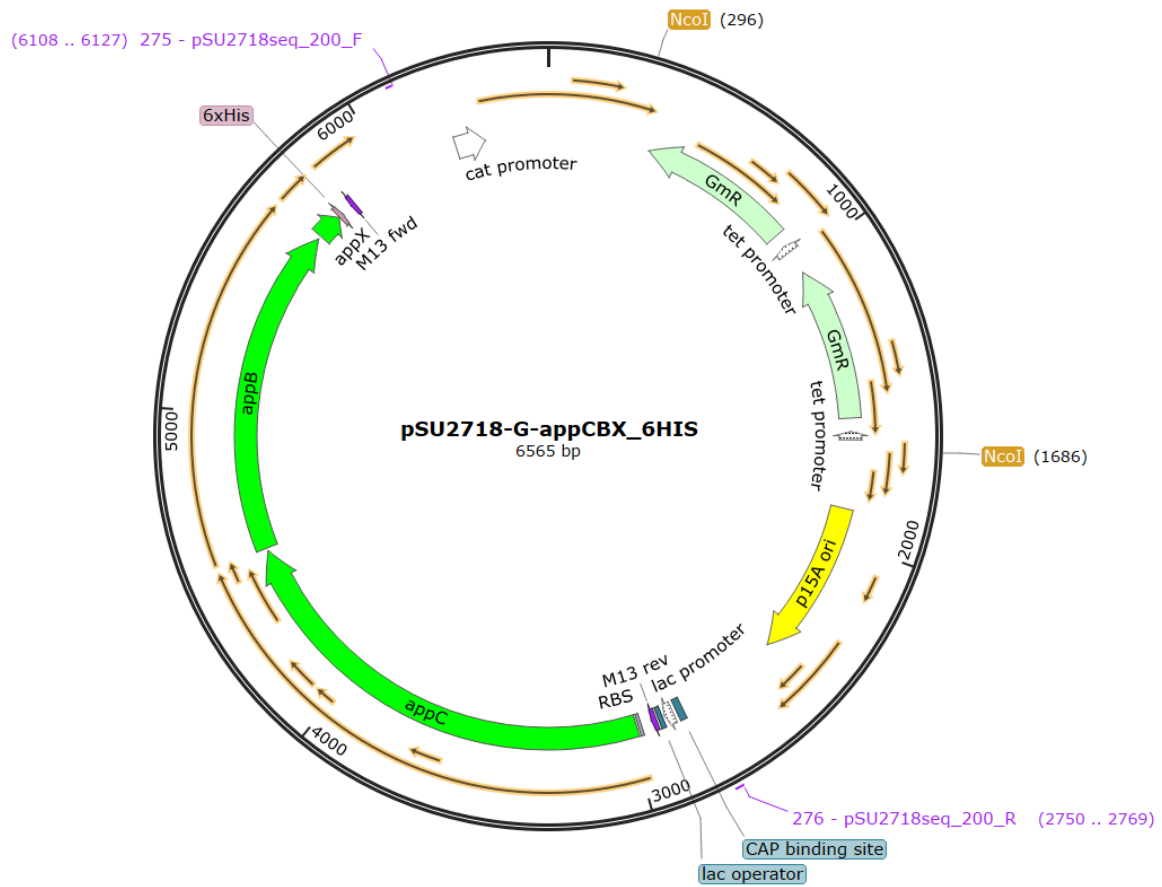


Figure 3.10. Plasmid map of *E. coli* cytochrome *bd-II* plasmid. The operon shows *E. coli* *bd-II* plasmid, pSU2718-G-*appCBX_6HIS*, with 2 gentamicin resistant cassettes and a 6*His tag attached to *appX*.

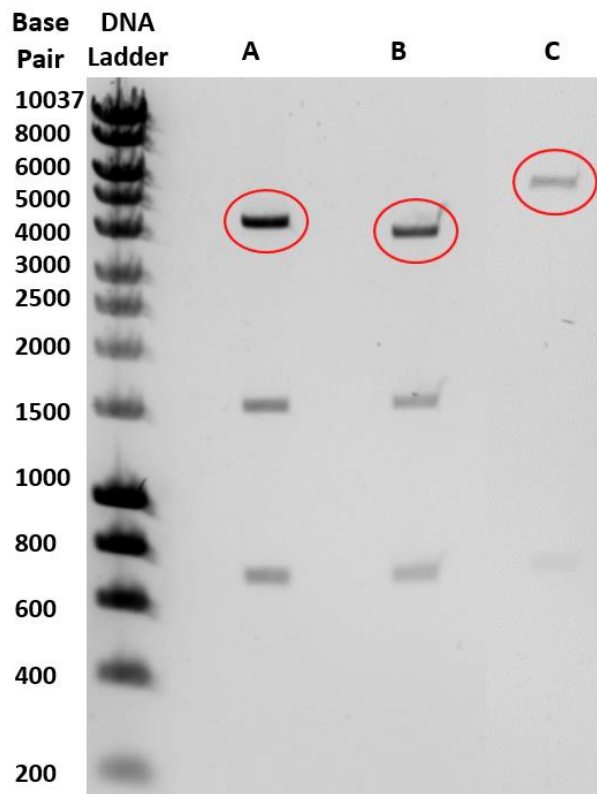


Figure 3.11. Restriction digest to confirm *E. coli* cytochrome *bd* plasmids in strains. Gel electrophoresis was conducted on 1% agarose gel. NcoI enzyme was used to perform a restriction digest to confirm the presence of **A)** *E. coli* cytochrome *bd*-I plasmid in another strain that is not relevant to this study. **B)** *E. coli* cytochrome *bd*-I plasmid (pSU2718-cydABX-HIS6) in *E. coli* DH5 α cells with an expected band size of 3727 bp. In column B, NcoI enzyme had four sites on the operon where the first three sites made two cuts with equal sizes of 695 bp each. This accounted for three bands being present in column B. **C)** *E. coli* cytochrome *bd*-II plasmid (pSU2718G-appCBX-6HIS) in *E. coli* MG1655 'EcoM4' strain lacking all terminal respiratory oxidases with an expected band size of 5175 bp. For column C, the NcoI had two sites on the operon which accounts for equal two bands with expected sizes of 695 bp each.

3.3.4.4. Growth and spectral properties of newly expressed recombinant strains expressing *E. coli* cytochrome *bd*-I and *bd*-II oxidases

Analysis of growth was conducted for the newly expressed recombinant strains expressing either cytochrome *bd*-I or cytochrome *bd*-II in *E. coli* cells (Figure 3.12). Aerobic growth assays revealed that both strains exhibited a small lag in growth before entering exponential phase. Both strains had similar exponential phase and began to hit stationary

phase at the same period. However, *bd*-I only cells had a faster growth rate compared to *bd*-II only cells.

Whole cells were grown, harvested and the membranes isolated for membrane spectra for *bd*-I only and *bd*-II only recombinant strains. Firstly, reduced membrane spectra were obtained for both strains through the addition of sodium dithionite to the samples. After this, the same reduced samples were exposed to carbon monoxide for 5 min to get CO reduced spectra. The reduced data was subtracted from the CO reduced data to get CO difference spectra as shown in Figure 3.13. Here, distinctive peaks can be seen which are representative of the haem groups present in different cytochrome *bd* oxidases. One of the most distinctive features of a spectrum containing cytochrome *bd* is the presence of a peak at around 640 nm which is representative of the ferrous form of haem *d* (Poole *et al.* 1989). The troughs present at around 650 nm are because of the oxygenated form of the haem *d* cofactor (Poole *et al.* 1983). The peak seen at 558 nm is representative of cytochrome *b*₅₅₈ and the small peaks at around 595 nm is representative of cytochrome *b*₅₉₅ (Poole *et al.* 1989).

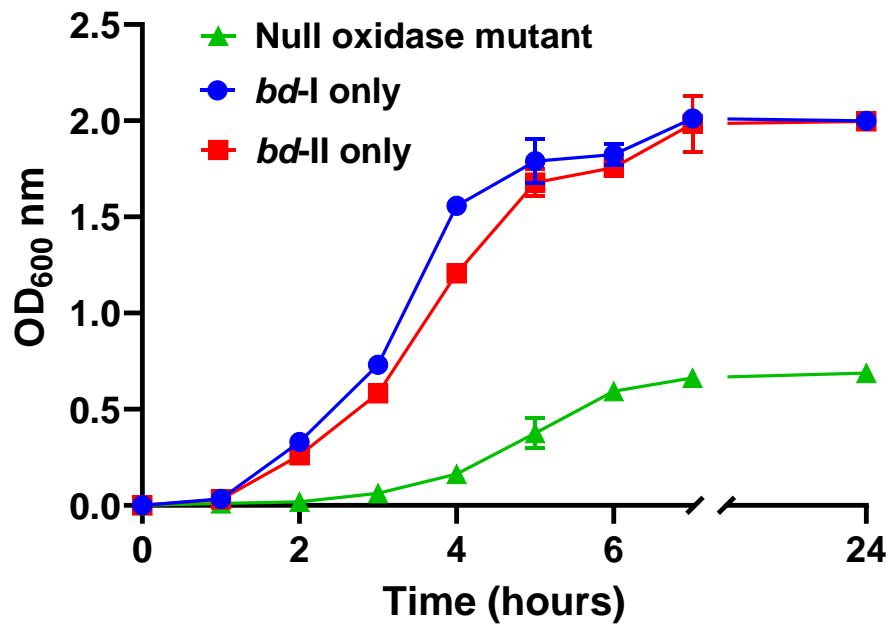


Figure 3.12. Aerobic growth curves for recombinant strains. ‘Null oxidase mutant’ consists of *E. coli* MG1655 EcoM4 cells with all oxidases knocked out. Curves marked as either ‘*bd-I* or *bd-II*’ consist of *E. coli* MG1655 EcoM4 cells with the specified transformed plasmid. Recombinant strains were grown under aerobic conditions in LB medium. Error bars represent +/- standard deviation from 2 biological repeats. The OD₆₀₀/h for each growth curve was obtained and a one-way ANOVA performed at timepoint 3 – 5. The p-value is 0.0008 which means that there is a statistical difference between the curves and the null hypothesis is rejected.

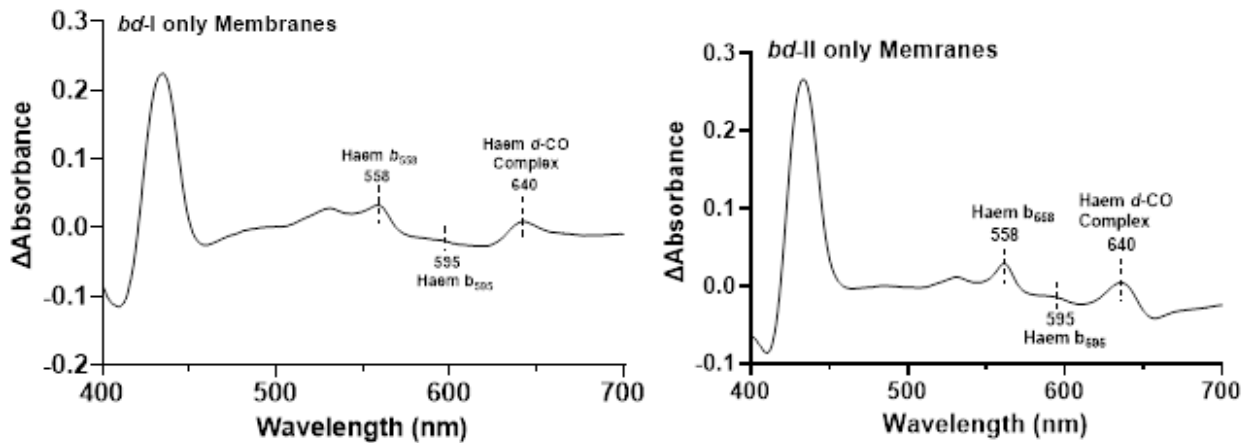


Figure 3.13. CO Difference spectral analysis of membranes isolated from recombinant strains expressing either *E. coli* EC958 *bd-I* only or *bd-II* only oxidases. Reduced spectra were obtained by addition of sodium dithionite after which the same samples were exposed to carbon monoxide for 5 min. The reduced spectra were subtracted from CO reduced spectra to obtain the CO difference spectra.

3.3.4.5. Oxygen consumption assay of recombinant strain expressing *E. coli* EC958 cytochrome *bd-II* only recombinant strain with TTFA

Published data (Meunier *et al.* 1995) and data from this study (Figure 3.5) have demonstrated that TTFA is an inhibitor of cytochrome *bd-I*. To establish the inhibitory effect of TTFA on *E. coli* cytochrome *bd-II*, oxygen consumption assay was performed on membranes of the newly constructed recombinant strain expressing *E. coli* cytochrome *bd-II* as its sole respiratory oxidase to determine its killing effect. As demonstrated in Figure 3.14, TTFA inhibits *E. coli* cytochrome *bd-II* with an IC_{50} of 2.66 ± 0.4 mM which is 1.26 times higher than that of cytochrome *bd-I*. To estimate IC_{50} , dose response data were fitted to the sigmoid $y = Bottom + (Top - Bottom) / (1 + 10^{((LogIC50 - X) * HillSlope)})$ equation using nonlinear regression (GraphPad).

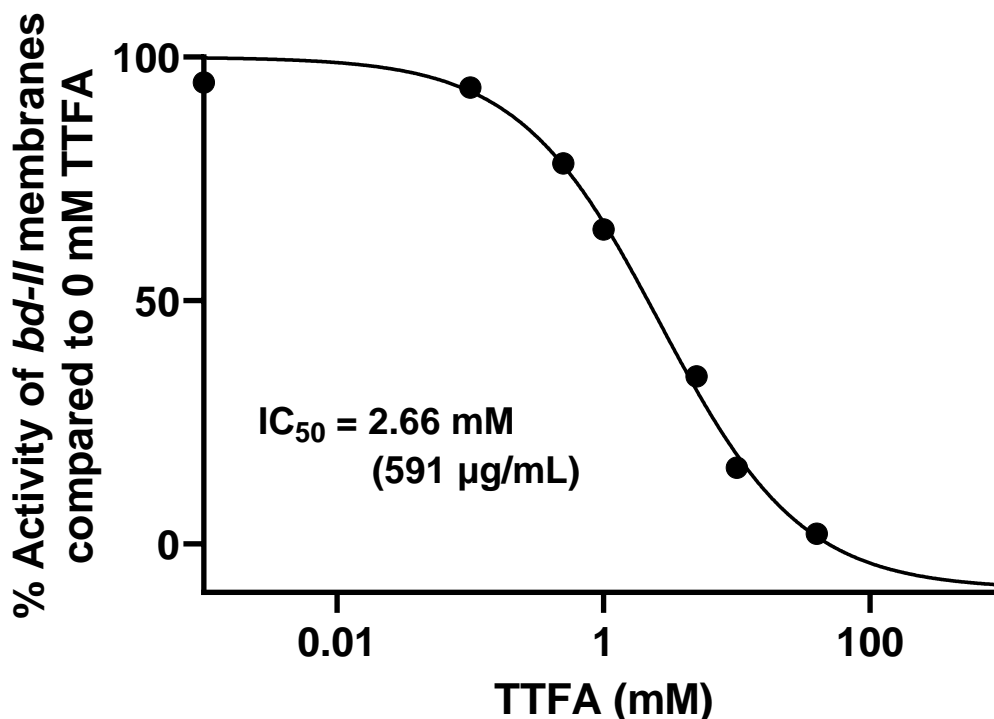


Figure 3.14. Oxygen consumption assay on membranes of recombinant strain expressing only *E. coli* cytochrome *bd-II* with TTFA. In the reaction chamber, 500 $\mu\text{g/mL}$ membranes were added to 50 mM HEPES (pH 7.5) with changing concentrations of TTFA in ethanol. Ethanol's concentration was set and remained at 2.5%. A final concentration of 8 mM succinate was added to start the reaction. *E. coli* cytochrome *bd-II* membranes were inhibited by TTFA at an IC_{50} of 2.66 ± 0.4 mM. Data points represent single experiments. Dose response data were fitted to the sigmoid $y = \text{Bottom} + (\text{Top} - \text{Bottom}) / (1 + 10^{((\text{Log}IC_{50} - X) * \text{HillSlope}))}$ equation using nonlinear regression (GraphPad).

3.3.5. Development of quinol site mutants to investigate drug resistance

3.3.5.1. Identifying important residues for mutation

Point mutations were introduced to the quinol-binding cleft of *E. coli* cytochrome *bd-I* to investigate whether this would affect the binding of inhibitors. This has implications for the design of future drugs and the emergence of resistance. These mutant complexes can potentially be used to simulate AA residue changes that could emerge if bacteria were exposed to inhibitors that bind to the quinol cleft.

Mutagenesis studies had identified residues that are of importance in the correct functioning of the quinol binding site (Zhang *et al.* 2004; Mogi *et al.* 2009; Goojani *et al.* 2020). *In silico* analysis was then performed to highlight these residues in the quinol binding site of CydA of *E. coli* cytochrome *bd-I*: L253A, F269A, Y387, I295 and F390 (Figure 3.15). Site-directed mutagenesis was performed on the specified amino acid residues. Appendix A.2. is a sequence alignment that shows the conservation of the amino acid residues. In Figure 3.15B, the residues are mutated to alanine. Haem *b*₅₅₈ is also shown and the main purpose of this haem is to oxidise ubiquinol to quinol. TTFA, a known inhibitor of *E. coli* cytochrome *bd-I*, is also bound to the quinol cleft.

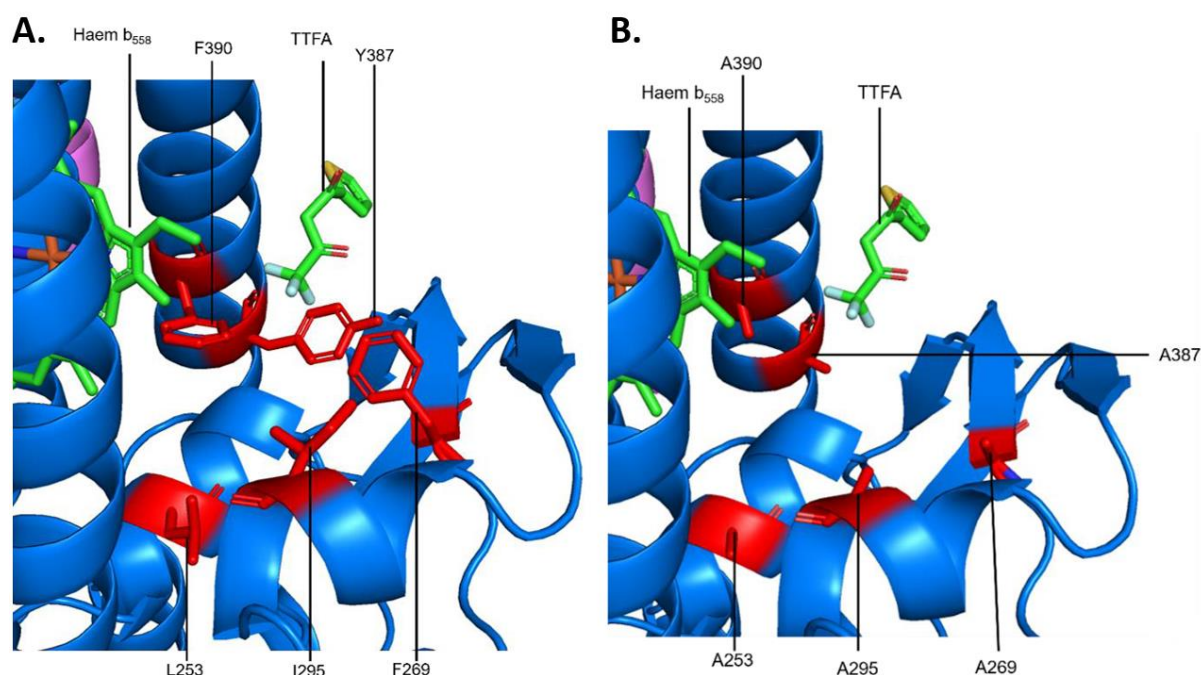


Figure 3.15. Residues of significance in the functioning of the quinol binding site of the cydA subunit of cytochrome *bd-I*. A) Residues L253, I295, F269, Y387 and F390 before mutation. B) Residues L253, I295, F269, Y387 and F390 after alanine mutation is introduced. Haem *b*₅₅₈ oxidises ubiquinol to quinol. TTFA is a known inhibitor of *E. coli* cytochrome *bd-I*.

3.3.5.2. Residues F269A and L253A were successfully mutated

Amino acid mutations were introduced to *E. coli* EC958 cytochrome *bd-I* plasmid (pSU2718G-app*CBX*-6HIS) isolated from an '*E. coli* TOP10' strain (MS402, Table 2.1, Shepherd Lab). Mutagenesis was performed using primers outlined in Table 2.3 (see section 2.1.3).

The mutagenesis products were transformed into NEB-5 alpha competent cells. Diagnostic restriction digests were carried out to confirm whether residues F269A and L253A have been successfully mutated. Plasmid maps show pSU2718G-app*CBX*-6HIS with the specific restriction enzyme used for residue F269A (Figure 3.16A) and L253A (Figure 3.17B). The mutagenesis process had added or removed a restriction site which can be determined through a restriction enzyme digest. Of the chosen residues, F269A and L253A were successfully mutated to alanine while the others failed.

Mutation F269A removed a BsmI site by introducing a GCC alanine codon and made a conservative codon change to GGT for Gly273. L253A with GCA alanine codon introduces a new PvuII site. Cutting a WT plasmid with BsmI would result in three large bands measuring 3004 bp, 2010 bp and 1803 bp (Figure 3.16B). However, F269A mutagenesis added 132 bp to the 2010 bp fragment to make it 2142 bp.

L253A with GCA alanine codon introduced a new PvuII site. Cutting WT plasmid with PvuII produced five large bands with 2864 bp, 1602 bp and 695 bp being the three largest. L253A mutation clipped the 1602 bp fragment into 984 bp and 618 bp (Figure 3.17B).

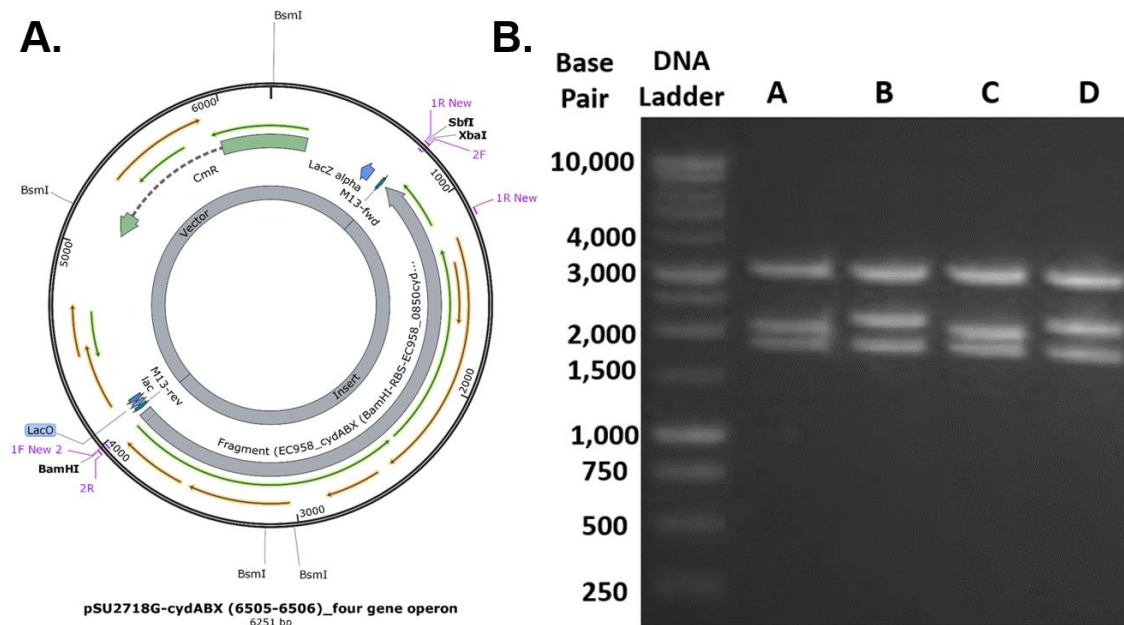


Figure 3.16. Plasmid map and restriction digest for F269A mutagenesis. **A)** Plasmid map for designing F269A mutant for mutagenesis work. **B)** Restriction digest for F269A mutagenesis. DNA ladder is ‘Promega 1Kb ladder’. Lane A represents WT *E. coli* EC958 cytochrome *bd-I* plasmid (pSU2718G-app*CBX*-6HIS) while lanes B and D show the DNA plasmid with F269A mutation added. Cutting WT DNA plasmid with BsmI would produce three large bands of 3004 bp, 2010 bp and 1803 bp. F269A mutagenesis added 132bp to the 2010 bp fragment making it 2142 bp.

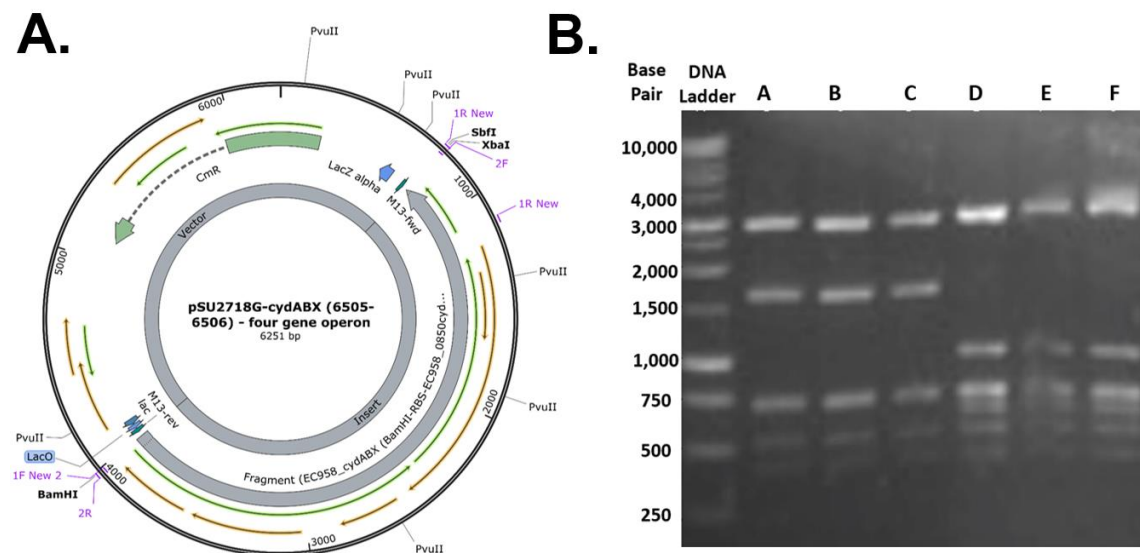


Figure 3.17. Plasmid map and restriction digest for L253A mutagenesis. **A)** Plasmid map for designing L253A mutant for mutagenesis work. **B)** Restriction digest for L253A mutagenesis. DNA ladder is ‘Promega 1Kb ladder’. Lanes A-C represent WT *E. coli* EC958 cytochrome *bd-I* plasmids (pSU2718G-app*CBX*-6HIS) while lanes D-E represent the plasmid with L253A mutation. L253A mutagenesis with GCA alanine codon introduced a new PvuII site. Cutting of WT plasmid with PvuII would produce five bands with three largest being 2864 bp, 1602 bp and 695 bp. L253A mutation clipped the 1602 bp fragment into 984 bp and 618 bp.

Following the site-directed mutagenesis of the residues of the quinol binding site, growth and spectral assays were performed to characterise the strains. As seen in Figure 3.18, F269A mutants grew relatively faster than the L253A mutants. However, both strains had similar growth patterns with the exponential phases commencing at the same time and both strains also entered the stationary phase at similar periods.

Whole cell spectra were obtained for both strains. Firstly, reduced spectra were obtained by the addition of sodium dithionite. The same reduced samples were exposed to carbon monoxide for 5 min to obtain CO reduced spectra. In Figure 3.19A, the distinctive peak at 640 nm is representative of haem *d* (Poole *et al.* 1989) which confirms the presence and correctly assembly of cytochrome *bd*-I in F289A mutants. There seem to have been a partial assemble of cytochrome *bd* complex in mutant L253A where cytochrome *b* is present, but haem *d* is absent (Figure 3.19B). This proposes that *E. coli* cytochrome *bd*-I was unable to assemble in L253A mutants.

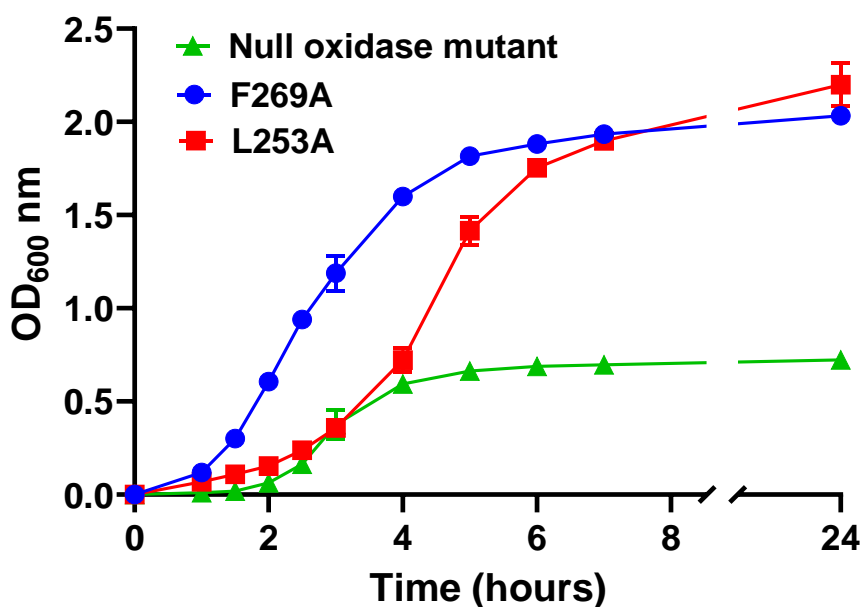


Figure 3.18. Aerobic growth curves of quinol site mutants F269A and L253A. Null oxidant mutant (*E. coli* MG1655 'EcoM4') contained no oxidase and was grown in 20 mM glucose to facilitate growth. Cells were grown aerobically in LB medium. Errors bars represent +/- standard deviation of 2 biological repeats. The OD₆₀₀/h for each growth curve was obtained and a one-way ANOVA performed at timepoint 2 – 4 h. The p-value was 0.0014 which means that there is a statistical difference between the curves and the null hypothesis is rejected.

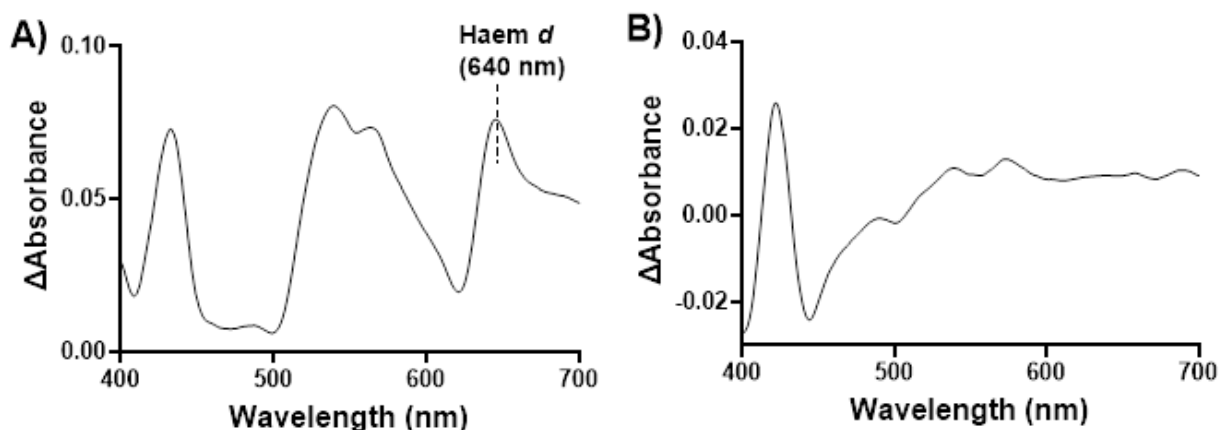


Figure 3.19. CO difference spectra of EcoM4 cells expressing *E. coli* cytochrome *bd-I* site-directed mutants. (A) F269A mutant with a distinctive peak at 640 nm which represents haem *d* of cytochrome *bd-I*. (B) L253A mutant does not have full assembly of cytochrome *bd* as haem *d* is absent.

3.3.5.3. F269A mutant led to oxygen consumption in purified membranes

To measure the ability of the newly engineered *E. coli* cytochrome *bd-I* quinol site-directed mutants to consume oxygen, oxygen electrode assays were carried out on purified membranes. Figure 3.20 shows that WT cytochrome *bd-I* only membranes isolated from *E. coli* cells harbouring pSU2718-G-*cydABX* (see MS402 in Table 2.1) consumed oxygen at a rate of 114 nM/s while F269A mutant consumed oxygen at a rate of 64 nM/s. Membranes harbouring L253A mutation were unable to consume any oxygen (Figure 3.20) which might be a result of *E. coli* cytochrome *bd-I* oxidase not being able to assemble (Figure 3.18B). An unpaired non-parametric t-test generated a p-value of 0.3 which indicates a non-statistically significant result (Figure 3.20).

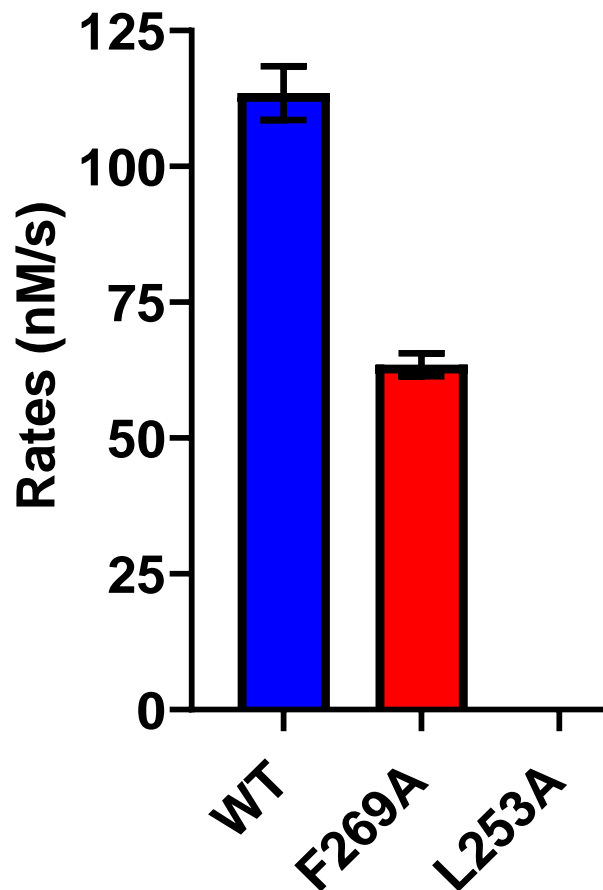


Figure 3.20. Oxygen consumption membrane assay on *E. coli* cytochrome *bd*-I quinol site-directed mutants. WT cytochrome *bd*-I only membranes isolated from *E. coli* TOP10 cells harbouring pSU2718-G-*cydABX* consumed oxygen at an average of 114 nM/s. F269A mutant consumed oxygen at an average of 64 nM/s. L253A mutant did not consume any oxygen. Error bars represent mean with standard deviation for two technical repeats. An unpaired, non-parametric t-test was performed that generated a p value of 0.3 which means that deviation from the null hypothesis is not statistically significant.

To determine whether a known inhibitor of *E. coli* cytochrome *bd*-I (TTFA) was able to inhibit the newly engineered *E. coli* cytochrome *bd*-I quinol site mutant (F269A), an oxygen electrode dose response curve was obtained for its membranes. Oxygen consumption activity was established for the F269A mutant in the presence of TTFA and an IC_{50} of 0.15 ± 0.05 mM was generated (Figure 3.21). To estimate median inhibitory concentrations (IC_{50}), dose response data were fitted to the sigmoid $y=Bottom + (Top-Bottom)/(1+10^{((LogIC50-X)*HillSlope)})$ equation using nonlinear regression (GraphPad). The IC_{50} obtained for the

F269A mutant is significantly lower than that of the unmutated cytochrome *bd*-I only membranes (Figure 3.5). This was not expected considering that mutations were introduced to this plasmid, and as such, this result was marked as an anomaly.

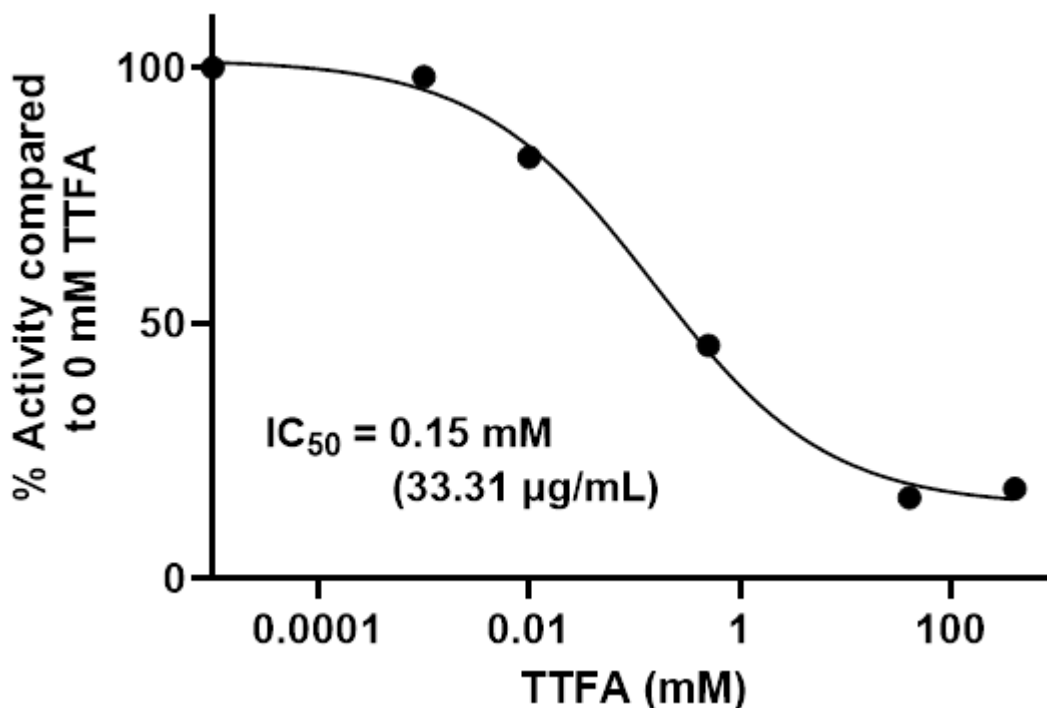


Figure 3.21. Oxygen consumption assay for *E. coli* cytochrome *bd*-I quinol site mutant (F269A) with TTFA. An oxygen electrode dose response curve was obtained for the membranes of F269A site-directed mutants that generated an IC_{50} of 0.15 ± 0.05 mM. In the reaction chamber, 500 $\mu\text{g/mL}$ membranes were added to 50 mM HEPES (pH 7.5) with changing concentrations of TTFA in ethanol. Ethanol's concentration was set and remained at 2.5%. A final concentration of 8 mM succinate was added to start the reaction. Data points represent single experiments. Dose response data were fitted to the sigmoid $y = \text{Bottom} + (\text{Top} - \text{Bottom}) / (1 + 10^{((\text{Log}IC_{50} - X) * \text{HillSlope}))}$ equation using nonlinear regression (GraphPad).

3.4. Discussion

3.4.1. Characterisation of *E. coli* EC958 cytochrome *bd-I* WT and mutant strains

A multidrug-resistant uropathogenic *E. coli* (Nicolas-Chanoine, Bertrand and Madec, 2014), EC958, was used for this study as it was able to determine the role that cytochrome *bd-I* play in a clinical pathogenic strain. *E. coli* has three known terminal respiratory oxidases, cytochrome *bd-I*, cytochrome *bd-II* and cytochrome *bo'* (Forte *et al.*, 2016). Having WT and mutant strains for *E. coli* EC958 bacteria allowed for direct comparisons and the formation of more conclusive experimental outcomes. Each respiratory oxidase has unique characteristics that make it easy to identify and understand them. To accurately study the terminal respiratory oxidases of *E. coli*, the growth and spectral properties were determined via the use of aerobic growth curves and spectral analysis.

The SDB4 spectrophotometer (Poole and Kalnenieks 2000) was used to generate CO difference and reduced *minus* oxidised whole cell spectra for the strains as this instrument can analyse highly turbid samples. It was also important for spectral readings to be obtained for purified membranes as the electron transport chain of prokaryotes are situated in plasma membranes. The haem groups of each terminal respiratory oxidase appear at different peaks when the oxidase assembles correctly which can be used to determine the type of terminal respiratory oxidases are present in a strain (Poole *et al.* 1989). Aerobic growth curves showed how well each strains grew as introducing mutations to bacteria can have significant effects on their function. *E. coli* WT strains grew the fastest which was expected as all three respiratory oxidases are present in this strain and the bacterium is working in its 'natural' element. Cytochrome *bd-I* only cells grew almost as fast as WT cells which attests to the ability of pathogenic bacteria to use this oxidase as a survival tool under almost any given conditions.

Cytochrome *bo'*-only cells grew much slower which proposes that this oxidase does not consume oxygen as well as cytochrome *bd*-I.

3.4.2. Designing experimental tools to repurpose drugs that target cytochrome *bd* oxidases

In the fight against AMR, new drug targets are needed to develop novel antimicrobials. Cytochrome *bd* oxidase is a good drug target because it is only found in prokaryotes and archaea (Borisov, Gennis, *et al.* 2011); it has been linked to virulence and stress tolerance in some of the most pathogenic strains of bacteria (Turner *et al.* 2003; Yamamoto *et al.* 2005) and the existence of high resolution structures for various cytochrome *bd* complexes from multiple organisms makes it easy to study the enzyme (Safarian *et al.* 2019; Grauel *et al.* 2021; Safarian *et al.* 2021).

One of the best ways to assess for the activity of cytochrome *bd*-I is through oxygen consumption assays on purified membranes. Therefore, an inhouse oxygen consumption assay was developed on the oxygen electrode using cytochrome *bd*-I only membranes. For positive control, a known and published inhibitor of *E. coli* cytochrome *bd*-I, TTFA, was analysed. Though effective, oxygen consumption assays on an electrode can be time consuming and could be made more time-efficient by use of a high-throughput fluorescence assay using a plate reader. This oxygen electrode membrane assay will form the basis of experimental drug screens in the lab as a follow-up of *in silico* approaches used in Chapters 4 and 5.

Recombinant strains were engineered that expressed *E. coli* EC958 cytochrome *bd*-type oxidases in an *E. coli* MG1655 'EcoM4' strain lacking all terminal respiratory oxidases. These recombinant strains expressed either *E. coli* cytochrome *bd*-I or cytochrome *bd*-II oxidases. The host lab is yet to design an *E. coli* cytochrome *bd*-II only strain so this newly designed recombinant *bd*-II only strain could allow for comparative analysis in future studies. Recombinant technology is a modern tool that is essential to drug development as it creates

more opportunities and flexibility for researchers to work with highly pathogenic and ‘dangerous’ microorganisms. The recombinant technology was successful in the host lab and could allow for the studying of highly pathogenic strains such as *Mycobacterium tuberculosis* if its cytochrome *bd* oxidase is successfully expressed in another non-pathogenic strain.

3.4.3. Development of quinol site mutants to investigate drug resistance

One of the greatest, but unpreventable, threats to antibiotics is the emergence of antibiotic resistance. Antibiotic is a global health threat that has increased by over 65% between 2000 to 2010 (Walsh *et al.* 2023). Antibiotic resistance is a naturally occurring phenomenon that allows bacteria to evade the antibacterial properties of antibiotics that they were once sensitive to (Pulingam *et al.* 2022). Though unpreventable, the occurrence of antibiotic resistance can be largely minimised by lowering the misuse and overuse of antibiotics (Aslam *et al.* 2018; EClinicalMedicine 2021). Introducing point mutations in the quinol-binding cleft has implications for the design of future drugs and the emergence of resistance. These mutant complexes can potentially be used to simulate AA residue changes that could emerge if bacteria were exposed to inhibitors that bind to the quinol cleft. Therefore, mutations were introduced to the quinol site of the *cydA* subunit of *E. coli* EC958 cytochrome *bd*-I through site-directed mutagenesis. Previous work has demonstrated the importance of the Q-loop and quinol binding site in the assembly and functioning of cytochrome *bd*-I (Goojani *et al.* 2020). CydA subunit holds a periplasmic hydrophilic loop called Q-loop that is proven fundamental for quinol oxidation (Goojani *et al.* 2020). Deletion or shortening of the Q-loop via mutation has resulted in loss of haem groups, prevented assembly of *E. coli* cytochrome *bd* or inactivation (Goojani *et al.* 2020). The amino acid residues that were predicted to be of most importance for ligand binding in the quinol site were earmarked for mutation. Of the five mutations attempted, only two were successful (F269A and L253A).

Spectral analysis demonstrated that mutation L253A prevented the assembling of *E. coli* cytochrome *bd-I* as the spectral analysis did not show any distinctive peaks that are unique to cytochrome *bd*, especially a peak at 640 nm which is representative of haem *d*. L253A signifies the original amino acid at position 253 in the protein sequence where “L” represents leucine. The letter “A” is representative of alanine, which is the amino acid used to replace leucine. L253A mutation is believed to have wide effects on the structure, function and interactions of a protein (Kamtekar *et al.* 2008)

F269A mutation affected the oxygen consumption of *E. coli* cytochrome *bd-I* only membranes as oxygen consumption activity were lower when compared to WT. However, oxygen consumption dose inhibition curve on isolated membranes revealed that mutation of F269A had no major impact on the on the inhibitory action of TTFA, suggesting that this residue is not involved in TTFA binding. F269A mutation refers to phenylalanine at position 269 in the protein sequence with an alanine substitution. It is believed that this mutation affects the ability of replication protein A to bind DNA and facilitate DNA repair processes (Chen *et al.* 2016). Replication protein A has vital roles in DNA replication, repair and recombination by binding to single-stranded DNA and interacting with other proteins (Chen *et al.* 2016).

3.4.4. Future Studies

This work generated a strain that expressed cytochrome *bd-II* as the sole respiratory oxidase, which will provide a useful tool for comparative work with other strains that express cytochrome *bd-I* or cytochrome *bo'* as the sole respiratory oxidases. In addition, this work developed a F269A variant of cytochrome *bd-I* that will be useful in future studies with potential drugs that bind in the quinol cleft. Although this residue is not important for the binding of TTFA, it may well be useful to simulate the emergence of resistance against other compounds that bind in this quinol pocket. The obvious extension of this work is to complete

the mutagenesis of all key residues in the quinol pocket, and then to undertake dose response experiments with putative quinol cleft inhibitors. This approach could be further extended to respiratory oxidases from other pathogens to gauge the likelihood of resistance emerging towards cytochrome *bd* inhibitors in a variety of pathogens.

Chapter 4

Assessing known antimicrobials as inhibitors of cytochrome *bd*

4.1. Summary

Atovaquone, 1,4-naphthoquinone, and madecassic acid are known antimicrobials with modes of actions that have previously been shown to target electron transport chains in different ways. Madecassic acid is an anticancer and antibacterial agent that has been a recent focus in novel therapeutic development. A madecassic acid derivative of interest has been recently developed that resulted in mitochondrial dysfunction through a decrease of mitochondrial membrane potential. Therefore, it was of interest to investigate if this compound had any effects on bacterial energetics. Atovaquone is an antimalarial and antipneumocystis agent that targets cytochrome *bc*₁ complex through competitive inhibition. Atovaquone is a hydroxy-naphthoquinone analogue, so the 1,4-naphthoquinone head group is highly likely to target ubiquinol-binding clefts as atovaquone does.

In silico analyses were performed for atovaquone, 1,4-naphthoquinone, and madecassic acid 1 to determine the molecular interactions between the compounds and the quinol site of *E. coli* cytochrome *bd*-1 and cytochrome *bo'*. Of the three compounds, atovaquone had the lowest K_d value for the quinol site of CydA for cytochrome *bd*-I (0.96 μ M) and subunit 1 for cytochrome *bo'* (5.2 μ M). Despite this, atovaquone was the only compound that possessed no inhibitory effects against oxygen consumption activity in *E. coli* *bd*-I only membranes. Madecassic acid 1 and 1,4-naphthoquinone were inhibitory against *E. coli* *bd*-I and *bo'*-only membrane oxygen consumption activity and cell growth. Neither of these compounds had inhibitory effects against cell viability. Madecassic acid 1 was derivatised to determine whether altering of its structure could increase its binding affinity for *E. coli* cytochrome *bd*-I quinol site. It was demonstrated that an added acetoxy group led to tighter binding to cytochrome *bd*-1 with IC_{50} as low as $8.8 \pm 3.5 \mu$ M ($5.6 \pm 2.2 \mu$ g/mL) for madecassic acid 2, compared to an IC_{50} of $46.80 \pm 15.7 \mu$ M ($23.62 \pm 7.9 \mu$ g/mL) for the original compound (madecassic acid 1).

4.2. Introduction

Madecassic acid is produced by *Centella asiatica* (Indian pennywort) and is a known anticancer and antibacterial agent (Valdeira *et al.* 2018; Valdeira *et al.* 2019; Wei, Cui and Liu 2023). Derivatives of madecassic acid were produced of which one (compound 29) showed growth inhibition against 26 various tumour cell lines (Valdeira *et al.* 2019). Atovaquone is an FDA-approved antimalarial medication known as Malarone which is used in the treatment of uncomplicated malaria in children (Nixon *et al.* 2013). Atovaquone is also given as a prophylactic treatment for *Pneumocystis jirovecii* immunocompromised patients (Cooley *et al.* 2014; Robin *et al.* 2017). Derivatives of 1,4-naphthoquinone have been proven to have antibacterial and antifungal properties against strains such as *E. coli*, *P. aeruginosa*, *S. aureus*, *L. monocytogenes* and various *Candida* species (Sánchez-Calvo *et al.* 2016; Ravichandiran *et al.* 2019). The antimicrobial properties of all three compounds make them interesting candidates for study as potential inhibitors of *E. coli* cytochrome *bd*-I. In addition, naphthoquinone is the head group of atovaquone, and both compounds are known to bind to quinol sites.

4.2.1. Madecassic Acid, Atovaquone and 1,4-Naphthoquinone as potential quinol site targets of *E. coli* Cytochrome *bd*-I

In protozoa, atovaquone inhibits the mitochondrial respiratory chain at the cytochrome *bc*₁ complex through competitive inhibition of ubiquinol binding (Fry and Pumey 1992; Nixon *et al.* 2013). Further studies show that this inhibition of the *bc*₁ complex diminishes the complete function of the mitochondria (Biagini *et al.* 2006). Hydroxy-naphthoquinones are also competitive inhibitors of cytochrome *bc*₁ complex (Kessl *et al.* 2007) and novel naphthoquinones have been designed and tested as substrate-based inhibitors of quinol/fumarate reductase *Wolinella succinogenes* (Nasiri *et al.* 2013). Cytochrome *bd* and

cytochrome bc_1 complexes are the only oxidases found in complex III of the electron transport chain and contains quinol binding sites. This makes the compounds atovaquone and naphthoquinone more interesting targets for the quinol site of *E. coli* cytochrome $bd-I$. Derivatives of madecassic acid have been synthesised and tested against tumour cell lines (Valdeira *et al.* 2018; Valdeira *et al.* 2019). A particular derivative (compound 29) resulted in a decrease of mitochondrial membrane potential and a subsequent mitochondrial dysfunction (Valdeira *et al.* 2019). Figure 4.1 illustrates a summary of the pharmacological properties of 1,4-naphthoquinone, atovaquone and madecassic acid which makes them potential candidates to target the ubiquinol site of *E. coli* cytochrome $bd-I$.

In the current work, whole cell and membrane assays were performed on *E. coli* EC958 strains to determine whether 1,4-naphthoquinone, atovaquone and madecassic acid are inhibitors of cytochrome $bd-I$. Derivatives of madecassic acid were designed, synthesised, and tested to determine whether binding affinity could be increased.

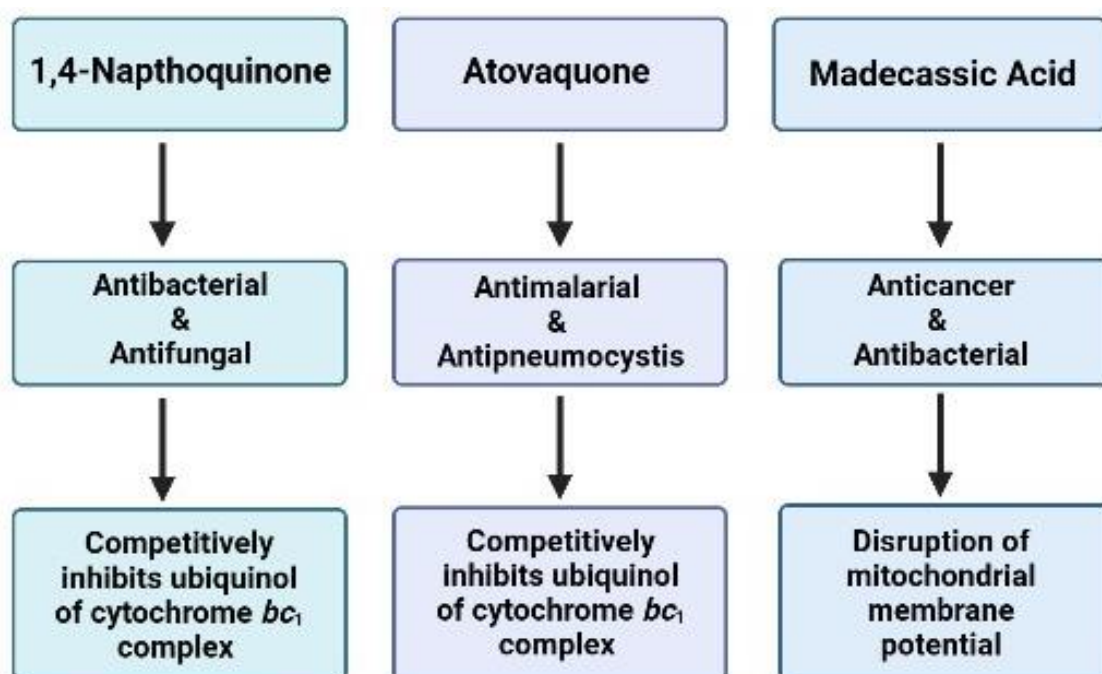


Figure 4.1. Pharmacological properties of 1,4-Naphthoquinone, Atovaquone and Madecassic Acid. All three compounds possess antimicrobial properties and mode of actions are associated with targeting of the mitochondrial electron transport chain.

4.3. Results

4.3.1. Docking of known antimicrobials to the AlphaFold 2 models of *E. coli* cytochrome *bd-I* and cytochrome *bo'*

An *in silico* analysis (Henry *et al.* 2024) was performed to investigate how well atovaquone, 2-hydroxy-1,4-naphthoquinone and madecassic acid 1 bind to the quinol sites of *E. coli* cytochrome *bd-I* (CydA) and cytochrome *bo'* (subunit 1). The drugs were docked to the quinol site of CydA for *E. coli* AlphaFold 2 cytochrome *bd-I* structural model and subunit 1 of cytochrome *bo'*. The dissociation constants predicted by AutoDock Vina for the known antimicrobials are shown in Table 4.1. Atovaquone had the lowest K_d value for both cytochrome *bd-I* and cytochrome *bo'* (Table 4.1). 2-hydroxy-1,4-naphthoquinone had a lower K_d value for cytochrome *bo'* (33.4 μM) compared to cytochrome *bd-I* (108.99 μM) (Table 4.1). Madecassic acid 1 (i.e. the native compound) had a K_d value 1.14 μM for cytochrome *bd-I* but 39.54 μM for cytochrome *bo'* which predicts the possibility of a tighter binding to cytochrome *bd-I* enzymes (Table 4.1). To establish how well the natural substrate (ubiquinol) of cytochrome *bd* and cytochrome *bo'* binds to the quinol site in CydA and subunit 1, respectively, ubiquinol-8 was also docked to these sites. Ubiquinol-8 had a high K_d value (108.4 μM) for cytochrome *bd-I* compared to other compounds such as atovaquone and madecassic Acid 1. For cytochrome *bo'*, 2-hydroxy-1,4-naphthoquinone had the same K_d value as ubiquinol-8, at 33.4 μM . Madecassic 1 also exhibited a K_d value close to those of 2-hydroxy-1,4-naphthoquinone and madecassic acid 1 of 39.54 μM .

Ligand	Enzyme	Binding Affinity (kcal/mol)	K _a Value (nM)	K _a Value (μM)
Ubiquinol-8	<i>E. coli</i> Cytochrome <i>bd</i> -I (CydA)	-5.1	180935.8	108.94
Atovaquone	<i>E. coli</i> Cytochrome <i>bd</i> -I (CydA)	-8.2	960.92	0.96
2-Hydroxy-1,4-Naphthoquinone	<i>E. coli</i> Cytochrome <i>bd</i> -I (CydA)	-5.4	108988	108.99
Madecassic Acid 1	<i>E. coli</i> Cytochrome <i>bd</i> -I (CydA)	-8.1	1137.81	1.14
Ubiquinol-8	<i>E. coli</i> Cytochrome <i>bo</i> ' (Subunit 1)	-6.1	33396.86	33.4
Atovaquone	<i>E. coli</i> Cytochrome <i>bo</i> ' (Subunit 1)	-7.2	5206.01	5.2
2-Hydroxy-1,4-Naphthoquinone	<i>E. coli</i> Cytochrome <i>bo</i> ' (Subunit 1)	-6.1	33396.86	33.4
Madecassic Acid 1	<i>E. coli</i> Cytochrome <i>bo</i> ' (Subunit 1)	-6.0	39544.63	39.54

Table 4.1. Docking of known antimicrobials to the ubiquinol sites in CydA of *E. coli* cytochrome *bd*-I and subunit 1 of *E. coli* cytochrome *bo*'. The natural substrate of cytochrome *bd*-I and cytochrome *bo*', ubiquinol-8, was also docked to the quinol sites of CydA and subunit 1, respectively.

Docking images illustrated the orientation of ubiquinol-8, atovaquone, madecassic acid 1 and 2-hydroxy-1,4-naphthoquinone in the quinol cleft of *E. coli* cytochrome *bd*-I CydA (Figure 4.2) and subunit 1 of *E. coli* cytochrome *bo*' (Figure 4.3). The natural substrate of cytochrome *bd* and cytochrome *bo*', ubiquinol-8, is docked to the quinol site in CydA of *E. coli* cytochrome *bd*-I (Figure 4.2) and subunit 1 of cytochrome *bo*' (Figure 4.3). The molecular

docking imaging (Figure 4.2) shows several hydrophobic residues present in the ubiquinol site of cytochrome *bd-I*. This means that there are high hydrophobic interactions between the compounds and cytochrome *bd-I* as demonstrated by multiple red areas on the protein. Alternatively, the ubiquinol site in subunit 1 of cytochrome *bo'* does not have as many hydrophobic interactions compared to cytochrome *bd-I* as several polar regions can be seen in blue (Figure 4.3).

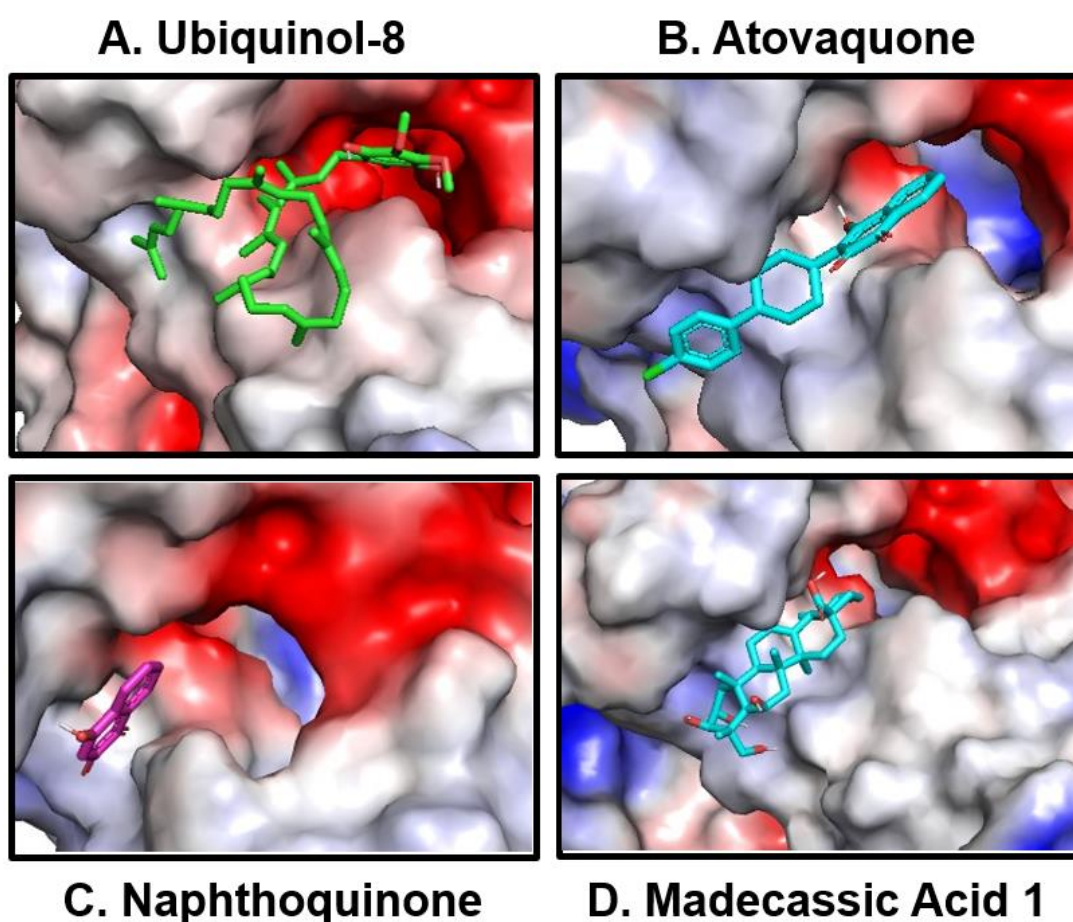


Figure 4.2. Docking images of known antimicrobial compounds and ubiquinol-8 bound to CydA of *E. coli* cytochrome *bd-I*. A) Ubiquinol-8, B) Atovaquone, C) 2-hydroxy-1,4-Naphthoquinone and D) Madecassic acid 1 bound to the ubiquinol site of *E. coli* AlphaFold 2 cytochrome *bd-I* model. Red = negative charge. White = hydrophobic. Blue = positive charge.

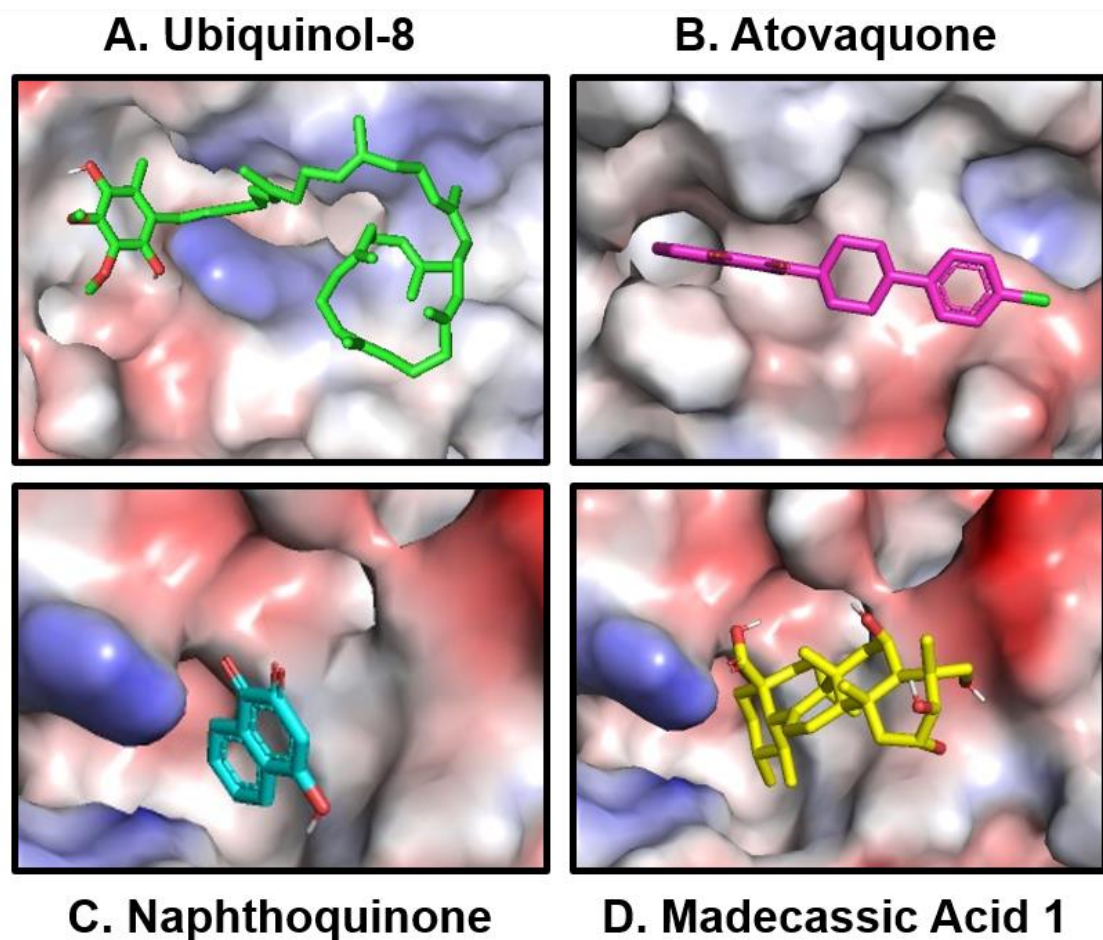


Figure 4.3. Docking images of known antimicrobial compounds and ubiquinol-8 bound to subunit 1 of *E. coli* cytochrome *bo'*. A) Ubiquinol-8, B) Atovaquone, C) 2-hydroxy-1,4-Naphthoquinone and D) Madecassic Acid 1 bound to subunit 1 of *E. coli* AlphaFold 2 cytochrome *bo'* model. Red = negative charge. White = hydrophobic. Blue = positive charge.

4.3.2. Investigation of Drug Efficacy/Specificity

4.3.2.1. Preliminary investigation of Atovaquone's efficacy/specificity

Of the three potential inhibitor scaffolds investigated in this chapter, atovaquone was predicted to have the highest affinity for ubiquinol sites of both cytochrome *bd-I* and cytochrome *bo'* (see section 4.3.1). To test the validity of this prediction, oxygen consumption assays were performed on *E. coli* EC958 membranes containing either cytochrome *bd-I* or cytochrome *bo'* as the sole respiratory oxidase. Atovaquone did not result in inhibition of

neither cytochrome *bd-I* nor cytochrome *bo'* only membranes (Figure 4.4), although it was predicted to have the highest affinity for the ubiquinol sites of both oxidases (see Table 4.1). Due to the lack of inhibition, atovaquone was excluded from further experiments and 2-hydroxy-1,4-naphthoquinone and madecassic acid 1 were investigated further.

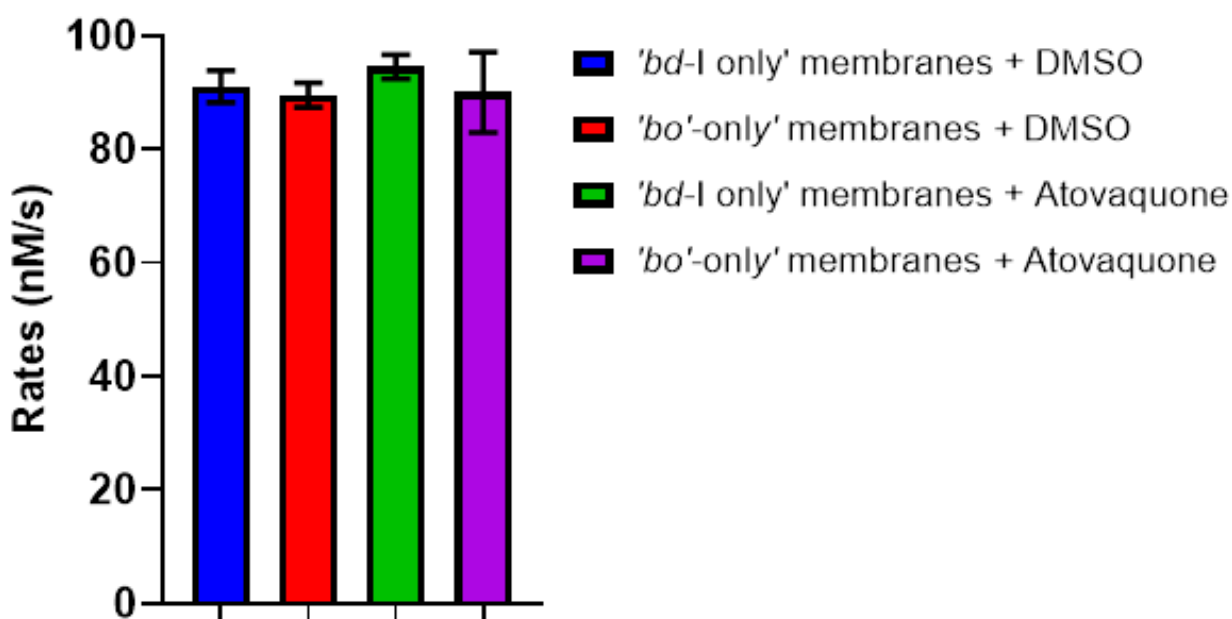


Figure 4.4. Oxygen consumption assay of *E. coli* EC958 cytochrome *bd-I* and cytochrome *bo'* only membranes against atovaquone. DMSO only experiments were used as negative controls. A high concentration of 1250 $\mu\text{g}/\text{mL}$ atovaquone does not inhibit *E. coli* EC958 cytochrome *bd-I* nor cytochrome *bo'*-only membranes. Error bars represent standard deviation of 2 technical repeats.

4.3.2.2. Oxygen consumption assays of madecassic acid 1 and 2-hydroxy-1,4-naphthoquinone against *E. coli* EC958 cytochrome *bd-I* and *bo'*-only membranes

Following *in silico* analysis of the known antimicrobials, atovaquone was found to be ineffective against the oxidoreductase activity of *E. coli* EC958 cytochrome *bd-I* and *bo'*-only membranes (see section 4.3.2.1). Contrastingly, both madecassic acid 1 and 2-hydroxy-1,4-naphthoquinone were inhibitory against *E. coli* cytochrome *bd-I* and *bo'* oxidases. Figure 4.5 shows that *E. coli* EC958 cytochrome *bd-I* only membranes were inhibited by madecassic acid 1 with an IC_{50} of $23.62 \pm 7.9 \mu\text{g}/\text{mL}$ ($46.80 \pm 15.7 \mu\text{M}$). Alternatively, 2-hydroxy-1,4-

naphthoquinone inhibited cytochrome *bd*-I only membranes with an IC_{50} of $1019 \pm 260 \mu\text{g/mL}$ ($6443 \pm 1644 \mu\text{M}$) (Figure 4.5). This corresponds to molecular predicted binding affinities which produced a high K_d value of $108.99 \mu\text{M}$ for 2-hydroxy-1,4-naphthoquinone, and a lower K_d value of $1.14 \mu\text{M}$ for madecassic acid 1 (Table 4.1). To estimate median inhibitory concentrations (IC_{50}), dose response data were fitted to the sigmoid $Y=Bottom + (Top-Bottom)/(1+10^{(X-LogIC50)})$ equation using nonlinear regression (GraphPad).

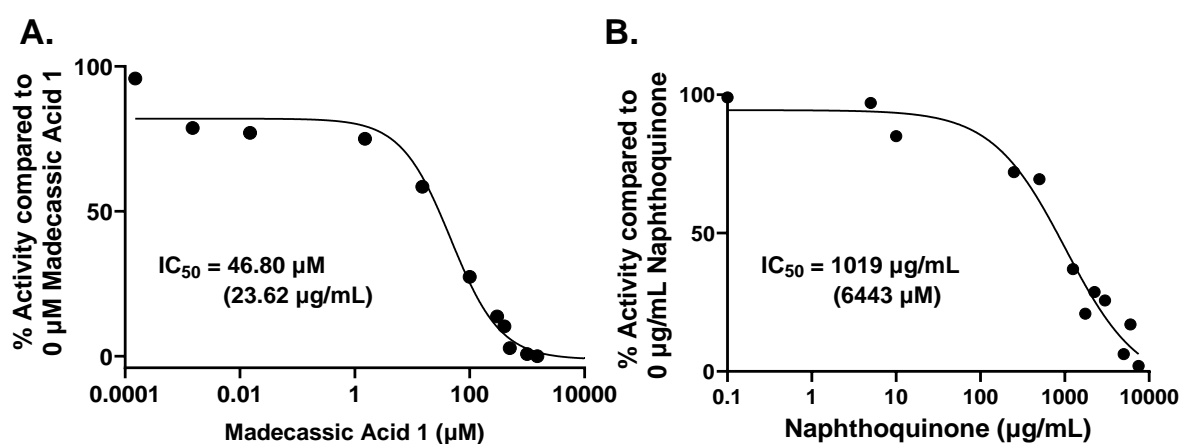


Figure 4.5. Dose inhibition curves of madecassic acid 1 and 2-hydroxy-1,4-naphthoquinone activities against *E. coli* EC958 cytochrome *bd*-I only membranes. A) Madecassic acid 1 inhibits cytochrome *bd*-I only membranes with an IC_{50} of $23.62 \pm 7.9 \mu\text{g/mL}$ ($46.80 \pm 15.7 \mu\text{M}$) while **B)** 2-hydroxy-1,4-naphthoquinone inhibits cytochrome *bd*-I only membranes at an IC_{50} of $1019 \pm 260 \mu\text{g/mL}$ ($6443 \pm 1644 \mu\text{M}$). Data points represent single experiments. Dose response data were fitted to the sigmoid $Y=Bottom + (Top-Bottom)/(1+10^{(X-LogIC50)})$ equation using nonlinear regression (GraphPad).

To assess the specificity of the compounds, oxygen consumption assays were performed on *E. coli* EC958 cytochrome *bo'* only membranes. Interestingly, madecassic acid 1 inhibited cytochrome *bo'* with an IC_{50} of $32.45 \pm 13.8 \mu\text{g/mL}$ ($64.3 \pm 27.3 \mu\text{M}$) which is lower than the measured IC_{50} for 2-hydroxy-1,4-naphthoquinone of $1027 \pm 483 \mu\text{g/mL}$ ($6323 \pm 2974 \mu\text{M}$) (Figure 4.6). However, the predicted K_d values of madecassic acid 1 and 2-hydroxy-1,4-naphthoquinone for cytochrome *bo'* oxidase were $39.54 \mu\text{M}$ and $33.4 \mu\text{M}$, respectively (Table 4.1). To estimate median inhibitory concentrations (IC_{50}), dose response

data were fitted to the sigmoid $Y=Bottom + (Top-Bottom)/(1+10^{(X-LogIC50)})$ equation using nonlinear regression (GraphPad).

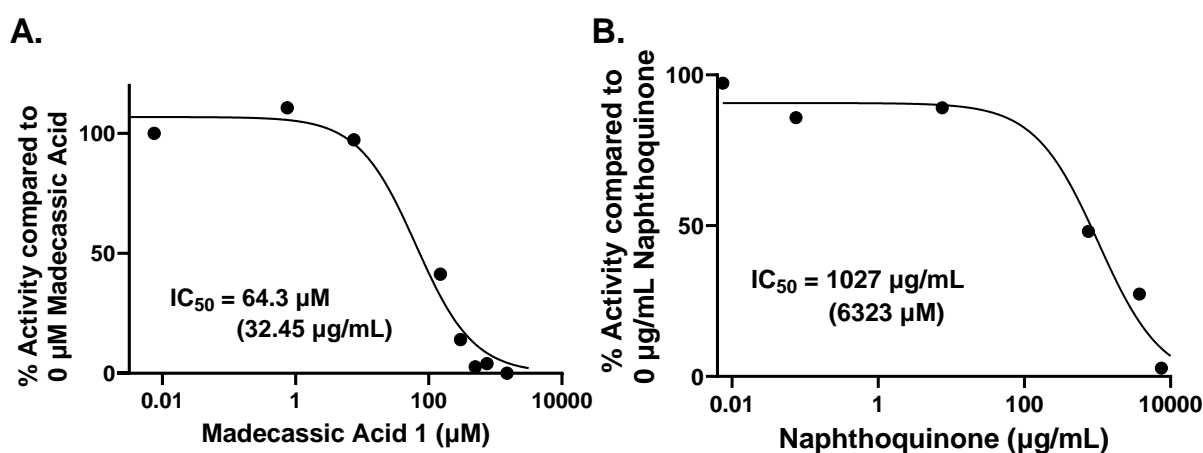


Figure 4.6. Dose inhibition curves of madecassic acid 1 and 2-hydroxy-1,4-naphthoquinone activities against *E. coli* EC958 cytochrome *bo'*-only membranes. A) Madecassic acid 1 inhibits cytochrome *bo'*-only membranes with an IC_{50} of $32.45 \pm 13.8 \mu\text{g/mL}$ ($64.3 \pm 27.3 \mu\text{M}$), while B) 2-hydroxy-1,4-naphthoquinone inhibits cytochrome *bo'*-only membranes with an IC_{50} of $1027 \pm 483 \mu\text{g/mL}$ ($6323 \pm 2974 \mu\text{M}$). Data points represent single experiments. Dose response data were fitted to the sigmoid $Y=Bottom + (Top-Bottom)/(1+10^{(X-LogIC50)})$ equation using nonlinear regression (GraphPad).

4.3.2.3. Growth and Survival Assays of Madecassic Acid 1 and 2-hydroxy-1,4-naphthoquinone against *E. coli* WT, cytochrome *bd-I* only and cytochrome *bo'*-only cells.

This study has confirmed that madecassic acid 1 and 2-hydroxy-1,4-naphthoquinone are inhibitory against the activity of *E. coli* cytochrome *bd-I* only and *bo'*-only membranes (see section 4.3.2.2.). Herein, we assessed the ability of both compounds to inhibit the growth of *E. coli* EC958 WT, cytochrome *bd-I* only and cytochrome *bo'*-only cells. 2-hydroxy-1,4-naphthoquinone caused inhibition against all three strains which testifies to the ability of the drug to not only inhibit oxygen consumption activity in membranes, but to inhibit the growth of whole cells. *E. coli* WT cells had the lowest IC_{50} of $0.04 \pm 0.03 \mu\text{g/mL}$ ($0.25 \pm 0.2 \mu\text{M}$) followed by cytochrome *bo'*-only cells with an IC_{50} of $0.06 \pm 0.03 \mu\text{g/mL}$ ($0.38 \pm 0.19 \mu\text{M}$)

against 2-hydroxy-1,4-naphthoquinone activity (Figure 4.7). However, both WT (Figure 4.7A) and *bo'*-only (Figure 4.7C) cells showed residual activity with only 42% inhibition occurring for both strains. This means that that maximum inhibition did not take place. Cytochrome *bd*-I only cells were inhibited by 2-hydroxy-1,4-naphthoquinone by up to 80% with an IC₅₀ of 2.9 ± 1.1 µg/mL (18 ± 6.8 µM) (Figure 4.7B).

Madecassic acid 1 was assessed to see its inhibitory effects on the growth of *E. coli* EC958 WT, cytochrome *bd*-I only and cytochrome *bo'*-only cells (Figure 4.8). The growth of WT cells was inhibited with an IC₅₀ of 39.45 ± 19 µM (19.91 ± 9.6 µg/mL) (Figure 4.8A). Cytochrome *bd*-I only cells showed a bit more specificity to the drug as they were inhibited at an IC₅₀ of 10 ± 5.8 µM (5 ± 2.9 µg/mL) (Figure 4.8B). *Bo'*-only cells showed the least amount of sensitivity towards madecassic acid 1 with an IC₅₀ of 180.7 ± 144.7 µM (91.2 ± 73 µg/mL) (Figure 4.8). To estimate median inhibitory concentrations (IC₅₀), dose response data were fitted to the sigmoid $y = \text{Bottom} + (\text{Top} - \text{Bottom}) / (1 + 10^{-(X - \text{LogIC}_{50})})$ equation using nonlinear regression (GraphPad).

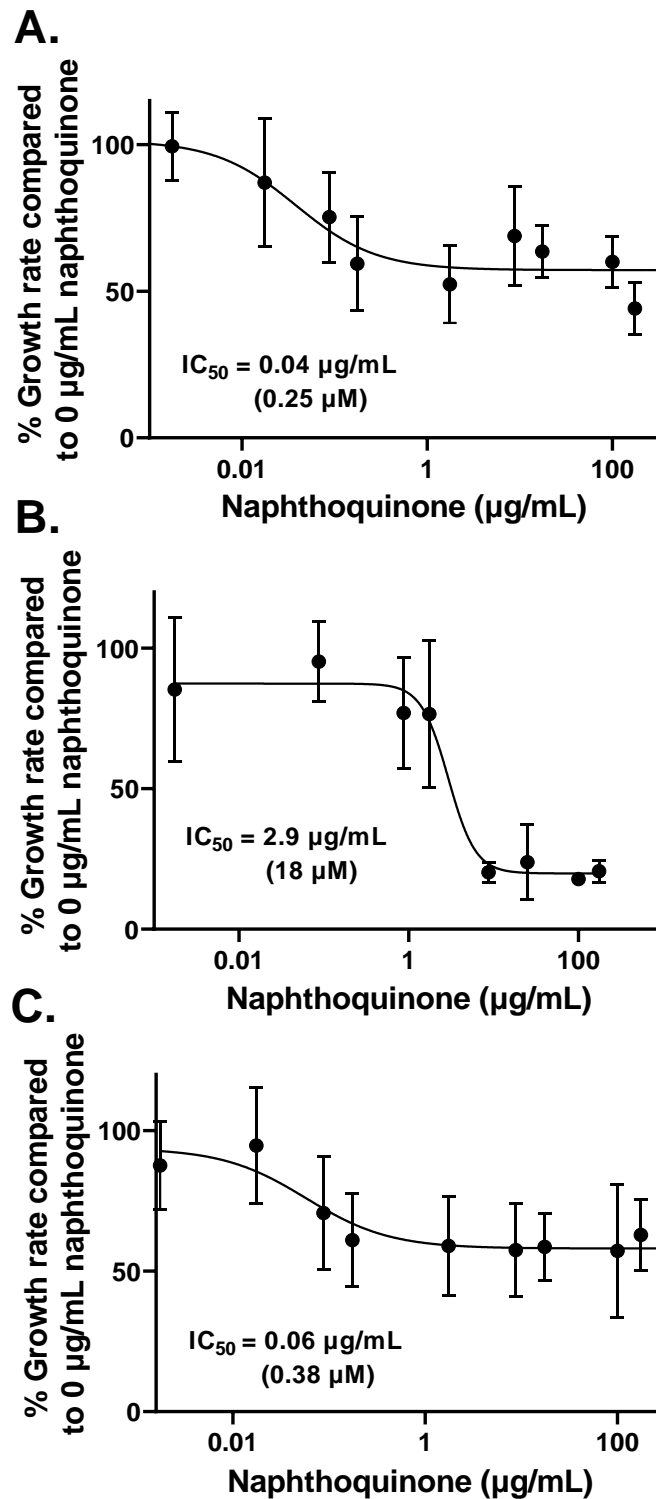


Figure 4.7. Growth Assays of 2-hydroxy-1,4-naphthoquinone against *E. coli* EC958 WT, cytochrome *bd*-I only and cytochrome *bo'*-only cells. 2-hydroxy-1,4-naphthoquinone inhibits growth of *E. coli* **A)** WT cells at IC₅₀ of 0.04 ± 0.03 µg/mL (0.25 ± 0.2 µM), **B)** *bd*-I only cells at an IC₅₀ of 2.9 ± 1.1 µg/mL (18 ± 6.8 µM) and **C)** *bo'*-only cells with an IC₅₀ of 0.06 ± 0.03 µg/mL (0.38 ± 0.19 µM). Dose response data were fitted to the sigmoid $y = Bottom + (Top - Bottom) / (1 + 10^{-(X - LogIC50)})$ equation using nonlinear regression (GraphPad). Error bars represent the mean with standard deviations for 6 technical repeats.

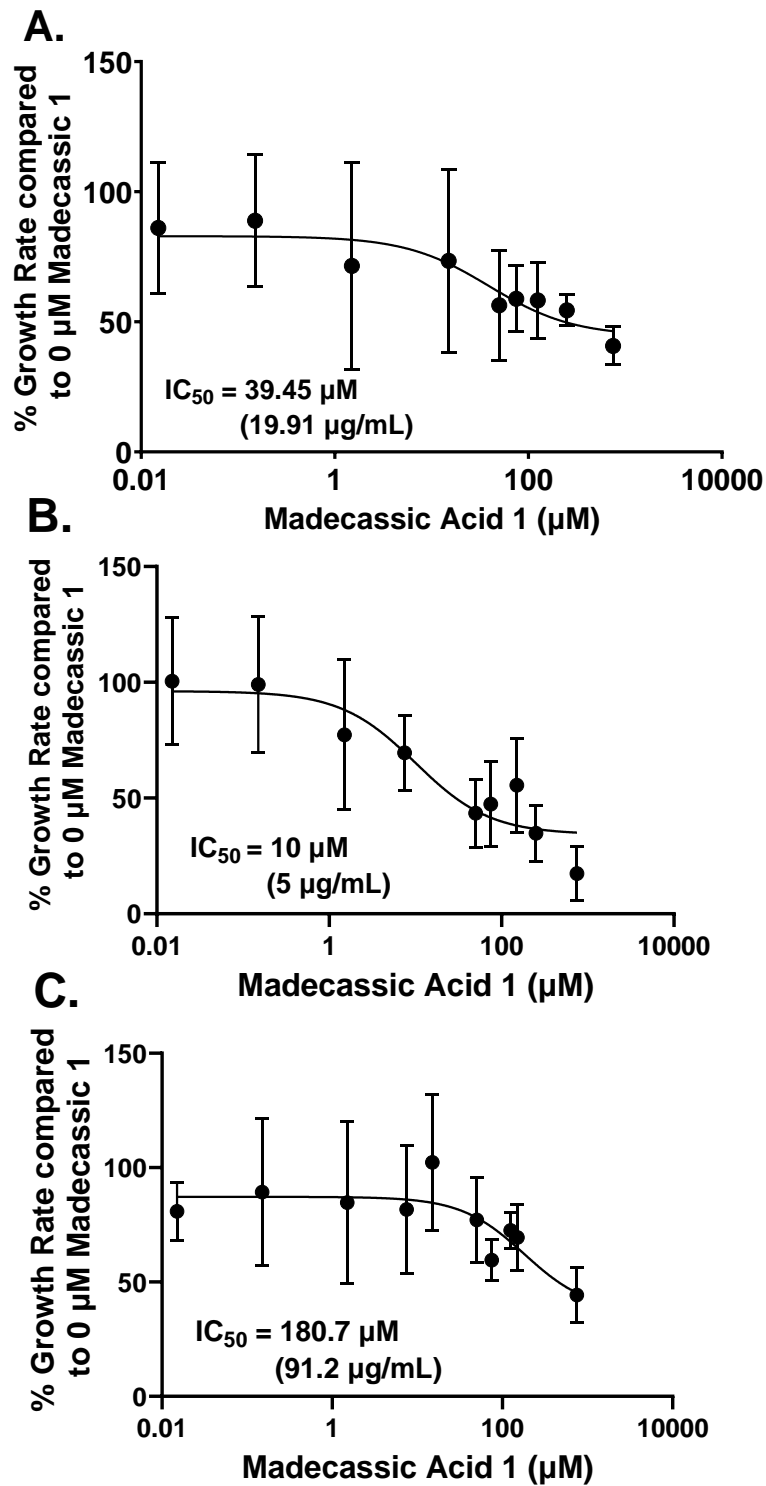


Figure 4.8. Growth Assays of madecassic acid 1 against *E. coli* WT, cytochrome *bd-I* only and cytochrome *bo'*-only cells. Madecassic acid 1 inhibits growth of *E. coli* **A)** WT cells at IC_{50} of $39.45 \pm 19 \mu\text{M}$ ($19.91 \pm 9.6 \mu\text{g/mL}$), **B)** *bd-I* only cells with an IC_{50} of $10 \pm 5.8 \mu\text{M}$ ($5 \pm 2.9 \mu\text{g/mL}$) and **C)** *bo'*-only cells at an IC_{50} of $180.7 \pm 144.7 \mu\text{M}$ ($91.2 \pm 73 \mu\text{g/mL}$). Dose response data were fitted to the sigmoid $y = \text{Bottom} + (\text{Top} - \text{Bottom}) / (1 + 10^{-(X - \text{Log}IC_{50})})$ equation using nonlinear regression (GraphPad). Error bars represent standard deviation for 6 technical repeats.

To further investigate the impact of 2-hydroxy-1,4-naphthoquinone and madecassic acid 1 upon *bd-I*-only and *bo'*-only strains, viability assays were conducted. It was shown that 2-hydroxy-1,4-naphthoquinone was not lethal against *E. coli* EC958 WT, *bd-I* only nor *bo'*-only cells (Figure 4.9). Viability assays were also undertaken with madecassic acid 1 and *E. coli* EC958 WT, *bd-I* and *bo'*-only cells, although it was confirmed not to kill any of the strains tested (Figure 4.10).

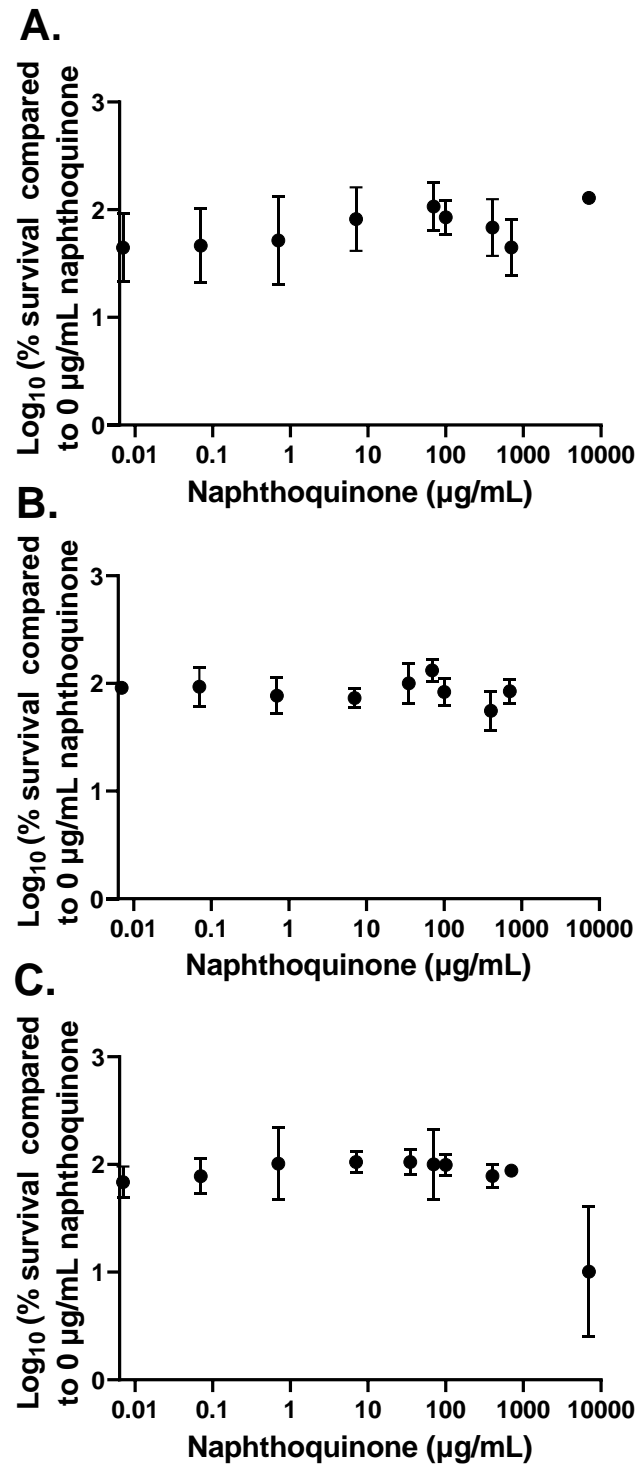


Figure 4.9. Viability assays of 2-hydroxy-1,4-naphthoquinone against *E. coli* EC958 WT, cytochrome *bd-I* only and cytochrome *bo'*-only cells. 2-hydroxy-1,4-naphthoquinone does not kill *E. coli* **A)** WT cells **B)** *bd-I* only cells nor **C)** *bo'*-only cells. Error bars represent the mean with standard deviations for 6 technical repeats.

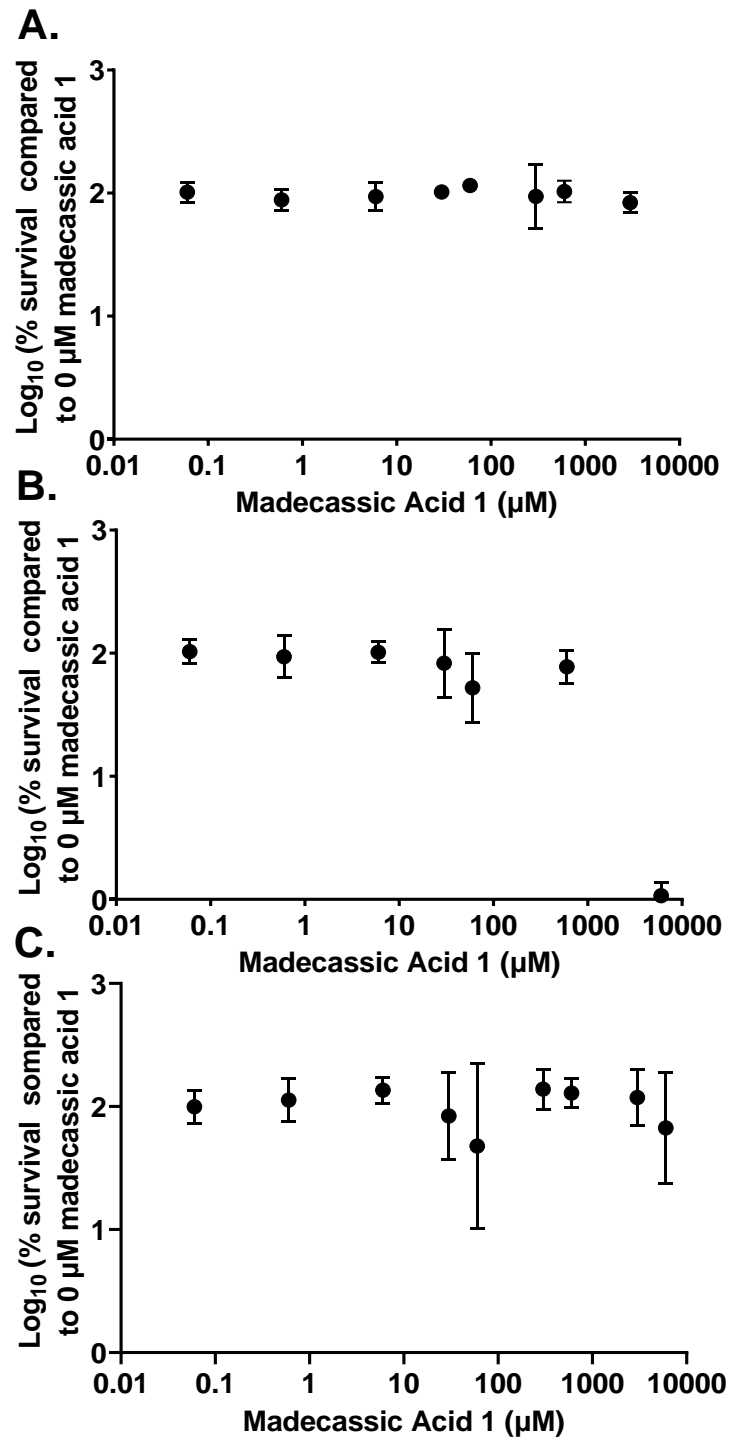


Figure 4.10. Viability assays of madecassic acid 1 against *E. coli* EC958 WT, cytochrome *bd-I* only and cytochrome *bo'*-only cells. Madecassic acid 1 does not kill *E. coli* A) WT cells B) *bd-I* only cells nor C) *bo'*-only cells. Error bars represent the mean with standard deviations for 6 technical repeats.

4.3.3. Assessing derivatives of madecassic acid 1 as *E. coli* cytochrome *bd-I* inhibitors

4.3.3.1. *In silico* analysis of madecassic acid 1 derivatives

Through collaboration with Dr Chris Serpell at the University of Kent, madecassic acid derivatives were chosen to investigate if alteration of several moieties could improve binding to the quinol site of cytochrome *bd*. To predict binding affinities of the madecassic acid 1 derivatives, an *in silico* analysis was performed (Table 4.2). Three madecassic acid 1 derivatives (madecassic acid 2, madecassic acid 3 and madecassic acid 4) were docked to the ubiquinol binding site of *E. coli* cytochrome *bd-I* AlphaFold 2 model (Figure 4.11). Docking images revealed multiple hydrophobic interactions between the compounds and the quinol binding site of *E. coli* cytochrome *bd-I* (Figure 4.11). The original compound, madecassic acid 1, displayed several hydrophobic residues (Figure 4.2) and a low K_d value of 1.14 μM (Table 4.2). Modifications made to the original madecassic acid 1 compound along with the predicted binding affinities are shown in Table 4.2.

The first derivative, madecassic acid 2, had hydroxy groups being replaced by acetoxy groups at the bottom left region of the structure. This change from hydroxy to acetoxy had resulted in a slightly lower K_d value of 0.96 μM . Madecassic acid 3 retained the acetoxy groups from the first derivative but added a $\text{NH}(\text{CH}_2)_{10}\text{NH}_2$ chain which increased the K_d value to 14.35 μM . Madecassic 4 had the acetoxy group removed but retained the $\text{NH}(\text{CH}_2)_{10}\text{NH}_2$ group which resulted in a molecular predicted K_d value of 8.64 μM . This data suggests that the presence of an acetoxy group instead of a hydroxy group result in tighter binding as seen by the decreased K_d value. However, a $\text{NH}(\text{CH}_2)_{10}\text{NH}_2$ chain results in weaker binding with an increased K_d value.

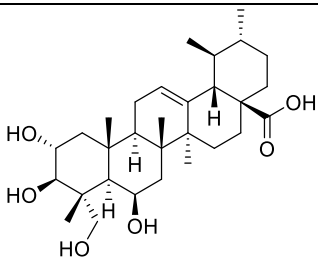
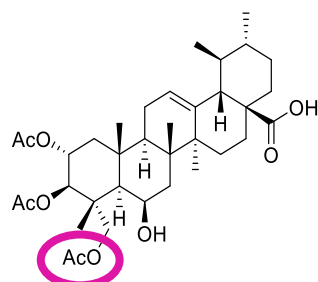
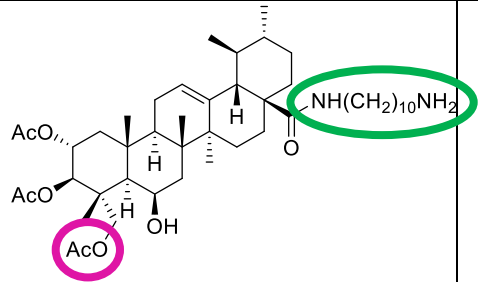
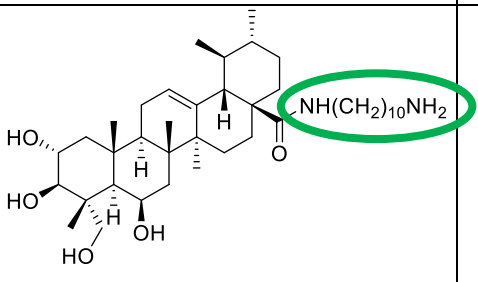
Compound	Structure	Molecular Weight	K_d Value (μM)
Madecassic Acid 1 (Original compound)		504.7	1.14
Madecassic Acid 2		630.8	0.96
Madecassic Acid 3		785.1	14.35
Madecassic Acid 4		659	8.64

Table 4.2. Madecassic acid derivatives structures, molecular weights and predicted binding affinities. Madecassic acid 1 (original compound) has a low K_d value of 1.14 μM . An acetoxy group was added madecassic acid 1 which resulted in madecassic acid 2 having a lower K_d value of 0.96 μM . The acetoxy group remained on madecassic acid 3 but a new chain was added ($\text{NH}(\text{CH}_2)_{10}\text{NH}_2$) which resulted in a predicted K_d value of 14.35 μM . The final compound, madecassic acid 4, kept only the long chain ($\text{NH}(\text{CH}_2)_{10}\text{NH}_2$) and had a predicted K_d value of 8.64 μM

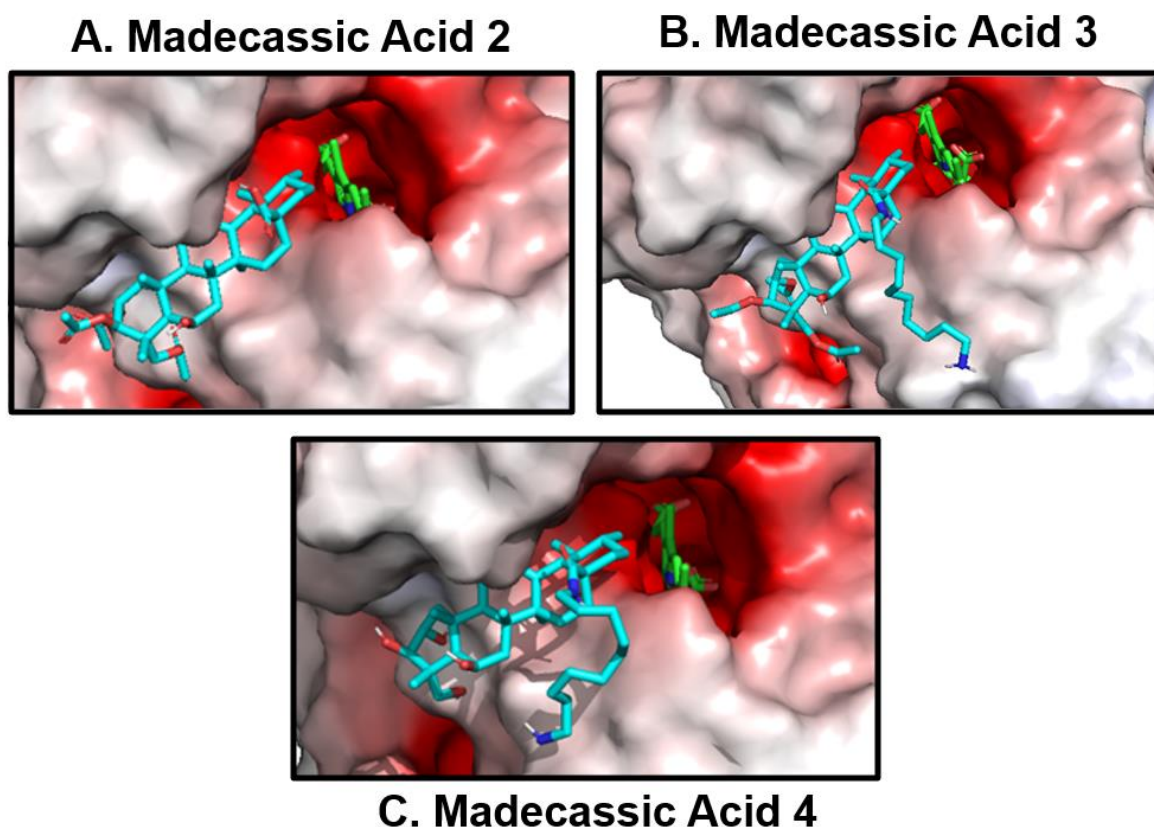


Figure 4.11. Madecassic acid derivatives docked to *E. coli* AlphaFold 2 cytochrome *bd-I* model. Three madecassic acid derivatives were docked to the haem *b*₅₅₈ quinol-binding pocket of *E. coli* cytochrome *bd-I* AlphaFold 2 model. These compounds are identified as **A)** madecassic acid 2, **B)** madecassic acid 3 and **C)** madecassic acid 4. Red = negative charge. White = hydrophobic. Blue = positive charge.

4.3.3.2. Oxygen consumption, growth and lethality of madecassic acid derivatives against *E. coli* EC958 cytochrome *bd-I* only cells.

To further investigate madecassic acid derivatives as inhibitors of *E. coli* cytochrome *bd-I* oxidase, microbiological assays were performed. Firstly, oxygen consumption assays were carried out to determine the ability of each derivative to inhibit oxygen consumption activity in *E. coli* EC958 cytochrome *bd-I* only membranes (Figure 4.12). *E. coli* cytochrome *bd-I* only membranes were inhibited by madecassic acid 2 with an IC₅₀ of 8.8 ± 3.5 μM (5.6 ± 2.2 μg/mL) (Figure 4.12). Madecassic acid 3 inhibited *E. coli* cytochrome *bd-I* only membranes with an IC₅₀ of 10.2 ± 1.1 μM (8 ± 0.9 μg/mL) (Figure 4.12). Interestingly, madecassic acid 4 also led

to inhibition of *E. coli* cytochrome *bd*-I only membranes but at a much higher IC_{50} of $92.8 \pm 47.3 \mu\text{M}$ ($61.2 \pm 31.2 \mu\text{g/mL}$) (Figure 4.12). This data coincides with the *in silico* analysis which proposed that the presence of acetoxy groups being added to madecassic acid 2 had led to a lower predicted K_d value (see Table 4.3). This is evident in the oxygen consumption membrane assays as madecassic acid 2 had led to the lowest IC_{50} regarding inhibition of *E. coli* cytochrome *bd*-I only membranes. Madecassic acid 3 had acetoxy groups present but a newly added $\text{NH}(\text{CH}_2)_{10}\text{NH}_2$ chain may have increased the predicted binding affinity hugely (see Table 4.2). Despite the addition of this $\text{NH}(\text{CH}_2)_{10}\text{NH}_2$ chain to madecassic acid 3, the presence of the acetoxy groups may have resulted in IC_{50} of $10.2 \pm 1.1 \mu\text{M}$. However, the acetoxy groups were removed from madecassic acid 4 and the $\text{NH}(\text{CH}_2)_{10}\text{NH}_2$ chain remained (see Table 4.3). This led to a much higher IC_{50} of $92.8 \pm 47.3 \mu\text{M}$.

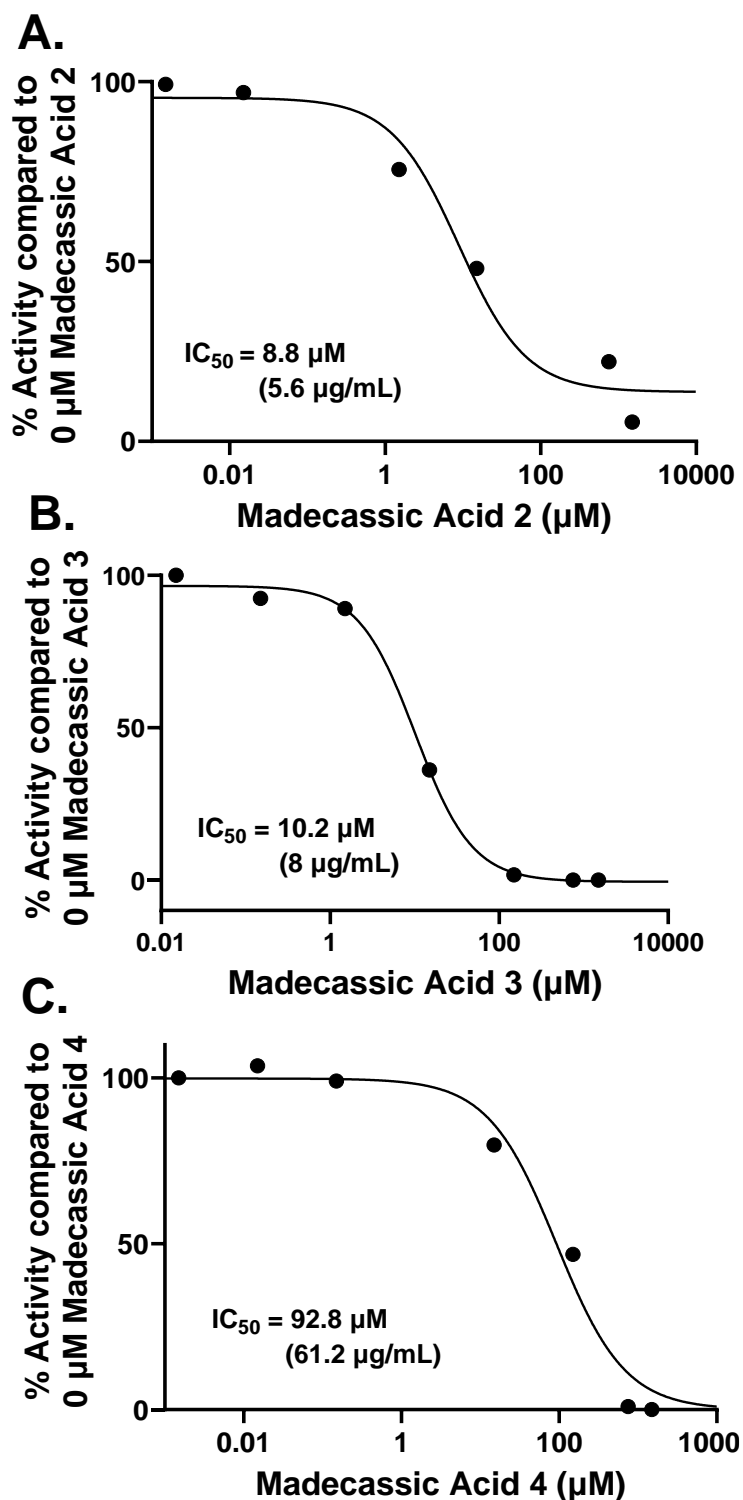


Figure 4.12. Madecassic acid derivatives inhibit *E. coli* EC958 cytochrome *bd*-I only membranes. A) Madecassic acid 2 inhibited *E. coli* cytochrome *bd*-I only membranes with an IC_{50} of $8.8 \pm 3.5 \mu\text{M}$ ($5.6 \pm 2.2 \mu\text{g/mL}$), B) Madecassic acid 3 inhibited *E. coli* cytochrome *bd*-I only membranes with an IC_{50} of $10.2 \pm 1.1 \mu\text{M}$ ($8 \pm 0.9 \mu\text{g/mL}$) and C) Madecassic acid 4 inhibited *E. coli* cytochrome *bd*-I only membranes with IC_{50} of $92.8 \pm 47.3 \mu\text{M}$ ($61.2 \pm 31.2 \mu\text{g/mL}$). Data points represent single experiments. Dose response data were fitted to the sigmoid $y = \text{Bottom} + (\text{Top} - \text{Bottom}) / (1 + 10^{-(X - \text{LogIC}_{50})})$ equation using nonlinear regression (GraphPad).

It has been confirmed that the madecassic acid derivatives are capable of inhibiting oxygen consumption activity of *E. coli* EC958 cytochrome *bd-I* membranes. Herein, experiments were conducted on whole cells to determine the effects of these derivatives on the growth and survival of *E. coli* EC958 cytochrome *bd-I* only cells. Madecassic acid derivatives inhibited the growth of *E. coli* cytochrome *bd-I* only cells with madecassic acid 3 having the lowest IC_{50} of $0.2 \pm 2.5 \mu\text{M}$ ($0.16 \pm 2 \mu\text{g/mL}$) (Figure 4.13B). Madecassic acid 2 had the second lowest IC_{50} of $58.6 \pm 14.4 \mu\text{M}$ ($36.97 \pm 9.1 \mu\text{g/mL}$) (Figure 4.13A). Madecassic acid 4 showed the least inhibition with an IC_{50} of $151 \pm 9.4 \mu\text{M}$ ($99.5 \pm 6.2 \mu\text{g/mL}$) (Figure 4.13C). Viability assays with madecassic acid derivatives demonstrate that madecassic acid 2 and 3 does not kill *E. coli* *bd-I* only cells (Figure 4.14). However, madecassic acid 4 showed inhibition to *E. coli* EC958 cytochrome *bd-I* only cells with an IC_{50} of $327.69 \pm 103.7 \mu\text{M}$ ($215.95 \pm 68.34 \mu\text{g/mL}$).

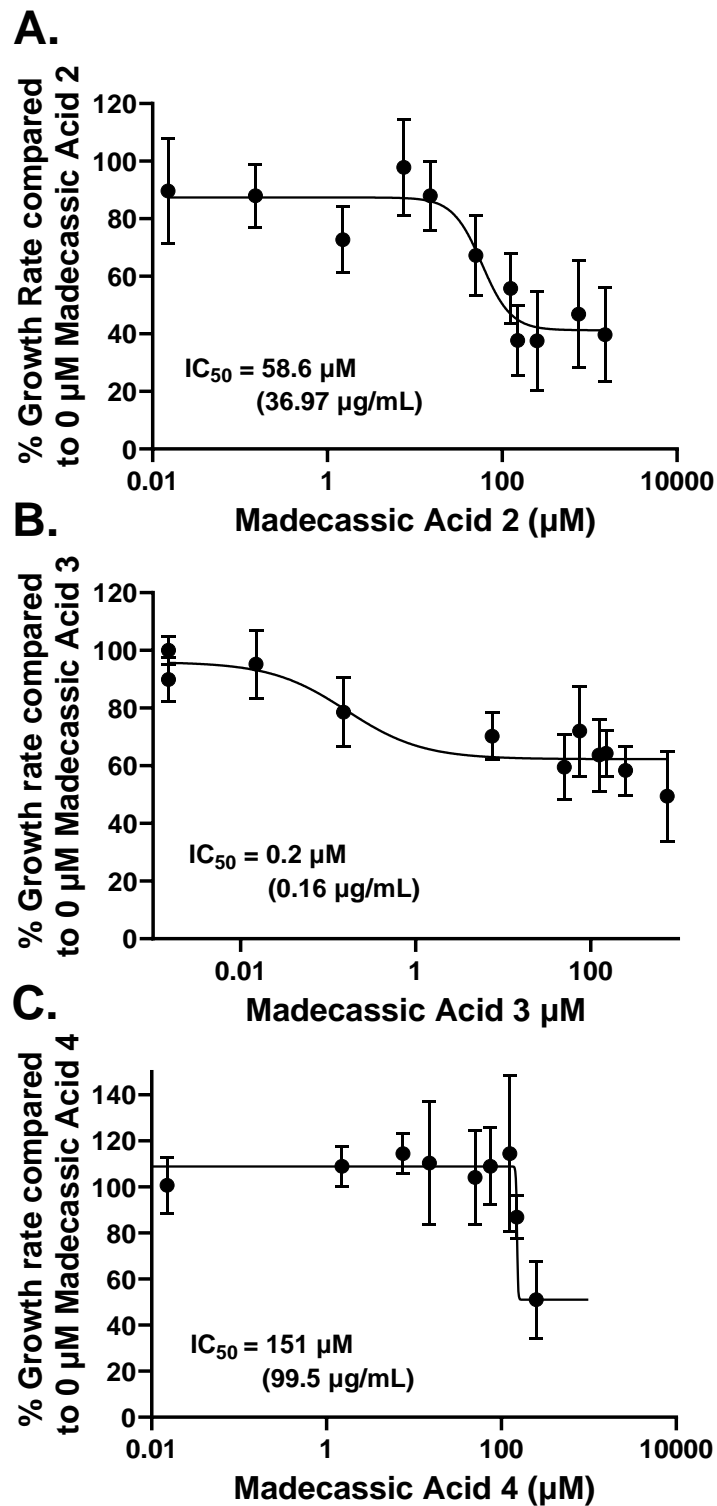


Figure 4.13. Madecassic acid derivatives inhibit the growth of *E. coli* EC958 cytochrome *bd-I* only cells. A) Madecassic acid 2 inhibited growth of *E. coli* EC958 cytochrome *bd-I* only cells with an IC_{50} of $58.6 \pm 14.4 \mu\text{M}$ ($36.97 \pm 9.1 \mu\text{g/mL}$), B) Madecassic acid 3 of *E. coli* EC958 cytochrome *bd-I* only cells at an IC_{50} of $0.2 \pm 2.5 \mu\text{M}$ ($0.16 \pm 2 \mu\text{g/mL}$) and C) Madecassic acid 4 of *E. coli* EC958 cytochrome *bd-I* only cells at an IC_{50} of $151 \pm 9.4 \mu\text{M}$ ($99.5 \pm 6.2 \mu\text{g/mL}$). Dose response data were fitted to the sigmoid $y = \text{Bottom} + (\text{Top} - \text{Bottom}) / (1 + 10^{((\text{LogIC}_{50} - X) * \text{HillSlope}))}$ equation using nonlinear regression (GraphPad). Error bars represents standard deviation of 6 technical repeats.

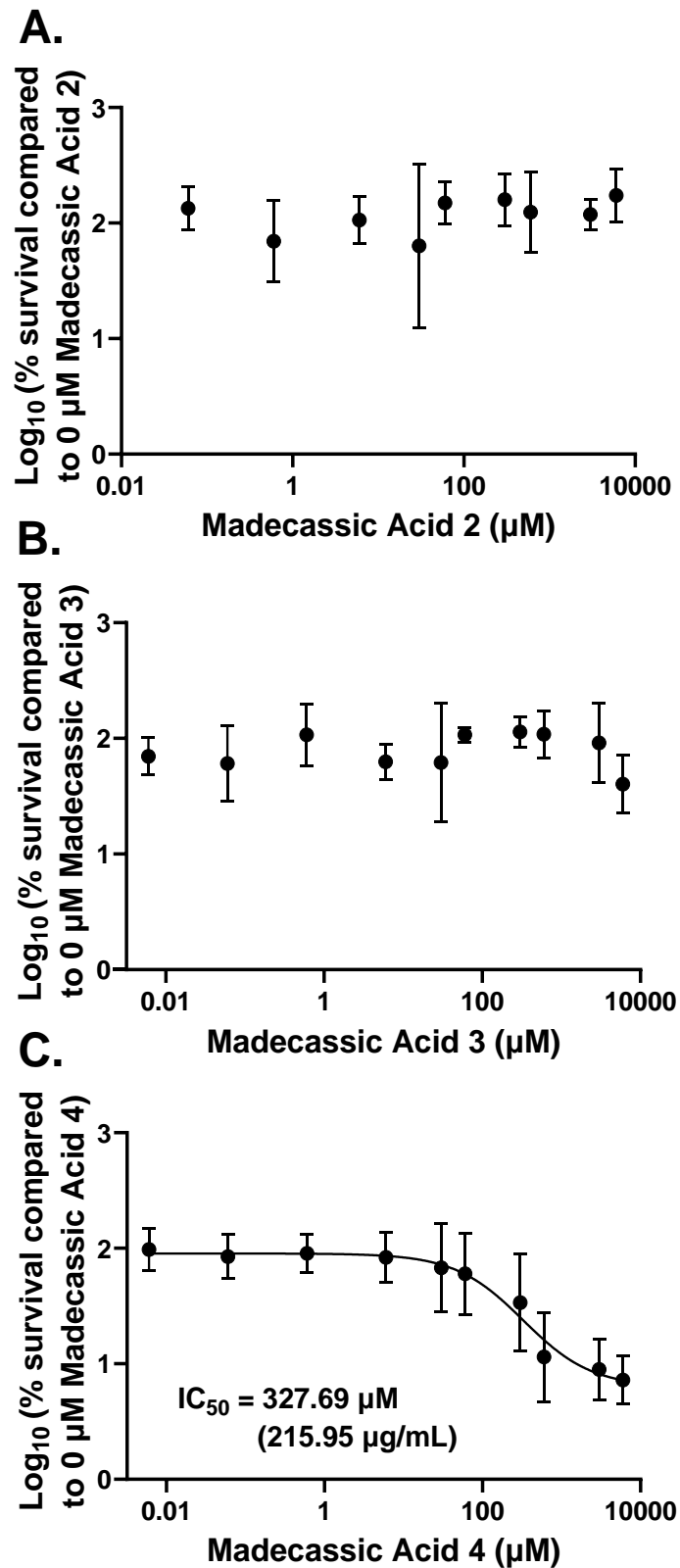


Figure 4.14. Madecassic acid derivatives survival assay on *E. coli* EC958 cytochrome *bd-I* only cells. A) Madecassic acid 2 did not kill *E. coli* EC958 cytochrome *bd-I* only cells. B) Madecassic acid 3 did not kill *E. coli* EC958 cytochrome *bd-I* only cells. C) Madecassic acid 4 killed *E. coli* EC958 cytochrome *bd-I* only cells at an IC₅₀ of 327.69 ± 103.7 μM (215.95 ± 68.34 μg/mL). Error bars represent standard deviation of 6 technical repeats.

4.4. Discussion

4.4.1. Development of *in silico* and experimental tools to identify new potential inhibitors of cytochrome *bd-I*

As previously mentioned, cytochrome *bd* is a good drug target due to its absence in eukaryotes and it plays a vital role in virulence of many highly pathogenic strains of bacteria (Borisov *et al.* 2020). There are high resolution published structures which make this respiratory oxidase easy to study (Safarian *et al.* 2019; Grauel *et al.* 2021). To predict the molecular binding affinities of the known antimicrobials for *E. coli* cytochrome *bd-I*, a molecular docking pipeline was developed. AlphaFold 2 models were predesigned in the host laboratory through structural modelling (Webster, C.M. (2023) PhD thesis, University of Kent). An FDA-approved drug library from e-Drug3D (Pihan *et al.* 2012) containing 1993 drugs was screened against the quinol site of *E. coli* cytochrome *bd-I* model via AutoDock Vina. Analyses of the results were achieved using PyMOL. The use of an FDA-approved drug library posed a few advantages, the major one being that the drugs have been proven safe for human consumption and stages of clinical trials could be skipped subsequently lowering drug development time (Pushpakom *et al.* 2018; Farha and Brown 2019). The *in silico* docking pipeline exploited in this study is a transferrable tool that can be adopted for oxidases in various pathogens as well as to explore other potential binding sites present in these oxidases.

A uropathogenic strain of *E. coli* EC958 was used as this is a clinical pathogenic strain isolated from a UTI patient. *E. coli* has three known respiratory oxidases: cytochrome *bd-I*, *bd-II* and *bo'*. Therefore, it was important to develop mutant strains expressing single respiratory oxidases to determine the effect of repurposed drugs on each oxidase. Lambda-Red mutagenesis was previously used by the host laboratory to produce strains that expressed either cytochrome *bd-I* or cytochrome *bo'* as the sole respiratory oxidase. Having a cytochrome *bo'*

only strain allowed for the specificity of repurposed compounds to cytochrome *bd* to be determined. Growth and survival assays were also essential to determine the effects of the compounds on whole cells.

4.4.2. Known antimicrobials as inhibitors of cytochrome *bd*

Atovaquone is a known quinol site inhibitor and is therefore highly relevant to this study (Mather *et al.* 2005). Atovaquone functions as a ubiquinone analogue that targets the respiratory chain of cytochrome *bc*₁ complex of *P. falciparum* and compactivity inhibits ubiquinol (Nixon *et al.* 2013). The molecular docking imaging results of atovaquone to the quinol binding site of *E. coli* cytochrome *bd*-I has shown numerous hydrophobic interactions. There are many residues that are important for binding within the quinol binding cleft but Arg391, Ile295 and Phe390 were highlighted as some of the most important residues for this interaction. The binding of atovaquone to the ubiquinol site in subunit 1 of cytochrome *bo'* showed less hydrophobic reactions than that of cytochrome *bd*-I. Atovaquone had the lowest molecular predicted K_d value of 0.96 M for the AlphaFold 2 model of *E. coli* cytochrome *bd*-I. However, this low K_d value was not proven reliable in the experimental assays as atovaquone did not cause any inhibition to *E. coli* cytochrome *bd*-I nor cytochrome *bo'* only membranes.

The next drug to be docked was 2-hydroxy-1,4-naphthoquinone, the head group of atovaquone. 1,4-naphthoquinone (lawsone) is a naturally occurring plant dye that has demonstrated great interest to medical research. 1,4-naphthoquinone possesses antibacterial properties through increasing ROS generation and activating apoptotic cell death (Ravichandiran *et al.* 2019). As well as being antibacterial, 1,4-naphthoquinones have shown properties that are anti-ischaemic, cardioprotective, hepatoprotective and neuroprotective (Aminin and Polonik 2020). Additionally, a recent study generated 3-alkylated derivatives of 1,4-naphthoquinone to target *E. coli* cytochrome *bd*-I and cytochrome *bo'* oxidases (Elamri *et*

al. 2020). The study was able to identify 2-hydroxy-1,4-naphthoquinone derivatives that were selective inhibitors of cytochrome *bo'* oxidase activity and had no effect on cytochrome *bd-I* (Elamri *et al.* 2020). This research revealed that the molecular K_d value of 2-hydroxy-1,4-naphthoquinone was significantly higher than that of atovaquone and madecassic acid 1 for docking to CydA of *E. coli* cytochrome *bd-I*. Despite this, 2-hydroxy-1,4-naphthoquinone resulted in the inhibition of *E. coli* cytochrome *bd-I* which was proven impossible for atovaquone that demonstrated an extremely lower K_d value. The K_d value for 2-hydroxy-1,4-naphthoquinone to subunit 1 of *E. coli* cytochrome *bo'* was 3.3 times lower than that of cytochrome *bd-I* (Table 4.2), however, there were no significant changes observed in the potency of the compound to both oxidases. This study demonstrated that atovaquone and 2-hydroxy-1,4-naphthoquinone bind at similar locations on cytochrome *bd-I* oxidase model (Figure 4.2), despite 2-hydroxy-1,4-naphthoquinone having a much higher predicted K_d value than atovaquone (Table 4.2). However, the binding of 2-hydroxy-1,4-naphthoquinone to cytochrome *bo'* showed a slightly different binding location within the ubiquinol binding pocket when compared to atovaquone (Figure 4.3).

Madecassic acid 1 was the third known antimicrobial to be docked to *E. coli* cytochrome *bd-I* and *bo'* AlphaFold 2 models. Madecassic acid is produced by *Centella asiatica* (Indian pennywort) and is a known anticancer (Valdeira *et al.* 2019) and antibacterial (Wei, Cui and Liu 2023) agent. Molecular docking images revealed that madecassic acid 1 can potentially bind well to the quinol binding site of *E. coli* cytochrome *bd-I*. There were more hydrophobic interactions between madecassic acid 1 and the quinol binding pocket of *E. coli* cytochrome *bo'* than the natural substrate, ubiquinol-8 had. The K_d value generated for madecassic acid 1 when docked to CydA of *E. coli* cytochrome *bd-I* was quite low (1.14 μM) and corresponded with a relatively low IC_{50} value of 46.80 μM in *bd-I* only membranes.

However, the IC₅₀ value generated in cytochrome *bo'* membranes was 64.3 μM which did not coincide with a relatively high *K_d* value of 39.54 μM generated in the molecular docking.

The inconsistency seen in the molecular *K_d* values and IC₅₀ values could propose that molecular docking tools are not always reliable and effective for use in drug repurposing. Though effective in narrowing down potential inhibitors of a drug target when posed with a long list of compounds, the molecular docking tool could potentially miss vital hits that have been ranked with lower binding affinities for a target. A computational study (Ramírez and Caballero, 2016) was done to establish the trustworthiness of docking energies by comparing two complexes between a target protein and enantiomeric pairs. AutoDock Vina, the docking tool used in this PhD research, was among the docking software tested. It was discovered that accurate predictions of binding energies in docking are heavily dependent on chance (Ramírez and Caballero, 2016). The study further revealed that scoring functions that accompanies popular docking programs do not always generate reliable predictions as it relates to binding affinities of ligands to proteins (Ramírez and Caballero, 2016).

4.4.3. Derivatisation enhances inhibitory activity of madecassic acid against *E. coli* EC958 cytochrome *bd-I*

Derivatives of madecassic acid were synthesised for various *in vitro* analyses for their ability to improve drug action. Three of these derivatives were used for testing on *E. coli* EC958 membranes to assess their ability to inhibit oxygen consumption activity. Comparisons were drawn between the derivatives and madecassic acid 1 original compound to determine whether derivatisation improved drug action. The results suggest that the acetoxy derivatives (Madecassic Acid 2 and 3) are tighter binders of *E. coli* cytochrome *bd-I* quinol site and are therefore more potent inhibitors of the oxidase. Acetylation is often used in medicinal chemistry to enhance drug physiochemical properties (Churchill *et al.* 2021). One of the main

results of this is increased permeability and the ability for drugs to cross membranes more easily (Churchill *et al.* 2021).

Other studies have showcased the pharmacological properties of madecassic derivatives in research. Madecassic derivatives were synthesised and tested against various cancer cell lines to determine anticancer properties (Valdeira *et al.* 2019). Of these derivatives, compound 29 was the most potent, showing anticancer activity against 26 different tumour cell lines and selectivity for one colon and two melanoma tumour cell lines (Valdeira *et al.* 2019). A recent study assessed the antibacterial ability of madecassic acid against eight pathogenic strains of bacteria including MRSA, *Escherichia coli*, *Pseudomonas aeruginosa*, *Bacillus subtilis* and *Bacillus megaterium* (Wei, Cui and Liu 2023). The study confirmed that madecassic acid is highly inhibitory against *S. aureus* through destruction of the cell membrane and cell wall (Wei, Cui and Liu 2023). It was also proposed that madecassic acid could decrease the activities of succinate dehydrogenase and malate dehydrogenase (Wei, Cui and Liu 2023). This raises questions around the ability of the compound to inhibit oxygen consumption activity through specifically inhibiting terminal respiratory oxidases such as cytochrome *bd*.

Chapter 5

**Drug screening approaches to
identify novel inhibitors of
cytochrome *bd***

5.1. Summary

Drug repurposing is a strategy used to develop drugs to treat a new condition from an existing approved drug. This tool can also be used computationally to perform *in silico* drug repurposing. It has a few advantages when compared to *de novo* drug discovery approaches considering that it is cheaper and generally takes a shorter time for a repurposed drug to hit the market. Challenges associated with drug repurposing is that the method is prone to failure and questions often arise around the novelty of the drug considered that it was already approved for treating a different condition. Despite this, drugs such as Anastrozole was discovered for inducing ovulation but was repurposed for the treatment of breast cancer.

Molecular docking is a form of *in silico* drug repurposing technique that measures the affinity of a small drug ligand to a protein structure. This method was used in this study to find drugs that has high affinity for the ubiquinol site of CydA subunit of *E. coli* cytochrome *bd-I*. Among the top 50 hits were the steroid drugs ethinylestradiol, quinestrol and mestranol. These drugs were screened in the laboratory via an oxygen consumption membrane assay on cytochrome *bd-I* only membranes and it was determined that quinestrol was the most potent. Quinestrol was proven the most potent of the three repurposed-drugs, and further work was performed on *E. coli* and MRSA strains to determine the effects of the synthetic hormone on Gram-negative and Gram-positive organisms.

5.2. Introduction

5.2.1. Drug Repurposing Progresses and Challenges

Drug repurposing, also called drug repositioning, may be defined as a process by which new uses are given to old therapeutic agents that have already been approved for treating other medical conditions (Roy, Dhaneshwar and Bhasin 2021; Kulkarni *et al.* 2023). Traditional methods of drug discovery are proven to be more expensive, time-consuming with many stages that involve identifying and optimising the target followed by a series of clinical and pre-clinical trials (Shaker *et al.* 2021). It has been estimated that it takes \$1.8 billion USD (Paul *et al.* 2010) for a new drug to be introduced to the market from drug discovery (Table 5.1). The cost in drug repurposing is significantly reduced as several major steps such as preclinical trials are not required, cutting the cost to about \$300 million USD (Nosengo 2016) (Table 5.1).

One of the major advantages of drug repurposing is that drug candidates have already been proven to be adequately safe in various stages of clinical trials for human consumption (Talevi and Bellera 2020). In addition, if a dose that is comparable to the previously approved dose is effective against the new target, then the initial stages of preclinical testing can be bypassed to further stages along the clinical testing (Talevi and Bellera 2020). There are several drugs that have gone through stages of clinical development but were not successful due to reasons that exclude safety. An example is Viagra that was first developed for the treatment of hypertension but was later repurposed for a better use which is to treat erectile dysfunction (Kulkarni *et al.* 2023). Another drug, Anastrozole, was discovered for inducing ovulation but was later repurposed for the treatment of breast cancer (Aggarwal *et al.* 2021).

Despite the myriads of advantages that drug repurposing offers, there are many challenges that accompany this approach. Firstly, the approach is not always successful and there are times when the process fails. An example is Topiramate that was originally discovered

to treat epilepsy and was attempted to be repurposed for inflammatory bowel disease treatment (Pushpakom *et al.* 2018). The drug was successful in a rodent model to treat inflammatory bowel disease but later failed in a cohort study (Crockett *et al.* 2014). Secondly, there are legal concerns that could prevent the patenting of a drug for a new medical use (Kulkarni *et al.* 2023). Some legislations oppose the patenting of a drug for a second medical indication. Thirdly, many potential repurposing uses are sometimes reported in literature or is offered clinically as an off label which raises debates around novelty (Pushpakom *et al.* 2018). Finally, there are challenges around availability to data or the compound as access to some valuable data such as clinical trials are limited to the public (Talevi and Bellera 2020). Not all pharmaceutical companies are open and willing to share their chemical library that include failed drugs to the public which may limit the pool of compounds there are to choose from (Talevi and Bellera 2020).

DE NOVO DRUG DISCOVERY	DRUG REPURPOSING
Includes 5 Stages: <ul style="list-style-type: none"> ○ Drug discovery and preclinical ○ Safety review ○ Clinical research ○ FDA review ○ FDA post-market and safety monitoring 	Include 4 stages: <ul style="list-style-type: none"> ○ Compound Identification (1-2 years) ○ Compound Acquisition (0-2 years) ○ Development (1 – 6 years) ○ FDA post-market safety monitoring
Time: 10 – 17 years	Time: 3 – 12 years
High cost: estimated \$1.8 billion USD	Less investment: estimated \$300 million USD
Higher risk of failing	Lower risk of failing
Safety profile requires evaluation	Safety profiles already exist

Table 5.1. Modern drug repurposing approaches compared to *de novo* drug discovery. Modern drug repurposing tools are proven more advantageous than the conventional *de novo* drug discovery approaches as it relates to time, costs, and success.

5.2.2. Approaches for Drug Repurposing

The review of the literature herein has demonstrated that the modern drug repurposing is generally a much faster and cheaper strategy in discovering new drugs to treat a disease than the conventional *de novo* method (Table 1.2). There are usually three main steps that are involved in drug repurposing which include identification of the compound that will be repurposed, acquisition of the compound and development of the compound which often involves phase II clinical trials (Pushpakom *et al.* 2018). The strategies used to achieve these steps are a part of two broader approaches of drug repurposing which are computational and experimental (Pushpakom *et al.* 2018). All approaches of drug repurposing usually fall under these two approaches but both approaches are often employed together to achieve the best outcome.

Computational approaches, as the name suggests, largely involves the analysis of data (e.g., electronic health records, gene expression and chemical structure) (Hodos *et al.* 2016). Data of this sort are usually large and complex and therefore, computational approaches are used to simplify the data to accelerate the drug discovery process (Hodos *et al.* 2016). Popular computational approaches in drug repurposing include signature matching, pathway mapping, retrospective clinical analysis, genetic association novel data sources and molecular docking (Pushpakom *et al.* 2018). The computational approach used throughout this study is molecular docking. Molecular docking is a common tool that uses three-dimensional modelling to dock a drug ligand into a protein-binding pocket allowing the affinity and interaction to be determined by the pairing (Hodos *et al.* 2016). This is a highly effective tool as it can allow researchers to screen large drug libraries with up to millions of compounds to find lead compounds that are potential drugs (Alvarez and Shoichet 2005). However, molecular docking relies on the existence of a three-dimensional model for the protein being studied which means that the absence of this poses a major limitation to the technique.

Molecular docking approaches are usually followed up with experimental approaches to validate the predicted interaction between drug and target. Experimental approaches are often performed synergistically with *in silico* methods to determine the pharmacological effect of the drug *in vitro* or *in vivo*. Popular experimental techniques include drug-target interactions that include binding assays and phenotypic screening for identifying compounds that exhibit effects of disease relevance in models (Pushpakom *et al.* 2018). Other reviews have classified experimental approaches under target-based screening, binding assays, drug-centric screening, and phenotype-based screening (Ng, Salim and Chu 2021). The experimental approach used throughout this study is a target-based screening approach, which measures the efficacy of a drug based on how well it binds to a set target which is usually a gene or protein (Sams-Dodd 2005; Ng, Salim and Chu 2021). In the case of the PhD study described in this thesis, the target of interest is cytochrome *bd*.

5.3. Results

5.3.1. *In silico* drug screen identified FDA-approved steroid drugs as potential inhibitors of cytochrome *bd*

In the fight against antimicrobial resistance, cytochrome *bd* is a suitable drug target for many reasons. Cytochrome *bd* is only found in prokaryotes and archaea (Borisov *et al.* 2021) giving rise to the ability of drugs to be developed which are not toxic to humans. Studies have shown that deletion severely attenuates virulence in some of the most pathogenic strains of bacteria such as Salmonella (Jones-Carson *et al.* 2016; Duc *et al.* 2020) and Mycobacterium (Lu *et al.* 2015). Lastly, cytochrome *bd* is induced by innate immune response and is highly expressed in *E. coli* during infection (Giuffrè *et al.* 2014).

Using AutoDock Vina, FDA-approved drugs were docked to the quinol binding site of *E. coli* cytochrome *bd*-I AlphaFold 2 (Table 5.2) (Webster, C.M. (2023) PhD thesis, University of Kent). There were several steroid drugs that appeared in the top hits which sparked an interest in assessing the ability of steroid drugs to bind to the quinol binding site of cytochrome *bd*. Ethinylestradiol, quinestrol and mestranol have similar structures including a distinctive hydrophobic steroid backbone which can be docked in similar configuration to the quinol site of cytochrome *bd*-I (Figure 5.1). The docking of all three steroid drugs to the quinol site of *E. coli* cytochrome *bd*-I reveals multiple hydrophobic interactions (Figure 5.1). The hydrophobic nature of all three drugs is an ideal characteristic for the compounds accessing the membranes. As shown in Table 5.3, all three steroid drugs have high predicted affinities for *E. coli* cytochrome *bd*-I. However, quinestrol has the highest predicted affinity with a K_d value of 0.49 μM followed by mestranol with 1.6 μM and ethinylestradiol with 1.89 μM (Table 5.3).

To draw molecular comparisons between the above data and a Gram-positive pathogen, all three FDA-approved steroid drugs (ethinylestradiol, quinestrol and mestranol) were docked

to the quinol site of *S. aureus* CydA subunit. The AlphaFold 2 model of CydA subunit was used as there are no PDB structures for *S. aureus* cytochrome *bd* oxidase. Like *E. coli* cytochrome *bd*-I, quineestrol exhibited the lowest predicted K_d value (1138 nM) to the AlphaFold 2 model of *S. aureus* quinol site of CydA (Table 5.4).

Ranking by predicted affinity	Drug Name	eDrug3D Database Number	Predicted Affinity (kcal/mol)	Estimated K_d (nM)
1	LOMITAPIDE	1572	-9.8	64
2	LEDIPASVIR	1731	-9.8	64
3	ERGOTAMINE	70	-9.6	90
4	IRINOTECAN	755	-9.4	127
5	NILOTINIB	1310	-9.4	127
6	CALCIPOTRIENE	1412	-9.4	127
7	DOXERCALCIFEROL	1417	-9.4	127
8	LUMACAFTOR	1782	-9.4	127
9	DROSPIRENONE	855	-9.3	150
10	ERGOCALCIFEROL	10	-9.2	177
11	ADAPALENE	718	-9.1	210
12	ALECTINIB	1819	-9.1	210
13	LIFITEGRAST	1824	-9.1	210
14	DIHYDROERGOTAMINE	36	-9	249
15	CYPROHEPTADINE	303	-9	249
16	DUTASTERIDE	883	-9	249
17	M DOXERCALCIFEROL	1556	-9	249
18	MIDOSTAURIN	1828	-9	249
19	M REVEFENACIN	1910	-9	249
20	ESTRADIOL CYPIONATE	20	-8.9	294
21	BROMOCRIPTINE	470	-8.9	294
22	BEXAROTENE	847	-8.9	294
23	CONIVAPTAN	927	-8.9	294
24	BETA CAROTENE	1380	-8.9	294
25	CALCITRIOL	480	-8.8	349
26	SIROLIMUS	853	-8.8	349
27	CANDICIDIN	1079	-8.8	349
28	PARITAPREVIR	1734	-8.8	349
29	M MIDOSTAURIN	1829	-8.8	349

30	M MIDOSTAURIN	1852	-8.8	349
31	MOXIDECTIN	1916	-8.8	349
32	ENTRECTINIB	1969	-8.8	349
33	HEXAFLUORENIUM	1336	-8.7	413
34	ELTROMBOPAG	1450	-8.7	413
35	SIMEPREVIR	1628	-8.7	413
36	VENETOCLAX	1822	-8.7	413
37	M ENTRECTINIB	1970	-8.7	413
38	CAPMATINIB	1983	-8.7	413
39	QUINESTROL	383	-8.6	489
40	MARAVIROC	958	-8.6	489
41	NYSTATIN	990	-8.6	489
42	ERGOLOID	1213	-8.6	489
43	CALCIFEDIOL	1390	-8.6	489
44	ABIRATERONE ACETATE	1519	-8.6	489
45	PONATINIB	1593	-8.6	489
46	NETUPITANT	1726	-8.6	489
47	TUCATINIB	1982	-8.6	489
48	LURBINECTEDIN	1986	-8.6	489
49	EXATECAN	1993	-8.6	489
50	PIMOZIDE	424	-8.5	579
51	DANAZOL	435	-8.5	579
52	TELMISARTAN	814	-8.5	579
53	HYDROCORTISONE CYPIONATE	1327	-8.5	579
54	VORAPAXAR	1710	-8.5	579
55	DASABUVIR	1735	-8.5	579
56	ELBASVIR	1815	-8.5	579
57	GLECAPREVIR	1850	-8.5	579
58	AVATROMBOPAG	1878	-8.5	579
59	BALOXAVIR	1914	-8.5	579
60	TRIFAROTENE	1944	-8.5	579
61	AVAPRITINIB	1968	-8.5	579
62	LOPERAMIDE	450	-8.4	685
63	ITRACONAZOLE	678	-8.4	685
64	RISPERIPERFORMED	713	-8.4	685
65	EXEMESTANE	795	-8.4	685
66	CHOLECALCIFEROL	824	-8.4	685
67	DACTINOMYCIN	1058	-8.4	685
68	TESTOSTERONE CYPIONATE	1335	-8.4	685
69	ERIBULIN	1505	-8.4	685
70	RILPIVIRINE	1516	-8.4	685

164	MESTRANOL	213	-7.9	1595
203	ETHINYL ESTRADIOL	18	-7.8	1889

Table 5.2. Top 70 potential *E. coli* cytochrome *bd*-I inhibitors ranked by predicted affinity to the quinol binding site of the AlphaFold 2 modelled structure. Steroid drugs quinestrol, ethinylestradiol and mestranol were highlighted as drugs of interest and were tested in the laboratory.

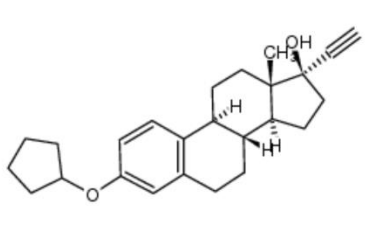
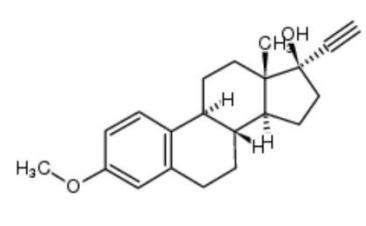
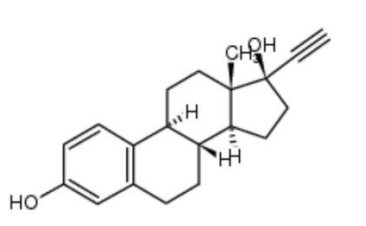
Ranking by predicted affinity	Drug Name	eDrug3D Database Number	Predicted Affinity (kcal/mol)	Estimated K_d (μ M)
39	Quinestrol 	383	-8.6	0.49
164	Mestranol 	213	-7.9	1.6
203	Ethinyl Estradiol 	18	-7.8	1.89

Table 5.3. FDA-approved steroid compounds and their binding affinities to the quinol binding site of *E. coli* cytochrome *bd*-I. Compounds were manually selected based on a combination of binding affinity, hydrophobicity, and modelled interactions with CydA. A cyclopentane group is present for quinestrol and absent in mestranol and ethinylestradiol.

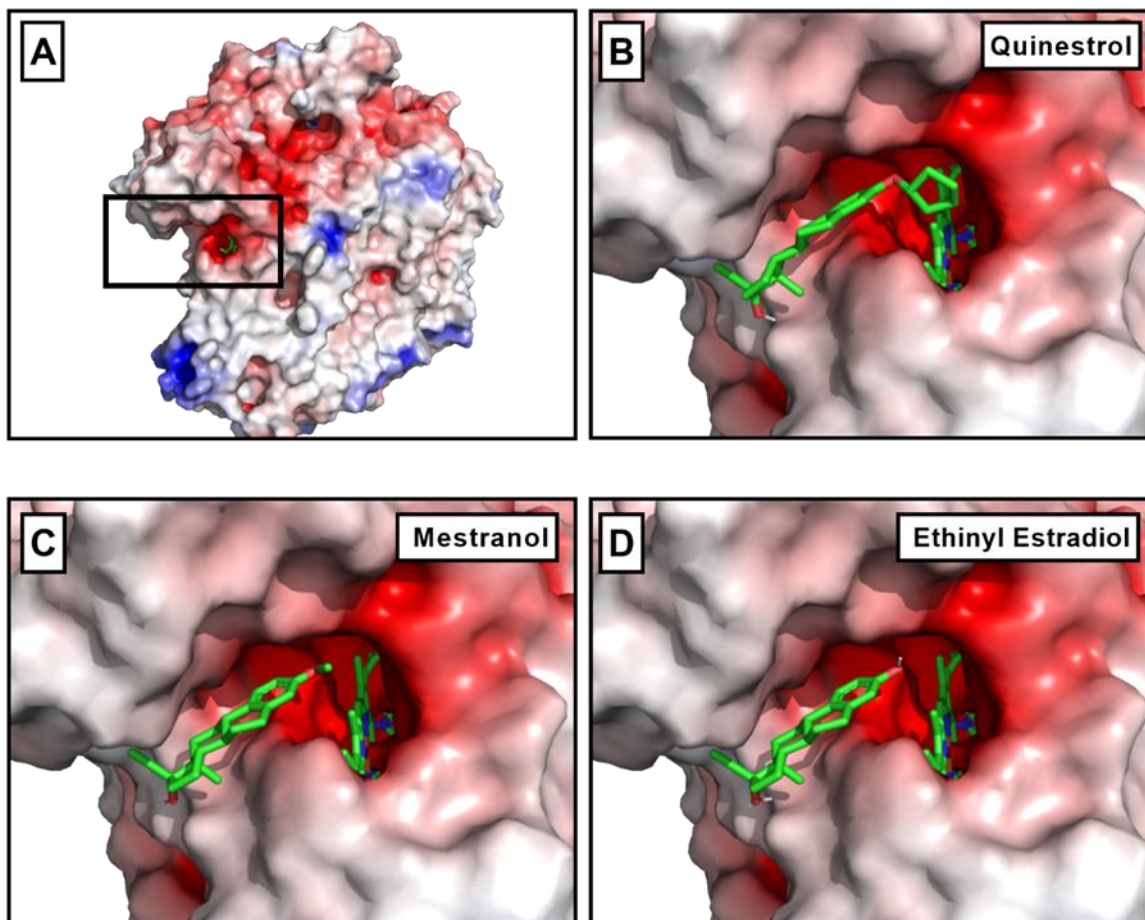


Figure 5.1. Docking of FDA-approved steroid drugs to the quinol binding site of *E. coli* cytochrome *bd-I* AlphaFold2 model. *A*) *E. coli* cytochrome *bd-I* structure with highlighted quinol binding site. *B*) Quinestrol docked in the quinol binding site *C*) Mestranol docked in the quinol binding site *D*) Ethinylestradiol docked in the quinol binding site. Red = negative charge. White = hydrophobic. Blue = positive charge.

Drug Name	eDrug3D Database Number	Predicted Affinity (kcal/mol)	Estimated K_d (μ M)
Quinestrol	383	-8.1	1.13
Mestranol	213	-7.5	3.14
Ethinyl Estradiol	18	-7.2	5.21

Table 5.4. FDA-approved steroid compounds and their binding affinities to the quinol binding site of *S. aureus* CydA.

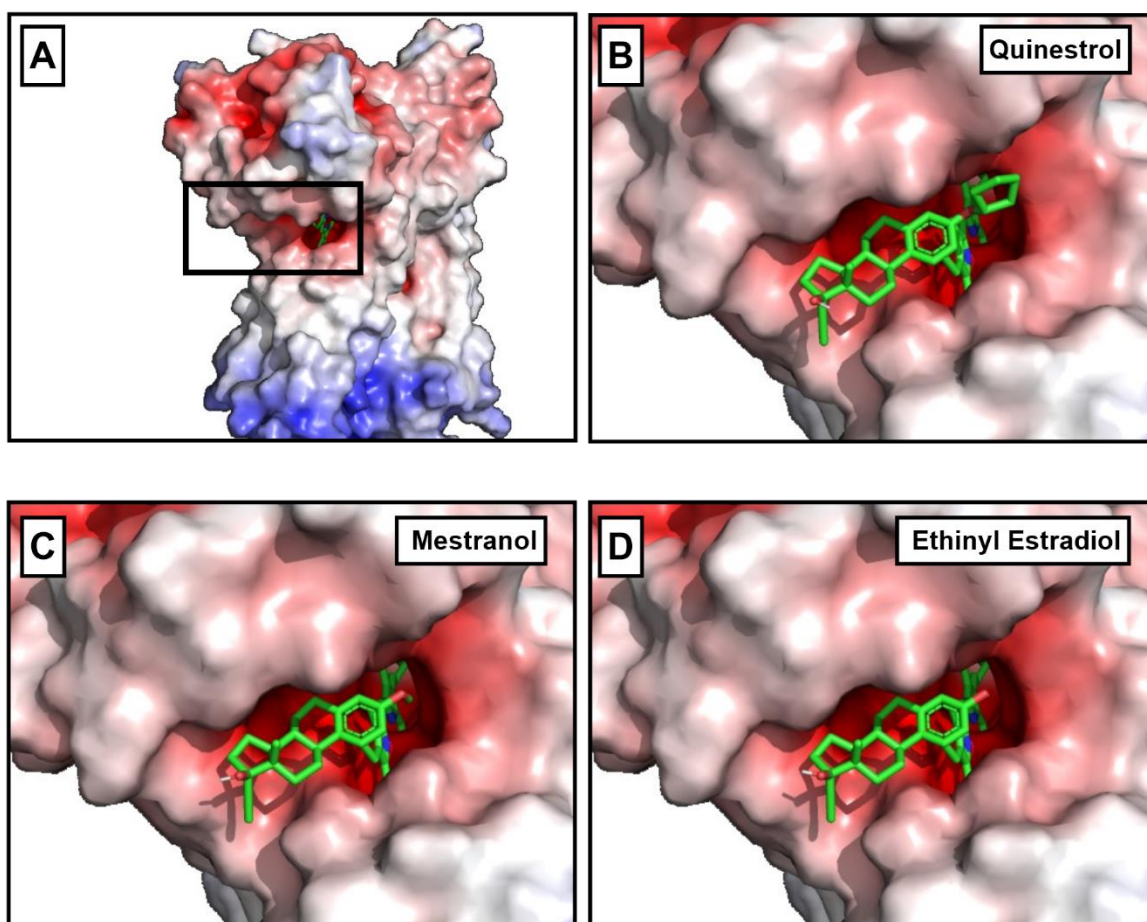


Figure 5.2. Docking of FDA-approved steroid drugs to the quinol site of *S. aureus* *cydA* subunit. *A*) Cytochrome *bd*-I CydA structure with highlighted quinol binding site. *B*) Quinestrol docked in the quinol binding site *C*) Mestranol docked in the quinol binding site *D*) Ethinyl estradiol docked in the quinol binding site. Red = negative charge. White = hydrophobic. Blue = positive charge.

5.3.2. *In vitro* approaches to confirm FDA-approved steroid drugs as inhibitors of cytochrome *bd*

5.3.2.1. FDA-approved steroid drugs inhibit oxygen consumption activity in *E. coli* EC958 *bd*-I only membranes and MRSA '*bd*-only' membranes

To confirm the steroid drugs as inhibitors of cytochrome *bd*-I, various experimental approaches were performed in the laboratory. Firstly, a drug screen was performed to test the effects of the steroid drugs on oxygen consumption activity in membranes of an *E. coli* EC958

strain that expresses cytochrome *bd*-I as its sole terminal respiratory oxidase (Figure 5.3). Of the three steroid compounds, mestranol did not lead to inhibition of oxygen consumption activity in *E. coli* EC958 *bd*-I only membranes (Figure 5.3A). Quinestrol led to the most inhibition of oxygen consumption activity in *E. coli* EC958 *bd*-I only membranes with an oxygen consumption rate of about 25 nM/s. Ethinylestradiol also led to inhibition and resulted in an oxygen consumption rate that doubled that of quinestrol (Figure 5.3A). Ethinylestradiol and quinestrol were proven the two most potent drugs that were capable of inhibiting the oxygen consumption activity of *E. coli* EC958 *bd*-I only membranes and so, a dose response curve was obtained for both (Figure 5.3B). Ethinylestradiol inhibited *E. coli* *bd*-I membranes with an IC_{50} of $47 \pm 28.9 \mu\text{g/mL}$ ($158 \pm 97.2 \mu\text{M}$) while quinestrol inhibited the membranes with an IC_{50} of $0.2 \pm 0.04 \mu\text{g/mL}$ ($0.5 \pm 0.1 \mu\text{M}$) (Figure 5.3B).

Moreover, preliminary studies were performed to determine whether quinestrol would inhibit the recombinant *E. coli* EC958 cytochrome *bd*-II that was expressed in an *E. coli* MG1655 'EcoM4' strain lacking all respiratory oxidases (Portnoy *et al.* 2010) (Figure 5.4). Quinestrol was able to inhibit *E. coli* cytochrome *bd*-II oxidase with an IC_{50} $0.4 \pm 0.3 \mu\text{g/mL}$ ($1 \pm 0.8 \mu\text{M}$) (Figure 5.4). This is close to the IC_{50} seen in *E. coli* EC958 *bd*-I only membranes. Quinestrol was the most potent of the two compounds, therefore, this drug was highlighted as the top hit of this study and formed the basis of future experiments.

MRSA USA300 LAC strains (see Table 2.1) were provided by Lindsey Shaw (University of South Florida, Tampa, FL) which were first obtained from the Network on Antimicrobial Resistance in *Staphylococcus aureus* (NARSA). MRSA USA300 membranes (see section 2.2.2) expressing cytochrome *bd* as its sole respiratory oxidase were analysed to determine the ability of quinestrol to inhibit oxygen consumption activity in a Gram-positive bacterial pathogen. Figure 5.5 demonstrates that MRSA '*bd*-only' membranes were inhibited by quinestrol with an IC_{50} of $0.98 \pm 0.1 \mu\text{g/mL}$ ($2.3 \pm 0.2 \mu\text{M}$).

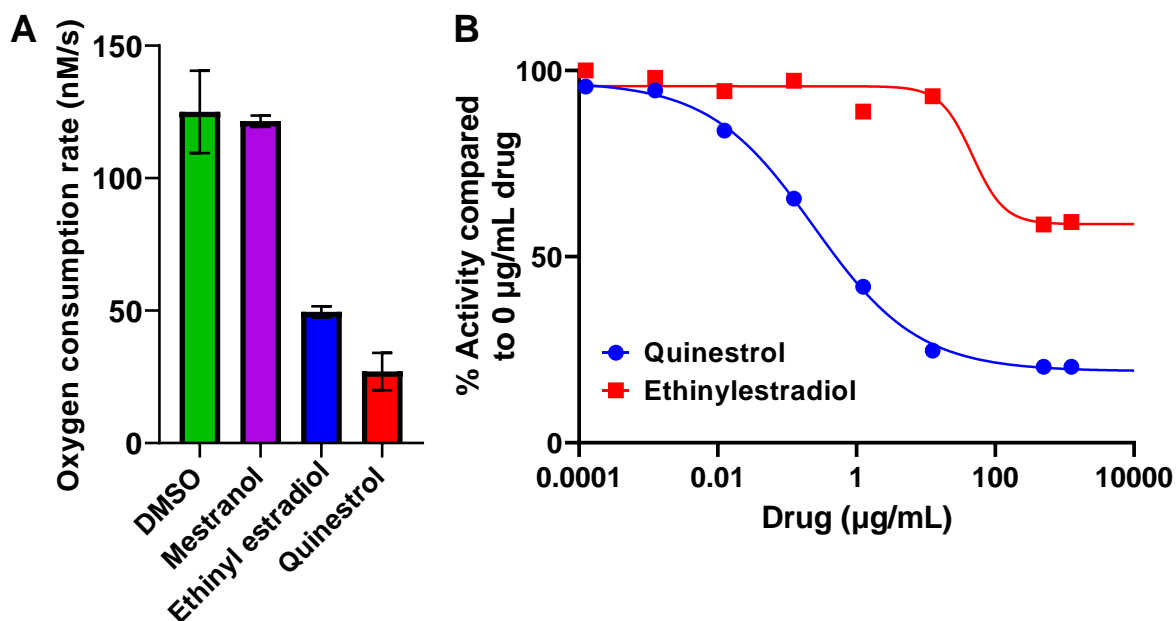


Figure 5.3. FDA-approved steroid drugs inhibit oxygen consumption activity of *E. coli* EC958 *bd-I* only membranes. Respiration was initiated by addition of 8 mM succinate as a substrate and the final concentration of membranes in the reaction chamber was 500 µg/mL. **A**) Initial screening of oxygen consumption using 100 µM drug (DMSO, Mestranol, Quinestrol, Ethinylestradiol). Drugs for (A) were tested in triplicates with error bars representing mean with standard deviation. **B**) Dose response with quinestrol and ethinylestradiol. Quinestrol exhibited an IC_{50} of 0.2 ± 0.04 µg/mL (0.5 ± 0.1 µM) while ethinylestradiol had an IC_{50} of 47 ± 28.9 µg/mL (158 ± 97.2 µM). Data points for (B) represent single experiments.

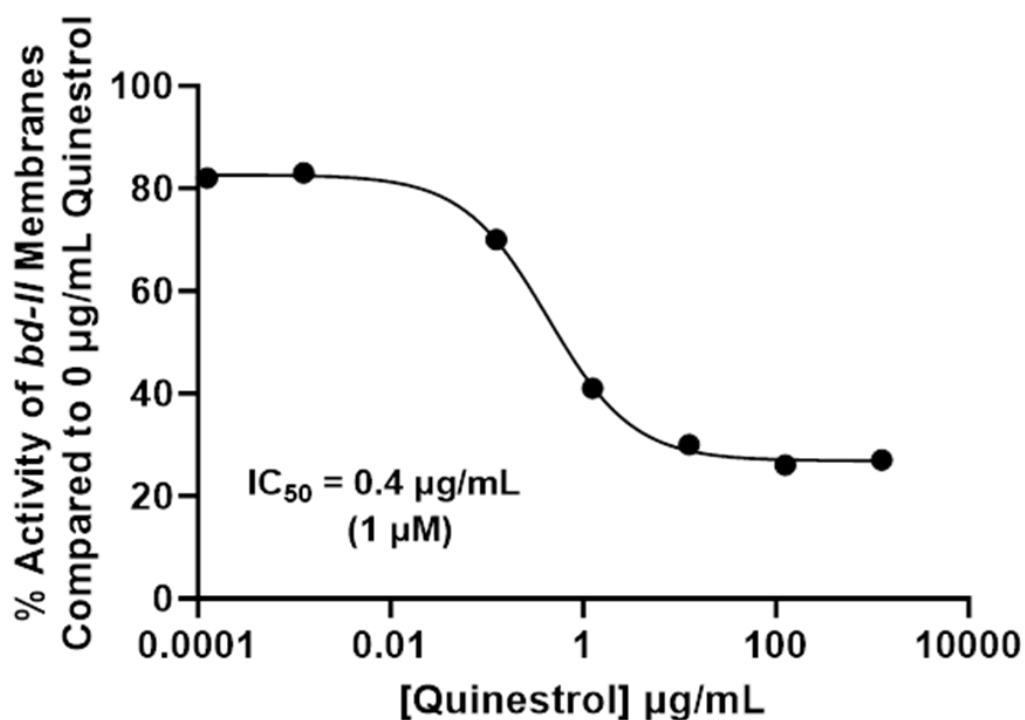


Figure 5.4. Quinestrol inhibits *E. coli* cytochrome *bd-II*. Oxygen consumption assay was performed on membranes of an *E. coli* recombinant oxidase that expresses *E. coli* EC958 cytochrome *bd-II*. The experiment consisted of various concentrations of quinestrol, and the reaction was started with 8 mM succinate. An IC_{50} of $0.4 \pm 0.3 \mu\text{g/mL}$ ($1 \pm 0.8 \mu\text{M}$) which is similar the IC_{50} seen in *E. coli* EC958 *bd-I* only membranes of $0.2 \pm 0.04 \mu\text{g/mL}$.

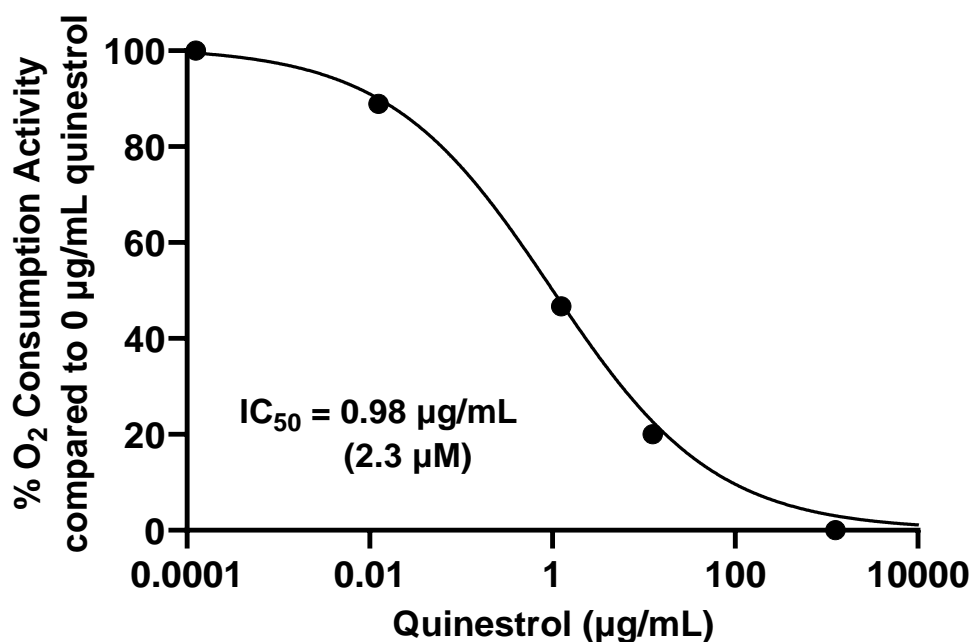


Figure 5.5. Quinestrol inhibits oxygen consumption activity of MRSA USA300 ‘*bd*-only’ membranes. The final concentration of membranes in the reaction chamber was 1 mg/mL and the reaction was initiated via the addition of 500 µM NADH as the substrate. Quinestrol exhibited an IC_{50} of $0.98 \pm 0.1 \mu\text{g/mL}$ ($2.3 \pm 0.2 \mu\text{M}$). Data points represent single experiments.

5.3.2.2. Kinetic assays confirm that quinestrol does not inhibit succinate dehydrogenase activity in *E. coli* EC958 *bd*- I only membranes

When using succinate as the electron donor (substrate) in oxygen consumption membrane assays, there is a chance that both succinate dehydrogenase or cytochrome *bd*-I (or both) are inhibited by quinestrol and ethinylestradiol. To exclude succinate dehydrogenase as a target for quinestrol, the activity of this respiratory complex was measured using previously described methods (Kolaj-Robin *et al.* 2011). The experiment was designed such that the conditions of the succinate dehydrogenase assay would match those of the oxygen consumption membrane inhibition assays. The succinate dehydrogenase assay showed that even at very high concentrations of quinestrol (125 µg/mL) and ethinylestradiol (500 µg/mL), there was no inhibition of succinate dehydrogenase (Figure 5.6). It was confirmed that both quinestrol and ethinylestradiol do not inhibit succinate dehydrogenase activity in *E. coli* EC958 *bd*-I only

membranes and that these assays measure the effect of quinestrol upon the cytochrome *bd-I* oxidase alone (Figure 5.6).

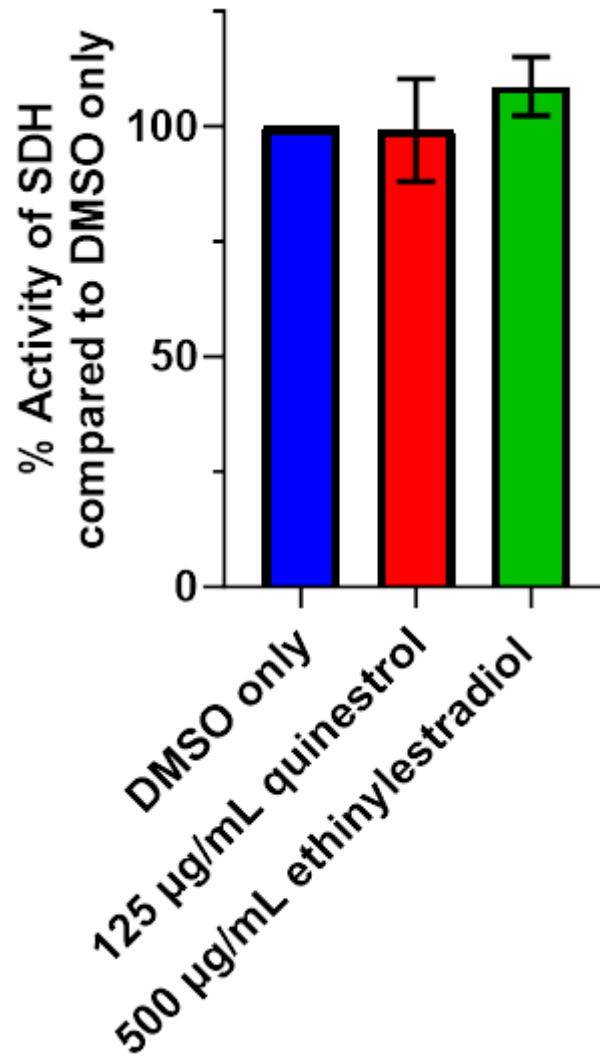


Figure 5.6. Succinate dehydrogenase (SDH) *E. coli* *bd-I* only membrane assay with quinestrol and ethinylestradiol. The activity of SDH was expressed as a percentage of the DMSO only control. Error bars represent the mean with standard deviation for three technical repeats.

5.3.2.3. Growth assays demonstrate that quineestrol inhibits the growth of bacterial cells expressing only cytochrome *bd* as their terminal respiratory oxidase

It was predicted that quineestrol had a high affinity for the quinol site of *E. coli* cytochrome *bd*-I (see section 5.3.1) and oxygen consumption assays confirmed that quineestrol inhibits *E. coli* *bd*-I only membranes (Figure 5.3). Growth curves were recorded in the presence of varying concentrations of quineestrol, and representative raw data is shown in Appendix A.3 to demonstrate how growth rates were calculated. The resultant dose response data for *E. coli* EC958 WT, '*bd*-I only' and '*bo*' only' strains is shown in Figure 5.7. Experiments with WT and '*bo*' only' strains produced IC₅₀ values of $0.1 \pm 0.02 \mu\text{g/mL}$ ($0.3 \pm 0.06 \mu\text{M}$) and $0.1 \pm 0.01 \mu\text{g/mL}$ ($0.3 \pm 0.03 \mu\text{M}$), respectively (Figure 5.7A, Figure 5.7C). Data for the strain expressing cytochrome *bd*-I as the sole respiratory oxidase (i.e., '*bd*-I only') produced a marginally lower IC₅₀ of $0.06 \pm 0.02 \mu\text{g/mL}$ ($0.2 \pm 7 \mu\text{M}$) (Figure 5.7B), although the errors of the fits suggest that there is no difference between all three IC₅₀ values for these *E. coli* strains.

Figure 5.7 demonstrated that quineestrol only led to roughly 50% inhibition in *E. coli* EC958 cells. Given the hydrophobic nature of quineestrol (LogP = 5.3), it was hypothesised that a limitation in solubility might be responsible for the residual cytochrome *bd* activity at higher concentrations. A solubility assay was performed in various growth media, solvents, and detergents to determine whether these conditions could improve solubility of quineestrol and maximise inhibition of *E. coli* cells (Appendix A.4). Attempts to solubilise quineestrol resulted in higher growth rates (Appendix A.4) which suggested that limitations in solubility were not responsible for residual activity, which was followed up with quineestrol derivatisation work (Section 5.3.2.5).

To investigate the activity of quineestrol against a Gram-positive pathogen, growth inhibition assays were conducted on WT, '*bd*-only' and '*aa*₃-only' strains of MRSA USA300.

Growth of all strains was inhibited by quineestrol (Figure 5.8), and data from the ‘*bd*-only’ experiments produced a significantly lower IC₅₀ of 2.2 ± 0.43 µg/mL (6.0 ± 1.2 µM).

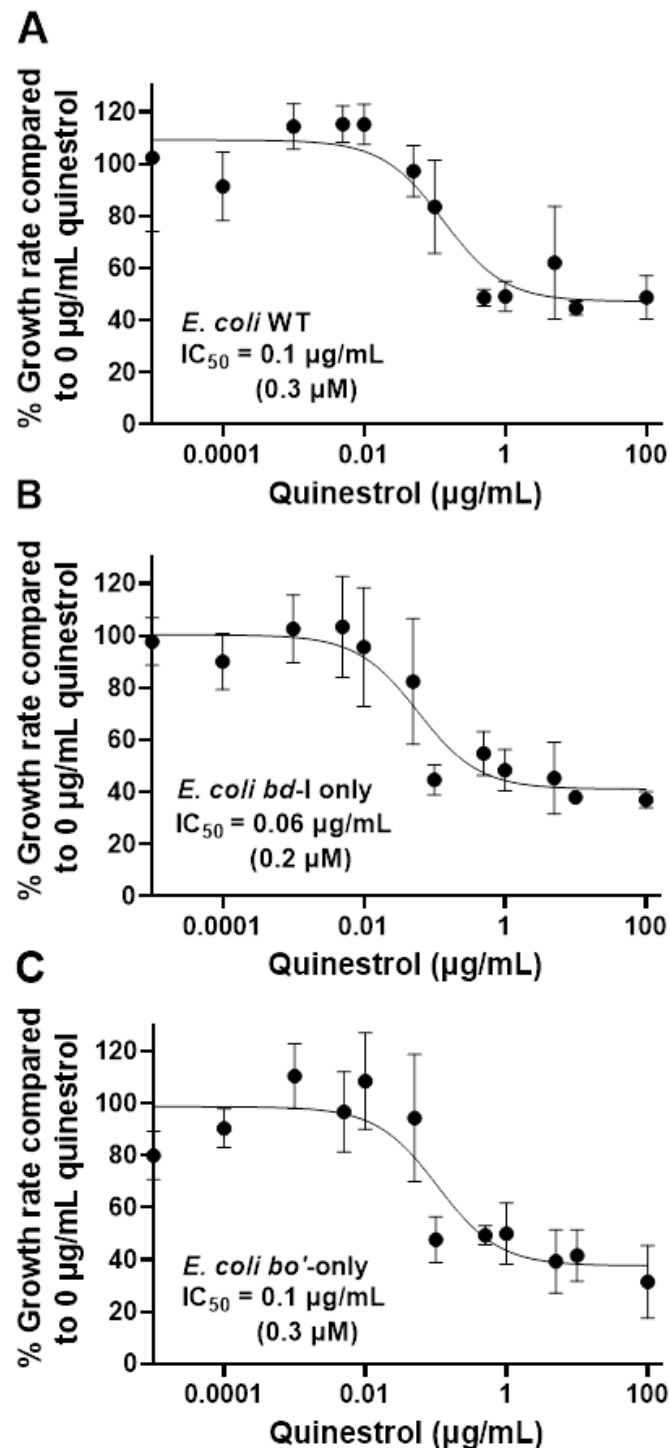


Figure 5.7. Quineestrol inhibits the growth of *E. coli* EC958 cells. Six repeats were performed for each drug concentration and are represented by the error bars showing mean with standard deviations. **A)** *E. coli* WT cells are inhibited by quineestrol at an IC₅₀ of 0.1 ± 0.02 µg/mL (0.3 ± 0.06 µM). **B)** *E. coli* ‘*bd*-I only’ cells are inhibited by quineestrol with an IC₅₀ of 0.06 ± 0.02 µg/mL (0.2 ± 7 µM). **C)** *E. coli* ‘*bo*’ only’ cells are inhibited by quineestrol at an IC₅₀ of 0.1 ± 0.01 µg/mL (0.3 ± 0.03 µM).

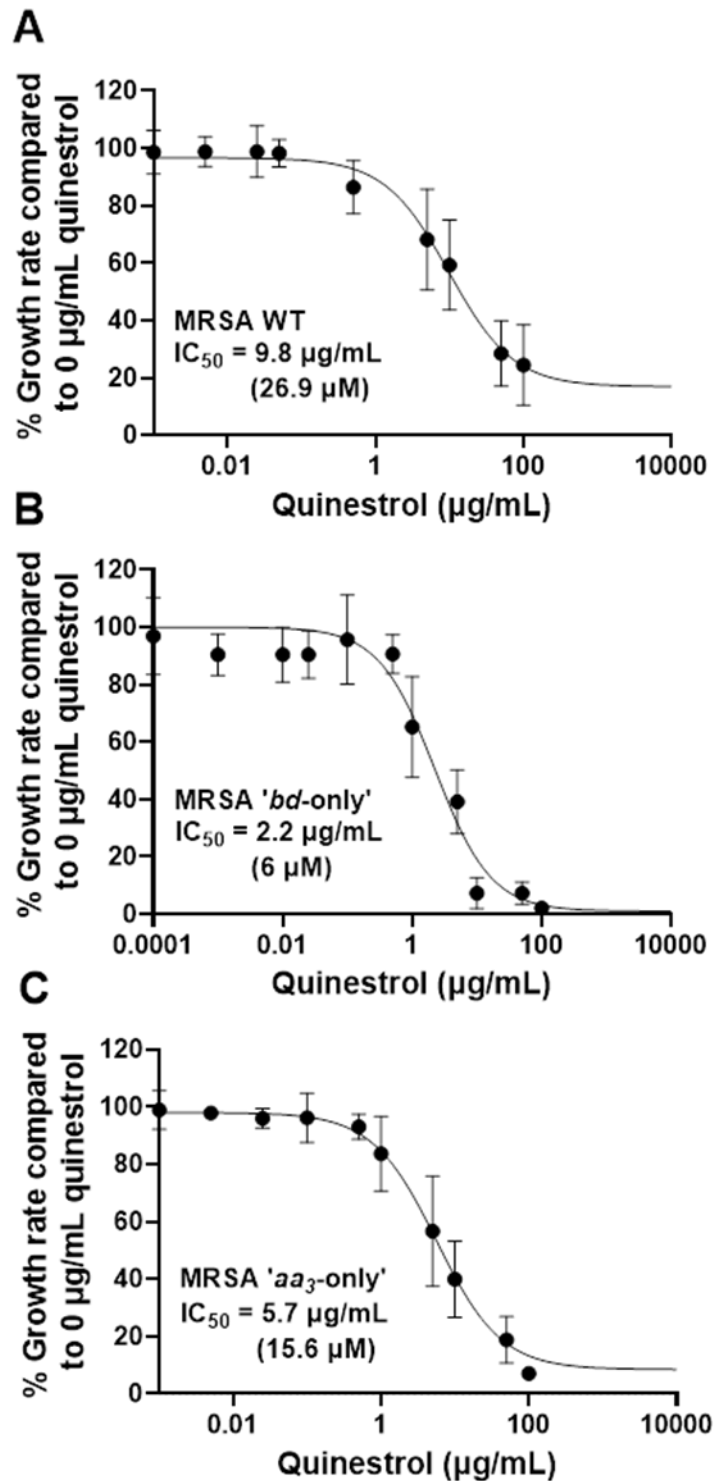


Figure 5.8. Quinestrol inhibits the growth of MRSA USA300. Six repeats were performed for each drug concentration and are represented by the error bars showing mean with standard deviations. **A)** Quinestrol inhibits the growth of WT MRSA cells with an IC_{50} of $9.8 \pm 1.95 \mu\text{g/mL}$ ($27.0 \pm 5.4 \mu\text{M}$). **B)** Quinestrol inhibits growth of MRSA '*bd* only' cells with an IC_{50} of $2.2 \pm 0.43 \mu\text{g/mL}$ ($6.0 \pm 1.2 \mu\text{M}$). **C)** Quinestrol inhibits MRSA '*aa*₃ only' cells with an IC_{50} of $5.7 \pm 1.2 \mu\text{g/mL}$ ($15.6 \pm 3.3 \mu\text{M}$)

To assess the ability of quinnestrol to kill Gram-positive bacteria, viability assays were carried out on *E. coli* EC958 and MRSA USA300 strains. While quinnestrol did not kill *E. coli* WT cells, MRSA WT cells were killed by quinnestrol with a median lethal concentration (LC₅₀) of $3.4 \pm 0.7 \mu\text{g/mL}$ ($9.3 \pm 1.9 \mu\text{M}$) (Figure 5.9A). Further work on *E. coli* mutants revealed that quinnestrol had no killing effects on 'bd-I only' or 'bo'-only' cells (data not shown), although quinnestrol killed 'bd-only' and 'aa₃-only' strains of MRSA with LC₅₀ values of $5.6 \pm 0.3 \mu\text{g/mL}$ ($13.7 \pm 0.7 \mu\text{M}$) and $9.0 \pm 0.6 \mu\text{g/mL}$ ($24.7 \pm 1.6 \mu\text{M}$), respectively (Figure 5.9B). This means that the Gram-positive MRSA cells were able to be killed directly by quinnestrol which is not the case for Gram-negative *E. coli*.

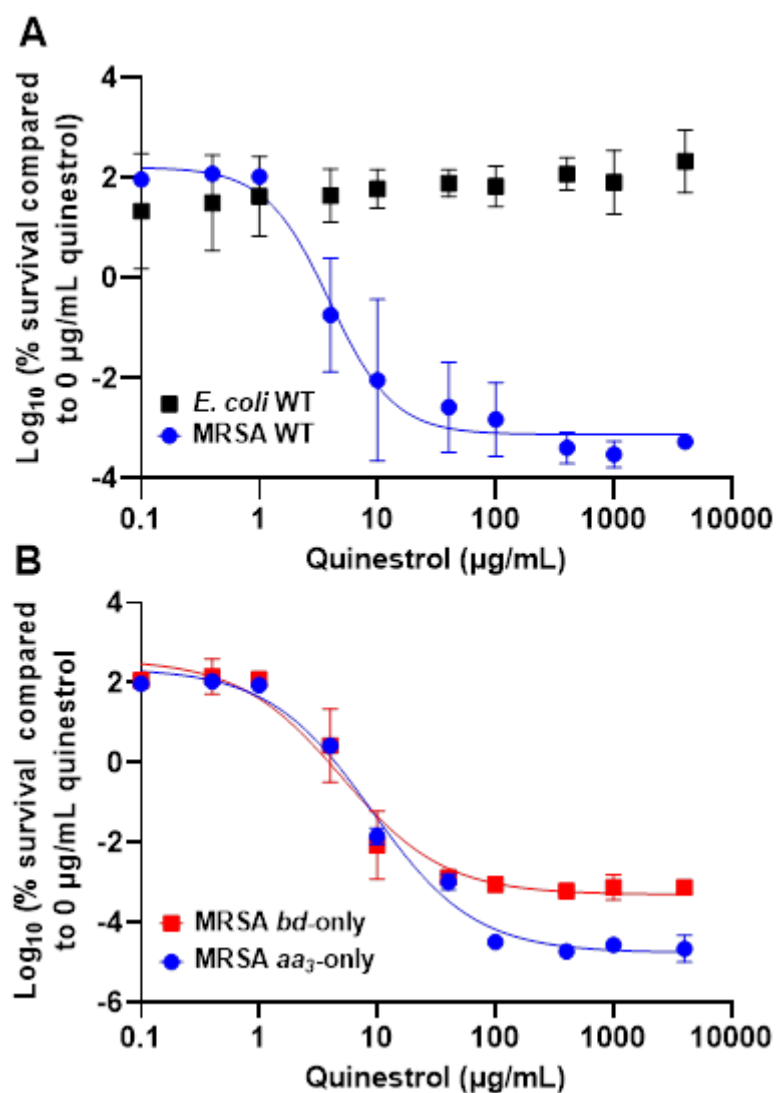


Figure 5.9. Quinestrol kills MRSA cells but not *E. coli*. Six repeats were recorded for each drug concentration and datapoints show the mean with error bars showing standard deviations. **A)** MRSA WT cells are killed by quinestrol at a median lethal concentration (LC₅₀) of $3.4 \pm 0.7 \mu\text{g/mL}$ ($9.3 \pm 1.9 \mu\text{M}$). Quinestrol does is not lethal towards *E. coli* WT cells. **B)** Quinestrol kills MRSA ‘*bd* only’ cells with a LC₅₀ of $5.6 \pm 0.3 \mu\text{g/mL}$ ($13.7 \pm 0.7 \mu\text{M}$). MRSA ‘*aa*₃ only’ cells are killed with an LC₅₀ of $9.0 \pm 0.6 \mu\text{g/mL}$ ($24.7 \pm 1.6 \mu\text{M}$).

5.3.2.4. Development of a PEG quinestrol derivative

Figure 5.6 demonstrated that quinestrol only led to roughly 50% inhibition in *E. coli* EC958 cells. To increase the solubility of quinestrol, an experiment was conducted to solubilise quinestrol but resulted in higher growth rates (Appendix A.4). It was hypothesised that it is the mode of binding and inability of quinestrol to fully out-compete ubiquinol binding to CydA

that was causing the incomplete inhibition observed *E. coli* strains (see Figure 5.6). Therefore, a PEG quineestrol derivative was designed to improve binding affinity and potentially remove residual activity at higher concentrations. This was achieved through a CuAAC modification of quineestrol which changed the chemical formula from $C_{25}H_{32}O_2$ to $C_{34}H_{51}N_3O_6$ (Figure 5.10). There was also a change in molecular weight from 364.53 g/mol to 597.80 g/mol (Figure 5.10). 1H NMR was conducted to verify the structure of the CuAAC modified compound compared to the original quineestrol compound (Beal lab). These results revealed diagnostic chemical shift changes (Figure 5.11). In the product, there is an alkyne CH lost at 2.2 ppm and the formation of a triazole peak at 7.55 ppm (Figure 5.11). PEG signals are also introduced in the product (Figure 5.10). An oxygen consumption assay was conducted using *E. coli* *bd-I* only membranes to determine whether the derivatisation had made quineestrol more soluble. The results showed that maximum inhibition of cytochrome *bd-I* only membranes was achieved with an IC_{50} of 0.84 μM (Figure 5.12).

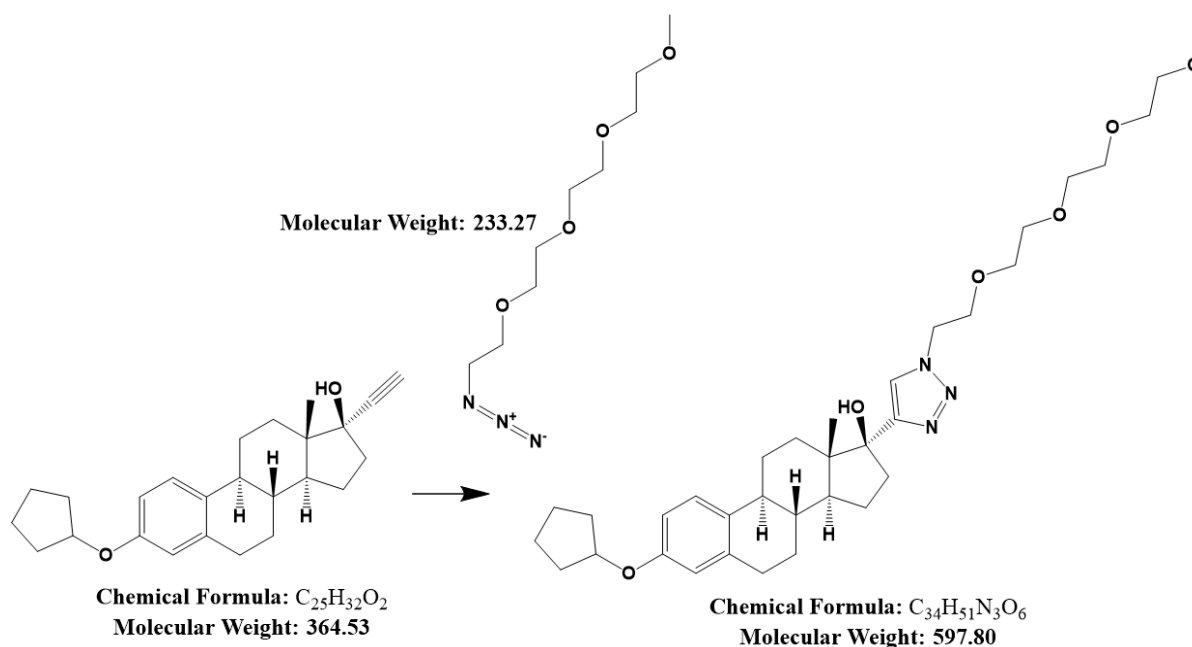


Figure 5.10. PEG derivatisation of quineestrol with a CuAAC modification.

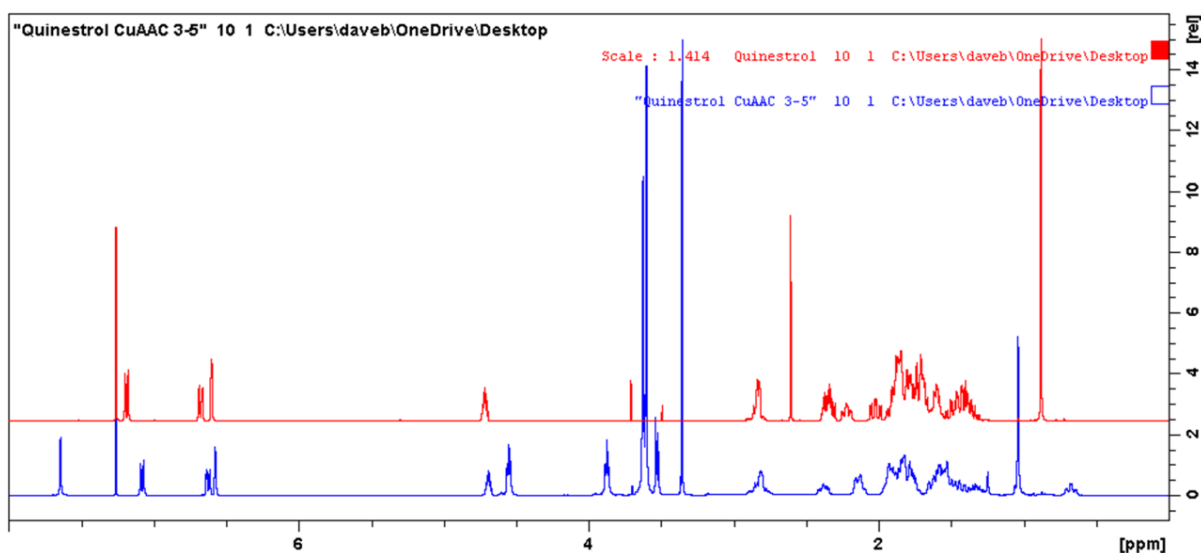


Figure 5.11. ^1H NMR of the quinestrol PEG derivative and the original quinestrol compound. The unmodified form of quinestrol is highlighted in red with its three highest peaks at approximately 0.8, 2.6 and 7.25 ppm. Data for the CuAAC PEG derivative of quinestrol is shown in blue. There are changes in the peaks of the CuAAC derivative producing its two highest peaks between 3.2 and 3.8 ppm. Most differences between the modified and unmodified quinestrol are seen between 0.5 and 5 ppm.

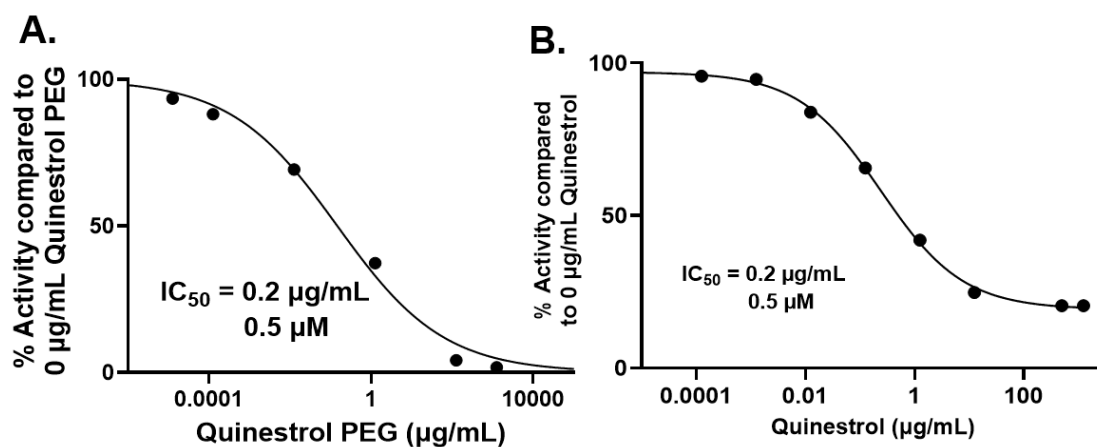


Figure 5.12. Quinestrol PEG derivative inhibits oxygen consumption activity in *E. coli* *bd-I* only membranes. **A)** *E. coli* *bd-I* only membrane inhibition by quinestrol PEG derivative. **B)** *E. coli* *bd-I* only membrane inhibition by quinestrol. Respiration was initiated by addition of 8 mM succinate as a substrate and the final concentration of membranes in the reaction chamber was 500 $\mu\text{g}/\text{mL}$. Both quinestrol PEG derivative and the original quinestrol compound inhibited oxygen consumption in *E. coli* *bd-I* membranes with an 0.2 ± 0.04 $\mu\text{g}/\text{mL}$ (0.5 ± 0.1 μM). Data points represent single experiments.

5.4. Discussion

5.4.1. Pharmacology of FDA-approved steroid drugs

A preliminary *in silico* drug screen generated a list of FDA-approved drugs with high binding affinities for the quinol site of an AlphaFold 2 model of a *E. coli* *bd-I* structure, which identified steroid drugs as promising candidates for binding to the quinol site. Subsequent *in vitro* analyses demonstrated that ethinylestradiol and quinestrol inhibited *E. coli* *bd-I* only membranes to varying degrees whereas mestranol exhibited no inhibitory effects, which suggested that subtle structural variations could elicit changes in binding affinity. The three steroids used in the current study differ only via the substituent on the C3 atom of the A ring: ethinylestradiol has a hydroxyl group, mestranol has a methyl ether, and quinestrol has a cyclopentyl ether. Together, these findings are consistent with the hypothesis that the A ring is in close proximity to the haem *b*₅₅₈ cofactor, and more hydrophobic substituents (i.e., cyclopentyl or methyl moieties) promote binding deep in the quinol pocket.

Ethinylestradiol is a synthetic oestrogen medication that is often used as a birth control in combination with progestins such as drospirenone (Keam and Wagstaff 2003). Previously, ethinylestradiol has been used to treat symptoms of menopause, hormone-sensitive cancers and disorders that are gynecologically related (Kuhl 2005). Ethinylestradiol is quickly and relatively completely absorbed by the gastrointestinal tract once ingested (Buchsbaum 2012). An oral dose of 50 mg ethinylestradiol would account for a concentration of 400 pg/mL in the blood (Barnes and Levrant 2007). Ethinylestradiol is usually excreted via urine and faeces as glucuronides and sulphates and succumbs to enterohepatic circulation (Eastell and Hannon 2007). It has been demonstrated that vaginal administration of 50 mg ethinylestradiol only results in circulating concentrations that are equivalent to 10 mg of orally ingested concentrations (Eastell and Hannon 2007).

Quinestrol is the cyclopentyl ether of ethinylestradiol and is used in hormone replacement therapy; as a hormonal birth control; for the treatment of menopause symptoms and for the treatment of some cancers such as breast and prostate (Shyu *et al.* 2011). Following gastrointestinal absorption, quinestrol is stored in the adipose tissue where it is slowly released and metabolised to the parent compound, ethinylestradiol (Shyu *et al.* 2011). However, quinestrol has a longer half-life than ethinylestradiol (over 5 days) and is taken less frequently as a result (Buchsbaum 2012). Estrovis, the brand name for quinestrol, was administered as 100 µg/day for 1 week, then 100-200 µg/week (Buchsbaum 2012).

Mestranol is an oestrogen medication and was the oestrogen component used in the first birth control pill (Sneider 2006) before being replaced by ethinylestradiol. The fate of mestranol is more variable, and it is assumed that mestranol and the active form, ethinylestradiol, reach peak levels in the body from 1 to 4 hours after ingestion (Buchsbaum 2012).

5.4.2. Novel inhibitors of cytochrome *bd*

Experimental analysis revealed the IC₅₀ of quinestrol for inhibiting oxygen consumption in *E. coli* *bd*-I only membranes as 0.2 ± 0.02 µg/mL (0.5 µM \pm 0.04 µM), although residual activity remained at around 20 % at higher concentrations. This residual activity suggests that quinestrol is unable to completely inhibit *E. coli* cytochrome *bd*-I terminal oxidase and further kinetic analyses will be required to elucidate the precise modes of binding. Indeed, this trend of low IC₅₀ with incomplete inhibition is mirrored by the growth assays for all the *E. coli* strains. Subsequent growth inhibition work for the *bd*-only mutant strain of MRSA produced an IC₅₀ value in the low micromolar range, and these data showed no residual growth suggesting that quinestrol is a more effective bactericidal agent against MRSA. The MRSA WT and '*aa*₃ only' strains exhibited IC₅₀ values slightly higher than the '*bd* only' strain,

suggesting that quineestrol binds to *bd* slightly more tightly than *aa3*. That said, quineestrol is clearly also a potent inhibitor of the cytochrome *aa3* complex as evidenced by the ‘*aa3* only’ strain having a lower IC₅₀ compared to the WT strain.

Stark differences were observed between *E. coli* and MRSA when bactericidal activity of quineestrol was assessed, where *E. coli* was completely resistant to killing and all MRSA strains exhibited several log-fold reductions in viability with median LC₅₀ in the low micromolar range. This is consistent with a previous screen where quineestrol was shown to inhibit the growth of vancomycin-resistant *Enterococcus faecium* and MRSA but not Gram-negative species (Younis *et al.* 2017), and perhaps reflects the suitability of steroid-based drugs for targeting bacterial species such as MRSA that lack an outer membrane. Surprisingly, the LC₅₀ for the MRSA WT strain is marginally lower than the IC₅₀ for this strain even though cell density was the same upon quineestrol exposure, although this difference in susceptibility could potentially be explained by the metabolic state of the cells being different in the static viability assays (less active) compared to the growth assays where orbital aeration may increase respiratory metabolism (more active). Indeed, it is well-known that some antibiotics target actively-growing cells more effectively while others target less metabolically active cells (Stokes *et al.* 2019). However, it is difficult to interpret the observed patterns of IC₅₀ and LC₅₀ between the WT and mutant MRSA strains, as loss of respiratory oxidases appears to diminish the lethality of quineestrol (i.e. increases LC₅₀) yet enhances the quineestrol-mediated growth inhibition (i.e. decreases IC₅₀). This could perhaps be linked to differences in metabolic activity between strains and experimental conditions, but it would be too speculative at this time to comment further on the bacteriostatic and bactericidal mechanisms. Notwithstanding these elusive insights, robust conclusions can be made: quineestrol can inhibit both *bd*-type and haem-copper oxidases and is lethal towards MRSA cells.

5.4.3. Derivatisation improves mode of binding of quinestrol

It was hypothesised that it was quinestrol's mode of binding that was resulting in residual activity at higher concentrations in *E. coli*. A well-known method for combating problems with binding affinity is by modification through PEGylation. The compound is modified via covalent conjugation with polyethylene glycol (PEG) which alters the chemical and physical properties of the compound (Veronese and Mero 2008). In this instance, CuAAC modification of quinestrol changed the chemical formula from $C_{25}H_{32}O_2$ to $C_{34}H_{51}N_3O_6$. PEGylation is known for improving the solubility of drugs and reduces immunogenicity (Veronese and Mero 2008). Modifying biological compounds by though PEGylation also increases the stability of drugs and drug retention in blood (Veronese and Mero 2008).

In vitro work with the PEG derivative of quinestrol resulted in maximum inhibition of *E. coli* *bd*-I membranes with no residual activity. However, both quinestrol PEG derivative and the original quinestrol compound inhibited oxygen consumption in *E. coli* *bd*-I membranes with an $0.2 \pm 0.04 \mu\text{g/mL}$ ($0.5 \pm 0.1 \mu\text{M}$). This is consistent with a previous study performed to measure the interactions of glycerol, tetraEG, and PEG groups with aromatic hydrocarbons and steroids (aromatic C, aliphatic C, amide N, hydroxyl O, cationic N, amide O and carboxylate O) (Knowles *et al.* 2015). PEG400 resulted in strong and favourable interactions with aromatic and aliphatic C and conclusions were drawn as to how PEG400 largely increases the binding affinities of aromatic compounds and steroids (Knowles *et al.* 2015). Overall, PEG modification appears to be a promising modification to the quinestrol scaffold to improve cytochrome *bd* inhibition.

5.4.4. Quinestrol as a novel inhibitor of cytochrome *bd*

The use of quinestrol as a novel inhibitor of cytochrome *bd* has its advantages and challenges. One of the most obvious benefits of having quinestrol as a novel inhibitor is that

the drug is FDA-approved, so it is safe for human use. However, the drug is a synthetic oestrogen so it can have off target effects if used continuously at non-physiological ranges. The aim of oestrogen replacement is to achieve blood levels like the early follicular phase in premenopausal women. Natural oestrogen blood plasma concentrations are within the picomolar range during early follicular phase. In hormone replacement therapy, blood plasma concentrations are also within the picomolar range. The IC_{50} of quinestrol in this study against was within the nanomolar range, so careful consideration of off target effects and dosage would be required should quinestrol analogues be used to treat bacterial infections. One potential solution might be to avoid circulatory delivery and to use these drugs to combat more localised areas, such as cutaneous infections or UTIs.

5.4.5. Future Work

There is a residual activity that is associated with the inhibition of *E. coli* by quinestrol that demonstrates that quinestrol is unable to cause maximum inhibition of the bacteria even at higher concentrations. This was not seen in MRSA cells. Though derivatisation with PEG appears to resolve the issue of incomplete inhibition (i.e. residual *bd* activity at high [quinestrol]), further kinetic studies will be required to elucidate the precise mode of binding for quinestrol and its derivatives to cytochrome *bd*. The use of molecular dynamics is one tool that can be used to study the binding of known inhibitors of the quinol binding site of *E. coli* cytochrome *bd-I*. This study used isolated membranes from the various strains to perform inhibition assays. However, future work with purified forms of the proteins could provide more mechanistic insights into the mode of binding and would eliminate specificity issues that might arise when linked assays (e.g. with succinate dehydrogenase) are employed.

Chapter 6

Final Discussion

6.1. Background

Antimicrobial resistance is a global health concern that needs urgent actioning. Various research is undergoing to find new ways to tackle this issue. Cytochrome *bd* is a terminal oxidoreductase that is found exclusively in prokaryotes and archaea and is a good drug target to discover new antimicrobials. It's presence in some of the most pathogenic strains of bacteria including uropathogenic *E. coli*, MRSA and *Mycobacterium tuberculosis* has highlighted its importance for virulence and host colonisation.

This study employed drug repurposing approaches to screen for potential new inhibitors of cytochrome *bd* from a series of FDA-approved drugs and known antimicrobials. A uropathogenic *E. coli* strain that was previously engineered to express single respiratory oxidases (cytochrome *bd*-I and *bo'*) was characterised. Herein, multidrug-resistant *E. coli* and methicillin-resistant *S. aureus* strains were tested against promising drug candidates against cytochrome *bd* discovered in this study. Membranes were isolated from whole cells to measure oxygen consumption activity. Figure 6.1 is a summary of the pipeline used to drive this project and generate research findings.

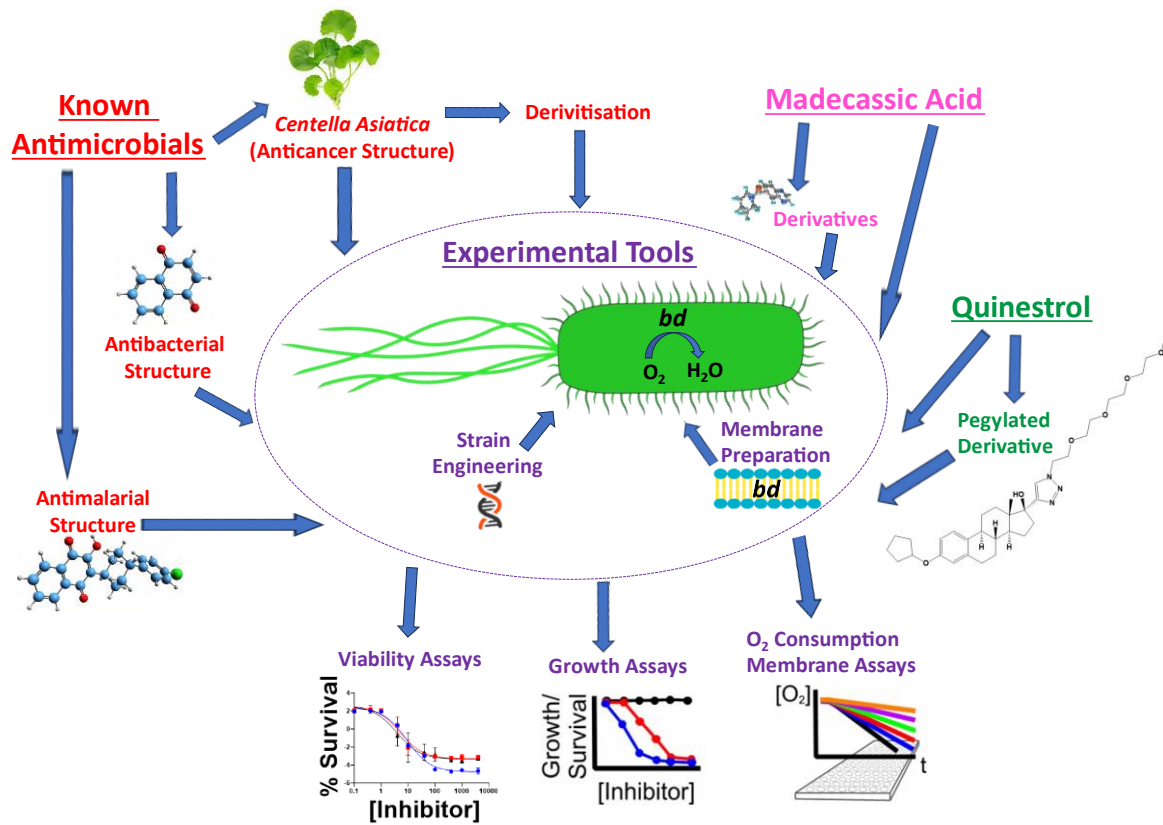


Figure 6.1. Summary of *in silico* and *in vitro* drug screening pipeline.

6.2. Conclusions

6.2.1. Engineering and characterisation of *E. coli* strains that express single respiratory oxidases

Antibiotic resistance is a major concern in some of the most pathogenic strains of bacteria, leading to multidrug resistance and often almost untreatable infections. The multidrug-resistant EC958 *E. coli* O25: H4-ST131 strain was used for this study. This strain was isolated from a patient with urinary tract infection and is resistant to most of the first-line antibiotics that was once used to treat an infection (Lau *et al.* 2008; Rogers, Sidjabat and Paterson 2011). A strain expressing cytochrome *bd*-I as its sole respiratory oxidase was previously engineered in the Shepherd lab via Lambda-Red mutagenesis (Webster, C.M. (2023) PhD thesis, University of Kent). Many attempts have been made to engineer a cytochrome *bd*-II only strain but were unsuccessful. The third *E. coli* respiratory oxidase, cytochrome *bo'*, was also expressed as the sole respiratory oxidase in the bacterium. A major tool used in our *in vitro* assays is the oxygen consumption assay that measures oxygen consumption in purified membranes. Membranes were isolated from the *E. coli* cytochrome *bd*-I only strain were tested against TTFA, a known inhibitor of cytochrome *bd*, to confirm the successful development of the assay. Recombinant strains of *E. coli* EC958 cytochrome *bd*-I and *bd*-II were successfully engineered to determine whether the cytochrome *bd* plasmid of highly pathogenic strains could be expressed in other strains that are less pathogenic.

Antibiotic resistance is a natural phenomenon that can result from prolonged exposure of bacteria to antibiotics. There are numerous residues within drug binding sites of enzymes, some of which are important for tight binding of various compounds. *In silico* analysis was used to identify key residues that are vital for the binding of drugs within the ubiquinol site of cytochrome *bd*. Mutagenesis can be employed to establish the effects that mutation of key

residues play in drug binding and potentially modelling the evolution of antibacterial resistance. To simulate this process, mutations were introduced to the amino acids (L253A, F269A, Y387, I295 and F390) located in the quinol cleft of cytochrome *bd* that are believed to be important in the proper functioning of the oxidase. Residues L253A and F269A were successfully mutated and oxygen consumption membrane assays in the presence of TTFA revealed that F269A membranes were able to consume oxygen. L253A was not able to consume oxygen, and this was believed to be because of the mutation.

6.2.2. Cytochrome *bd* as a modern drug target

Cytochrome *bd* complexes are restricted to the prokaryotic world which is an attractive trait when selecting potential drug targets. A small number of cationic amphiphilic peptides have been identified that bind to *E. coli* cytochrome *bd*-I, including Gramicidin S (Mogi *et al.* 2008), microcin J25 (Galván *et al.* 2018) and Cathelicidin LL-37 (Choi & Weisshaar, 2017). While these have IC₅₀ values in the μM range they have complex mechanisms of action thought to primarily involve membrane destabilisation rather than direct targeting of the *bd* complex. Cytochrome *bd* from *M. tuberculosis* has attracted much attention as a promising target for next-generation antibacterials (recently reviewed in [Borisov *et al.* 2021; Mascolo & Bald, 2020]). Bedaquiline, an FDA-approved treatment for tuberculosis and inhibitor of mycobacterial ATP synthases, has been found to increase in efficacy when cytochrome *bd* has been knocked out (Berney *et al.* 2014), highlighting future combinatorial treatments alongside cytochrome *bd* inhibitors as promising new therapies. Isoniazid, a first-line treatment for tuberculosis, works via a complex mechanism that involves perturbation of the respiratory chain, and loss of cytochrome *bd* synthesis (Dhar & McKinney, 2010) or inhibition with aurachin C (Zeng *et al.* 2019) enhances the efficacy of isoniazid. Furthermore, a recent *in silico* screen identified an inhibitor (MQL-H₂: 3-[[2-(4-chlorophenyl)ethylamino]methyl]-1-ethyl-indole-2-carboxylic) that binds to the menaquinol-binding pocket of *Mycobacterium*

tuberculosis cytochrome *bd*, and efficacy was tested using ATP assays on *M. smegmatis* mutants revealing an IC₅₀ of 34 µM towards a ‘*bd* only’ strain (Harikishore *et al.* 2020). A subsequent study identified a series of 2-aryl-quinolone inhibitors that target *M. tuberculosis* cytochrome *bd* (Jeffreys *et al.* 2023), and a very low IC₅₀ of 3 nM was calculated for the CK-2-63 compound from inhibition kinetic data for the purified recombinant *M. tuberculosis* cytochrome *bd* isolated from an *E. coli* respiratory mutant strain. Finally, *in silico* screening of FDA-approved drugs docking to the *Geobacillus thermodenitrificans* cytochrome *bd* structure and subsequent efficacy assays led to the development of the synthetic compound 8d from the quinoline moiety of ivacaftor and roquinimex (Zhou *et al.* 2023). This ‘8d’ compound was shown to bind to purified mycobacterial cytochrome *bd* with a *K_d* value of 4.17 µM and to inhibit a ‘*bd*-only’ strain of *M. smegmatis* with a MIC value of 6.25 µM. These recent studies highlight the potential for targeting *bd*-type oxidases using derivatives and mimics of natural quinones found in bacteria, which differs from the current study that highlights the novel utility of steroid drugs as respiratory inhibitors.

6.2.3. Drug screening approaches to identify novel inhibitors of cytochrome *bd*

Drug repurposing is a more modern tool used in the development of novel drugs compared to conventional drug discovery techniques. An *in silico* drug repurposing pipeline was developed in the host lab (Webster, C.M. (2023) PhD thesis, University of Kent) to screen FDA-approved drugs for their ability to bind the quinol site of *E. coli* cytochrome *bd*-I. Herin, a series of steroid compounds were selected from the top-hits and screened for inhibitory activity against the quinol site of *E. coli* cytochrome *bd*-I. In addition, known antimicrobials that target the electron transport chain of various organisms were ran through the docking pipeline to determine binding affinities for the quinol site of *E. coli* cytochrome *bd*-I before performing *in vitro* analyses. The binding affinities generated from the molecular docking did not often coincide with the *in vitro* data. Compounds such as atovaquone produced an

extremely low molecular K_d value (0.49 μM) but was proven completely ineffective against *E. coli* cytochrome *bd*-I only membranes. However, other compounds such as naphthoquinone had a significantly higher K_d value (108.99 μM) for *E. coli* cytochrome *bd*-I but led to complete inhibition of oxygen consumption in membranes. This questions the reliability of the scoring functions present in molecular docking software such as AutoDock Vina.

Though there are questions around the reliability of molecular docking as a tool in drug repurposing, several research have continued to employ this approach and have been proven effective in highlighting potential inhibitors of cytochrome *bd*. The most recent drug-repurposing work done on *Mycobacterium tuberculosis* cytochrome *bd* oxidase had screened over 523,192 compounds via molecular docking (Seitz *et al.* 2024). From this, 102 inhibitors were screened experimentally to determine inhibitory effects against cytochrome *bd* in inverted membrane vesicles of *Mycobacterium tuberculosis* (Seitz *et al.* 2024). A total of six new inhibitors of cytochrome *bd* were identified from this study (Seitz *et al.* 2024).

6.3. Future Work

Considering questions around the reliability of molecular docking scoring functions for binding affinity, future work needs to focus on assessing the trustworthiness of this feature and improving its precision. A comparative test can be performed between different docking software such as Glide, GOLD, MOE-Dock and the software used in this research, AutoDock to determine whether there is consistency in the docking scores for ligands to protein. Based on the results obtained from this, optimisation studies can be done to improve the scoring function through use of known inhibitors of cytochrome *bd* such as aurachin D. Chapter 5 aimed to repurpose a group of steroids from the results of an in silico docking where quinestrol was the lead compound. Quinestrol is a steroid compound that is a synthetic form of oestrogen. It is proven to have a high binding affinity (K_d of 0.49 μM) for the quinol site of *E. coli* cytochrome *bd*-I. Further testing should be performed to determine whether all naturally occurring steroids in the body would be inhibitory to cytochrome *bd* or whether the molecular docking tool is providing high binding affinity values by chance.

To determine the mode of binding of the repurposed drugs in this study, a cryo-EM structure with the drugs bound to the various subunits of cytochrome *bd* in *E. coli* and MRSA should be employed. A recent study has performed this method successfully using aurachin D bound to *E. coli* cytochrome *bd*-II oxidase at 3 Å resolution (Grauel *et al.* 2021). In addition, the method of molecular dynamics can be employed to establish the modes of binding of each drug to the quinol site of cytochrome *bd*. This approach could use known inhibitors of cytochrome *bd* as positive controls in understanding the interaction between the quinol site and the drugs. The repurposed drugs in this study can then be studied to form comparison to known inhibitors of the quinol site. Molecular dynamics is a useful tool as the results can provide insights into drug derivatisation which is useful in improving drug binding. Molecular dynamic

simulation and structure-based pharmacophore modelling have been previously used to identify novel inhibitors of cytochrome *bc₁* (Gangwal *et al.* 2013) and is a technique that can be adopted for future work in this study.

Cytochrome *bd* holds different properties depending on the organism it is present in and this should be considered when looking into future studies to improve this project. The pathogens studied in this project were *E. coli* EC958, a MDR clinical isolate, and MRSA. Future work should include a wider range of pathogens to study the inhibitory effects of the drugs repurposed in this study. *E. coli* EC958 cytochrome *bd*-I and *bo'* were previously engineered by the host laboratory but the engineering of cytochrome *bd*-II in this study was unsuccessful. A further attempt should be made to engineer *E. coli* cytochrome *bd*-II via Lambda Red mutagenesis so that comparative analysis can be made between *E. coli* *bd*-type oxidases. Conducting future work with purified forms of the proteins could provide more mechanistic insights into the mode of binding and would eliminate specificity issues that might arise when linked assays (e.g. with succinate dehydrogenase) are employed. Lastly, kinetic analyses with purified cytochrome *bd* complexes could provide mechanistic insights into modes of inhibitor binding (i.e., to validate the hypothesis that quineestrol is a competitive inhibitor with respect to ubiquinol).

References

- Abramson, J., Riistama, S., Larsson, G. (2000). The structure of the ubiquinol oxidase from *Escherichia coli* and its ubiquinone binding site. *Nature Structural Biology* **7**:910.
- Adedeji, W.A. (2016). The treasure called antibiotics. *Annals of Ibadan postgraduate medicine* **14**:56-57.
- Aggarwal, S., Verma, S. S., Aggarwal, S., & Gupta, S. C. (2021). Drug repurposing for breast cancer therapy: Old weapon for new battle. *Seminars in Cancer Biology* **68**:8–20.
- Ahmad, M., Wolberg, A. and Kahwaji, C.I. (2023). Biochemistry, Electron transport chain. <https://www.ncbi.nlm.nih.gov/books/NBK526105/>.
- Alvarez, J. and Shoichet, B. (2005). Virtual screening in drug discovery. *Virtual Screening in Drug Discovery* [Online]:1–470.
- Aminin, D. and Polonik, S. (2020). 1,4-Naphthoquinones: Some Biological Properties and Application. *Chemical and Pharmaceutical Bulletin* **68**:46–57.
- Antos-Krzeminska, N. and Jarmuszkiewicz, W. (2012). Direct evidence for *Acanthamoeba castellanii* alternative oxidase gene function. *Biochimica et Biophysica Acta (BBA) - Bioenergetics* **1817**:S104–S105.
- Arai, H. *et al.* (2014). Enzymatic characterization and *in vivo* function of five terminal oxidases in *Pseudomonas aeruginosa*. *Journal of Bacteriology* **196**:4206–4215.
- Asadi Karam, M.R., Habibi, M. and Bouzari, S. (2019). Urinary tract infection: Pathogenicity, antibiotic resistance and development of effective vaccines against Uropathogenic *Escherichia coli*. *Molecular Immunology* **108**:56–67.
- Aslam, B., Wang, W., Arshad, M.I., Khurshid, M., Muzammil, S., Rasool, M.H, Nisar, M.A., Alvi, R.F., Aslam, M.A., Qamar, M.U., Salamat, M.K.F. and Baloch, Z. (2018). Antibiotic resistance: a rundown of a global crisis. *Infection and Drug Resistance* **11**:1645–1658.
- Atlung, T., Knudsen, K., Heerfordt, L. and Brøndsted, L. (1997). Effects of sigmas and the transcriptional activator Appy on induction of the *Escherichia coli* *Hya* and *CbdAB-AppA* operons in response to carbon and phosphate starvation. *American Society for Microbiology*. **179**:2147-2146.
- Bae, T., Class, E.M., Schneewind, O. and Missiakas, D. (2007). Generating a collection of insertion mutations in the *Staphylococcus aureus* genome using *bursa aurealis*. *Methods Mol Biol*. **416**:103–116.
- Bajeli, S., Baid, N., Kaur, M., Pawar, G.P., Chaudhari, V.D. and Kumar, A. (2020). Terminal respiratory oxidases: a targetable vulnerability of Mycobacterial bioenergetics? *Frontiers in Cellular and Infection Microbiology* **10**:589318.
- Barnes, R.B. and Levrant, S.G. (2007). Pharmacology of Estrogens. In: *Menopause*. Academic Press, pp. 767–777.
- Bartoletti, R. *et al.* (2016). Treatment of Urinary Tract Infections and Antibiotic Stewardship. *European Urology, Supplements* **15**:81–87.

- Baughn, A. and Malamy, M. (2004). The strict anaerobe *Bacteroides fragilis* grows in and benefits from nanomolar concentrations of oxygen. *Nature* **427**:441–444.
- Bekker, M., de Vries, S., Ter Beek, A., Hellingwerf, K.J., de Mattos, M.J. Respiration of *Escherichia coli* can be fully uncoupled via the nonelectrogenic terminal cytochrome *bd*-II oxidase. *Journal of Bacteriology*. **191**:5510-5517.
- Berney, M., Hartman, T.E. and Jacobs, W.R. (2014). A *Mycobacterium tuberculosis* cytochrome *bd* oxidase mutant is hypersensitive to bedaquiline. *mBio* **5**:e01275-14.
- Biagini, G.A. *et al.* (2006). Functional characterization and target validation of alternative complex I of *Plasmodium falciparum* mitochondria. *Antimicrobial Agents and Chemotherapy* **50**:1841–1851.
- Bien, J., Sokolova, O. and Bozko, P. (2012). Role of uropathogenic *Escherichia coli* virulence factors in development of urinary tract infection and kidney damage. *International Journal of Nephrology* **2012**.
- Bonomo, R.A. (2014). Overview of aminoglycosides and enzyme-mediated bacterial resistance. *Clinical Implications*. 1–6.
- Borisov, V.B. *et al.* (2015). Cytochrome *bd* protects bacteria against oxidative and nitrosative stress: A potential target for next-generation antimicrobial agents. *Biochemistry (Moscow)* **80**:565–575.
- Borisov, V.B. *et al.* (2004). Interaction of the bacterial terminal oxidase cytochrome *bd* with nitric oxide. *FEBS Letters* **576**:201–204.
- Borisov, V.B. *et al.* (2006). Nitric oxide reacts with the ferryl-oxo catalytic intermediate of the CuB-lacking cytochrome *bd* terminal oxidase. *FEBS Letters* **580**:4823–4826.
- Borisov, V.B., Gennis, R.B., *et al.* (2011). The cytochrome *bd* respiratory oxygen reductases. *Biochimica et Biophysica Acta - Bioenergetics* **1807**:1398–1413.
- Borisov, V.B., Murali, R., *et al.* (2011). Aerobic respiratory chain of *Escherichia coli* is not allowed to work in fully uncoupled mode. *Proceedings of the National Academy of Sciences of the United States of America* **108**:17320–17324.
- Borisov, V.B., Nastasi, M.R. and Forte, E. (2023). Cytochrome *bd* as antioxidant redox enzyme. *Molecular Biology* **57**:1077–1084.
- Borisov, V.B. and Siletsky, S.A. (2019). Features of organization and mechanism. *Biochemistry*. **84**:1390-1402.
- Borisov, V.B., Siletsky, S.A., Paiardini, A., Hoogewijs, D., Forte, E., Giuffrè, A. and Poole R.K. (2021). Bacterial oxidases of the cytochrome *bd* Family: Redox enzymes of unique structure, function and utility as drug targets. *Antioxidants & Redox Signaling* **34**:1280-1318.
- Borisov, V.B. and Verkhovsky, M.I. (2009). Oxygen as Acceptor. *EcoSal Plus* **3**.

- Bota, D.A., Mason, W., Kesari, S., Magge, R., Winograd, B., Elias, I., Reich, S.D., Levin, N., Trikha, M., and Desjardins A. (2021). Marizomib alone or in combination with bevacizumab in patients with recurrent glioblastoma: Phase I/II clinical trial data. *Neuro-oncology advances* **3**:vdab142.
- Brøndsted, L. and Atlung, T. (1996). effect of growth conditions on expression of the acid phosphatase (*Cyx-AppA*) operon and the *AppY* gene, which encodes a transcriptional activator of *Escherichia Coli*. *Journal of Bacteriology* **178**:1556-1564.
- Brumbaugh, A.R., Smith, S.N. and Mobley, H.L.T. (2013). Immunization with the yersiniabactin receptor, FyuA, protects against pyelonephritis in a murine model of urinary tract infection. *Infection and Immunity* **81**:3309–3316.
- Buchsbaum, H.J. (2012). The Menopause. In: Buchsbaum, H. J. ed. *The Menopause*. p. 60.
- Bush, K. and Bradford, P.A. (2016). β -Lactams and β -Lactamase Inhibitors: An Overview. *Cold Spring Harbor Perspectives in Medicine*. **6**:a025247.
- Calhoun, M.W., Newton, G. and Gennis, R.B. (1991). *E. coli* map. Physical map locations of genes encoding components of the aerobic respiratory chain of *Escherichia coli*. *Journal of Bacteriology* **173**:1569.
- Chang, W. *et al.* (2006). Global transcriptome analysis of *Staphylococcus aureus* response to hydrogen peroxide. *Journal of Bacteriology* **188**:1648–1659.
- Charbon, G. *et al.* (2017). Re-wiring of energy metabolism promotes viability during hyperreplication stress in *E. coli*. *PLoS Genetics* **13**:e1006590.
- Chen, R., Subramanyam, S., Elcock, A. H., Spies, M., & Wold, M. S. (2016). Dynamic binding of replication protein a is required for DNA repair. *Nucleic Acids Research* **44**:5758–5772.
- Chepuri, V. *et al.* (1990). The sequence of the *Cyo* operon indicates substantial structural similarities between the cytochrome *o* ubiquinol oxidase of *Escherichia coli* and the Aas-type family of cytochrome *c* oxidases. *J. Biol. Chem* **265**:11185–11192.
- Choi, H., Yang, Z. and Weisshaar, J.C. (2017) Oxidative stress induced in *E. coli* by the human antimicrobial peptide LL-37. *PLoS Pathog* **13**:e1006481.
- Churchill, G. C., Strupp, M., Factor, C., Bremova-Ertl, T., Factor, M., Patterson, M. C., Platt, F. M. and Galione, A. (2021). Acetylation turns leucine into a drug by membrane transporter switching. *Scientific Reports* **1**.
- Clements, M.O. *et al.* (1999). CtaA of *Staphylococcus aureus* is required for starvation survival, recovery, and cytochrome biosynthesis. *Journal of Bacteriology* **181**:501-507.
- Cook, M.A. and Wright, G.D. (2022). The past, present, and future of antibiotics. *Science Translational Medicine* **14**:7793.
- Cooley, L. *et al.* (2014). Consensus guidelines for diagnosis, prophylaxis and management of *Pneumocystis jirovecii* pneumonia in patients with haematological and solid malignancies. *Internal Medicine Journal* **44**:1350–1363.

- Crockett, S.D. *et al.* (2014). Topiramate use does not reduce flares of inflammatory bowel disease. *Digestive Diseases and Sciences* **59**:1535–1543.
- Croxall, G. *et al.* (2011). Molecular epidemiology of extraintestinal pathogenic *Escherichia coli* isolates from a regional cohort of elderly patients highlights the prevalence of ST131 strains with increased antimicrobial resistance in both community and hospital care settings. *Journal of Antimicrobial Chemotherapy* **66**:2501–2508.
- Cunningham L. and Williams H.D. (1995) Isolation and characterization of mutants defective in the cyanide-insensitive respiratory pathway of *Pseudomonas aeruginosa*. *J Bacteriol.* **177**:432-8.
- Dassa, J. *et al.* (1991). A new oxygen-regulated operon in *Escherichia coli* comprises the genes for a putative third cytochrome oxidase and for pH 2.5 acid phosphatase (*AppA*). *Molecular and General Genetics* **229**:341-352.
- Delaney, J.M., Wall, D. and Georgopoulos C. (1993). Molecular characterization of the *Escherichia Coli HtrD* Gene: cloning, sequence, regulation, and involvement with cytochrome *d* Oxidase *Journal of Bacteriology* **175**:166-175.
- Dhar N, McKinney JD. (2010). *Mycobacterium tuberculosis* persistence mutants identified by screening in isoniazid-treated mice. *Proc Natl Acad Sci U S A* **107**:12275–12280.
- Dincturk, H.B., Demir, V. and Aykanat, T. (2011). *Bd* oxidase homologue of photosynthetic purple sulfur bacterium *Allochromatium vinosum* is co-transcribed with a nitrogen fixation related gene. *Antonie van Leeuwenhoek, International Journal of General and Molecular Microbiology* **99**:211–220.
- D’Mello, R., Hill, S. and Poole, R.K. (1995). The oxygen affinity of cytochrome *bo'* in *Escherichia coli* determined by the deoxygenation of oxyleghemoglobin and oxymyoglobin: K_m values for oxygen are in the submicromolar range. *Journal of Bacteriology* **177**:867–870.
- D'mello, R., Hill, S. and Poole R.K. (1996). The cytochrome *bd* quinol oxidase in *Escherichia coli* has an extremely high oxygen affinity and two oxygen-binding haems: implications for regulation of activity in vivo by oxygen inhibition. *Microbiology (Reading)* **4**:755-763.
- Donia, M.S. *et al.* (2014). A systematic analysis of biosynthetic gene clusters in the human microbiome reveals a common family of antibiotics. *Cell* **158**:1402–1414.
- Duc, K.M. *et al.* (2020). The small protein CydX is required for cytochrome *bd* quinol oxidase stability and function in *Salmonella enterica* serovar *typhimurium*: A phenotypic study. *Journal of Bacteriology* **202**:e00348-19.
- Durand, G.A., Raoult, D. and Dubourg, G. (2019). Antibiotic discovery: history, methods and perspectives. *International Journal of Antimicrobial Agents* **53**:371-382.
- Eastell, R. and Hannon, R.A. (2007). *Biochemical Markers of Bone Turnover*. [Online]. Elsevier. Available at: <http://www.sciencedirect.com:5070/book/9780123694430/treatment-of-the-postmenopausal-woman> [Accessed: 15 November 2023].

- EClinicalMedicine (2021). Antimicrobial resistance: a top ten global public health threat. *eClinicalMedicine* **41**:101221.
- Edwards, S.E. *et al.* (2000). Mutation of cytochrome *bd* quinol oxidase results in reduced stationary phase survival, iron deprivation, metal toxicity and oxidative stress in *Azotobacter vinelandii*. *FEMS Microbiology Letters* **185**:71–77.
- Elamri, I. *et al.* (2020). Synthesis and biological screening of new lawson derivatives as selective substrate-based inhibitors of cytochrome *bo₃* ubiquinol oxidase from *Escherichia coli*. *ChemMedChem* **15**:1262–1271.
- Endley, S., McMurray, D. and Ficht, T.A. (2001). Interruption of the *CydB* locus in *Brucella abortus* attenuates intracellular survival and virulence in the mouse model of infection. *Journal of Bacteriology* **183**:2454–2462.
- Everse, J. (2013). HeMe proteins, in *Elsevier eBooks*. pp. 532–538.
- Farha, M.A. and Brown, E.D. (2019). Drug repurposing for antimicrobial discovery. *Nat Microbiol* **4**:565– 577.
- Fey, P.D., Endres, J.L., Yajjala, V.K., *et al.* (2013). A genetic resource for rapid and comprehensive phenotype screening of nonessential *Staphylococcus aureus* genes. *mBio*. **4**:e00537-12.
- Forde, B.M. *et al.* (2014). The complete genome sequence of *Escherichia coli* EC958: A high-quality reference sequence for the globally disseminated multidrug resistant *E. coli* O25b:H4-ST131 Clone. *PLOS ONE* **9**:e104400.
- Forte, E., Borisov, V.B., Vicente, J.B. and Giuffrè, A. (2017). Cytochrome *bd* and gaseous ligands in bacterial physiology. *Adv Microb Physiol*. **71**:171-234.
- Forte, E. *et al.* (2016). The terminal oxidase cytochrome *bd* promotes sulfide-resistant bacterial respiration and growth, *Scientific Reports* **6**.
- Forte, E. *et al.* (2019). In the respiratory chain of *Escherichia coli* cytochromes *bd*-I and *bd*-II are more sensitive to carbon monoxide inhibition than cytochrome *bo₃*. *Biochimica et Biophysica Acta (BBA) - Bioenergetics* **1860**:148088.
- Forte, E., Nastasi, M.R. and Borisov, V.B. (2022). Preparations of terminal oxidase cytochrome *bd*-II isolated from *Escherichia coli* reveal significant hydrogen peroxide scavenging activity. *Biochemistry (Moscow)* **87**:720–730.
- Forte, E., Siletsky, S.A. and Borisov, V.B. (2020). In *Escherichia coli* ammonia inhibits cytochrome *bo₃* but activates cytochrome *bd*-I. *Antioxidants (Basel, Switzerland)* **10**:1–15.
- Friedrich, T., Wohlwend, D. and Borisov, V.B. (2022). Recent advances in structural studies of cytochrome *bd* and its potential application as a drug target. *International Journal of Molecular Sciences* **23**:3166.

- Fry, M. and Pumey, M. (1992). Site of action of the antimalarial hydroxynaphthoquinone, 2-[trans-4-(4'-chlorophenyl) cyclohexyl]-3-hydroxy-1,4-naphthoquinone (566C80). *Biochem Pharmacol* **43**:1545-53.
- Fu, H.A., Iuchi, S. and Lin, E.C.C. (1991). The requirement of ArcA and Fnr for peak expression of the *cyd* operon in *Escherichia coli* under microaerobic conditions. *Mol Gen Genet* **226**:209–213.
- Galván, A.E., Chalón, M.C., Schurig-Briccio, L.A., *et al.* (2018) Cytochromes *bd*-I and *bo*₃ are essential for the bactericidal effect of microcin J25 on *Escherichia coli* cells. *Biochim Biophys Acta Bioenerg* **1859**:110–118.
- Gangwal RP, Dhoke G v., Damre M v., *et al* (2013) Structure-Based virtual screening and molecular dynamic simulation studies to identify novel cytochrome *bc*₁ inhibitors as antimalarial agents. *Journal of Computational Medicine* **2013**:1–9.
- Garneau-Tsodikova, S. and Labby, K.J. (2016). Mechanisms of resistance to aminoglycoside antibiotics: overview and perspectives. *MedChemComm.* **7**:11–27.
- Giuffrè, A. *et al.* (2014). Cytochrome *bd* oxidase and bacterial tolerance to oxidative and nitrosative stress. *Biochimica et Biophysica Acta - Bioenergetics* **1837**:1178–1187.
- Goojani, H. G., Konings, J., Hakvoort, H., Hong, S., Gennis, R. B., Sakamoto, J., Lill, H. and Bald, D. (2020). The carboxy-terminal insert in the Q-loop is needed for functionality of *Escherichia coli* cytochrome *bd*-I. *Bioenergetics*, **1861**:5–6.
- Götz, F. and Mayer, S. (2013). Both terminal oxidases contribute to fitness and virulence during organ-specific *Staphylococcus aureus* colonization. *mBio* **4**:e00976-13.
- Grael, A. *et al.* (2021). Structure of *Escherichia coli* cytochrome *bd*-II type oxidase with bound aurachin D. *Nature Communications* **12**:6498.
- Grund, T.N. *et al.* Mechanistic and structural diversity between cytochrome *bd* isoforms of *Escherichia coli*. *Proc Natl Acad Sci U S A* **118**:e21114013188.
- Gulder, T.A.M. and Moore, B.S. (2010). Salinosporamide natural products: potent 20 S proteasome inhibitors as promising cancer chemotherapeutics. *Angewandte Chemie International Edition* **49**:9346–9367.
- Haas, L.F. (1999). Papyrus of Ebers and Smith. *Journal of neurology, neurosurgery, and psychiatry* **67**:578.
- Hammer, N.D. *et al.* (2013). Two heme-dependent terminal oxidases power *Staphylococcus aureus* organ-specific colonization of the vertebrate host. *mBio* **4**:e00241-13.
- Harikishore, A. *et al.* (2020). Targeting the menaquinol binding loop of mycobacterial cytochrome *bd* oxidase. *Molecular Diversity* **25**:517–524.
- Hata-Tanaka, A. *et al.* (1987). Electron flow and heme-heme interaction between cytochromes *b*₅₅₈, *b*₅₉₅ and *d* in a terminal oxidase of *Escherichia Coli*. *Biochimica et Biophysica Acta* **893**:289-295.

- Henry, S. A., Webster, C. M., Shaw, L. N., Torres, N. J., Jobson, M-E., Totzke, B. C., Jackson, J. J., McGreig, J. E., Wass, M. N., Robinson, G.K. and Shepherd, M. (2024). Steroid drugs inhibit bacterial respiratory oxidases and are lethal towards methicillin-resistant *Staphylococcus aureus*. *Journal of Infectious Diseases*. Oxford University Press.
- Hemp .J. and Gennis R.B. (2008). Diversity of the heme-copper superfamily in archaea: insights from genomics and structural modeling. *Results Probl Cell Differ*. **45**:1-31.
- Hiramatsu, K. *et al.* (2014). Multi-drug-resistant *Staphylococcus aureus* and future chemotherapy. *Journal of Infection and Chemotherapy* **20**:593–601.
- Hodos, R.A. *et al.* (2016). *In silico* methods for drug repurposing and pharmacology. *Wiley Interdisciplinary Reviews: Systems Biology and Medicine* **8**:186–210.
- Hoeser, J. *et al.* (2014). Subunit CydX of *Escherichia coli* cytochrome *bd* ubiquinol oxidase is essential for assembly and stability of the di-heme active site. *FEBS Letters* **588**:1537–1541.
- Hutchings, M., Truman, A. and Wilkinson, B. (2019). Antibiotics: past, present and future. *Current Opinion in Microbiology* **51**:72-80.
- Hyduke, D.R. *et al.* (2007). Integrated network analysis identifies nitric oxide response networks and dihydroxyacid dehydratase as a crucial target in *Escherichia Coli*. *Proc Natl Acad Sci U S A*. **104**:8484-9.
- Jackson, R.J., Elvers, K.T., Lee, L.J., Gidley, M.D., Wainwright, L.M., Lightfoot, J., Park, S.F. and Poole, R.K. (2006). Oxygen reactivity of both respiratory oxidases in *Campylobacter jejuni*: the *cydAB* genes encode a cyanide-resistant, low-affinity oxidase that is not of the cytochrome *bd* type. *J Bacteriol*. **189**:1604-15.
- Jeffreys, L.N. *et al.* (2023). Identification of 2-Aryl-Quinolone inhibitors of cytochrome *bd* and chemical validation of combination strategies for respiratory inhibitors against *Mycobacterium tuberculosis*. *ACS Infectious Diseases* **9**:221–238.
- Jones, S.A. *et al.* (2007). Respiration of *Escherichia coli* in the mouse intestine. *Infection and Immunity*. **75**:4891–4899.
- Jones-Carson, J. *et al.* (2016). Cytochrome *bd*-dependent bioenergetics and antinitrosative defenses in Salmonella Pathogenesis. *mBio* **7**:e02052-16.
- Kaila, V.R.I. and Wikström, M. (2021). Architecture of bacterial respiratory chains. *Nature Reviews Microbiology*. **19**:319–330.
- Kaminski, P.A. *et al.* (1996). *Azorhizobium Caulinodans* uses both cytochrome *bd* (Quinol) and cytochrome *cbb₃* (cytochrome *c*) terminal oxidases for symbiotic N₂ fixation. **178**:5989-94.
- Kamtekar, S., Jia, L., Emig, R., Miller, E., Lee, W. H., & Inc, P. B. O. C. (2008). *US10975362B2 - Recombinant polymerases for improved single molecule sequencing - Google Patents*. <https://patents.google.com/patent/US10975362B2/en>
- Keam, S.J. and Wagstaff, A.J. (2003). Ethinylestradiol/drospirenone: A review of its use as an oral contraceptive. *Treatments in Endocrinology* **2**:49–70.

- Kelly, D.J., Hughes, N.J. and Poole, R.K. (2014) Microaerobic physiology: aerobic respiration, anaerobic respiration, and carbon dioxide metabolism. pp. 111–124.
- Kelley, L.A. *et al.* (2015). The Phyre2 web portal for protein modeling, prediction and analysis. *Nature Protocols* **10**:845–858.
- Kennedy, A.D., Otto, M., Braughton, K.R., *et al.* (2008). Epidemic community-associated methicillin-resistant *Staphylococcus aureus*: Recent clonal expansion and diversification. *Proc Natl Acad Sci U S A.* **105**:1327–1332.
- Kessl, J.J. *et al.* (2007). Parameters determining the relative efficacy of hydroxy-naphthoquinone inhibitors of the cytochrome *bc1* complex. *Biochimica et Biophysica Acta - Bioenergetics* **1767**:319–326.
- Kitchen, D.B. *et al.* (2004). Docking and scoring in virtual screening for drug discovery: methods and applications. *Nature Reviews Drug Discovery* **3**:935–949.
- Knowles, D.B. *et al.* (2015). Chemical interactions of polyethylene glycols (PEGs) and glycerol with protein functional groups: applications to effects of peg and glycerol on protein processes. *Biochemistry* **54**:3528–3542.
- Kolaj-Robin, O. *et al.* (2011). Biochemical and biophysical characterization of succinate: Quinone reductase from *Thermus thermophilus*. *Biochimica et Biophysica Acta - Bioenergetics* **1807**:68–79.
- Korshunov, S., Imlay, K.R.C. and Imlay, J.A. (2016). The cytochrome *bd* oxidase of *Escherichia coli* prevents respiratory inhibition by endogenous and exogenous hydrogen sulfide. *Molecular Microbiology* **101**:62–77.
- Kot, B. (2019). Antibiotic resistance among uropathogenic *Escherichia coli*. *Polish Journal of Microbiology* **68**:403–415.
- Kracke, F., Vassilev, I. and Krömer, J.O. (2015). Microbial electron transport and energy conservation - the foundation for optimizing bioelectrochemical systems. *Frontiers in Microbiology* **6**.
- Kuhl, H. (2005). Pharmacology of estrogens and progestogens: influence of different routes of administration. *Climacteric* **8**:3–63.
- Kulkarni, V.S. *et al.* (2023). Drug Repurposing: An effective tool in modern drug discovery. *Russian Journal of Bioorganic Chemistry* **49**:157.
- Laemmli, U.K. *et al.* (1991). Properties of the Two Terminal Oxidases of *Escherichia Coli*. **30**:3936-42.
- Lau, S.H. *et al.* (2008). UK epidemic *Escherichia coli* strains A–E, with CTX-M-15 β -lactamase, all belong to the international O25:H4-ST131 clone. *Journal of Antimicrobial Chemotherapy* **62**:1241–1244.
- Lee, B.S. *et al.* (2020). Dual inhibition of the terminal oxidases eradicates antibiotic-tolerant *Mycobacterium tuberculosis*. **13**:e13207.

- Li, J. *et al.* (2021). Cryo-EM structures of *Escherichia coli* cytochrome *bo*₃ reveal bound phospholipids and ubiquinone-8 in a dynamic substrate binding site. *Proceedings of the National Academy of Sciences of the United States of America* **118**:e2106750118.
- Lindqvist, A. *et al.* (2000). Roles of respiratory oxidases in protecting *Escherichia coli* K12 from oxidative stress. *Comparative Study* **78**:23–31.
- Lobanovska, M. and Pilla, G. (2017) *Focus: Drug Development: Penicillin's discovery and antibiotic resistance: Lessons for the future?*
<https://www.ncbi.nlm.nih.gov/pmc/articles/PMC5369031/>.
- Loisel-Meyer, S. *et al.* (2005). Differential use of the two high-oxygen-affinity terminal oxidases of *Brucella suis* for *in vitro* and intramacrophagic multiplication. *Infection and Immunity* **73**:7768–7771.
- Lorence, R.M., Gennis, R.B. and Koland, J.G. (1986). Coulometric and spectroscopic analysis of the purified cytochrome *d* Complex of *Escherichia coli*: evidence for the identification of “Cytochrome a1” as Cytochrome *b*₅₉₅. *Biochemistry* **25**:2314–2321.
- Lu, P. *et al.* (2018). The anti-mycobacterial activity of the cytochrome *bcc* inhibitor Q203 can be enhanced by small-molecule inhibition of cytochrome *bd*. *Scientific Reports* **8**:1–7.
- Lu, P. *et al.* (2015). The cytochrome *bd*-type quinol oxidase is important for survival of *Mycobacterium smegmatis* under peroxide and antibiotic-induced stress. *Scientific Reports* **5**:10333.
- March-Vila, E. *et al.* (2017). On the integration of *in silico* drug design methods for drug repurposing. *Frontiers in Pharmacology* **8**:298.
- Mascolo L, Bald D. Cytochrome *bd* in *Mycobacterium tuberculosis*: A respiratory chain protein involved in the defense against antibacterials. (2020). *Prog Biophys Mol Biol* **152**:55–63.
- Mason, M.G. *et al.* (2009). Cytochrome *bd* confers nitric oxide resistance to *Escherichia coli*. *Nature Chemical Biology* **5**:94–96.
- Mather, M.W. *et al.* (2005). Uncovering the molecular mode of action of the antimalarial drug atovaquone using a bacterial system. *Journal of Biological Chemistry* **280**:27458–27465.
- Matsumoto, Y. *et al.* (2006). Mass spectrometric analysis of the ubiquinol-binding site in cytochrome *bd* from *Escherichia coli*. *Journal of Biological Chemistry* **281**:1905–1912.
- Meunier, B. *et al.* (1995). New inhibitors of the quinol oxidation sites of bacterial cytochromes *bo* and *bdt*. *Biochemistry* **34**:1076-83.
- Mogi, T. (2009). Probing the haem *d*-binding site in cytochrome *bd* quinol oxidase by site-directed mutagenesis. *J Biochem.* **145**:763-70.
- Mogi, T., Ui, H., Shiomi, K., Omura, S. and Kita, K. (2008) Gramicidin S identified as a potent inhibitor for cytochrome *bd*-type quinol oxidase. *FEBS Lett* **582**:2299–2302.

- Mora-Ochomogo, M. and Lohans, C.T. (2021). β -Lactam antibiotic targets and resistance mechanisms: from covalent inhibitors to substrates. *RSC Medicinal Chemistry*. **12**:1623–1639.
- Morales, G., Ugidos, A. and Rojo F. (2006). Inactivation of the *Pseudomonas putida* cytochrome *o* ubiquinol oxidase leads to a significant change in the transcriptome and to increased expression of the CIO and *cbb3-1* terminal oxidases. *Environ Microbiol*. **8**:1764–74.
- Morris, G.M. *et al.* (2009). AutoDock4 and AutoDockTools4: Automated docking with selective receptor flexibility. *Journal of Computational Chemistry* **30**:2785–2791.
- Mowat, C.G. and Chapman, S.K. (2013) *Cytochromes*, in Springer eBooks, pp. 428–433.
- Mullins, J. (2022). Drug repurposing *in silico* screening platforms. *Biochem Soc Trans* **50**:747–758.
- Munita, J.M. and Arias, C.A. (2016). Mechanisms of antibiotic resistance. *Microbiology spectrum* **4**:4:10.1128.
- Murray, C.J. *et al.* (2022). Global burden of bacterial antimicrobial resistance in 2019: a systematic analysis. *The Lancet* **399**:629–655.
- Nasiri, H.R. *et al.* (2013). Design, synthesis, and biological testing of novel naphthoquinones as substrate-based inhibitors of the quinol/fumarate reductase from *Wolinella succinogenes*. *J Med Chem* **56**:9530–41.
- Nicolas-Chanoine, M.H., Bertrand, X. and Madec, J.Y. (2014). *Escherichia coli* ST131, an intriguing clonal group, *Clinical Microbiology Reviews* **27**:543–574.
- Ng, Y.L., Salim, C.K. and Chu, J.J.H. (2021). Drug repurposing for COVID-19: Approaches, challenges and promising candidates. *Pharmacology & Therapeutics* **228**:107930.
- Nicholls, P. *et al.* (2013). Sulfide inhibition of and metabolism by cytochrome *c* oxidase. *Biochemical Society Transactions* **41**:1312–1316.
- Nixon, G.L. *et al.* (2013). Antimalarial pharmacology and therapeutics of atovaquone. *Journal of Antimicrobial Chemotherapy* **68**:977–985.
- Nosengo, N. (2016). Can you teach old drugs new tricks? *Nature* **534**:314–316.
- Oelschlaeger, P. (2021). β -Lactamases: Sequence, Structure, Function, and Inhibition. *Biomolecules*. **11**:986.
- Osborne, J.P. and Gennis, R.B. (1998). Sequence analysis of cytochrome *bd* oxidase suggests a revised topology for subunit I.
- Palmer, G. and Reedijk, J. (1992). Nomenclature Committee of the International Union of Biochemistry (NC-IUB). Nomenclature of electron-transfer proteins. Recommendations 1989. *Journal of Biological Chemistry* **267**:665–677.
- Paul, S.M. *et al.* (2010). How to improve R&D productivity: the pharmaceutical industry's grand challenge. *Nature Reviews Drug Discovery* **9**:203–214.

- Pihan, E. *et al.* (2012). e-Drug3D: 3D structure collections dedicated to drug repurposing and fragment-based drug design. *Bioinformatics* **28**:1540–1541.
- Poole, R.K., Chellappa, K., Salmon, I. and Britton, C. (1983). The 650 mμc chromophore in *Escherichia coli* is an ‘oxy-’ or oxygenated compound, not the oxidized form of cytochrome oxidase *d*: an Hypothesis. *Journal of General Microbiology* **129**:1335-1344.
- Poole, R.K. (1983). Bacterial cytochrome oxidases a structurally and functionally diverse group of electron-transfer protein. *Biochimica et Biophysica Acta (BBA) - Reviews on Bioenergetics* **726**:205–243.
- Poole, R.K. *et al.* (1989). Mutations affecting the cytochrome *d*-containing oxidase complex of *Escherichia coli* K12: identification and mapping of a fourth locus, *cydD*. *Journal of general microbiology* **135**:1865–1874.
- Poole, R.K. and Kalnenieks, U. (2000). Introduction to light absorption: visible and ultraviolet spectra. *Spectrophotometry and Spectrofluorimetry*. Available at: <https://academic.oup.com/book/41698/chapter/353943288> [Accessed: 29 September 2023].
- Poole, R.K. and Williams, H.D. (1988). Formation of the 680 nm-absorbing form of the cytochrome *bd* oxidase complex of *Escherichia coli* by reaction of hydrogen peroxide with the ferric form. *FEBS Letters* **231**:243–246.
- Portnoy, V.A. *et al.* (2010). Deletion of genes encoding cytochrome oxidases and quinol monooxygenase blocks the aerobic anaerobic shift in *Escherichia coli* K-12 MG1655. *Applied and Environmental Microbiology* **76**:6529–6540
- Portnoy, V.A., Herrgård, M.J. and Palsson, B. (2008). Aerobic fermentation of D-glucose by an evolved cytochrome oxidase-deficient *Escherichia coli* strain. *Applied and Environmental Microbiology* **74**:7561–7569.
- Price, E.P. *et al.* (2018). Transcriptomic analysis of longitudinal *Burkholderia pseudomallei* infecting the cystic fibrosis lung. *Microbial genomics* **4**:e000194.
- Pulingam, T. *et al.* (2022). Antimicrobial resistance: Prevalence, economic burden, mechanisms of resistance and strategies to overcome. *European Journal of Pharmaceutical Sciences* **170**:106103.
- Pushpakom, S. *et al.* (2018). Drug repurposing: progress, challenges and recommendations. *Nature Reviews Drug Discovery* **18**:41–58.
- Quesada A., Guijo, M.I., Merchán, F., Blázquez, B., Igeño, M.I. and Blasco, R. (2007). Essential role of cytochrome *bd*-related oxidase in cyanide resistance of *Pseudomonas pseudoalcaligenes* CECT5344. *Appl Environ Microbiol* **73**:5118-24.
- Ramírez, D. and Caballero, J. (2016). Is it reliable to use common molecular docking methods for comparing the binding affinities of enantiomer pairs for their protein target? *International Journal of Molecular Sciences* **17**:525.

- Rammelkamp, C.H. and Maxon, T. (1942). Resistance of *Staphylococcus aureus* to the action of penicillin. *Experimental Biology and Medicine* **51**:386–389.
- Ravichandiran, P. *et al.* (2019). 1,4-Naphthoquinone analogues: Potent antibacterial agents and mode of action evaluation. *Molecules* **24**:1437.
- Redgrave, L.S., Sutton, S.B., Webber, M.A. and Piddock, L.J.V. (2014). Fluoroquinolone resistance: mechanisms, impact on bacteria, and role in evolutionary success. *Trends in Microbiology* **22**:438–445.
- Reygaert, W. C. (2018). An overview of the antimicrobial resistance mechanisms of bacteria. *AIMS Microbiology* **4**:482–501.
- Rivera-Chávez, F. *et al.* (2016). Depletion of butyrate-producing clostridia from the gut microbiota drives an aerobic luminal expansion of Salmonella. *Cell Host and Microbe* [Online] **19**:443–454.
- Robert K. Poole and Huw D. Williams (1987). Proposal that the function of the membrane-bound cytochrome *a*₁-like haemoprotein (cytochrome *b*-595) in *Escherichia coli* is a direct electron donation to cytochrome *d*. *FEBS Letters* **217**:49–52.
- Robin, C. *et al.* (2017). Plasma concentrations of atovaquone given to immunocompromised patients to prevent *Pneumocystis jirovecii*. *Journal of Antimicrobial Chemotherapy* **72**:2602–2606.
- Rogers, B.A., Sidjabat, H.E. and Paterson, D.L. (2011). *Escherichia coli* O25b-ST131: a pandemic, multiresistant, community-associated strain. *The Journal of antimicrobial chemotherapy* [Online] **66**:1–14.
- Rolfe, M.D. *et al.* (2011). Transcript profiling and inference of *Escherichia coli* K-12 ArcA activity across the range of physiologically relevant oxygen concentrations. *Journal of Biological Chemistry* **286**:10147–10154.
- Roy, S., Dhaneshwar, S. and Bhasin, B. (2021). Drug repurposing: an emerging tool for drug reuse, recycling and discovery. *Current drug research reviews* **13**:101–119.
- Rutter, J., Winge, D.R. and Schiffman, J.D. (2010). Succinate dehydrogenase – assembly, regulation and role in human disease. *Mitochondrion* **10**:393–401.
- Safarian, S. *et al.* (2019). Active site rearrangement and structural divergence in prokaryotic respiratory oxidases. *Science* **366**:100–104.
- Safarian, S. *et al.* (2016). Structure of a *bd* oxidase indicates similar mechanisms for membrane integrated oxygen reductases. *Science* **352**:583–586.
- Safarian, S. *et al.* (2021). The cryo-EM structure of the *bd* oxidase from *M. tuberculosis* reveals a unique structural framework and enables rational drug design to combat TB. *Nature Communications* **12**.
- Sams-Dodd, F. (2005). Target-based drug discovery: is something wrong? *Drug Discovery Today* [Online] **10**:139–147.

- Sánchez-Calvo, J.M. *et al.* (2016). Synthesis, antibacterial and antifungal activities of naphthoquinone derivatives: a structure–activity relationship study. *Medicinal Chemistry Research* **25**:1274–1285.
- Sarti, P. *et al.* (2012). Mitochondria and nitric oxide: Chemistry and pathophysiology. *Advances in Experimental Medicine and Biology* **942**:75–92.
- Sato-Watanabe, M. *et al.* (1994). Structure-function studies on the ubiquinol oxidation site of the cytochrome *bo* complex from *Escherichia coli* using p-benzoquinones and substituted phenols. *Journal of Biological Chemistry* **269**:28899–28907.
- Seeliger, D. and De Groot, B.L. (2010). Ligand docking and binding site analysis with PyMOL and Autodock/Vina. *Journal of Computer-Aided Molecular Design* [Online] **24**:417–422.
- Seitz, C., Ahn, S., Wei, H., Kyte, M., Cook, G. M., Krause, K. L., & McCammon, J. A. (2024). Targeting Tuberculosis: Novel scaffolds for inhibiting cytochrome *bd* oxidase. *Journal of Chemical Information and Modeling*.
- Serra, D.O., Richter, A.M. and Hengge, R. (2013). Cellulose as an architectural element in spatially structured *Escherichia coli* biofilms. *J Bacteriol.* **195**:5540-54.
- Shaker, B. *et al.* (2021). *In silico* methods and tools for drug discovery. *Computers in biology and medicine* **137**:104851.
- Shepherd, M., Poole, R.K. (2013). *Bacterial Respiratory Chains*. In: Roberts, G.C.K. (eds) Encyclopedia of Biophysics. Springer, Berlin, Heidelberg.
- Shepherd, M. *et al.* (2010). Compensations for diminished terminal oxidase activity in *Escherichia coli*: Cytochrome *bd*-II-mediated respiration and glutamate metabolism. *Journal of Biological Chemistry* **285**:18464–18472.
- Shepherd, M. *et al.* (2016). The cytochrome *bd*-I respiratory oxidase augments survival of multidrug-resistant *Escherichia coli* during infection. *Scientific Reports* **6**:35285.
- Shi, L. *et al.* (2005). Changes in energy metabolism of *Mycobacterium tuberculosis* in mouse lung and under *in vitro* conditions affecting aerobic respiration. *Proc Natl Acad Sci U S A* **25**:15629-34.
- Shyu, C. *et al.* (2011). Quinestrol. *Toxicology and Applied Pharmacology* **250**:322–326.
- Siletsky, S. (2013). Steps of the coupled charge translocation in the catalytic cycle of cytochrome *c* oxidase. *Frontiers in Bioscience*. **18**:36.
- Small, J.L. *et al.* (2013). Perturbation of cytochrome *c* maturation reveals adaptability of the respiratory chain in *Mycobacterium tuberculosis*. *mBio* **4**.
- Smelov, V., Naber, K. and Bjerklund Johansen, T.E. (2016). Improved classification of urinary tract infection: future considerations. *European Urology, Supplements* **15**:71–80.

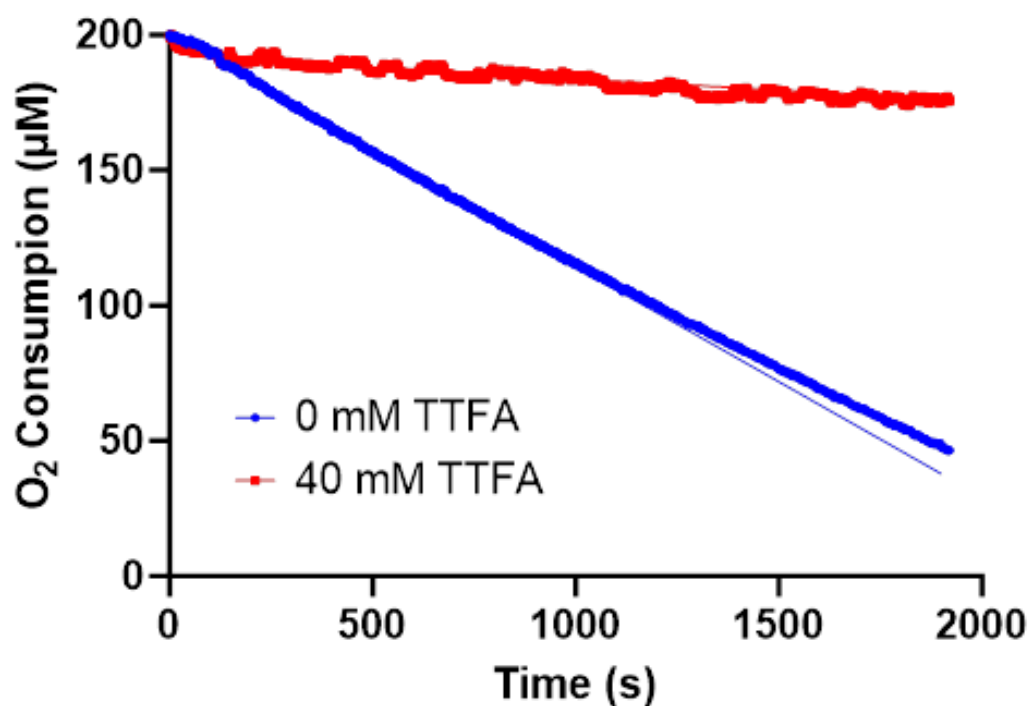
- SnapGene®, (n.d.). *Snapgene Viewer: Free software for plasmid mapping, Primer Design, and Restriction Site Analysis, SnapGene*. Available at: <https://www.snapgene.com/snapgene-viewer> (Accessed: 11 February 2024).
- Sneader, W. (2006). Drug Discovery: A History. *Drug Discovery: A History* [Online]:1–468.
- Soballe B. and Poole R.K. (1999). Microbial ubiquinones: multiple roles in respiration, gene regulation and oxidative stress management. *Microbiology*. **145**:1817–30.
- Sousa, F.L. *et al.* (2012). The superfamily of heme–copper oxygen reductases: Types and evolutionary considerations. *Biochimica et Biophysica Acta (BBA) - Bioenergetics* **1817**:629–637.
- Stokes JM, Lopatkin A.J., Lobritz M.A., Collins J.J. (2019). Bacterial metabolism and antibiotic efficacy. *Cell Metab* **30**:251–259.
- Sturr, M.G., Krulwich, T.A. and Hicks, D.B. (1996). Purification of a cytochrome *bd* terminal oxidase encoded by the *Escherichia coli* *App* locus from a *Cyo Cyd* strain complemented by genes from *Bacillus firmus* *OF4* **176**:1742-9.
- Taber, H.W. and Morrison, M. (1964). Electron transport in Staphylococci. Properties of a particle preparation from exponential phase *Staphylococcus aureus*. *Archives of Biochemistry and Biophysics* **105**:367–379.
- Talevi, A. and Bellera, C.L. (2020). Challenges and opportunities with drug repurposing: finding strategies to find alternative uses of therapeutics. *Expert Opinion on Drug Discovery* **15**:397–401.
- Terlizzi, M.E., Gribaudo, G. and Maffei, M.E. (2017). UroPathogenic *Escherichia coli* (UPEC) infections: Virulence factors, bladder responses, antibiotic, and non-antibiotic antimicrobial strategies. *Frontiers in Microbiology* **8**:1566.
- Theßeling, A. *et al.* (2019). Homologous *bd* oxidases share the same architecture but differ in mechanism. *Nature Communications* **10**:5138.
- Tomlinson, B.R., Malof, M.E. and Shaw, L.N. (2021). A global transcriptomic analysis of staphylococcus aureus biofilm formation across diverse clonal lineages. *Microbial Genomics* **7**:000598.
- Totsika, M. *et al.* (2011). Insights into a multidrug resistant *Escherichia coli* pathogen of the globally disseminated ST131 lineage: Genome analysis and virulence mechanisms. *PLoS ONE* **6**.
- Trott, O. and Olson, A.J. (2010). AutoDock Vina: Improving the speed and accuracy of docking with a new scoring function, efficient optimization, and multithreading. *Journal of Computational Chemistry* **31**:455–461.
- Turner, A.K. *et al.* (2003). Contribution of proton-translocating proteins to the virulence of *Salmonella enterica* serovars Typhimurium, Gallinarum, and Dublin in chickens and mice. *Infection and Immunity* **71**:3392–3401.

- Tynecka, Z. *et al.* (1999a). Energy conservation in aerobically grown *Staphylococcus aureus*. *Research in Microbiology* **150**:555–566.
- Uden, G. and Dünnwald, P. (2008). The aerobic and anaerobic respiratory chain of *Escherichia coli* and *Salmonella enterica*: enzymes and energetics. *Ecosal Plus* **3**.
- Valdeira, A.S.C. *et al.* (2019). Madecassic Acid Derivatives as Potential Anticancer Agents: Synthesis and Cytotoxic Evaluation. *Journal of Natural Products* **82**:2094–2105.
- Valdeira, A.S.C. *et al.* (2018). Synthesis and Biological evaluation of new madecassic acid derivatives targeting ERK cascade signaling. *Frontiers in Chemistry* **6**:434.
- Vanorsdel, C.E. *et al.* (2013). The *Escherichia coli* CydX protein is a member of the CydAB cytochrome *bd* oxidase complex and is required for cytochrome *bd* oxidase activity. *Journal of Bacteriology* **195**:3640–3650.
- Veronese, F.M. and Mero, A. (2008). The impact of PEGylation on biological therapies. *BioDrugs* **22**:315–329.
- Villar-Hernández, R., Ghodousi, A., Konstantynovska, O., Duarte, R., Lange, C., & Raviglione, M. (2023). Tuberculosis: current challenges and beyond. *Breathe* **19**:220166.
- Voggu, L. *et al.* (2006). Microevolution of cytochrome *bd* oxidase in Staphylococci and its implication in resistance to respiratory toxins released by Pseudomonas. *Journal of Bacteriology* **188**:8079–8086.
- Walsh, T.R. *et al.* (2023). Antimicrobial Resistance: addressing a global threat to humanity. *PLoS medicine* **20**:e1004264.
- Way, S.S. *et al.* (1999). Impact of either elevated or decreased levels of cytochrome *bd* expression on *Shigella flexneri* virulence. *Journal of Bacteriology* **181**:1229–1237.
- Webster, C.M. (2023). *Escherichia Coli* aerobic respiratory complexes as modulators of aminoglycoside susceptibility and targets for drug discovery. University of Kent. PhD Thesis.
- Webster, C.M. *et al.* (2022). Proton motive force underpins respiration-mediated potentiation of aminoglycoside lethality in pathogenic *Escherichia coli*. *Archives of Microbiology* **204**:120.
- Wei, C., Cui, P. and Liu, X. (2023). Antibacterial activity and mechanism of madecassic acid against *Staphylococcus aureus*. *Molecules* **28**:1895.
- Weiss, S.A. *et al.* (2009). Characterization of cytochrome *bo*₃ activity in a native-like surface-tethered membrane. *Biochemical Journal* **417**:555–560.
- Welchen, E. and Gonzalez, D.H. (2016). Cytochrome *c*, a hub linking energy, redox, stress and signaling pathways in mitochondria and other cell compartments. *Physiologia Plantarum* **157**:310–321.
- Whelan, S., Lucey, B., & Finn, K. (2023). Uropathogenic *Escherichia coli* (UPEC)-Associated Urinary Tract Infections: The Molecular Basis for Challenges to Effective Treatment. *Microorganisms* **11**:2169.

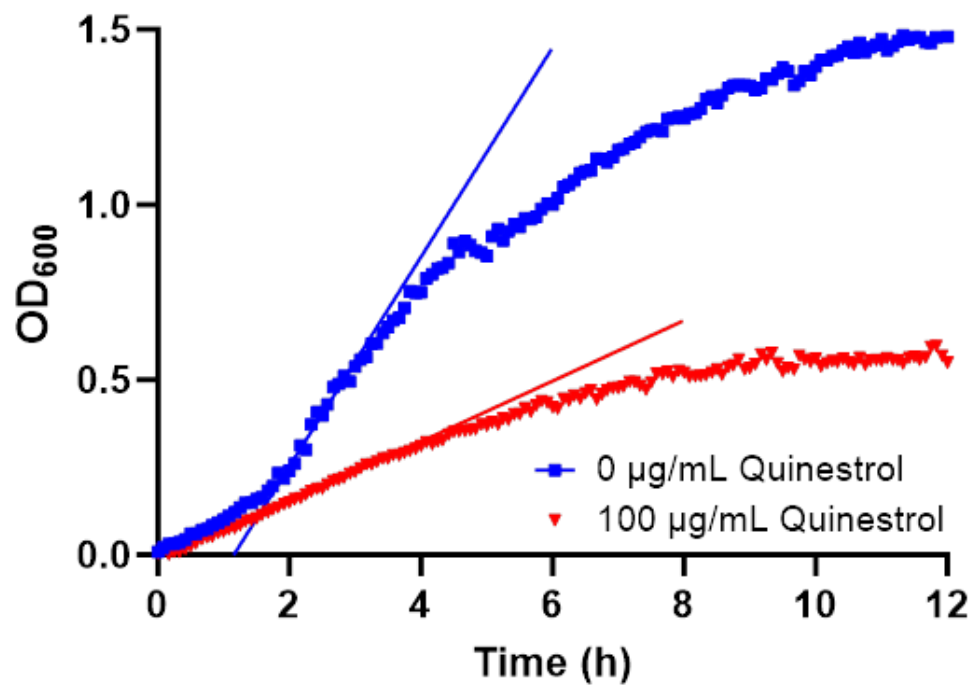
- Whitehouse, D.G., May, B. and Moore, A.L. (2019) Respiratory chain and ATP synthase, in *Elsevier eBooks*.
- World Health Organization (2021). Antimicrobial Resistance. Available at <https://www.who.int/news-room/fact-sheets/detail/antimicrobial-resistance> . [Accessed: January 03, 2024].
- Yamamoto, Y. *et al.* (2005). Respiration metabolism of Group B Streptococcus is activated by environmental haem and quinone and contributes to virulence. *Molecular Microbiology* **56**:525–534.
- Younis, W. *et al.* (2017). *In Vitro* screening of an FDA-approved library against ESKAPE pathogens. *Current Pharmaceutical Design* **23**:2147-2157.
- Zhang, J., Hellwig, P., Osborne, J. P., & Gennis, R. B. (2004). Arginine 391 in Subunit I of the cytochrome *bd* quinol oxidase from *Escherichia coli* stabilizes the reduced form of the hemes and is essential for quinol oxidase activity. *Journal of Biological Chemistry* **279**:53980–53987.
- Zhou Y, Shao M, Wang W, et al. Discovery of 1-hydroxy-2-methylquinolin-4(1H)-one derivatives as new cytochrome *bd* oxidase inhibitors for tuberculosis therapy. *Eur J Med Chem* **245**:114896.
- Zeng S, Soetaert K, Ravon F, *et al.* (2019). Isoniazid bactericidal activity involves electron transport chain perturbation. *Antimicrob Agents Chemother* **63**:e01841-18.
- Zipperer, A. *et al.* (2016). Human commensals producing a novel antibiotic impair pathogen colonization. *Nature* **535**:511–516.
- Zlosnik, J.E.A. *et al.* (2006). Investigation of the physiological relationship between the cyanide-insensitive oxidase and cyanide production in *Pseudomonas aeruginosa*. *Microbiology* **152**:1407–1415.

APPENDIX

Appendix A.1. Raw traces of oxygen consumption TTFA assay with *E. coli* cytochrome *bd-I* only membranes. *E. coli* EC958 *bd-I* membranes were exposed to various concentrations of TTFA. The substrate used to start the oxygen consumption reaction was succinate dehydrogenase. One reaction ran for about 30 min and raw voltage data was collected. A timepoint was selected for the oxygen consumption data (μM) and the rate of reaction was calculated. From the calculated rates (nM/s), an inhibition curve was generated and IC_{50} determined.



Appendix A.3. Raw traces of *E. coli* 'bd-only' growth curves in the presence of quineestrol. μ_{max} was calculated via linear regression of datapoints from the region of most rapid growth (2 - 3 h) and allows direct comparison of all quineestrol concentrations.



Appendix A.4. Solubility assay for quinestron against *E. coli* cells. *E. coli* EC958 WT cells were grown in the presence of growth media (TSB, LB or M9 minimal media), detergents (triton or tween), and solvents (DMSO and EtOH). A high inhibitory concentration of quinestron, 100 µg/mL, was used for all experiments. Cells were grown for 12 hours, and a time point within the exponential phase was selected to calculate the rate of growth. Error bars represent the standard deviation of 4 technical repeats.

